UNIVERSITE NICE SOPHIA ANTIPOLIS – UFR Sciences
Ecole Doctorale de Sciences Fondamentales et Appliquées

THESE

pour obtenir le titre de
Docteur en Sciences
de l'UNIVERSITE Nice Sophia Antipolis
Discipline : Chimie

présentée par
Andrea SABĂU

Mécanismes d'interaction du nickel et de l´europium avec la calcite

Interaction mechanisms of europium and nickel with calcite

Thèse dirigée par Prof. Nicolas MARMIER

Soutenue publiquement le 27 Mars 2015 devant le jury composé de

Président du Jury :

Dr. Vinzenz Brendler, Chercheur, Helmholtz-Zentrum Dresden Rossendorf, Institute of Resource Ecology

Rapporteurs :

Dr. habil. Grégory Lefèvre, Chargé de recherche, Chimie ParisTech-CNRS

Dr. habil. Isabelle Le Hécho, Maître de conférences, Université de Pau

Examinateurs :

Dr. Nelly Toulhoat, Ingénieur-chercheur, CEA/IPNL, Université de Lyon

Dr. Eric Giffaut, Ingénieur de recherche, ANDRA

Dr. Nicolas Marmier, Professeur, Université Nice Sophia Antipolis

Dr. Norbert Jordan, Chercheur, Helmholtz-Zentrum Dresden Rossendorf, Institute of Resource Ecology

Dr. Claire Lomenech, Maître de conférences, Université Nice Sophia Antipolis

Acknowledgements

First, I would like to be thankful to *Vinzenz Brendler* for accepting to be the president of the jury for my Ph.D. defense. Beside this, I am thankfull for all discussions about science, for all advices and all the feedbacks for reports/presentations and other documents and all late meetings to prepare new stays in Dresden. I would like to be grateful to *Grégory Lefèvre* and *Isabelle Le Hécho* for having accepted to referee my thesis and to *Nelly Toulhoat* for taking part in the defense jury.

First I would like to express my recognition to ANDRA for founding this thesis, and without which this project would not be possible. I would like to express my distinguish thanks Eric Giffaut from Transfert Division of ANDRA, who is responsible of project managing, for believing in my capacities and understanding me. I will not forget Scott Altman, for the scientific encouragements and discussions.

I would like to express my gratitude to all people who supported me during my thesis: my four Ph.D. advisors, for what I've learned from them, scientifically (but not only!) and for the autonomy to doing things in my way.

- *Nicolas Marmier* – many thanks for all scientific advices, for his diplomatic touch and optimism.
- *Norbert Jordan* – my sincere thanks for accepting me as your first Ph.D. student (hope this experience didn't discourage you for future ...never knows!) for all long scientific discussions and advices, dedication, careful observation of my work and experiments performed over these years. Also, thank you for giving me a new vision about science and for all the precious time spend to correct all the documents/reports/presentations.
- *Claire Lomenech* – my sincere thanks for your implication in this project and for your unconditioned scientific support over these years and for all the time you give to correct all my presentations, reports and my manuscript.

Also I am grateful to:

- *Nelly Toulhoat*, *Yves Pipon* and *Nathalie Moncoffre* for their hospitality during my trips to Lyon and RBS measurements at INPL, for introducing me in RBS world and for all the corrections that they integrated to my manuscript.

- *Caroline Raepset* for RBS preliminary measurements at IRAMIS.
- *Suzy Surblé* for accepting the project and for a great introduction into IBA techniques; but also for all the explanations you give me during the long days and nights spent to the RBS facility to IRAMIS (CEA, Saclay).
- *Astrid Barkleit* for introducing me in TRLFS and for fruitful discussions about this technique, and of course for all tips and corrections of my manuscript.
- HZDR-IRE staff: *Weiß Stephan* (I'll never forget your unconditioned scientific support!!!), *Heim Karsten, Eckardt Carola, Müller Christa, Neubert Heidrun, Ritter Aline, Müller Katharina* and *Moll Henry.*
- All the people from other institutes of HZDR who helped me in various ways: *Hübner René, Christalle Elfi* and *Scholtz Andrea.*

I am happy to meet and to "grow up" in the wonderful team of ECOMERS Laboratory where *Salomé, Brice, Inès, Yassine* and *Mehwish* (...and others) supported me and helped me a lot to improve my French level. Thank you for still being my friends after various experiences and having the patience to tolerate me...I have a difficult character ☺
Also, I would like to thank to *Charlotte Hurel* who integrated me very well in the team and who supported me in my difficult steps.

Sunt recunoscătoare părinților mei care m-au vegheat de la început. De la amandoi am învățat cea mai importantă lecție de viață: SĂ FII OM!
(I am grateful to my parents which have been behind of me from the very beginning. From both of them I learned the most important lesson of my life: **to be human**).

Per Roberto - Questo breve ringraziamento non basta a ripagare l'incondizionato sostengo e tuo amore datomi durante la stesura del mio lavoro di tesi in quest'ultimo anno.

All the people that I forget and I should have mentioned...I am sorry for that.

Résumé en français

Mécanismes d'interaction de l´europium et du nickel avec la calcite

Le parlement français a adopté la loi du 30 décembre 1991 (dite loi Bataille) relative à la gestion des déchets radioactifs. L'Agence Nationale pour la gestion des Déchets RAdioactifs (l'ANDRA) s'est vue confiée l'axe 2 de cette loi, à savoir l'étude de la faisabilité de l'exploitation de laboratoires souterrains en formation géologique profonde, dans le but d'y stocker les déchets de Haute Activité à Vie Longue (HAVL) et de Moyenne Activité à Vie Longue (MA-VL). A cette fin, un laboratoire de recherche souterrain a été construit sur la commune de Bure (Meuse, France) au sein d'une formation argileuse du Callovo-Oxfordien (COx), à environ 490 m de profondeur.

Suite au bilan des travaux effectués durant quinze années, une nouvelle loi a été votée le 28 juin 2006. Cette dernière a confirmé la faisabilité du stockage réversible en formation géologique profonde. L´ANDRA est responsable de la conception et de l´implantation du centre de stockage dans le cadre du projet CIGEO (Centre Industriel de stockage GEOlogique).

Afin d´établir la sûreté d´un centre de stockages sur le long terme, il est nécessaire d´étudier et d´élucider les mécanismes régulant le transfert des radionucléides. Généralement, la sorption par des phases minérales gouverne la migration de ces éléments, de même que la dissolution des phases solides potentiellement formées. La sorption peut être considérée comme une première étape à cinétique rapide de la fixation des ions, mais les différentes étapes entre la chimie de surface et l'incorporation des ions sont encore peu comprises. Les mécanismes d'interaction entre cations et minéraux peuvent inclure des processus d'adsorption, de (co-) précipitation de surface, et aller jusqu'à l'incorporation au sein du matériau, ce qui peut entraîner l'irréversibilité de certaines réactions de sorption. Les argilites du COx sont constituées principalement de trois phases minérales: une phase argileuse (illite, smectite et micas), une phase carbonatée (principalement la calcite et l'ankérite) et le quartz. Les eaux interstitielles du COx ont un pH proche de la neutralité ou légèrement alcalin, imposé par les phases en présence.

Le minéral choisi pour cette étude est la calcite, présente dans les argilites du Callovo-Oxfordien et également produit d'altération des ciments, ce qui justifie son intérêt pour l'évaluation de la sûreté d'un site de stockage de déchets radioactifs en formation géologique profonde.

Le but de cette thèse est d´étudier et de quantifier les processus conduisant à l'incorporation de cations au sein d'une matrice carbonatée. L'accent a été mis sur la mise en évidence de l'existence ou non de processus d'incorporation dans les systèmes Eu−NaCl−CO_2–calcite et Ni−NaCl−CO_2–calcite, dans des conditions atmosphériques où le milieu tamponné par la calcite a un pH voisin de 8,3, et pour une partie de l'étude à pression partielle plus élevée de CO_2 (10^{-2} atm), correspondant à la valeur d'équilibre au sein de la formation du COx. L'europium est choisi en tant qu'analogue pour certains actinides trivalents, ainsi que pour ses propriétés de fluorescence qui permettent l´utilisation de la Spectrométrie Laser à Résolution Temporelle (SLRT). Le nickel, notamment les isotopes ^{59}Ni et ^{63}Ni, est quant à lui un produit d'activation neutronique des composants métalliques du combustible irradié. Notre étude combine des expériences macroscopiques de type batch et des études spectroscopiques (SLRT et spectrométrie de rétrodiffusion de Rutherford - RBS) pour caractériser les systèmes choisis. Des observations complémentaires en microscopie électronique à balayage (MEB) des surfaces minérales couplées à des analyses EDXS ont également été menées, afin d´évaluer l´homo/hétérogénéité des échantillons.

Dans un premier temps, une caractérisation poussée de calcites sous forme de poudres (en provenance de différentes sources) nous a permis de sélectionner un matériau de départ approprié pour les expériences de sorption et de spectroscopie. Une calcite SOLVAY (SOCAL U1-R), avec une taille de particule fine et une surface spécifique élevée (18,4 m^2/g), a été retenue pour les expériences de SLRT. Pour les expériences RBS, notre choix s´est porté sur la calcite OMYA (BL 200), avec une taille de particule plus élevée et une surface spécifique de 0,66 m^2/g. Afin d'éviter la présence d'artefacts sur des échantillons de calcite compactés au cours des mesures RBS, nous avons également choisi de travailler avec des cristaux millimétriques de calcite (Alfa Aesar). L'absence de contamination majeure et d'autres polymorphes de $CaCO_3$ (vatérite, aragonite) a été confirmée par DRX, ATR-FT-IR et ICP-MS après digestion.

Les études de sorption de l'europium et du nickel ont ensuite été menées, avec préalablement une étude de la chimie en solution carbonatée de ces deux éléments dans les conditions des expériences.

Le comportement de l'europium en solution a été étudié en milieu carbonaté obtenu à l´aide de solutions pré-équilibrées avec la calcite. L'étude a porté notamment sur l'influence de la concentration initiale et du temps de contact. Ceci a servi de référence et de support afin de mieux appréhender l'interaction de l'europium avec la calcite. Les calculs de spéciation faits sous conditions atmosphériques à pH=8,3 en utilisant une gamme de concentrations variant de 10^{-6} à

10^{-3} mol.L^{-1} ont prédit une précipitation de l'europium sous la forme de $Eu_2(CO_3)_3{:}3H_2O_{(s)}$ et $Eu(CO_3)OH_{(s),}$ à 10^{-3} mol.L^{-1} et à $\leq 10^{-4}$ mol.L^{-1} Eu(III) initiale, respectivement. Ces calculs ont été confirmés par des expériences à l'échelle macroscopique qui ont révélé une précipitation de l'Eu(III) pour des concentrations supérieures à 10^{-5} mol.L^{-1}. A 10^{-6} mol.L^{-1}, aucune précipitation n'a été observée. La formation de $Eu_2(CO_3)_3{:}3H_2O_{(s)}$ et $Eu(CO_3)OH_{(s),}$ a été confirmée par TRLFS et DRX.

Les expériences de sorption de l'europium ont été menées sous conditions atmosphériques ($pCO_2 = 10^{-3.5}$ atm) en milieu NaCl 10^{-1} mol.L^{-1}, pour des concentrations d'europium variant de 10^{-3} (en sursaturation) à 10^{-6} mol.L^{-1} et des temps de contact variant de quelques heures à 6 mois. Les analyses ICP-MS/ICP-AES des surnageants ont montré un taux de rétention de l'Eu(III) par la calcite supérieur à 95 % quelles que soient les conditions expérimentales utilisées dans cette étude.

Les résultats de SLRT montrent un comportement différent de l'europium en fonction de la concentration initiale et du temps de contact. Pour les concentrations les plus élevées (supérieures à 10^{-4} mol.L^{-1}), les espèces identifiées semblent correspondre à un (co-)précipité de surface et un complexe de surface. Pour les concentrations plus faibles (inférieures à 10^{-5} mol.L^{-1}), les temps de vie observés sur l'une des espèces, beaucoup plus longs, semblent indiquer une incorporation de l´europium au sein du matériau.

Des expériences par RBS ont également été effectuées sur millisonde nucléaire à l'Institut de Physique Nucléaire de Lyon, ainsi que sur microsonde au CEA-Saclay en utilisant des concentrations initiales en Eu(III) de 10^{-4} et 10^{-5} mol.L^{-1} sur monocristaux. Cette technique est bien adaptée pour discriminer les processus de sorption tels que: (i) adsorption ou (co)-précipitation sur les surfaces minérales ou (ii) incorporation dans la structure minérale (grâce à la diffusion par exemple).

Les résultats RBS ont démontré une accumulation de l'Eu(III) à la surface, probablement sous la forme d'un co-précipité de surface. La distribution hétérogène de l'Eu(III) à la surface de la calcite a été établie par des mesures SEM-EDXS complémentaires. Cette accumulation de surface est accompagnée d'une incorporation de l'Eu(III) dans la calcite sur une profondeur allant jusqu'à 250 nm après 2 mois de contact pour les échantillons à 10^{-5} mol.L^{-1} et 5 mois de contact pour les échantillons à 10^{-4} mol.L^{-1}. Les profils de concentration ont été modélisés en utilisant des coefficients de diffusion apparents, de l'ordre de 10^{-22} – 10^{-21} $m^2.s^{-1}$ et incompatibles avec un mécanisme de diffusion.

La rétention de l'europium dans la calcite semble procéder par trois mécanismes différents, au vu des mesures SLRT, RBS et SEM-EDXS : (i) l'accumulation hétérogène de surface ((co-)précipité de surface), (ii) la formation d'un complexe de sphère interne et (iii) l'incorporation dans le solide, vraisemblablement par un processus de dissolution/re-précipitation pour former une solution solide.

Le comportement du nickel en solution carbonatée a été étudié dans des solutions pré-équilibrées avec la calcite, en fonction de la concentration initiale et du temps de contact. La précipitation du nickel a été observée pour des concentrations initiales comprises entre 10^{-5} et 10^{-3} mol.L^{-1}, contrairement à 10^{-6} mol.L^{-1} pour laquelle le nickel ne précipite pas. La formation de $Ni(OH)_{2(s)}$ pour une concentration initiale de 10^{-3} mol.L^{-1} a été confirmée par DRX, conformément aux calculs de spéciation. La précipitation du nickel s'est avérée être un processus à cinétique lente pouvant durer jusqu'à plusieurs mois.

Les expériences de sorption en batch pour des concentrations du nickel variant de 10^{-6} à 5×10^{-5} mol.L^{-1} ont abouti à des taux de sorption élevés (>65%) et des taux moins élevés (40 %) pour 10^{-4} mol.L^{-1} et 5×10^{-4} mol.L^{-1} pour un rapport masse de calcite/volume de suspension égal à 1 g.L^{-1}. Pour toutes les concentrations étudiées, une désorption du nickel a été observée. Les indices de désorption ont révélé une réversibilité quasi-totale pour les faibles concentrations (<10^{-5} mol.L^{-1}). Le degré d'irréversibilité augmente avec la concentration initiale en nickel. Les expériences de sorption et de désorption en fonction du temps, couplées au calcul d'un indice de désorption, ont permis de mettre en évidence un mécanisme de sorption composé de deux processus: (i) un processus d'adsorption, rapide et réversible (ii) un mécanisme plus lent et partiellement réversible, probablement une précipitation de surface.

Une accumulation du nickel à la surface de monocristaux de calcite a été observée par milli et µ-RBS, avec une distribution hétérogène du nickel, confirmée par des mesures MEB-EDXS. Cette observation serait en accord avec les mécanismes proposés sur la base des expériences de sorption/désorption en batch, c'est-à-dire de l'adsorption et /ou de la précipitation de surface. La distribution non uniforme d'un précipité de surface $Ni(OH)_{2(s)}$ expliquerait les différences observées par la RBS et le SEM-EDXS en fonction du temps de contact.

Table of contents

List of Figures

List of Tables

Context of the study

Context of the study

All anthropogenic activities produce waste. Nuclear waste is all the radioactive material that should be stored in special conditions. France has been one of the first countries to vote a law in December 1991 (loi Bataille), regarding the repository of the nuclear waste, especially high-level ones.

Radioactive waste - where does it come from?

Most of the waste is coming from nuclear activities, such as nuclear energy production (fission of ^{235}U) or scientific research activities. From these activities, some isotopes like ^{239}Pu, ^{237}Np, ^{241}Am, ^{243}Am, ^{244}Cm, ^{245}Cm, ^{129}I are formed in reactor fuel assemblies. The various type of the radioactive waste produced in France vary by their activity and half-life (Table 0.1). The treatment and the final disposal solution must be therefore adapted to each type of waste.

Table 0.1: Classification of radioactive waste [1].

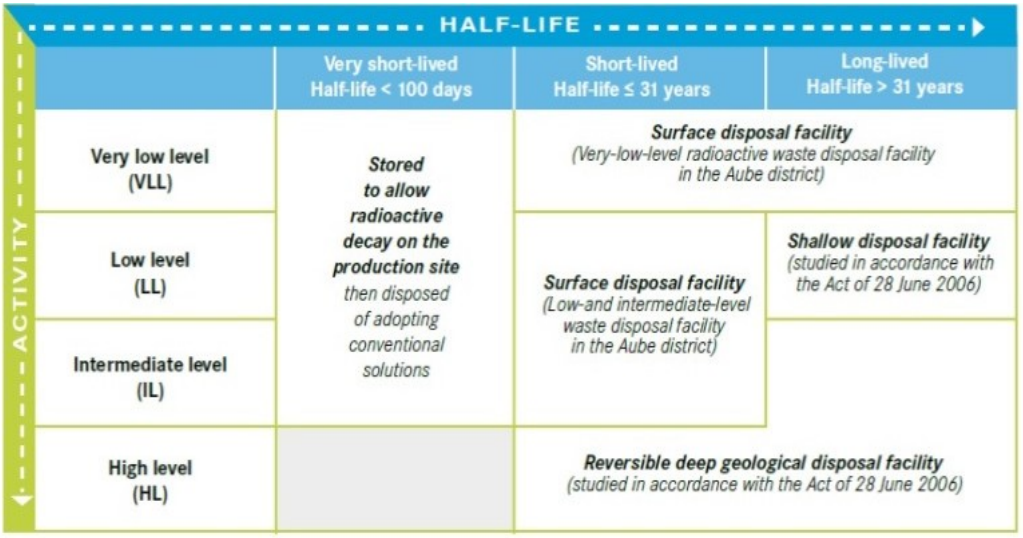

Radioactive waste management in France

The law voted in 1991 (research in radioactive waste management) organized the research focusing on nuclear waste management in three axes:

- separation and transmutation of long-lived elements
- conditioning and long term surface storage of low and intermediate level waste

- reversible disposal of intermediate level long lived (IL–LL) and high level (HL) waste in deep geological formation

The first point refers to reduce the volume and the harmfulness of radioactive waste, by transforming it in isotopes with a lower activity and/or much shorter half-life. The second point refers to design new storage installation or to improve the existent surface storage sites to meet the requirements imposed by the law. These two axes were assigned to the CEA (Commissariat à l'énergie atomique et aux énergies alternatives).

The last axis is aiming at proving the capacities of geological formations to store the IL-LL and HL radionuclides. The French National Radioactive Waste Management Agency (ANDRA-Agence Nationale pour la Gestion des Déchets RAdioactifs), the public institution in charge of the radioactive waste management, was responsible of this topic.

ANDRA has performed feasibility studies in two clay rock (Bure and Marcoule, in Meuse/Haute-Marne and Gard districts, respectively) and one granitic (La Chapelle-Bâton, in Vienne district) geological formations. Studies have established weak robustness of a disposal project in granite in Vienne district. Among the two clay rock formations, it was concluded that the Callovo-Oxfordian (COx) geological formation (Bure) is the best solution in France.

Based on the strategy act of law voted in 2006 (program on sustainable management of radioactive materials and waste), ANDRA has the mission to design and implement a repository in the COx formation to store IL–LL and HL waste. This project is called CIGEO (Centre Industriel de stockage GEOlogique) and is based on the studies regrouped in Dossier 2005 Argile [2, 3].

Purpose of the work

Proving the safety of a nuclear waste repository requires a better understanding of migration of pollutants into environment and the processes occurring there. Generally, the sorption of radioelements onto mineral phases controls their migration together with solubility of the solid bearing phases formed.

The pore waters in the COx (Callovian Oxfordian) clay rocks impose equilibrium of the investigated system. The presences of the carbonates in the system impose a pH close to neutral or

alkaline. The COx clay rocks are made of three main mineralogical phases: argillaceous phase (illite, smectite et micas), carbonate phase (mainly calcite) and quartz.

Interactions between cations and natural or synthetic $CaCO_3$ – calcite (including aragonite) may include processes like adsorption, surface (co)-precipitation up to incorporation within the material, which may cause irreversibility of some uptake reactions.

The interest of this Ph.D. is based on the capacity of calcite to sorb heavy metal contaminants such as transition metals (in particularly nickel as activation product) and lanthanides (especially europium as analogue for trivalent actinides) over a long time scale and to characterize the mechanisms occurring at the solid/liquid interface.

Calcite has already been shown to be an appropriate material to strongly retain europium [4-7]. There are studies determining the partition coefficient [8] of sorbed Eu(III) onto calcite powders [7], but these empirical values do not give information about the structure of the element on the surface of the investigated solid or the on-going mechanisms. Studies characterizing the Eu(III) interaction with calcite at spectroscopic level are scarce [4, 6, 7, 9, 10]. Due to the fact that Eu(III) ionic radii (95 pm) is close to Ca ionic radii (100 pm), Eu(III) can be incorporated into calcite by isomorphic substitution. This was observed by Marques-Fernandes et al. [4], who synthesized calcite in presence of Eu(III) traces (using the mixed-flow reactor procedure), by means of Time-Resolved Laser Fluorescence Spectroscopy (TRLFS).

Ni(II) interaction with calcite and its sorption on calcite has been presented as an ionic exchange process with Ca^{2+} ions or metal complexation with CO_3^{2-} groups on a hydrated surface layer [11]. Hoffmann and Stipp [12] came to a similar conclusion from their study of the mechanisms of Ni(II) incorporation, using surface sensitive techniques. Carlsson and Aalto [13] studied Ni(II) co-precipitation with calcite by liquid scintillation counting and observed Ni incorporation during re-crystallization. The sorption and reversibility of the nickel-calcite system was investigated for various pH scales and different ionic strengths by Lamana [14] and Zachara [11] who noted that Ni(II) sorption increases with pH and is not desorbing readily.

Although some information is available, a series of open questions are still existent about Eu(III) and Ni(II) interaction with calcite:

- How does contact time and concentration influence Eu(III)/Ni(II) interaction with calcite? Is there an irreversible process over time?
- Which conditions promote surface complexation and surface precipitation?
- Which mechanisms could lead to incorporation of Eu(III)/Ni(II) into calcite? Is it possible that a solid state diffusion of these elements occur in calcite, as shown by S. Stipp and collaborators for other elements (i.e. Cd^{2+}, Zn^{2+}) [15, 16]?

Our approach to answer these main questions is to investigate the mechanisms governing the interaction of Eu(III)/Ni(II) at the calcite interface both from a macroscopic and a microscopic approach. The methodology developed consists into designing appropriate time-dependency batch sorption experiments on calcite powders and single crystals with Eu(III) and Ni(II) solutions at different concentrations. Indeed, if the mechanisms depend on the concentration, they might be different in the near field where the concentrations of radionuclides can be rather high, and in the far field where the concentrations are always very low. Then, spectroscopic techniques such as TRLFS and RBS (Rutherford Backscattering Spectrometry) were applied to characterize the systems at the molecular level. While TRLFS has been extensively used to study Eu(III) speciation, RBS is a spectroscopic tool well adapted to obtain information on the depth distribution of elements from the upmost surface layers to the bulk of solids – it has for example been used to study diffusion of Eu in clay minerals [17]. Therefore, it should be a powerful tool to characterize and quantify the incorporation of Eu/Ni in calcite. Additional techniques such as SEM, SEM-EDXS were used in the study to help us to have a better understanding of the interaction mechanisms.

This work is regrouped in four chapters. The first chapter sums up the existent bibliographic data of calcite, europium and nickel. The structure, aqueous behavior and reactivity of calcite are highlighted. For each element, the aqueous chemistry, complexation with carbonates and interaction with calcite are presented in order to have an overview of the investigated system.

The second chapter regroups as a first step a careful characterization of each type of calcite that was used in this study. Then, the second step is a detailed description about the experimental procedure for sorption and spectroscopic experiments.

Chapter three presents all the results obtained on Eu(III). The first part presents the speciation diagrams and the macroscopic data of complexation of Eu(III) with carbonates together with TRLFS studies supported by XRD (X-Ray Diffraction). The second part is dedicated to Eu(III) interaction with calcite under several conditions, which are carefully presented from macroscopic and spectroscopic point of view. TRLFS and RBS results are detailed together with SEM-EDXS and compared with macroscopic ones in order to identify the mechanisms occurring in this system.

The last chapter is dedicated to Ni(II). The first part is presenting the complexation of Ni(II) with carbonates, then a detailed sorption/desorption study gives the macroscopic results. A detailed RBS study is presented as well, completed with SEM-EDXS investigations.

Chapter 1:
State of the art

1. State of the art

The mobility of elements in natural systems strongly depends on the geological environment and both on their solution chemistry and sorption properties. Different group of elements exhibit a particular reactivity toward calcite, giving interest to this work. Due to its high reactivity, calcite plays a key role in the aqueous geochemistry by regulating the pH and alkalinity by means of dissolution and precipitation in closed systems. Surface techniques such as XPS (X-ray Photoelectron Spectroscopy), LEED (Low Energy Electron Diffraction) and AFM (Atomic Force Microscopy), showed that in humid air calcite has an ordered and crystalline surface, while in vacuum a surface reconstruction occurs [18, 19]. Kept in water for a long time, surface of calcite is rearranging [19-21]. In aqueous environment, calcite is therefore influencing the chemical behavior of soils and sediments [22]. Via sorption reactions, calcite may affect the mobility and geochemical cycling of trace metal that can be found in the aquatic environment [23, 24]. The reactivity of calcite, surface makes it an important sorbent for heavy metals, metalloids and contaminants in the environment.

This chapter gathers the bibliographic review of calcite interaction with metals. The first part focuses on calcite, on its environmental occurrence and significance, as well as its bulk structure and its surface reactivity in aqueous solutions. The second part is a review of past studies dealing with the interaction of Eu(III) with aqueous carbonates, with an emphasis on TRLFS studies. This was followed by a review on the literature data on Eu(III) interaction with calcite. Finally, the third part is devoted to the aqueous chemistry of Ni(II) and especially its interaction with aqueous carbonate species, which have to be taken into account when studying their sorption on calcite. Likewise, a bibliographic review of Ni(II) behavior in presence of calcite is presented in the same section.

1.1. Calcite: environmental occurrence and significance, structure and surface reactivity

1.1.1. Environmental occurrence and significance

Calcium carbonate ($CaCO_3$) can be found in three polymorphic forms: calcite, aragonite and vaterite [25]. Taking into account the solubility products K_{sp} at 25°C of each polymorphic form (Table 1.1), we can see that calcite is the most stable in the $CaCO_3$ series. Vaterite behaves as a precursor in calcite/aragonite formation, resulting in a polymorph phase mixture.

Table 1.1: Solubility products of calcium carbonates at 25 °C.

Phase	$\log_{10}$ Ksp (I=0)	Reference
Calcite	−8.42	Jacobsen and Langmuir [26]
	−8.45	Berner [27]
	−8.48	Plummer and Busenberg[28]
Aragonite	−8.28	Berner [27]
	−8.28	Plummer and Busenberg [28]
	−8.31	Garvin et al. [29]
Vaterite	−7.91	Plummer and Busenberg [28]
	−7.90	Garvin et al. [29]

Calcite is widely found in sedimentary rocks and cementitious materials and is expected to precipitate as a result of the interaction of concrete with carbonated water or organic waste [30]. From highly supersaturated calcium carbonate solutions, metastable vaterite may precipitate as a precursor phase and later transform to calcite [31]. In addition to calcium carbonate polymorphs for high alkaline pH, it is important to consider $Ca(OH)_2$ - portlandite too.

Precipitated calcite as well as primary phases are expected to trap dissolved radionuclides, especially lanthanides and actinides [32]. Calcite is also known to retain divalent trace metals onto its surface and to incorporate them into the lattice by cationic substitution [16].

1.1.2. Structure of calcite

Calcite crystallization form is rhombohedra being included in $R\bar{3}2/m$ group space. The cell dimensions differ slightly for different calcite crystals depending e.g. on the purity, the conditions during crystal growth, temperature, and pressure. Hexagonal cell parameters are: $b_1 = b_2 = 5.58$ Å, $b_3 = 17.060$ Å, $\alpha = \beta = 90°$, and $\gamma = 120°$ [33] (Figure 1.1).

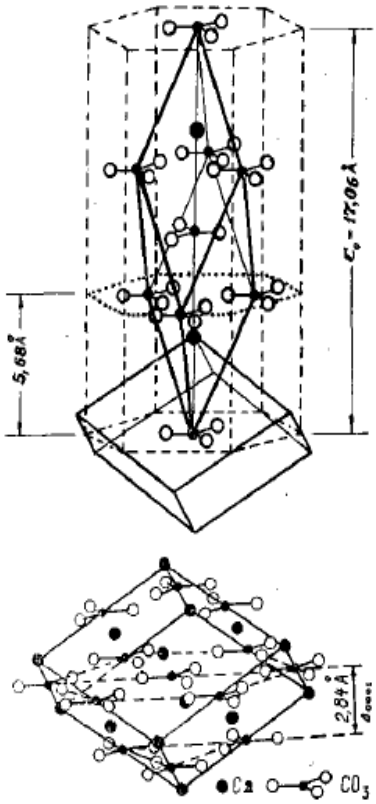

Figure 1.1: Structure of calcite [34].

Calcite structure can be described using the hexagonal representation, with Miller or Bravais-Miller indices. The Miller indices, is a group of three numbers that indicates the orientation of a plane or set of parallel planes of atoms in a crystal. The orientation of a surface or a crystal plane may be defined by considering how the plane (or the parallel plane) intersects the main crystallographic axes of solid. The application of a set of rules leads to the assignement of Miller indices, (h, k, l); a set of number which quantify the intercepts and thus may be used to uniquely identify the plane or surface. If four axes are defined in the crystal, and not three as presented before, this leads to four Bravais-Miller indices which can be written (h, k, i, l).In this work, in order to be internally consistent, notations using three Miller indices were used.

The primitive rhombohedral unit cell of calcite contains ten atoms (two $CaCO_3$ formula units) and consists of alternating (111) planes of Ca atoms and carbonate groups. Ca atoms are situated at 0 and 1/2 along [111], and carbonate groups are located at 1/4 and 3/4 along this vector [35]. In calcite, carbonate groups are characterized by weak ionic bonds with calcium cations (Figure 1.1).

The most common cleavage face for calcite is (104). This surface is the most stable and is often identified on crystal growth, calcite cleavage and dissolution. So, rhombohedral crystals are therefore also the most dominant morphology of calcite observed in the natural environment. During growth, calcite contains some shallow pyramids named growth hillock as was observed by DIC (differential interface contrast) microscopy in Paquette and Reeder [36] study. Surfaces are composed most of (001), (110), (012), and (104) faces, but the (104) face is by far the most abundant and the most stable. This face is corresponding to $[\bar{4}41]$ and $[48\bar{1}]$ directions. The abundance of faces can be explained by PBC theory - Periodic Bond Chain Theory. The crystal morphology can be derived from the crystal structure, according to Hartman and Perdok theory. According to this theory, the $[\bar{4}41]$ is considered to be the most stable. This explains the high stability of the calcite crystal face and its reason for the high abundance on this face on crystal grown from solution.

Ruiz-Agudo [37] observed the atomic steps on the crystal surfaces reflect its rhombohedral symmetry, with two steps intersecting the (104) cleavage face at an acute angle ($[\bar{4}41]$ and $[48\bar{1}]$) and two steps intersecting at an obtuse angle ($[441]_+$ and $[481]_+$). Increasing the pH to 12 led to the nucleation of 2D islands with rounded $[441]_+/[481]_+$ corners. Paquette and Reeder [36] identified three nonequivalent PBCs in the calcite structure along the $[\bar{4}41]$, the $[2\bar{2}1]$ and the $[101]$ direction.

The lowest energy on the surface of calcite surface is on the face (104), which also characterizes the rhombohedral morphology of calcite [38, 39]. Ca^{2+} and CO_3^{2-} form a rectangular lattice on this plane. The ratio Ca^{2+}/CO_3^{2-} and the geometry of CO_3^{2-} depend of the orientation of the crystal face. In the case of (104) face, these ions are present in a ratio 1:1. The surface density of the (104) face is 4.95 atoms. nm^{-2} (8.226 µmol surface sites. m^{-2}) [40].

1.1.3. Surface reactivity of calcite

1.1.3.1. pH and surface charge of calcite

The pH of saturated calcite suspensions has been often investigated, because it is strongly dependent on calcite dissolution, calcite surface speciation, Ca^{2+} concentration and solid surface charge (pH_{zpc}). The charged surface of a mineral affects adsorption. A positively charged surface will attract anions and reject cations. A charge of a mineral, including calcite is directly linked to

pH. The pzc (point of zero charge) is defined as the pH value where the net total particle charge is equal to zero [41]. Values of pzc for calcite were found between 8 and 9.5 [42].

If it is assumed that Ca^{2+} or CO_3^{2-} has the same affinity for the calcite surface, the pzc is the point where the concentrations of Ca^{2+} or CO_3^{2-} are equal. It is important to understand the effect of physical parameters (e.g. temperature) and of the chemical parameters (e.g. pH, pCO_2, ionic strength and investigated element concentration or additional organic ligands) on the investigated system [43]. When these parameters vary the sorption can be strongly influenced (reduced or promoted metal sorption) [44]. This is the reason why several early studies are based on classical "batch" experiments where the influences of different parameters like pH, pCO_2, metal concentration, ionic strength, background electrolyte and time are varied [14].

The surface reactivity of calcite has been described by thermodynamic approaches such as surface complexation modeling (SCM). Based on the model developed by Stumm [45] where the integration of surface speciation into kinetic models of oxides and silicates was made, Van Cappellen and co-workers proposed a SCM model which is presently the main reference in SCM modeling of calcite [23]. Principles of SCM modeling will not be described in details in this bibliographic review since the Ph.D. study has been focused on the first steps before carrying out modeling, which are the identification of mechanisms that should be later considered when modeling the data: structural studies on the surface chemistry are thus presented in detail in the next section.

1.1.3.2. Structural studies of the calcite/water interface

Surface spectroscopic techniques such as XPS (X-ray photoelectron spectroscopy), LEED (low energy electron diffraction), AFM or XAS (X-ray absorption spectroscopy) give information at atomic level on bonding environment on carbonate/water surface.

Chiarelo and Sturchio [46] and Stipp and Hochella [18] showed, respectively by X-ray reflectivity and XPS, that the spacing and the long range ordering of the near-surface lattice are from a statistic point of view identical to those in the bulk of calcite [47]. Their studies reveal that structural distortion of the mineral lattice due to hydration does not penetrate deeper than 1-2 atomic layers. Using atomic force microscopy (AFM), several studies on calcite showed that dissolution and growth occur at high energy level defect sites, on the borders of solid under near-equilibrium

conditions (Dove and Hochella [48]; Teng et al. [49]). The saturation index (S.I) can be defined as logarithm between the IAP (ionic activity product) and solubility product (K_{sp}):

$$S.I. = \log \frac{IAP}{K_{sp}} \qquad \text{(Eq.1.1)}$$

Three cases can be distinguished:

- IAP<Ksp then S.I. < 0 means that the mineral dissolves.
- IAP>Ksp then the S.I. > 0, means that the mineral precipitates.
- IAP=Ksp, then S.I. = 0 means that the mineral is in equilibrium with the solution.

It should be noted that there is dissolution/precipitation even when the system is closed to equilibrium, which highly impacts the surface reactivity of calcite.

At S.I. = 0.2 Dove and Hochella [48] found spiral growth and growth at available molecular steps as the dominant growth mechanisms. At S.I. = 0.4, spiral growth and surface nucleation exist together.

According to Heberling et al. [50], studies by surface diffraction documented that the structure of the calcite (104) face corresponds to a large degree to the termination along this crystallographic direction expected from the bulk crystal structure. Two layers of adsorbed surface hydration water at 2.3 and 3.4 Å above the surface have been identified.
Stipp and Hochella [18], using XPS and LEED, identified two distinct hydrated species using ultra-high vacuum, namely $>CaOH^0$ and $>CO_3H^0$ after exposing calcite to water. LEED is a technique which permits to identify pattern on atomic level (Å order) in a solid. XPS permits the identification of compounds on near surface and their binding in solid.

Fenter et al. [51] studied calcite-water interface at various pH 6.8, 8.3 and 12.1 under atmospheric conditions by means of X-ray reflectancy. At pH 8.3, the best fit of the reflectancy model is presented at 1.0±0.4 monolayer of hydroxyl species. They report on a full monolayer of water or hydroxyl at 2.50±0.12 Å above the surface. They modeled their data without including calcium carbonate inner-sphere complexes. Surface diffraction is generally very sensitive to inner–sphere

adsorption. A surface diffraction study analyzing the 3D structure of the calcite–water interface at pH 8.3 in equilibrium with air was performed by Geissbühler et al. [52]. Their results show that there are two well-ordered water layers with the first 2.30 ± 0.1 Å above the surface and the second one 3.45±0.2 Å above the surface. The ions in the first two monolayers of the surface slightly relax from their bulk positions. The surface carbonate ions are tilted towards the surface by 11.3°. The distance between the surface calcium and the closest water molecule is 2.97 ± 0.12 Å.

In the case of carbonates, dissociation of water molecules adsorbed on the surface form two distinct types of hydration sites. In the case of our material of interest, calcite, hydration of calcite show two different surface sites that are formed $>CaOH^0$ and $>CO_3H^0$ having 1:1 stoichiometry on the surface. The presence of these two surface sites was highlighted using spectroscopic techniques by Pokrovky and Schott [53] used performed an IR study (DRIFT- diffuse reflectance infrared Fourier transform) of the surface of calcite. They identified two bands at 3400 cm^{-1} and 1420 cm^{-1} as surface hydroxyl groups and carbonate groups. For the solutions that have a low pH, they noticed an increase of the hydroxyl band and explain it by an increase of hydrated calcium- surface complexes.

Changes in calcite structure are expected, due to the dynamics of system and re-crystallisation processes coinciding with the adsorption of radionuclides [19]. Surface re-crystallization may cause partial incorporation of radionuclides into the calcite structure.

With a better understanding of calcite surface and its behavior in solution, a bibliographic review of aqueous behavior and interaction of Eu(III) and Ni(II) with calcite is presented below.

1.2. Lanthanide: europium

1.2.1. Aqueous chemistry of europium

In natural environment, europium is generally present in +III oxidation state. Under reducing conditions, it can be also found under +II oxidation state. The most common and stable europium isotopes are ^{151}Eu and ^{153}Eu, the more abundant being ^{153}Eu. The most common radioactive isotope is ^{152}Eu, which is a β-emitter. Other Eu(III) isotopes found in radioactive waste is ^{155}Eu which is a fission product, but also in a small quantity produced by neutron capture on ^{153}Eu. Another radioactive Eu isotope is ^{154}Eu which is produced by neutron activation of ^{153}Eu.

Eu(III) is an important metal because of its similar behavior to Cm(III), Am(III), Pu(III) and Bk(III), which mobility in groundwater systems has to be assessed since they are among the radioactive species (^{242}Cm, ^{243}Cm, ^{244}Cm and ^{241} Am) present in radioactive waste. Its fluorescent properties enable the use of TRLFS as an interesting tool to investigate aqueous speciation and sorption mechanisms at the molecular level.

A multitude of chemical species exists in the system Eu−NaCl−CO_2−calcite. Over time, the aqueous speciation as well as the solubility of the solid phases has been investigated. Thermodynamic data are available for speciation and solubility calculations at standard conditions for europium solutions and solid phases and have been selected in several projects, among which the Thermochimie database, which provided consistency to the numerous and sometimes ambiguous data in the literature. At pH smaller than 7, europium hydrolyzes slightly while at basic pH Eu(III) can form strong hydroxide precipitates. Aqueous carbonate ions are well known to be very strong inorganic ligands complexing actinides/lanthanides [54, 55]. Trivalent solid carbonates have been determined to be the most important solubility - controlling phases for trivalent elements under natural environment conditions [56]. Speciation diagrams for the conditions of our experimental studies will be given in Chapter 3. Spectroscopic studies on the aqueous Eu(III) complexes and Eu(III) containing solid phases are presented in this section, with an emphasis on spectrofluorimetry results, since this technique is the one used during this Ph.D. work.

Runde et al. [56] focused their research on synthesis and spectroscopic characterization of isolated solid phases of Eu(III) and Am(III). Structural information on crystalline and amorphous compounds was obtained by spectroscopic techniques like FTIR, XRD and XAS. Finally, they used TRLFS to get a deeper understanding of the obtained compounds. By DTA/TGA (Differential Thermal Analysis/Thermal Gravimetric Analysis), they showed that the mixed hydroxy-carbonate $EuOHCO_{3(s)}$ does not contain water molecules [56, 57]. The absence of water molecules for $EuOHCO_{3(s)}$ was evidenced by the presence of a very narrow IR band at 3479 cm^{-1} confirming the presence of a hydroxo group. For $Eu_2(CO_3)_3$:2-3 $H_2O_{(s)}$, it was very difficult to establish exactly the correct number of water molecules, contrary to $NaEu(CO_3)_2$:$5H_2O_{(s)}$ where the number of water molecules was determined to be 5 by DTA/TGA. By FT-IR, the presence of water was confirmed. TRLFS allowed to distinguish between Eu(III) hydroxides and carbonates which cause a different splitting into discrete crystal field levels; this technique also allowed to distinguish between Eu(III)

solid carbonates. They used the fluorescence lifetimes to estimate the number of water molecules surrounding Eu for two species: $Eu_2(CO_3)_3{:}2\text{-}3H_2O_{(s)}$, τ = 234 ± 10 μs (nH_2O = 2.8 ± 0.5) and $NaEu(CO_3)_2{:}5H_2O_{(s)}$, τ = 208 ± 8 μs (nH_2O = 4.5 ± 0.5). The correlation between inner-sphere water molecules and lifetimes were done by applying an equation developed by Horrocks [58, 59] and Chopin [60] :

$$n_{H_2O} = \frac{x}{\tau_{H_2O}} - y \qquad \text{(Eq.1.2)}$$

For Eu(III) the constants values are determined by Chopin [60] and are x=1.05 and y=0.70. The obtained results for water molecules confirms their DTA/TGA data [60]. XAS and TRLFS were successfully used to determine the coordination environment of Eu(III) carbonates in solution, as well as solids.

Later, Plancque [61] and his collaborators investigated Eu(III) complexes formed with hydroxide, carbonate and humic substances by TRLFS. They varied ligand concentration and pH using a fixed Eu(III) concentration in order to obtain the aqueous speciation of Eu(III) carbonates $Eu(CO_3)^+$, $Eu(CO_3)_2^-$ and $Eu(CO_3)_3^{3-}$. The first species that they identified is the free europium ion at pH = 2 under atmospheric conditions obtaining a lifetime of 110 ± 10 μs. This value has been obtained until pH = 6, for a total concentration of Eu(III) of ~ 6.6×10^{-6} $mol.L^{-1}$. In Table 1.2, Table 1.3 and Table 1.4 the calculated lifetimes for the europium carbonate aqueous and solid species are summarized.

Table 1.2: Eu(III) literature lifetimes for aqueous Eu(III) hydroxo species.

Species	Wavelength (nm)			F_1/F_2 ratio	Lifetime (µs)	nH_2O	Temperature (K)	References
	Transitions							
	$^5D_0 \rightarrow {}^7F_0$	$^5D_0 \rightarrow {}^7F_1$	$^5D_0 \rightarrow {}^7F_2$					
$Eu^{3+}_{(aq)}$	580	593	618	8/1	110 ± 5	9	298	Stumpf et al. [62]
					110 ± 10		298	Moulin et al. [63]
					110 ± 10		293	Plancque et al. [61]
		591.7	616.4	1/0.5	110	8.9	297	Heller et al. [64]
$EuOH^{2+}_{(aq)}$	580	593	615	1/1	50 ± 5	-	293	Plancque et al. [61]
$Eu(OH)_2^{+}{}_{(aq)}$	580	593	615	1/1	40 ± 5	-	293	Plancque et al. [61]
$Eu(OH)_{3\,(aq)}$	580	593	615	1/1	40 ± 5	-	293	Plancque et al. [61]
$Eu(OH)_4^{-}{}_{(aq)}$	580	593	616	1/1	30 ± 5	-	293	Plancque et al. [61]

Table 1.3: Eu(III) literature lifetimes for aqueous Eu(III) carbonate species.

Species	Wavelength (nm)			F_1/F_2 ratio	Lifetime (μs)	nH_2O	Temperature (K)	References
	Transitions							
	$^5D_0 \rightarrow {}^7F_0$	$^5D_0 \rightarrow {}^7F_1$	$^5D_0 \rightarrow {}^7F_2$					
$EuCO_3^{+}{}_{(aq)}$	580	591	616	1/2	180 ± 10	5.3	293	Plancque et al. [61]
	579	592	617		170	5.7	298	Kim et al. [68]
$Eu(CO_3)_2^{-}{}_{(aq)}$	580	592	616	1/3	290	3.1	293	Plancque et al. [61]
	580	592	617		230	4.0	298	Kim et al. [65]
$Eu(CO_3)_3^{3-}{}_{(aq)}$	580	594	617	1/4	440	1.8	293	Plancque et al. [61]
		592	615		385	2.2	298	Kim et al. [65]
	580	593	614/618	1/6	400	2.1	293	Moulin et al. [63]

Table 1.4: Eu(III) literature lifetimes for Eu(III) hydroxide, hydroxo-carbonate and carbonate solid phases.

Species	Wavelength (nm)			Lifetime (µs)	Temperature (K)	References
	Transitions					
	$^5D_0 \rightarrow {}^7F_0$	$^5D_0 \rightarrow {}^7F_1$	$^5D_0 \rightarrow {}^7F_2$			
$Eu(OH)_{3(s)}$	577.50	591.40 594.88	616.26	21.6 ± 3.3	298.15	Runde et al. [56]
$Eu(OH)_{3(s)}$	579.71	592.42	616.90	220		Pointeau [66]
$EuOHCO_{3(s)}$	577.47	586.17 587.92 600.10	610.13 617.09 621.23	109.8 ± 7.7	298.15	Runde et al. [56]
$Eu_2(CO_3)_3$:2-3$H_2O_{(s)}$	579.24	591.4 593.61 606.21	613.16 615.12 617.51	233.6 ± 9.8	298.15	Runde et al. [56]
$Eu_2(CO_3)_3$:3$H_2O_{(s)}$	/	/	/	270 ± 27	298.15	Vu-Do [67]
$NaEu(CO_3)_2$:5$H_2O_{(s)}$	578.80	588.17 592.52 594.46	613.65 616.71 619.08	207.7 ± 8.2	298.15	Runde et al. [56]

1.2.2. Eu(III) sorption onto calcite

Adsorption should be the first step leading to incorporation and is very important to be studied and understood. If a contaminant is incorporated rather than simply adsorbed on the surface, then desorption process is less probable to take place. So, the contaminant is considered to be immobilized until the physico-chemical conditions of the host rock do not change.

Calcite should be a material that satisfy these conditions in the case of Eu(III) as presented by Parekh et al. [68] and Palmer [69]. The simple structure of calcite and its high reactivity makes relevant the study of its interaction with trivalent elements, which could replace Ca^{2+} in the calcite lattice by heterovalent substitution [4].

Zhong and Mucci [70] studied the co-precipitation of calcite with Rare Earth Elements (REE) from prepared seawater. Their experiments were performed under steady-state conditions using the constant addition method. Their method is very convenient because it allows the synthesis of solids with constant composition by controlling the precipitation rate. They also performed batch-type sorption experiments under atmospheric conditions, where a cocktail of 12 REE were introduced having a concentration of ~ 6.5×10^{-7} mol.L^{-1} and the measured K_d for Eu(III) was 1500 mL.g^{-1}. Also, an important influence was noticed for Na on the partition coefficient, which depends on REE concentration, and they suggested that Na^{+} might offset the excess charge created by substitution of REE in Ca^{2+} sites. From their study, the selective adsorption of soft REE is noticed rather than the adsorption of the heavy ones.

Eu(III) sorption onto calcite was investigated by Piriou et al. [6] and Yeghicheyan [7], both with kinetic and batch experiments at room temperature and 50°C and pH= 8.3. For kinetic experiments they used a constant initial concentration and the sorbed concentration was measured as a function of time, and for sorption isotherms, the initial concentration of Eu(III) was varied and the contact time was fixed at 5 hours. For fluorescence measurements a selection of samples was done with an Eu(III) concentration varying from 2 up to 7.6×10^{-5} mol.m^{-2}. For kinetic experiments the delay to reach a plateau was 4 hours and the steady state was reached after 24 hours for concentrations of 10^{-7} - 10^{-5} mol.L^{-1}. For the sorption isotherms the concentrations were determined at 50°C as a function of the concentration remaining in the supernatant. A log/log variation was observed and finally a plateau was reached at 7.6×10^{-5} mol.m^{-2}, which excludes the formation of a precipitate.

From fluorescence measurements they deduced that Eu(III) sorbed on calcite is incorporated in a hydrated/hydroxylated layer with two different families of sites and a minor fraction of Eu(III) substitutes Ca^{2+} in calcite.

Stipp et al. [10] reported some results obtained combining the co-precipitation method and surface-sensitive techniques to investigate affinity of calcite for Eu^{3+} from oxidized solutions. The goal was to study the partitioning of dissolved Eu^{3+} between solution and calcite for a fixed concentration, by precipitating from a slightly supersaturated solution (with respect to calcite) to determine the amount of europium that can be trapped into calcite. The co-precipitation process can be distinguished by two approaches: the solid solution models and distribution models based on the phenomenological partition coefficients. In parallel they performed some experiments onto single crystals of calcite exposed to 10^{-2} mol.L^{-1} $Eu(NO_3)_3$ solution during 1 minute, which were analyzed by AFM. From these results it turned out that the crystal has no measurable effect on the pH, its value remaining constant in the range of 3-4. Concomitant samples of freshly cleaved calcite and a sample of calcite exposed to deionized water for 1 minute were analyzed by AFM. The calcite exposed to air has some flat and smooth terraces, but for the sample exposed to deionized water (pH = ~5.6, atmospheric conditions) a rhombohedral shape on the surface was noticed. AFM and XPS observations showed the high affinity of Eu for calcite, and that Eu is adsorbed to surface and does not precipitate.

Later, Lakshtanov and Stipp [71] investigated the partitioning of Eu(III) sorbed on calcite. They collected data on partition coefficients in order to better understand the incorporation mechanisms. For their work they used the coprecipitation method (constant addition method - also used by Tresoriero and Pankow [72]) and showed that Eu(III) was strongly retained from the solution by calcite. A similar behavior was noticed also for sorption of Cm(III) onto calcite [30]. Also, Curti [32] investigated the partition of some radionuclides in calcite, with the purpose to provide a consistent set of data for modeling. From the data reviewed, empirical correlations were derived that relate experimentally determined partition coefficients (λ_{Me}) to measurable chemical properties of the co-precipitated metals (ionic radii of the incorporated trace metals, solubility products of the pure metal carbonates).

Sorption of An and Ln (Eu(III), Sm(III), Np(V), Pu(V) and Pu(IV)) onto calcite was investigated by Zavarin et al. [73] as a function of pH and alkalinity. Based on Pokrovsky and Schott [53] surface

speciation model, they built up a surface complexation model for Sm(III), Eu(III), Np(V), and Pu(IV). For Eu(III) sorption was studied under atmospheric conditions ($pCO_2=10^{-3.5}$ atm) and under higher $pCO_2 =10^{-2}$ atm. They fitted the data using 1-2 surface species and could account for the effect of pH and CO_2 fugacity on sorption. For lower pH values, which are imposed in closed system by pCO_2, the sorption decreased. The experiments were done for two contact times: 1 day and 30 days and K_d values were determined. For 24 hours K_d vary from 1300-8800 $mL.g^{-1}$ and for 30 days sorption K_d values are situated between 3600-51000 $mL.g^{-1}$ and were attributed to slow incorporation.

Studies based on spectroscopic investigation and surface techniques are needed to provide depth information about the chemical environment. The optical properties of 4f elements, Eu^{3+} being a part of them, can be used to obtain information about their chemical environment, identification of main crystallographic sites, hydration state and their symmetry. Time resolved laser fluorescence spectroscopy has been used to determine speciation of Eu(III) onto calcium carbonate.

The interaction of Eu(III) with calcite was investigated by the co-precipitation method by Marques Fernandes et al. [4] with the aim of studying the possible incorporation of Eu(III) in the lattice structure and charge mechanisms compensation. The Eu(III)-doped calcite samples were synthesized in the presence of Na^+ and K^+. In the presence of Na^+, the results are in agreement with a partial incorporation of Eu(III) in the calcite lattice as a coupled substitution proceeds in the co-precipitate $An/LnNa(CO_3)_2–CaCO_3$, namely $2Ca^{2+} \leftrightarrow Na^+ + An^{3+}/Ln^{3+}$. TRLFS investigation showed that interaction of Eu^{3+} with calcite allowed the discrimination of three discrete Eu(III) sites and the characterization of their symmetry and degree of hydration. Also, the interaction of Eu(III) with a polymorph phase of calcite, aragonite and gypsum, was investigated by the same spectroscopic tool [74]. The purpose of the work was to investigate the interaction between trivalent actinides/lanthanides (Cm^{3+} and Eu^{3+}) under Ca-bearing mineral phases at the molecular level. Doped samples were prepared in MFR (mixed flow reactor), and then investigated by TRLFS and the results were in agreement with an incorporation of Eu^{3+}/Cm^{3+} in aragonite and inner-sphere surface complex formation in the case of gypsum.

Interaction of Eu(III) with calcite and the influence of anions were studied by Hofmann et al. [9] Coprecipitation experiments and batch experiments were performed in order to study the influence of background electrolyte ($NaNO_3$) on the formation of solid solutions in the calcite/Eu(III) system.

Batch experiments were done on 100 mg natural calcite, using 0.01 mol.L^{-1} $NaClO_4$ and 10^{-6} mol.L^{-1} $Eu(ClO_4)_3$ and kinetic experiments were performed (1 day, 2 weeks and 1 month). The second set of experiments was performed using the conditions mentioned before and in addition 3×10^{-6} mol.L^{-1} $NaNO_3$ was added. The reaction times were 1 and 2 months. The third set of experiments are on synthesized Eu(III) (10^{-5} mol.L^{-1}) doped $NaNO_3$ single crystals. From the sorption isotherm, the impact of nitrates onto sorption of Eu(III) on calcite was revealed. A difference of Eu(III) sorbed onto calcite being one order of magnitude higher than in the absence of nitrates. AFM showed serious damages created by nitrates (even at low concentrations such as 10^{-7} mol.L^{-1}) on calcite and the formation of an extra layer. Spectroscopic tools (TRLFS) were used as well to characterize this system and they highlighted the incorporation of Eu(III) in the new layer formed while Eu(III) was losing its hydration sphere.

A short bibliographic review of TRLFS data on Eu(III) sorbed on a selection of solids is presented in Table 1.5 and Table 1.6.

Table 1.5: Literature lifetimes of Eu(III) species in interaction with $CaCO_3$ solids.

System	Lifetime / µs	TRLFS temperature measurements (K)	Literature
Eu/calcite	A: 9000 B: 550 - 850 C: 450	15	Piriou et al. [6]
Eu/calcite (recrystallization experiments – 1 day)	160 ±20 440±50 1060±220	<20	Hofmann et al. [9]
Eu/calcite (recrystallization experiments – 12 days)	680 ±50	<20	Hofmann et al. [9]
Eu/calcite (recrystallization experiments – 14 days)	110 ±10 460±50	<20	Hofmann et al
Eu/calcite (recrystallization experiments – 30 days)	200 ±20 740 ±90	<20	Hofmann et al. [9]
Eu/calcite/$NaNO_3$ (recrystallization experiments – 12 days)	660 ±50	<20	Hofmann et al. [9]
Eu/calcite/$NaNO_3$ (recrystallization experiments – 30 days)	580 ±50	<20	Hofmann et al. [9]
Eu/calcite/$NaNO_3$ (recrystallization experiments – 50 days)	540 ±60	<20	Hofmann et al. [9]
Eu/calcite (on MFR experiments – 14 days)	450 ±70 3500±450 3700±200	<20	Hofmann et al. [9]
Eu/calcite/$NaNO_3$ (on MFR experiments – 14 days)	670 ±50	<20	Hofmann et al. [9]
Eu/calcite (on MFR experiments)	A : 800-1080 C : 3570-3760	<20 and 300	Fernandes et al. [4]
Eu/ aragonite	1636 (0.0 ± 0.5 H_2O)	<20	Schmidt et al. [74]

Table 1.6: Literature lifetimes of Eu(III) species in interaction with different solids.

System	Lifetime / µs	Temperature (K)	Literature
Eu/ hydrotalcite	305	10	Stumpf et al. [62]
Eu/ montmorillonite	250 (for aluminol sites) 135 (for silanol sites)	298	Kowal – Fouchard et al. [75]
Eu/gypsum	199 (4.8 ± 0.5 H_2O)	<20	Schmidt et al. [74]
Eu/alumina	350 ±15 µs (aluminol sites) 350 (210 – for other sites)	298	Ghaleb et al. [76]
Eu/$SrCO_3$	1600	16	Holliday et al. [77]
Eu/$SrSO_4$	3100	16	Holliday et al. [77]

Ion beam techniques are often used in geochemistry to study diffusion processes as presented in earlier studies (Cherniak [78], Cherniak [79], Alonso et al. [17]).

Chemical diffusion of divalent elements (Pb(II) and Sr(II)) into calcite was investigated by Cherniak [78] under anhydrous conditions by solid state diffusion. Experiments with Pb(II) were performed in silica glass tubes and sealed under vacuum and in the same time, a small amount of calcite powder was added to ensure calcite stability. For Sr experiments, the starting materials are $SrCO_3$ and calcite, which were placed in Pt tubes, then in silica glass tubes and annealed at 1 atm in furnaces for different time contacts (15 h – 3 months). Temperatures for Sr were ranged from 440 – 800°C, but for Pb some problems were encountered above 440-650°C (the tubes exploded). After the reaction time, the samples were cooled in air. The depth profiles were determined using RBS. These elements diffuse very quickly in calcite. Isotopic and chemical signatures showed that diffusion is the main process affecting alteration. Several studies showed that Eu(III), Cm(III) and Am(III) can be incorporated into the calcite lattice during crystal growth

1.3. Transition metal: nickel

1.3.1. Aqueous chemistry of nickel

Nickel is a toxic divalent heavy metal both for stable isotopes as well as in its radioactive form. Radioactive contamination may result from long-term degradation of radioactive waste repositories. ^{59}Ni and ^{63}Ni are produced by neutron activation of ^{58}Ni and ^{62}Ni (both naturally occurring and stable isotopes of nickel) in the structural steels and internal components of nuclear reactor vessels. ^{63}Ni represents a special case with an intermediate radioactive half-lifetime of 100 years and is present in many waste packages having a relatively high activity level [2]. The mean concentration of natural nickel in several COx clays samples is 30 ppm. Ni is released from natural and anthropogenic sources, and it is often found in industrial waters and mining areas.

Nickel is a transition metal with the electronic configuration [Ar]$3d^8 4s^2$ and can exist with the formal oxidation states in the range -I - +IV. In aqueous chemistry Ni(II) can be found in +II oxidation state [80]. It can form complexes with organic and inorganic ligands as well. The absence of any other oxidation state of comparable stability to the +II state implies that compounds of Ni(II) are largely immune to typical redox reactions.

Over the pH range of most natural waste waters and in alkaline medium the complexes $NiHCO_3^-$, $NiCO_{3(aq)}$ and the solids $NiCO_3$ and $Ni(OH)_2$ may be formed. The stability constant of $Ni(CO_3)_{(aq)}$ has a very large discrepancy as mentioned by Gamsjäger et al. [81] ($2.56 \leq \log K \leq 6.87$).

Under atmospheric conditions, temperature of 25°C and ionic strength of 1 $mol.kg^{-1}$ the species $NiCO_{3(aq)}$ is formed for pH>8.5, and starting from pH>9 is the only species that predominates [81].

Divalent metal carbonates can be found in nature as anhydrous form, but it is not the case for Ni(II) as $NiCO_3$ [82]. In hyperalkaline conditions, both solid species $Ni(OH)_{2(s)}$ and $NiCO_{3(s)}$ can be formed. According to Guillard and Lewis [83], $NiCO_{3(s)}$ can be formed only in competition with $Ni(OH)_{2(s)}$. $Ni(OH)_2$ as solid has other possible variesties such as β-$Ni(OH)_2$, α-$Ni(OH)_2$ and α*-$Ni(OH)_2$. The last two ones differ from the β-$Ni(OH)_2$ which is the most stable from thermodynamically point of view [81].

Chloride as a complexing ligand showed a great importance in sorption experiments. Previous studies on Ni(II) interaction with calcite such as Zachara et. al. [11], Hoffman and Stipp [12]. Lakshtanov and Stipp [84], Belova et al. [85] performed experiments using $NaClO_4$.

Solubility measurements as a function of pH and temperature have been performed by Palmer et al. [86] using flow techniques and potentiometric methods. For solubility measurements hydrogen−electrode concentration cell was designed. A more detailed description is given elsewhere [87]. From their study, one can notice that, $NiO_{(cr)}$ is metastable for several days at 0°C, time which is required for hydrogen−electrode concentration cell equilibration. β-$Ni(OH)_{2(cr)}$ can persist up to 200°C for almost 1 day in hydrogen−electrode concentrationcell. In aqueous solutions,$NiOH^+$ is almost the only hydrolysis product, which stability constant is known. Plyasunova et al. [88] showed some stability constants for Ni(II) hydrolysis products at 25°C. Also, Plyasunova et al. [88] obtained values for two crystalline compounds. $Ni(OH)_{2(cr)}$ by dehydration at temperature, forms $NiO_{(cr)}$. The stability constants are:

$$Ni(OH)_{2(cr)} = Ni^{2+}_{(aq)} + 2\ OH^-_{(aq)} \qquad \log K\ (298.15\ K) = -17.48 \pm 0.54 \qquad \text{(Eq.1.3)}$$

The solubility product for $Ni(OH)_{2(cr)}$ reported by Mattigod et al. [89] is different from that of Plyasunova et al. [88] the expressed value being −16.1.

From the speciation calculations of Lamana [14], in the conditions imposed in their study (ambient temperature of 25 ± 2ºC, and atmospheric $pCO_2 = 10^{-3.41}$ atm) in calcite-saturated 0.1 $mol.L^{-1}$ and 0.7 $mol.L^{-1}$ NaCl solutions over a range of pH (7.5 to 8.9) and total Ni concentrations- $[Ni]_{total}$- (10^{-4} $mol.L^{-1}$) no precipitation was expected. For 0.1 $mol.L^{-1}$ below pH 7.7 Ni^{2+} is the dominant species, between pH 7.7.-8.7 $NiCO_{3(aq)}^{0}$ and $Ni(CO_3)_2^{2-}$ is the most important specie above 8.7. For 0.7 $mol.L^{-1}$ there is a decrease in the relative abundance of the $NiCO_{3(aq)}^{0}$ complex at pH 8.3) as well as Ni^{2+} at pH 7.3), coupled with increase in total chloride species, in particular $NiCl_{2(aq)}$. It should be emphasized that strong uncertainties are associated to the stability constants of these two species.

Nickel halides are soluble salts, so in aquatic chemistry they are almost negligible and they are not found in environment. In environmental chemistry, carbonates are often found and the most common mineral found and used is $NiCO_{3(cr)}$, which will be found in our calculations too.

1.3.2. Ni(II) sorption onto calcite

Divalent metals are known to interact very well with calcite. The adsorption of divalent metals on calcite is considered to be strongly pH-dependent [11, 84, 90-92]. In these studies, classical batch-type experiments were done, and the influence of parameters such as pH, pCO_2, metal concentration, background electrolyte, ionic strength and duration of experiments are examined [93].

Zachara et al. [11] investigated the sorption of divalent metals (Cd, Zn, Mn, Co, Ni, Ba) in calcite pre-equilibrated solutions with a pH ranging from 7 to 9.5 at 25°C under atmospheric conditions and an initial metal concentration of 10^{-7} mol.L^{-1}. The maximum sorption fraction was reached for a pH value that slightly exceeds 9 and was around 60%. The sorption fractions of all the divalent studied metals increased as pH increased. The authors present the sorption of these elements as an ion-exchange reaction, with Ca^{2+} ions present on the calcite surface or complexing with carbonate groups on a hydrated surface. The authors concluded on studied metals that the capacity of sorption on calcite was sufficiently large and calcite could act as an important sorbent for the removal of those metals in calcite-rich environments.

Belova et al. [85] tried to obtain data for safety assessment investigating sorption of Ni(II) onto chalk. The experiments were performed under atmospheric conditions at 25°C in a pH range between 7.6 and 8.8 using an initial metal concentration of 10^{-6} mol.L^{-1} Ni(II). Maximum adsorption in this case was 65% at pH 8.7.

Lamana et al. [14] did another elaborate study of the sorption of Ni(II) onto calcite at 2 different ionic strengths, 10^{-1} mol.L^{-1} and 7×10^{-1} mol.L^{-1} NaCl. Kinetic experiments showed the dual nature of the process, whereby a significant fraction of total Ni(II) was sorbed to the surface within the first few hours (< 24 hours) of metal-mineral contact and sorption increased with increasing pH. The processes are followed by either a plateau or slow progressive sorption with time, interpreted as metal co-precipitation or diffusion into the bulk solid phase.

The most common mechanisms for nickel sorption may be cation exchange or surface complexation, which means that parameters such as pH or ionic strength may have an influence on the process. Monovalent (Na^+, K^+ and Cl^-) ions have an important contribution during re-crystallization of calcite [16], and should therefore have an influence on sorption. Experimental studies of Stipp et al. [15], Belova et al. [85], Rouff et al.[93] on Ni(II) as well as other divalent metal cations (e.g., Pb^{2+}, Cd^{2+}) have obtained similar results. Cherniak [78] used RBS as a tool to investigate Pb^{2+} and Sr^{2+}diffusion into calcite by solid state experiments. Carlsson and Aalto [13] investigated co-precipitation of Ni(II) with calcite, at the pH of saline waters (pH of 8-9) in the near field of Finnish nuclear repositories. Samples were spiked with ^{45}Ca and ^{63}Ni and kinetic experiments were performed (42 days). The aim was to highlight the ion exchange during the re-crystallization process and to see if incorporation occurs. This process was observed by an increase of ^{45}Ca in solution as a function of time. For low concentrations like 10^{-6} mol.L^{-1}, the interaction between Ni(II) and calcite increased as a function of time and precipitation was excluded, while for the strong concentration, 10^{-4} mol.L^{-1}, Ni(II) incorporation seemed to be independent of contact time between nickel and calcite. Liquid scintillation and SEM/EDS measurements proved that Ni(II) in solution can be incorporated forming a nickel-compound like $Ni(OH)_2$ or NiO. According to Hummel and Curti [94] and citations mentioned therein NiO is not stable at more than 290 K and eventually covered by $Ni(OH)_2$ which means that is not very probably to form NiO. Also, Plyasunova et al. [88] showed that $Ni(OH)_{2(s)}$ is thermodynamically more stable than $NiO_{(s)}$.

Ni(II) and Mn(II) interaction (sorption and co-precipitation) with calcite has been studied by Zavarin et Doner [95] and characterized by EXAFS to define possible mechanism at Ni(II)/calcite interface. These two elements were chosen due to the close values of their ionic radii (Ni(II):0.69 Å and Mn(II): 0.80 Å) to Ca(II) (1.00Å), and because $MnCO_3$ has a similar structure to calcite. Ni(II) substitution in calcite is less likely, because the solid needs a greater deformation. The concentration of Ni(II) was quite high, ranging between 5-100 ppm, which means that the samples were supersaturated with respect to solid phases such as $Ni(OH)_2$ or $MnCO_3$. Sorption and co-precipitation experiments were conducted by pH-stat method at 0.03% and 0.25% pCO_2 using 10^{-1} mol.L^{-1} background electrolyte.

For sorption samples, no important changes occurred on spectra, which suggest that in few hours of contact time between nickel and calcite no significant restructuration on calcite occurred. For co-

precipitation experiments, a set of data were analyzed by XAS. The co-precipitation data fits suggests that substitution of Ca^{2+} for Ni^{2+} in calcite results in the distortion of interatomic distances in calcite. So, Ni(II) substitution perturbed the atom lattice positions to at least 5 Å resulting that Ni^{2+} substitutes directly for Ca^{2+} in calcite.

Ni^{2+} interaction with calcite was investigated by AFM, XPS and ToF-SIMS (Time of Flight Secondary Ion Mass Spectrometry) by Stipp and her team [84] with the purpose to determine whether Ni(II) sorption proceeds by a diffusion mechanism or a simple adsorption onto the surface of calcite. AFM is a suitable technique that allows in situ experiments and allows getting information on what happens at the micrometric scale. Natural calcite single-crystals were cleaved and immersed in 10^{-3} and 10^{-2} $mol.L^{-1}$ $Ni(ClO_4)_2$ (solutions were under saturated with respect of the possible solid phase formation - $Ni(OH)_{2(s)}$ and $NiCO_{3(s)}$). They used ClO_4^- as anion, because of its low tendency to form ion-pairs. The pH of samples was kept very low (pH 4.4 - 4.6) to avoid precipitation. ToF-SIMS and XPS results revealed that Ni^{2+} was simply adsorbed, while AFM showed dissolution of calcite.

Based on early co-precipitation studies [70, 72, 96], Curti [32] defines that partition coefficient for those works (repartition of trace metals in calcite) and describes it as:

$$\lambda = \frac{n_{Me}}{n_{Ca}} \cdot \frac{[Ca]_0}{[Me]_0} \qquad \text{(Eq.1.4)}$$

where: n_{Me} and n_{Ca} are the the amounts of trace metals and Ca^{2+} added to the solution during the co-precipitation experiments and $[Ca]_0$ and $[Me]_0$ are the calcium and trace metal concentration which are always equal to initial concentrations.

From the partition coefficients obtained by Curti [32], Ni(II) incorporation will be moderate ($\lambda \sim 0.8$-6), but this partition coefficient is problematic due to the high variety of solubility products of $NiCO_3$ reported at that period.

Taking Curti [32] formula, Stipp and Lakshtanov [84] calculated the partition coefficient (λ) for Ni(II) in calcite between 0.1 and 6, depending of the solubility product of $NiCO_3$. From their

experiments they estimated the partition coefficient to 1 and to be weakly dependent on calcite precipitation rate.

Partition of Ni^{2+} sorbed onto calcite was also investigated by Lakshtanov and Stipp [84] in order to determine distribution and partition coefficients, and to investigate the possible incorporation of Ni(II). Co-precipitation experiments were carried out on calcite powders using the constant addition method under atmospheric conditions and pCO_2=1 atm. The precipitation of calcite was induced as a function of desired precipitation rate, and Ni(II) concentration was varied so that precipitation of Ni(II) in a separate phase was avoided. Ni(II) adsorption experiments were also performed, at 25°C with atmospheric CO_2 partial pressure, in calcite pre-equilibrated solutions. The purpose was to establish the role of adsorption on Ni(II) incorporation during calcite growth. From sorption experiments of Ni(II) onto calcite, a fast adsorption by complexation with surface groups, then a slow uptake corresponding to a co-precipitation/re-crystallization was proposed. These results are supported also by some previous studies such as McBride [97], Lorens [96], Davis [90], Zachara [11] for other divalent metals.

As a conclusion to this bibliographic review, many macroscopic and spectroscopic studies were performed on sorption of different metals onto calcite. But, few of them are focusing on time sequence experiments and variation of concentration, which makes the objective of this study. Understanding and quantifying of non-reversible trapping mechanisms can be assumed to be an important improvement for a geological barrier or a backfill material performance in the safety assessment. Not too many things are known about transfer processes from surface until bulk material. As presented in this bibliographic study, trapping of Eu(III)/Ni(II) can be done by incorporation into lattice or dissolution/precipitation processes.

The first step of the Ph.D. work was to further investigate the solution chemistry of Eu(III)/Ni(II) in carbonate medium in the conditions of our study since the literature data are not complete enough to directly apply them to our study.

The Ph.D. work was then focused on a combination of macroscopic sorption (classical batch experiments) and spectroscopic studies on the Eu−NaCl−CO_2−calcite and Ni−NaCl−CO_2−calcite systems. Among the different spectroscopic techniques relevant for the study of these systems and already cited in this review, TRLFS (exclusively for Eu(III)) and Rutherford Backscattering

Spectrometry (for both) were selected to elucidate mechanisms occurring over time and at various Eu(III) and Ni(II) concentrations. Incorporation which is the key process of this study was carefully investigated by macroscopic and spectroscopic studies.

Chapter 2:
Experimental details

2. Experimental details

This section presents the reagents that were used for preparation of samples, the choice of the adsorbent and a description of all performed experiments (batch and spectroscopic studies). The methods used to determine the Specific Surface Area (SSA) and total organic carbon (TOC) of calcite are introduced in Appendix A. The principle of standard analytical and microscopic techniques such as X-ray Diffraction (XRD), Infrared spectroscopy (IR), Inductively Coupled Plasma Mass Spectrometry (ICP-MS) and Inductively Coupled Plasma Optical Emission Spectrometry (ICP-OES), as well as Scanning Electron Microscopy coupled with energy dispersive X-ray spectroscopy (SEM-EDXS) is also given in Appendix A.

The principle of the advanced spectroscopic techniques applied to characterize the reacted samples, e.g. Time-Resolved Laser induced Fluorescence Spectroscopy (TRLFS) and Rutherford Backscattering Spectrometry (RBS) are detailed in Appendix B and Appendix C, respectively, together with a detailed description of the experimental parameters used to record the data.

2.1. Reagents and solutions

Having the purpose to make experiments using trace concentrations, the reagents used were of high purity (>99 %). In order to avoid possible contamination of the solutions by silicate, polypropylene or polycarbonate flasks were used for all experiments. All laboratory materials used for experiments were cleaned with 10% hydrochloric acid for at least 24 hours, then rinsed several times with Milli-Q water and dried in air. Stock solutions were prepared with high purity reagent grade materials without any further treatment. $EuCl_3.6H_2O$ (Sigma-Aldrich, 99.99 %, trace metal basis) was dissolved in Milli-Q water to obtain europium stock solution having an initial concentration of 5×10^{-3} mol.L^{-1}. As for europium, fresh nickel stock solutions of 5×10^{-3} and 10^{-3} mol.L^{-1} have been prepared starting from a nickel salt, $NiCl_2.6H_2O$ (Sigma-Aldrich, 99.99 %, trace metal basis). The initial concentrations of the stock solutions were checked before starting every experiment by ICP-MS. No acidification of the stock solutions has been done. As background electrolyte, NaCl (Sigma-Aldrich, p.a., ACS reagent, ≥99.5%) with an ionic strength of 10^{-1} mol.L^{-1} was used.

2.2. Choice of the adsorbent - calcite

A thorough characterization of the starting material and a detailed knowledge of its behavior in solution are of high importance. In order to establish a common calcite material and to ensure data consistency between the different used techniques, preliminary studies were carried out on a series of commercial (Merck, Alfa Aesar or Sigma Aldrich) and natural calcite (from Mexico) samples. Industrial calcites were also supplied by OMYA (HYDROCARB 90 and BL200) and SOLVAY (SOCAL U1-R).

The most common characterization tools, such as XRD, IR or ICP-MS (for total digestion) were used to determine the purity and texture of the starting material. In some cases, the Total Organic Carbon (TOC) was also determined to get a better characterization of the samples. The influence of the organic matter can be thoroughly tested, but for this an experimental protocol has to be developed. Identifying the organic additives or impurities requires time and since it was not our aim, it was not part of our experimental plan.

Determination of specific surface area and TOC of different calcite materials

All the first tested calcites (except the OMYA (HYDROCARB 90)) turned out to have a very low specific surface area, which can be a drawback for sorption and subsequent spectroscopic experiments. However, the OMYA (HYDROCARB 90) calcite had high organic matter content (Table 2.1).

Table 2.1: Specific surface area and TOC of commercial and natural calcites.

Sample	SSA ($m^2.g^{-1}$)	TOC ($mg.g^{-1}$)
$CaCO_3$ (Alfa Aesar)	0.20	n.d.*
$CaCO_3$ (Sigma Aldrich)	0.20	n.d.*
$CaCO_3$ (Merck)	0.35	n.d.*
$CaCO_3$ OMYA (HYDROCARB 90)	10.8	2.01 ± 0.05
$CaCO_3$ (Mexico)	0.20	n.d.*

*n.d. = not determined

Two other types of industrial calcite supplied by SOLVAY (SOCAL U1- R) and OMYA (BL 200) were then tested with the purpose to match with the requirements of a good sorbent material: high

specific surface area and high purity. Before use, OMYA BL200 was sieved through a 50 µm sieve in order to remove the largest particles and thus to improve the surface specific area. The specific surface areas and TOC were determined (Table 2.2).

Table 2.2: Specific surface area of commercial and natural calcites.

Sample	SSA ($m^2.g^{-1}$)	TOC ($mg.g^{-1}$)
$CaCO_3$ (SOLVAY(SOCAL U1-R))	18.4	0.29 ± 0.05
$CaCO_3$ (OMYA(BL200))	0.66	0.33 ± 0.05

Both of them exhibited low TOC content, while the SOLVAY calcite had the highest SSA. Our attention was consequently focused on natural grinded calcites SOLVAY (SOCAL U1-R), OMYA (BL 200) and natural single crystals from Alfa Aesar (Reference no: L07W052/Stock no: 44520).

2.3. Characterization of the selected calcite materials

The paragraphs below, present in details the characterization of calcites powders SOLVAY (SOCAL U1-R) and (OMYA (BL 200), as well as calcite single-crystals. Before starting all experiments, it is important to know if other phases or impurities are present in the adsorbent.

2.3.1. XRD characterization of SOLVAY (SOCAL U1-R), OMYA (BL 200) and Alfa Aesar calcites

The XRD patterns are presented in Figure 2.1, and show that SOLVAY (SOCAL U1-R) and OMYA (BL 200) are pure calcite phases, since the observed diffraction lines (012) (22.95, 2θ), (104) (29.35, 2θ), (113) (39.35, 2θ) etc. matched well with the ICDD 01-083-0577 file.

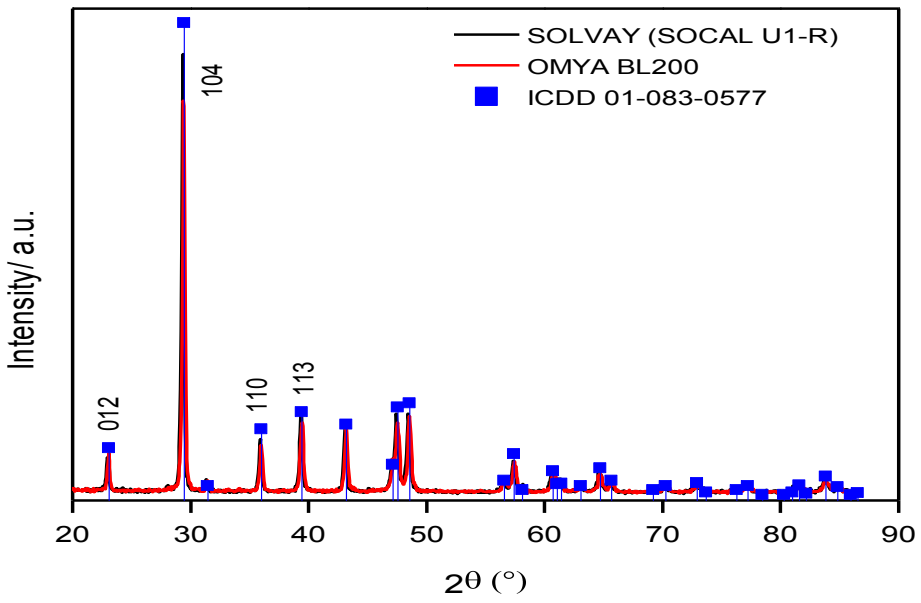

Figure 2.1: XRD pattern for SOLVAY (SOCAL U1-R) (black) and OMYA (BL 200) (red) calcites, with reference pattern of calcite (blue), ICDD card 01-083-0577.

In addition, the presence of other impurities or allotropic form was not observed with this technique. By comparing the XRD patterns to the ICDD card 01-083-0577 (calcite), ICDD card 01-071-2392 (aragonite), ICDD card 01-074-1867 (vaterite), the native single crystal samples can be identified as a pure calcite phase. Based on the obtained X-ray diffractogram, the presence of aragonite and vaterite can be excluded (Figure 2.2).

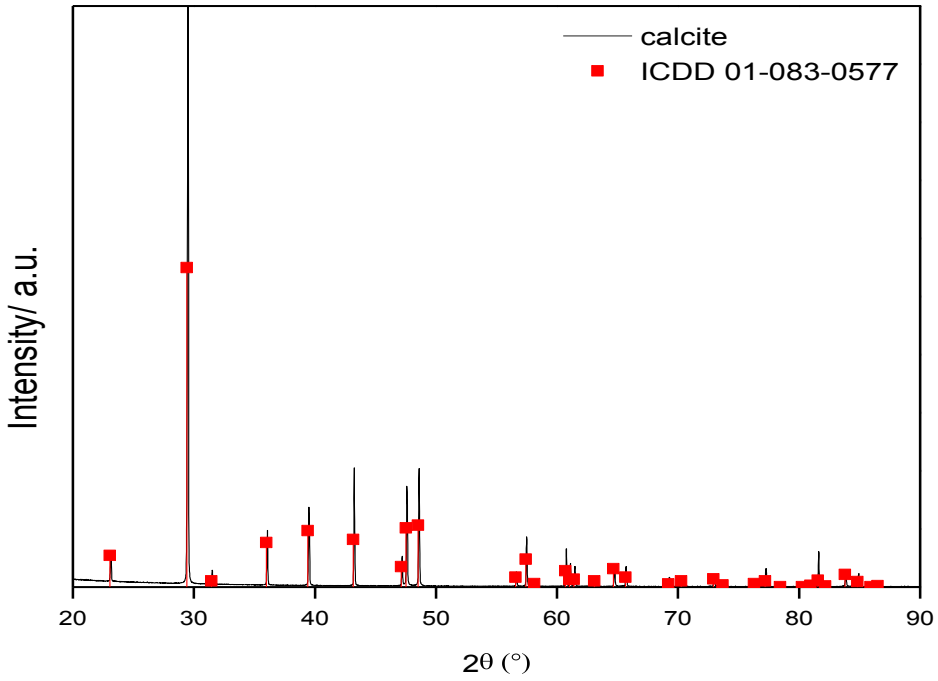

Figure 2.2: Experimental X-ray powder pattern (black) of a crystal, with reference pattern of calcite (red), ICDD card 01-083-0577.

The high relative intensity of the (104) reflection (29.4° 2θ) is to be attributed to preferred orientation. The majority of the crystallites must, hence, be oriented in such a way that the (104)-faces are parallel to the sample holder, a single crystalline Si plate.

In order to explore which facets were exposed to the solution during sorption experiments, several crystals were characterized by single crystal X-ray diffraction. The face indexing of four different calcite crystals investigated on the diffractometer revealed the (104)-faces as limiting ones (Figure 2.3).

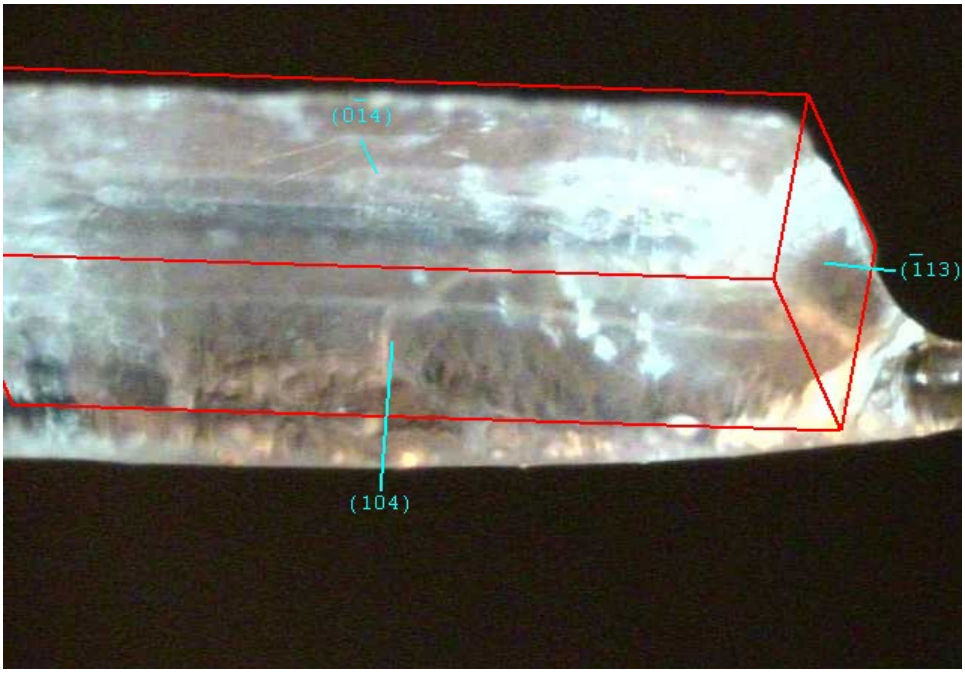

Figure 2.3: Optical photograph of one of the investigated native calcite crystals with face indexes.

The results are to a small extent, though, biased by the quality of the crystals. The diffraction images always showed reflections of several calcite domains with a slight misorientation.

2.3.2. Infra-red characterization of SOLVAY (SOCAL U1-R) and OMYA (BL 200) calcites

The presence of other phases in adsorbent was investigated by ATR-FT-IR. For that, a suspension of 2.5 $g.L^{-1}$ was prepared then a drop of the suspension was put on the crystal and analyzed. This procedure was respected for both calcites. The IR spectrum is presented in Figure 2.4.

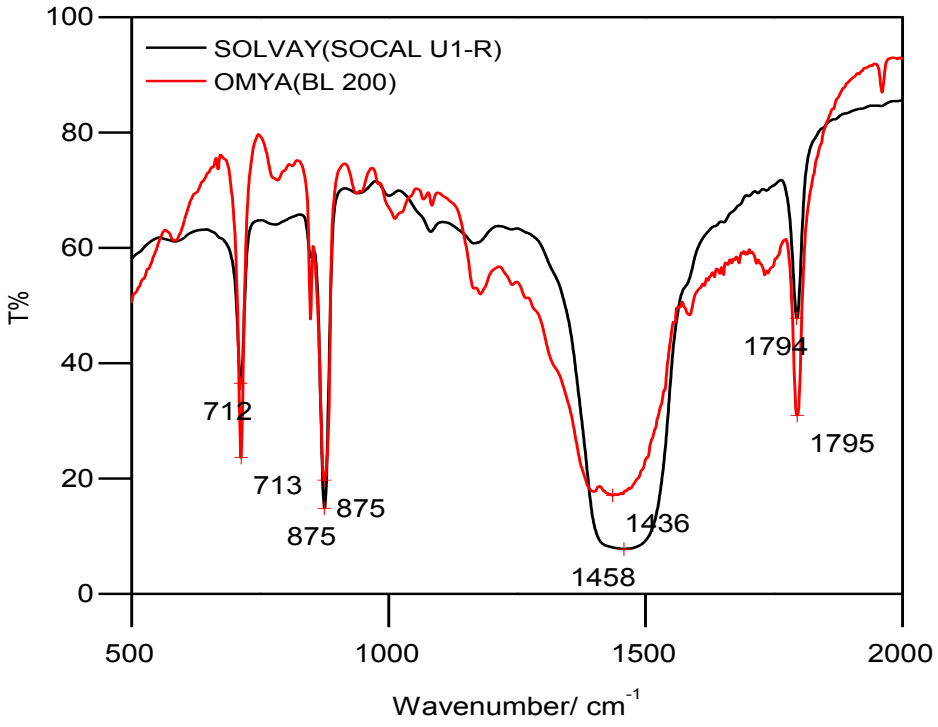

Figure 2.4: IR spectra of SOLVAY (SOCAL U1-R) and OMYA (BL200) calcites.

The absence of vaterite, which would have appeared at 750 cm^{-1}, or other impurities was confirmed. Aragonite presents a specific band at υ_4=715 / 700 cm^{-1}, which is not detected in our samples. The adsorbent presents the characteristic bands for calcite, υ_3=1470 cm^{-1}, υ_2=875 cm^{-1}, υ_4=713 cm^{-1}. These bands are comparable to those obtained by Sato and Matsuda [98] ,υ_3=1430 cm^{-1}, υ_2=874 cm^{-1}, υ_4=710 cm^{-1}. The band corresponding to 1794 cm^{-1} for SOLVAY (SOCAL U1-R) and 1795 cm^{-1} for OMYA (BL200) respectively are in agreement with Sivakumar et al. [99] and correspond to calcite too.

2.3.3. SEM characterization of SOLVAY (SOCAL U1-R) and OMYA (BL 200) calcites

SEM measurements were performed onto calcite powders and single crystals which were coated with a carbon layer. The SEM image of calcite SOLVAY (SOCAL U1-R) and OMYA (BL 200) are presented in Figure 2.5. The rhombohedra shape, characteristic for commercial calcite, is very difficult to be distinguished in the grain population presented below. In this case, it is also very

difficult to observe the (104) face of calcite, which is supposed to be the most abundant exposed face of this material [40, 50].

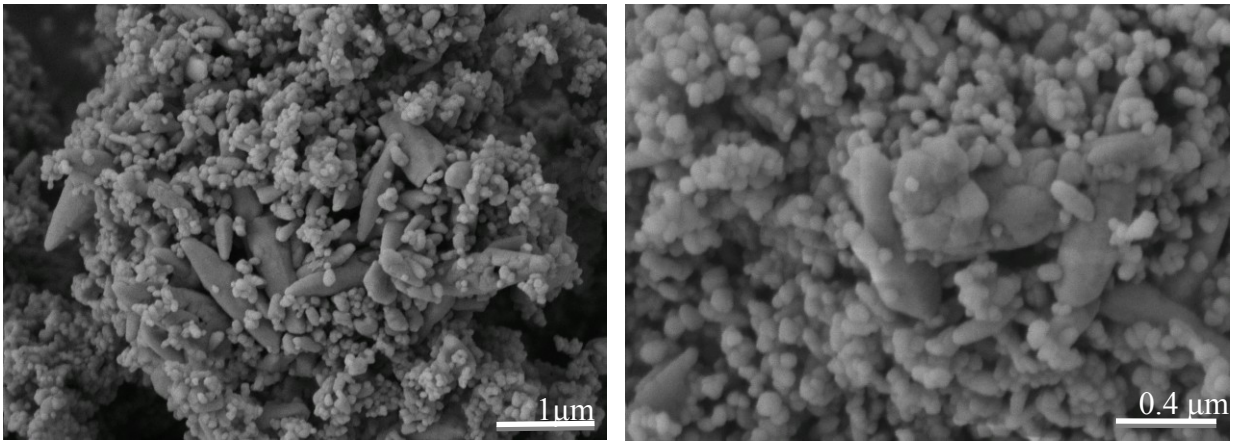

Figure 2.5: SEM image of SOLVAY (SOCAL U1-R) calcite at different scales.

The obtained pictures present an inhomogeneous distribution of the grain size with irregular shapes for calcite SOLVAY (SOCAL U1-R). There are a mixture of ”populations”, with different grain size. In the left side picture, granules with a larger size are shaded by small grains. A more detailed example is presented in the right side image, where the bigger grains present on the left side picture (around 0.5-1 µm) can be seen together with very small grains (around 100 nm or less).

For calcite OMYA (BL 200), the initial grain size was superior to 50 µm before the sieving of the material. The pictures presented here show the rhombohedra shape characteristic for calcite, especially on the right side image (Figure 2.6).

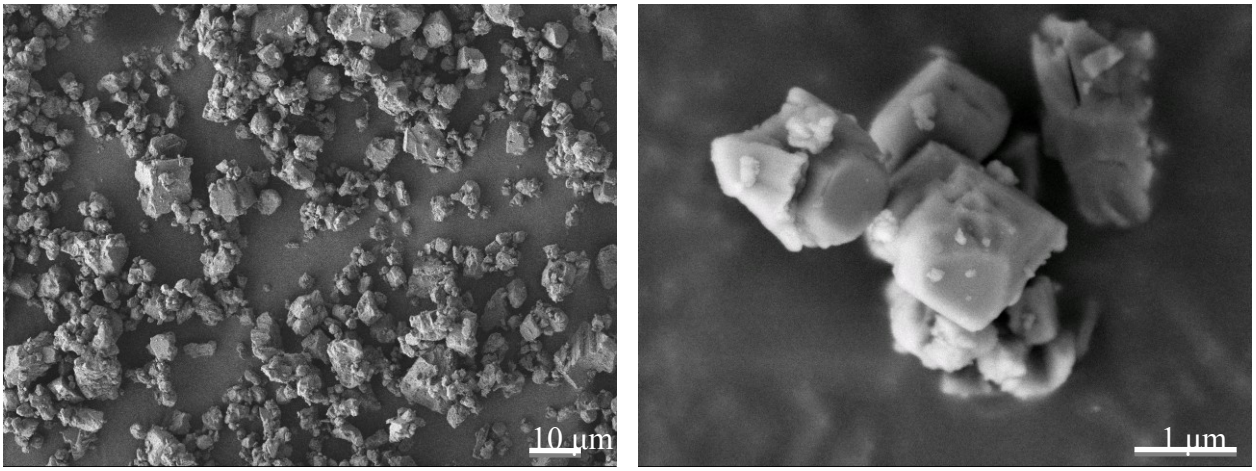

Figure 2.6: SEM image of OMYA (BL 200) calcite at different scales.

On the left side image, an overview of the dispersed grains is presented and some of them exceed 10 µm. On the right side image, an agglomerate of several grains is exposed, where the grain size is around 1 µm.

2.3.4. Total digestion of SOLVAY (SOCAL U1-R), OMYA (BL 200) and Alfa Aesar calcites

Total digestion of calcites was performed in order to determine the concentrations of impurities in the material using ICP-MS. The identified values for SOLVAY (SOCAL U1-R) were close to detection limit, 0.06 $\mu g.g^{-1}$ for Eu(III) and 0.01 $\mu g.g^{-1}$ for Ni(II) which means that this material is appropriate for sorption experiments. Eu(III) content in OMYA (BL 200) calcite is below the limit detection and the Ni(II) content is 13.11 $\mu g.g^{-1}$. Other element that was found in this calcite is U, with a content of 0.15 $\mu g.g^{-1}$.

In the same manner as for calcite powders, total digestion was done for single crystals (0.5 g). The Eu(III) concentration in the solid was 0.07 $\mu g.g^{-1}$, whereas Ni(II) concentration was 0.41 $\mu g.g^{-1}$. An iron content of 77 $\mu g.g^{-1}$ was found, but also of U 1.4 $\mu g.g^{-1}$, Pb 0.25 $\mu g.g^{-1}$. Other metals like As, Pd, Sm, Gd, Os, Ir were below 0.01 $\mu g.g^{-1}$. With these quite low contents of our elements of interest combined to low amount of impurities in the solid, the RBS measurements are not expected to be affected.

In conclusion, from a variety of calcite powder sources, our attention was mainly focused on three types of calcite, due to the experimental condition requirements and spectroscopic tools needs.

SOLVAY (SOCAL U1-R) has a high specific surface area and has been chosen as adsorbent material for batch-sorption experiments and TRLFS investigation. OMYA (BL 200) has a higher particle size and has been chosen for batch experiments as well as RBS studies. Also, because of RBS demands (high energy ion scattering), single crystals from Alfa Aesar were selected, too.

2.4. Preparation of samples

NaCl was chosen as background electrolyte in order to minimize the variations of the activity coefficients, but also because Na^+ and Cl^- ions are found in the COx interstitial pore waters. The ionic strength was set to 0.1 $mol.L^{-1}$ since this value is close to the one of the pore waters.

2.4.1. Preparation of calcite-equilibrated suspensions (CES)

In order to achieve the desired pH for our investigations, that is ~8.3 (corresponding to the pH of calcite equilibrated with air), the appropriate amount of calcite was stirred gently and permanently with NaCl (10^{-1} $mol.L^{-1}$) during 2 days directly in the reactors under atmospheric conditions. After this period of time, the desired pH of 8.3 was reached, then the metal introduced. This protocol was also used for calcite single crystals (~0.3 $g.L^{-1}$) to obtain a calcite single crystal equilibrated suspensions (CSC-ES). This time, it was necessary to add NaOH to increase the pH up to 8.3, and to wait a longer time (1 week) than for powders.

2.4.2. Preparation of calcite pre-equilibrated solutions (CPES)

A second method was implemented in order to control dissolution of calcite. In the second case, calcite powders or single crystals were put in contact with NaCl (0.1, 0.11 or 0.125 $mol.L^{-1}$) in order to maintain the ionic strength to a final value of 10^{-1} $mol.L^{-1}$ for the sorption experiments (after addition of the element of interest, the ionic strength will be modified due to high amount of stock solution).

The experimental device for pre-equilibration of calcite powder/single crystal consists in a polypropylene bottle with a PTFE stirring bar, where calcite and NaCl are introduced. In order to reach faster a pH to 8.3, a peristaltic pump was used to bubble atmospheric CO_2 (Figure 2.7).

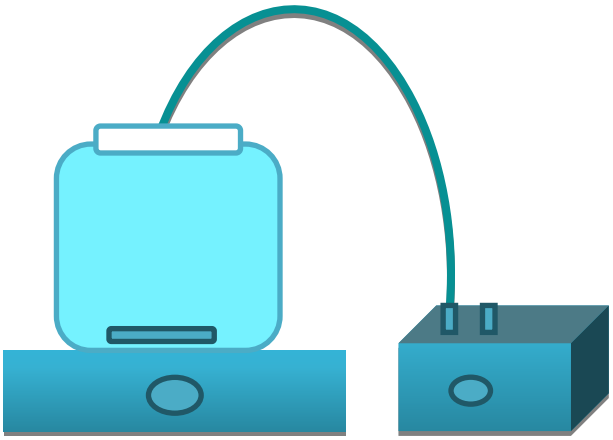

Figure 2.7: Experimental setup for calcite pre-equilibration.

For calcite powders, once pH 8.3 was reached, the suspension was centrifuged for 30 minutes using 500 mL polypropylene centrifugation tubes. The supernatant was first filtered through a fritted glass (porosity 4) and then through Sartorius® 0.45 µm filters (pre-conditioned with 200 mL of water to minimize additional release of dissolved organic carbon from the filter [100]). The resulting collected filtrate refers to CPES. The procedure relative to single crystals is detailed in the following section.

For experiments under $pCO_2=10^{-2}$ atm, the same equilibration method for calcite was performed in a glovebox, by pumping a gas mixture (1% CO_2/N_2).

2.4.3. Preparation of calcite single-crystals pre-equilibrated solutions (CSC-PES)

For these experiments, a similar method with those for powders was implemented. This method consists into equilibration of ~0.1 $g.L^{-1}$ of calcite single-crystals with the appropriate amount of NaCl (0.1, 0.11 or 0.125 $mol.L^{-1}$). The same separation procedure (centrifugation followed by filtration) described in section 2.4.2 was used to produce a CSC-PES solution.

2.5. Experimental setup and procedure for blanks experiments

Blank solution experiments (without calcite) were performed in order to study solution chemistry of Eu(III) and Ni(II) in carbonate medium. This serves as a preliminary study in order to better understand the Eu(III) and Ni(II)-calcite systems. Calcite pre-equilibrated solutions (CPES), at $pCO_2 = 10^{-3.5}$ atm and 10^{-1} mol.L^{-1} NaCl, were spiked with Eu(III) and Ni(II) (10^{-6} to 10^{-3} mol.L^{-1} in both cases). The stirring time was varied from 1 day until 2 months for Eu(III) and from 1 day to 5 months for Ni(II). Regular samplings were done as a function time, the aliquot were ultracentrifuged (1.5h at 230,500 g for Eu and 2h at 182,100 g for Ni(II)). Concentrations of Eu(III) and Ni(II) left in the supernatant were analyzed by ICP-MS. For selected samples and times, the phases precipitating were also identified. After a first centrifugation at 5300 rpm during 90 minutes, an ultracentrifugation was performed (32.000 rpm during 2 hours). The resulting pellets were dried overnight in an oven at 70 °C and measured by XRD. Besides the XRD measurements, additional TRLFS investigations were performed on Eu(III) suspensions.

2.6. Experimental setup and procedure for batch sorption experiments

The adsorption studies of the contaminants onto calcite are made in "batch" reactors (open with respect to CO_2). Europium sorption experiments were carried out in Teflon® (WVR® International) vials, in order to avoid sorption/interaction of europium onto reactor walls. For nickel, polypropylene vials were used. In the vials, a weighted quantity of calcite powder was put in contact with a defined volume of solution (CES or CPES) with an ionic strength of 10^{-1} mol.L^{-1} NaCl. A small magnetic stirring bar was placed in the middle of Teflon® vials in order to ensure the homogeneity of the suspension.

For single crystal, the manner to perform the experiments is by trapping new single crystals in manufactured Teflon clips (presented in Figure 2.8 left) placed in a Teflon® or polypropylene vial containing a CSC-PES solution. In every vial, 6 clips containing each one trapped crystal were introduced (under the 3 clips presented in the image, other 3 ones are inserted) (Figure 2.8 right). A small magnetic stirring bar is placed in the middle of the vials in order to ensure the homogeneity of the suspension.

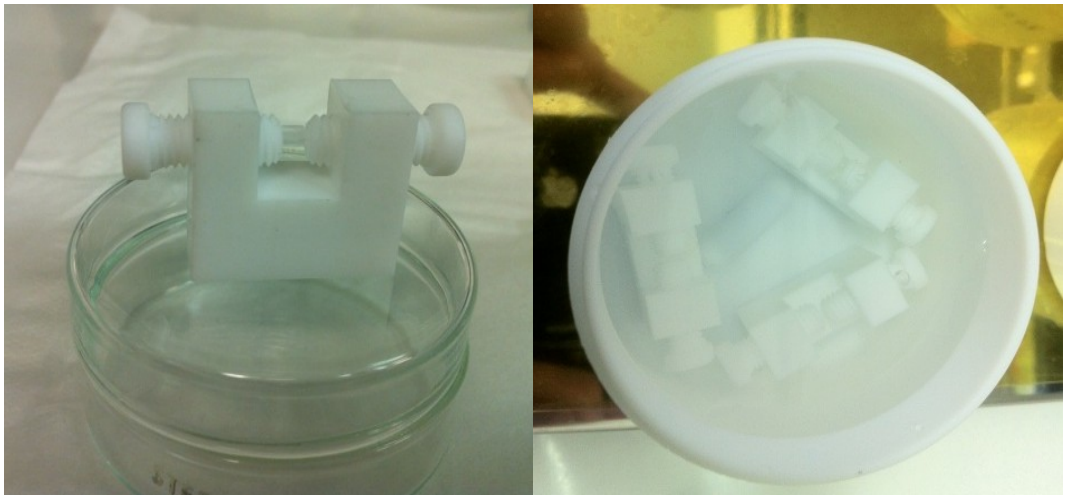

Figure 2.8: Experimental set-up for sorption experiments onto calcite single-crystals: clip containing the trapped crystal (left) and several clips in a vial (right).

Classical experiments were designed to investigate sorption of europium and nickel onto calcite. Samples were spiked with europium stock solution (5×10^{-3} mol.L^{-1}) or nickel stock solution (5×10^{-3} and 10^{-3} mol.L^{-1}). The pH of all samples was checked throughout the handling. pH was measured for calcite pre-equilibration, batch sorption experiments and blank solutions. Measurements were performed using a WTW 730 (Wissenschaftlich-Technische Werkstätten) and METTLER DELTA 345 pH meters using a WTW SenTix® Mic or InLab® Expert NTC30 electrodes in which an Ag/AgCl reference electrode is incorporated. The pH electrodes were calibrated before starting every measurement using NIST buffer solutions. The WTW SenTix® Mic electrode was calibrated with solutions having pH 6.86 and 9.18, and the METTLER DELTA 345 using pH 4, 6.08 and 10.01 at 25°C. The accuracy of the measurements is ± 0.1 pH units. The pH of the experiments is in most of the cases 8.3±0.1 and was imposed by the equilibrium of calcite with air, but some experiments were carried out with a higher pCO_2, namely 10^{-2} atm. For the second set of experiments, the equilibrium pH of calcite-CO_2-NaCl system is 7.5 ± 0.1. The experiments with highest pCO_2 were handled in glove-box (Braun) using a gas mixture (1% CO_2/N_2) and prepared in the same manner as those under atmospheric conditions.

Also, a protocol was developed to study desorption of nickel. For that, at the end of each sorption experiment, the suspension was centrifuged and the supernatant removed. A fresh CPES suspension was then added to the remaining solid with the aim to control calcite dissolution and to initiate

desorption of nickel. At the end of each experiment, after separating the liquid from the solid by centrifugation (1.5 hours at 6,800 g), the Eu(III) or Ni(II) concentration left in the supernatant was investigated by ICP-MS. For Nickel, colloids potentially left in the supernatant did not impact significantly sorption results. Indeed, identical Ni(II) concentrations were found in the supernatant after an ultracentrifugation (1.5 hours at 230,500 g). All the experiments were performed in duplicate.

Table 2.3 summarizes the experimental conditions used for batch experiments.

Table 2.3: Summary of experimental conditions for batch experiments.

Calcite	m/v ($g.L^{-1}$)	pCO_2 (atm)	Element	Medium	Concentration ($mol.L^{-1}$)	Duration
SOLVAY	1 and 5	$10^{-3.5}$	Eu(III)	CES	10^{-6}, 10^{-5}, 10^{-4} and 10^{-3}	1 day to 6 months
SOLVAY	1	$10^{-3.5}$	Eu(III)	CPES	10^{-6}, 10^{-5} and 5×10^{-5}	1 week
SOLVAY	1	10^{-2}	Eu(III)	CPES	10^{-6}, 10^{-5}, 10^{-4} and 10^{-3}	1 day and 1 week
SOLVAY	1	$10^{-3.5}$	Ni(II)	CPES	10^{-6}, 5×10^{-6},10^{-5}, 5×10^{-5}, 10^{-4} and 5×10^{-4}	1 day to 2 months

2.7. Spectroscopic elucidation of Eu(III) and Ni(II) interaction with calcite

To determine speciation of an element, the analytical technique must possess some properties like: selectivity, sensitivity to trace concentrations and it should preferentially be non-intrusive (not to modify the investigated sample) [61]. One of the techniques that meet the aforementioned attributes is TRLFS. RBS is a technique use to evaluate the concentration profiles of heavy elements in a light matrix.

2.7.1. TRLFS study

TRLFS enables the speciation of lanthanides (like Eu(III)) or actinides (like U(VI), Am(III) or Cm(III)) in solution, on water/mineral surface or in solids . Two types of information are given by this technique:

- changes in the emission spectra due to the variations in the first sphere of coordination of the investigated element
- analysis of the calculated fluorescence lifetimes which allows to determine the number of fluorescence quenched entities

TRLFS is based on excitation with a pulsed laser beam of a fluorescent element (in our case europium) followed by the measurement of fluorescence signal during a defined time interval. The main advantages of this technique are the rapidity of analysis, the sensibility, and the selectivity towards the investigated species. We use this technique in aqueous and solid medium where it can probe the first coordination sphere of the fluorescent element. Thus, we have chosen it to determine speciation in solutions, suspensions, and solids.

Sample preparation for TRLFS measurements

Three types of samples were prepared according to methods for calcite equilibration described in section 2.5 with the aim to differentiate the possible mechanisms such as adsorption, precipitation, or either incorporation occurring over time.

- the first series of samples blank solutions have the purpose to investigate the different behavior of Eu(III) in solution and its complexation with carbonates from

calcite pre-equilibrated solutions (CPES), at $pCO_2 = 10^{-3.5}$ atm and 10^{-1} mol.L^{-1} NaCl. Details are given in section 2.5.

- the second series of samples - consists in studying the sorption of Eu(III) onto calcite powder. For this, a calcite equilibrated solution (CES) was spiked with the Eu(III) stock solution in order to obtain the desired final concentration. The chosen concentrations, which should permit to discriminate distinct mechanisms at solid/solution interface, are ranging from 10^{-6} up to 10^{-3} mol.L^{-1}. The solid/liquid ratio chosen for the experiments is 1 g.L^{-1} and the stirring time was varied from 4 hours up to 6 months. The parameters that were kept constant during the whole time of experiments, are the pH of 8.3 ± 0.1 resulting from $pCO_2 = 10^{-3.5}$ atm, and 10^{-1} mol.L^{-1} NaCl.

- the third series of samples - consists in studying the impact of pCO_2 on the sorption of Eu(III) onto calcite powder by using a CPES solution. The parameters that were kept constant during the whole time of experiments, are the pH of 7.5 ± 0.1 resulting from $pCO_2 = 10^{-2}$ atm, and 10^{-1} mol.L^{-1} NaCl. The Eu(III) chosen concentrations are ranging from 10^{-6} up to 10^{-3} mol.L^{-1}. The reaction time was 1 day and 1 week.

- the fourth series of samples - consist in single crystals that were immersed in a CSC-PES solution and then spiked with Eu(III) stock solution to obtain the desired final concentration, as for previous samples. The chosen concentrations are similar as for the previous two sets of samples, from 10^{-6} to 10^{-3} mol.L^{-1}. The reaction time was varied from 2 weeks until 2 months.

2.7.2. RBS study

In our study, we have used Rutherford Backscattering Spectrometry (RBS). Indeed, RBS has already been used to follow the incorporation or migration of different elements in minerals. For instance, the incorporation of rare earth elements (REE) and Pb and Sr into calcite and into apatite has been studied by Cherniak and its collaborators [101, 102] by solid state diffusion. The comparison of the results of these studies proves that these elements diffuse rather rapidly into calcite in comparison to other minerals. Alonso et al. [17, 103] investigated the diffusion of Eu, U, Sr and Re into clay by means of RBS, and clearly showed different behaviors for Eu and U (strong

adsorbing elements) compared with Sr and Re. Carroll [104] combined a RBS study to SEM and EDS measurements and observed the incorporation of U(VI), Nd and Th(IV) in calcite as solid solutions. This analytical method is based on the interaction of an ion beam with a sample. It allows the determination of all elements from the periodic classification, given that the signals of the different elements do not interfere with each other. In our case, the study of a heavy atom (Ni(II) or even better Eu(III)) in the light matrix $CaCO_3$ is particularly well adapted. Depending on the beam (type of accelerated ion, energy...), several interactions are possible between the projectile and the target. They can be classified into two categories: electronic and nuclear interactions [105]. These interactions allow obtaining multi-elemental concentration distribution. The resulting technique has three major advantages: a large depth of penetration (≈ 1-2 µm), good sensitivity (it can be lower than 1 at. %) and especially quantitative elemental concentration.

Samples investigated by RBS

Several types of samples were investigated by RBS, either with a millimetric or a micrometric beam size, in two research facilities in IPNL in Lyon (milli-beam) and in CEA-Saclay (micro-beam). The two beam sizes have been chosen either to get an average characterization of the sample (milli-beam) or to focus the analysis on one grain or one selected area on the crystals (micro-beam). A summary of the analyzed samples with their composition is described as well as the used beam:

- milli-beam analysis of samples:
  - pressed pellets - these samples have the purpose to study the incorporation of Eu/Ni into calcite grains. For that calcite powders OMYA (BL 200) and SOLVAY (SOCAL U1-R) were reacted during 1 month with Eu(III) (10^{-4} and 10^{-3} mol.L^{-1}) and Ni(II) (10^{-3} mol.L^{-1}). For this, a CES medium was used. Other experimental parameters are pH 8.3 (pCO_2=$10^{-3.5}$ atm) and 10^{-1} mol.L^{-1} NaCl. After interaction with Eu and Ni, powders were pressed to pellets and were analyzed with a 4 MeV ^{4}He incident beam. At this energy, the depth resolution is about 35 nm near the surface.

  - single crystals - these samples have the same purpose as the pressed pellets, but the preparation method is different (use of a CSC-ES medium with addition of NaOH to reach pH 8.3). Single crystals were put into contact with Eu(III) solution (10^{-4} mol.L^{-1}) during 1 week and 1 month. The experiments were also carried out for 10^{-3} mol.L^{-1} Ni(II) with a

reaction time of 1 week and 3 weeks. The incident beam was set to 1.5 MeV in order to improve the depth resolution (25 nm) and the backscattering yield.

- μ-beam analysis of samples:

A μ−beam with energy of 1.5 MeV for a better depth resolution (25 nm) and backscattering yield was again used. For these experiments, calcite single−crystals were put in contact with CSC-PES solutions, then spiked with Eu(III) (initial concentration of 10^{-4} and 10^{-5} mol.L^{-1}) and Ni(II) (initial concentration of 10^{-4} or 10^{-3} mol.L^{-1}). The contact times were ranging between 1 day – 5 months for Eu(III) and 1 week − 2 months for Ni(II), respectively.

Chapter 3:
Interaction of europium with calcite

3. Interaction of europium with calcite

This chapter deals first with the solution chemistry of Eu(III) in carbonate medium, by combining macroscopic data together with TRLFS and XRD. This serves as a preliminary study in order to better understand the europium-calcite system. The interaction of Eu(III) with calcite was studied under atmospheric conditions by TRLFS, RBS and SEM-EDXS and results were compared with existent bibliographic data. The impact of the initial Eu(III) concentration as well as time was studied on both powders and single crystals. This study was completed by applying TRLFS on Eu(III) sorbed onto calcite powder and single crystals under $pCO_2=10^{-2}$ atm.

3.1. Solution chemistry of europium

Europium can be found as free ion, Eu^{3+}, in +III oxidation state, hydrolyzed or complexed with carbonates, chlorides or other ions from the aqueous environment.

Europium is a luminescent element used as an analogue to some actinides such as Cm^{3+}/Am^{3+}. The high luminescence sensitivity of Eu(III) makes it possible to investigate its complexation with carbonates and represents a preliminary study to Eu(III) sorption onto calcite. In COx pore water, the solubility of Eu(III) is inferior to 10^{-7} mol.L^{-1}, but different criteria (such as sensitivity) imposed by spectroscopic requirements motivated us to work at higher concentrations. A preliminary TRLFS test shows that for 10^{-7} mol.L^{-1} Eu(III), the detected signal was very weak. Thus, the minimal concentration to obtain analyzable spectra is 10^{-6} mol.L^{-1}. The concentration at which the investigations were performed were 10^{-6}, 10^{-5}, 10^{-4} and 10^{-3} mol.L^{-1} Eu(III). More details about experimental conditions are given in section 2.6.

3.1.1. Speciation calculations

The current data in the literature are various and sometimes incoherent. Some new speciation calculations were needed to understand the behavior of aimed elements under the COx conditions. In the literature, most of the researchers used the constants presented by Hummel et al. [106]. Speciation calculations were performed as well by J. Tits et al. [107] in ACW (artificial cement water) at pH 13.3 and the species they considered were close to those relevant for our investigations.

The main species determined at pH 13.3 in ACW, is $Eu(OH)_4^-$. The maximum concentration of soluble Eu(III) is estimated to be 8.6×10^{-6} mol.L^{-1}, assuming that $Eu(OH)_{3(am)}$ and $Eu(OH)_{3(cr)}$ are the phases governing the Eu(III) solubility. Other relevant complexation study of Eu(III) with carbonates/bicarbonates in Tris solutions and I=10^{-1} mol.L^{-1} was done by Rao and Chatt [108] using synergistic solvent extraction system of 1-nitroso-2-naphtol and 1,10-phenanthroline in chloroform. The concentration of bicarbonate was 5×10^{-3} to 10^{-1} mol.L^{-1}and carbonates 5×10^{-4} to 10^{-2} mol.L^{-1} and pH of 8-9.1 which simulates the ground water composition. Eu(III) concentration was between 10^{-9} and 10^{-7} mol.L^{-1}. They determined based on calculated bicarbonate/carbonate concentrations and Eu(III) radioactivity the distribution ratios. The influence of bicarbonates/carbonates concentrations on Eu(III) distribution ratios were tested by curve-fitting techniques. Anyway, according to their study, the main species identified for pH=8.3 in their experimental imposed conditions are $EuCO_3^+$ and $Eu(CO_3)_2^-$.

Speciation calculations performed by Zavarin et al. [73] using the aqueous species extracted from Haas et al. [109] and Spahiu and Bruno [110] revealed that under atmospheric conditions mono−($EuCO_3^+$) and dicarbonate ($Eu(CO_3)_2^-$) are the dominant species whereas tricarbonate species are not common for pH higher than 9. For a higher pCO_2 (1% CO_2), Zavarin et al. [73] presents the speciation diagram for 1% Eu(III) at I=10^{-1} mol L^{-1} and shows that for pH 8 the dominating species is $EuCO_3^+$. The contribution of $EuOH^+$ and $Eu(CO_3)^{3-}$ is minimized.

The ThermoChimie database (version 9) [111] from ANDRA was used for our speciation calculations. Calculations were performed at constant ionic strength (10^{-1} mol.L^{-1} NaCl), at pCO_2 $10^{-3.5}$ atm, at pH 8.3 and at 25°C. The initial europium concentrations, identical to those taken for the batch experiments, were ranging from 10^{-6} to 10^{-3} mol.L^{-1}. To reflect experimental conditions, a solution pre-equilibrated with calcite was used for the calculations. However, no calcite was introduced. The aqueous species and solid phases as well as their formation constants used for speciation diagrams are summarized in Table 3.1 and Table 3.2.

Table 3.1: Eu(III) aqueous species and their equilibrium constants ($I = 0$) used for speciation calculations.

Aqueous Species	log K
$Ca^{2+} + Eu^{3+} - 3H^{+} + 3H_2O \rightleftharpoons \mathbf{Ca(Eu(OH)_3)^{2+}}$	−26.300
$2Ca^{2+} + Eu^{3+} - 4H^{+} + 4H_2O \rightleftharpoons \mathbf{Ca_2(Eu(OH)_4)^{3+}}$	−37.200
$3Ca^{2+} + Eu^{+3} - 6H^{+} + 6H_2O \rightleftharpoons \mathbf{Ca_3(Eu(OH)_6)^{3+}}$	−60.700
$Eu^{3+} + Cl^{-} \rightleftharpoons \mathbf{EuCl^{2+}}$	0.760
$Eu^{3+} + 2Cl^{-} \rightleftharpoons \mathbf{EuCl_2^{+}}$	−0.050
$Eu^{3+} + CO_3^{2-} \rightleftharpoons \mathbf{Eu(CO_3)^{+}}$	7.900
$Eu^{3+} + 2CO_3^{2-} \rightleftharpoons \mathbf{Eu(CO_3)_2^{-}}$	12.900
$Eu^{3+} + 3CO_3^{2-} \rightleftharpoons \mathbf{Eu(CO_3)_3^{-3}}$	14.800
$Eu^{3+} + H^{+} + CO_3^{2-} \rightleftharpoons \mathbf{Eu(HCO_3)^{2+}}$	12.430
$Eu^{3+} - H^{+} + H_2O \rightleftharpoons \mathbf{Eu(OH)^{+2}}$	−7.800
$Eu^{3+} - 2H^{+} + 2H_2O \rightleftharpoons \mathbf{Eu(OH)_2^{+}}$	−15.700
$Eu^{3+} - 3H^{+} + 3H_2O \rightleftharpoons \mathbf{Eu(OH)_3}$	−26.200
$Eu^{3+} - 4H^{+} + 4H_2O \rightleftharpoons \mathbf{Eu(OH)_4^{-}}$	−40.700

Table 3.2: Eu(III) solid phases and their equilibrium constants ($I = 0$) used for speciation calculations.

Solids	log K
$\mathbf{EuCl(OH)_2(s)} \rightleftharpoons Eu^{3+} - 2H^{+} + Cl^{-} + 2H_2O$	9.130
$\mathbf{EuCl_2(s)} \rightleftharpoons Eu^{3+} + 2Cl^{-} + 0.5H_2O - H^{+} - 0.25O_2$	32.715
$\mathbf{EuCl_3(s)} \rightleftharpoons Eu^{3+} + 3Cl^{-}$	19.720
$\mathbf{EuCl_3{\cdot}6H_2O(s)} \rightleftharpoons Eu^{3+} + 3Cl^{-} + 6H_2O$	5.200
$\mathbf{Eu(CO_3)(OH)(cr)} \rightleftharpoons Eu^{3+} - H^{+} + CO_3^{2-} + H_2O$	−9.630
$\mathbf{Eu(CO_3)(OH){\cdot}0.5H_2O(s)} \rightleftharpoons Eu^{3+} - H^{+} + CO_3^{2-} + 1.5H_2O$	−7.800
$\mathbf{Eu(cr)} \rightleftharpoons Eu^{3+} + 1.5H_2O - 3H^{+} - 0.75O_2$	165.125
$\mathbf{EuOCl(s)} \rightleftharpoons Eu^{3+} - 2H^{+} + Cl^{-} + H_2O$	15.810
$\mathbf{Eu(OH)_3(am)} \rightleftharpoons Eu^{3+} - 3H^{+} + 3H_2O$	17.600
$\mathbf{Eu(OH)_3(cr)} \rightleftharpoons Eu^{3+} - 3H^{+} + 3H_2O$	15.460
$\mathbf{EuO(s)} \rightleftharpoons Eu^{3+} - 3H^{+} + 1.5H_2O - 0.25O_2$	66.265
$\mathbf{Eu_2(CO_3)_3{\cdot}3H_2O(s)} \rightleftharpoons 2Eu^{3+} + 3CO_3^{2-} + 3H_2O$	−35.000
$\mathbf{Eu_2O_3\ (cubic)} \rightleftharpoons 2Eu^{3+} - 6H^{+} + 3H_2O$	52.400
$\mathbf{Eu_2O_3\ (monoclinic)} \rightleftharpoons 2Eu^{3+} - 6H^{+} + 3H_2O$	53.470
$\mathbf{Eu_3O_4(s)} \rightleftharpoons 3Eu^{3+} - 9H^{+} + 4.5H_2O - 0.25O_2$	114.515
$\mathbf{NaEu(CO_3)_2{\cdot}5H_2O(s)} \rightleftharpoons Na^{+} + Eu^{3+} + 2CO_3^{2-} + 5H_2O$	−20.900

Taking into account all aqueous and solid species presented in Table 3.1 and

Table 3.2, the speciation diagram obtained is presented in Figure 3.1 under the physico-chemical conditions that were used for our experiments.

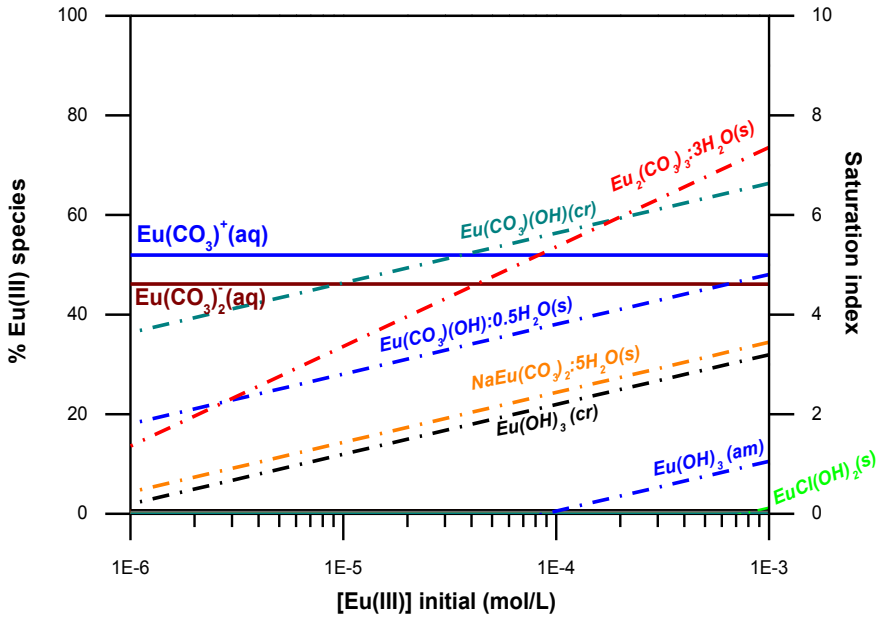

Figure 3.1: Chemical distribution of Eu(III) species as a function of the initial concentration(left ordinate) and saturation indexes for possible precipitated species (right ordinate) ($I=10^{-1}$ mol.L^{-1} (NaCl), $pCO_2 = 10^{-3.5}$ atm, pH=8.3±0.1).

The solid phases that are expected to form in our case at pH 8.3 are europium carbonates and europium hydroxy-carbonates. From our calculations, the main solid phases expected to precipitate at 10^{-3} mol.L^{-1} and at $\leq 10^{-4}$ mol.L^{-1} are $Eu_2(CO_3)_3{:}3H_2O_{(s)}$ and $Eu(CO_3)OH_{(cr)}$, respectively.

The main aqueous species that are obtained in our imposed experimental conditions are $EuCO_3^+$ 50% and in almost in the same percentage, $Eu(CO_3)_2^-$,~45% in the whole concentration range.

The distribution of species for each initial concentration as a function of pH is presented in Figure 3.2.

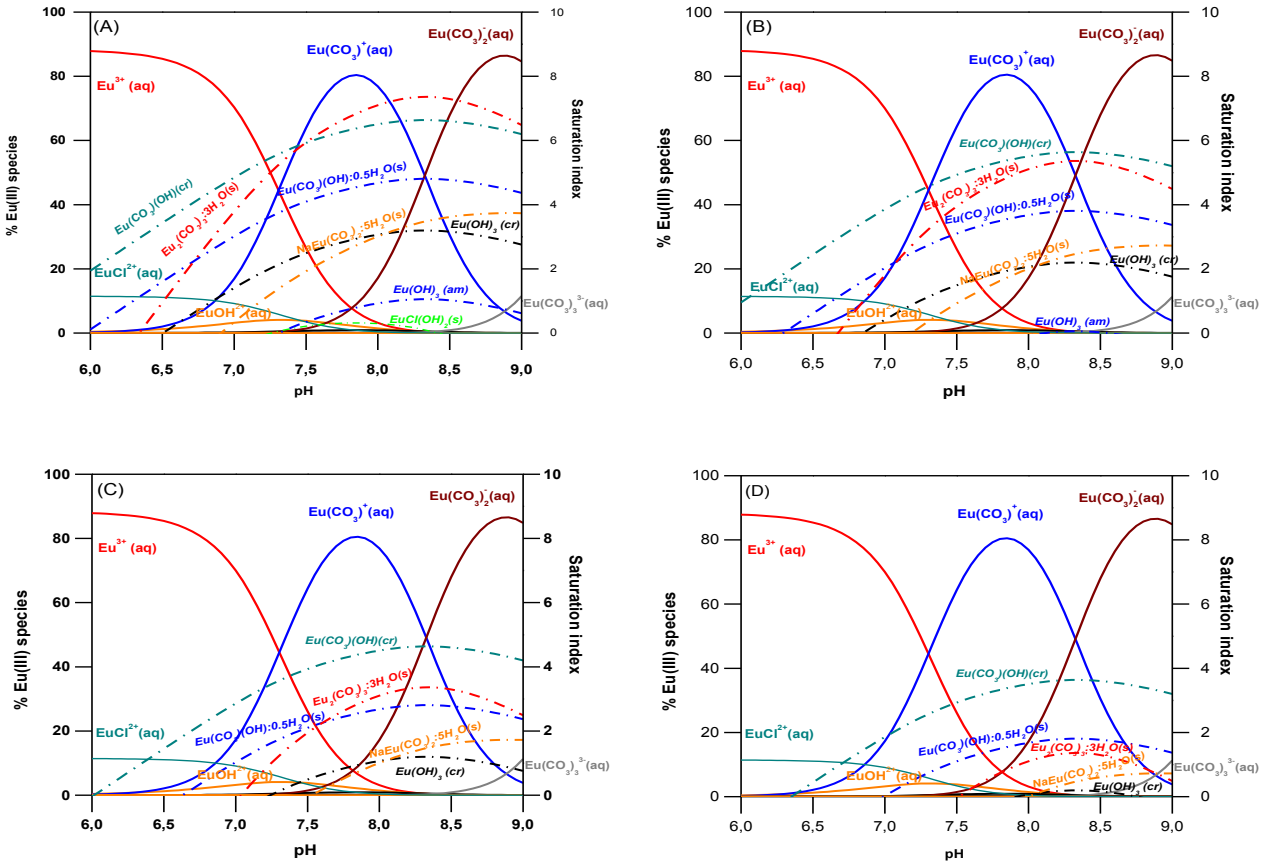

Figure 3.2: Chemical distribution of Eu(III) as a function of pH (left ordinate) and saturation indexes (right ordinate)for different initial concentrations (($[Eu]_0 = 10^{-3}$ (A), 10^{-4} (B), 10^{-5} (C) and 10^{-6} (D) mol.L^{-1}) (I=10^{-1} mol.L^{-1} (NaCl), $pCO_2 = 10^{-3.5}$ atm).

No matter the initial concentrations, the aqueous species are the same. Eu^{3+} is present as main species up to pH 7. From pH 7, its concentration is decreasing, and above pH 8 this species is not present anymore. The predominant species is then $EuCO_3^+$, being at a maximum at around pH 7.9. At pH higher than 8.5, the predominant species becomes $Eu(CO_3)_2^-{}_{(aq)}$. From 10^{-6} to 10^{-4} mol.L^{-1}, europium hydroxy-carbonate Eu(OH)CO_3(cr) shows the highest saturation index from pH 6 to 9. At 10^{-3} mol.L^{-1}, Eu(OH)CO_3(cr) is expected to precipitate below pH 7.6, while $Eu_2(CO_3)_3$:3H_2O(s) would be formed above pH 7.6.

Investigations of Eu(III) in CPES media were done in order to check the accuracy of the speciation calculations. A detailed understanding of Eu(III) aqueous speciation will help understanding its interaction with calcite.

3.1.2. Eu(III) speciation in CPES solution: macroscopic results

CPES solutions were spiked with a certain amount of Eu(III) to obtain desired concentration (from 10^{-6} up to 10^{-3} mol.L^{-1}). To evaluate in detail the behavior of Eu(III), regular samplings at different time intervals were done from 1 day to 2 months. After ultracentrifugation, the concentration of Eu(III) left in solution was investigated by ICP−MS in order to determine the amount of Eu possibly precipitating. In Figure 3.3, the amount of Eu(III) precipitating and the pH of the suspensions observed during the time-dependent experiments of Eu(III) complexation with carbonates are presented.

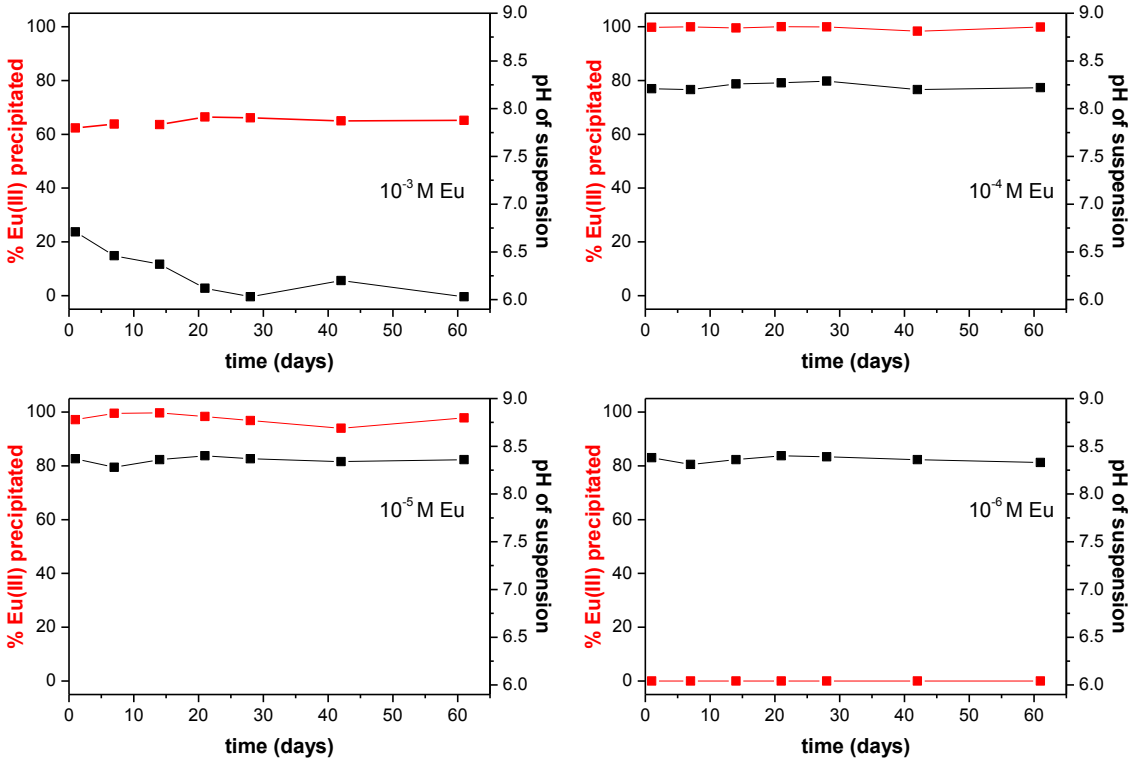

Figure 3.3: Percentage of Eu(III) precipitating as a function of time for different initial concentrations (left ordinate) and pH of the suspensions (right ordinate).

At 10^{-3} mol.L^{-1}, formation of white flakes occurred, the solutions became turbid and a decrease of the pH to ~ 6.3 was noticed. ICP-MS results evidenced that approximately 60 % of Eu(III) was precipitating.

At 10^{-4} and 10^{-5} mol.L^{-1}, precipitation could also be visually observed, with a light turbidity of the solutions at 10^{-5} mol.L^{-1} contrary to 10^{-4} mol.L^{-1}. More than 95 % of precipitation was revealed by ICP-MS at 10^{-4} mol L^{-1} and 10^{-5} mol.L^{-1}. The solutions at 10^{-6} mol.L^{-1} remained transparent up to 2 months, without any precipitation which was confirmed by ICP-MS. From 10^{-6} up to 10^{-4} mol.L^{-1}, the pH remained close to 8.3.

Precipitation of Eu(III) is a very fast kinetic process as shown in Figure 3.3 and proceeds even from the first hours of stirring as it has been observed visually. To determine the nature of both the formed precipitates and the aqueous species remaining in solution and their evolution with time, TRLFS and XRD were used.

3.1.3. Eu(III) speciation in CPES solution: TRLFS and XRD results

Relevant investigations of Eu(III) complexation with carbonates and with other ligands using TRLFS have been done by Moulin et al. [63], Runde et al. [56], Plancque et al. [61]. They present spectroscopic data (luminescence emission spectra and lifetimes), which is a basis for our work.

In Figure 3.4, the luminescence emission spectra of Eu(III) complexed with carbonates for different Eu(III) concentration are presented. TRLFS measurements were at first performed on the suspensions.

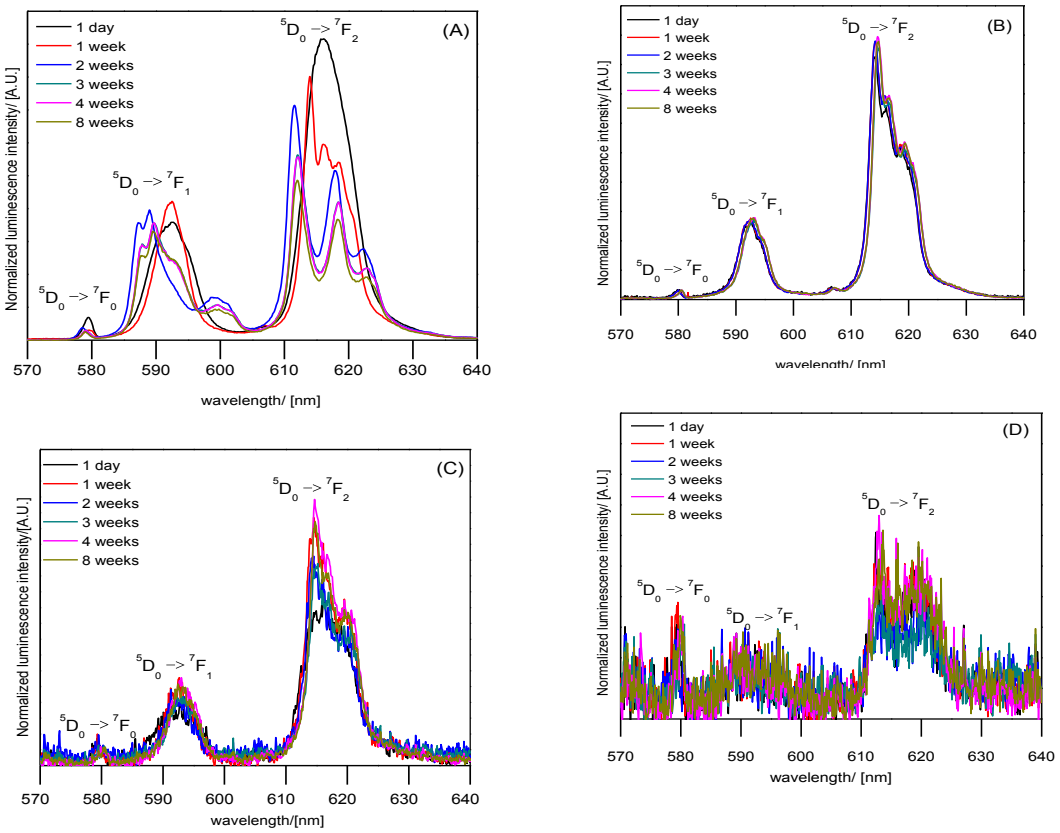

Figure 3.4: Luminescence emission spectra of Eu(III) suspensions as a function of initial Eu(III) concentration, 10^{-3} mol.L^{-1} (A), 10^{-4} mol.L^{-1} (B), 10^{-5} mol.L^{-1} (C) and 10^{-6} mol.L^{-1} (D).

In all spectra, intensity changes and splitting of the bands corresponding to $^5D_0 \rightarrow {}^7F_1$ and $^5D_0 \rightarrow {}^7F_2$ transitions are observed with Eu(III) coordination. For all initial Eu(III) concentrations except 10^{-6} mol.L^{-1}, precipitation was noticed as mentioned before from visual observations and confirmed by ICP-MS. The broad peaks for the main transitions $^5D_0 \rightarrow {}^7F_0$, $^5D_0 \rightarrow {}^7F_1$ and $^5D_0 \rightarrow {}^7F_2$ are comparable with Eu(III) solid phases studied by Runde et al. [56]. For 10^{-6} mol.L^{-1} Eu(III), the spectra (Figure 3.4 (D)) were too noisy for lifetime determination and subsequent species interpretation.

For all initial Eu(III) concentrations except 10^{-3} mol.L^{-1} the spectra shapes do not change significantly over time. The different spectra for 10^{-3} mol.L^{-1} Eu(III) recorded after 1 day, 1 week and 2 weeks are presented in Figure 3.5. After 2 weeks, no further changes of the spectra shape have been observed.

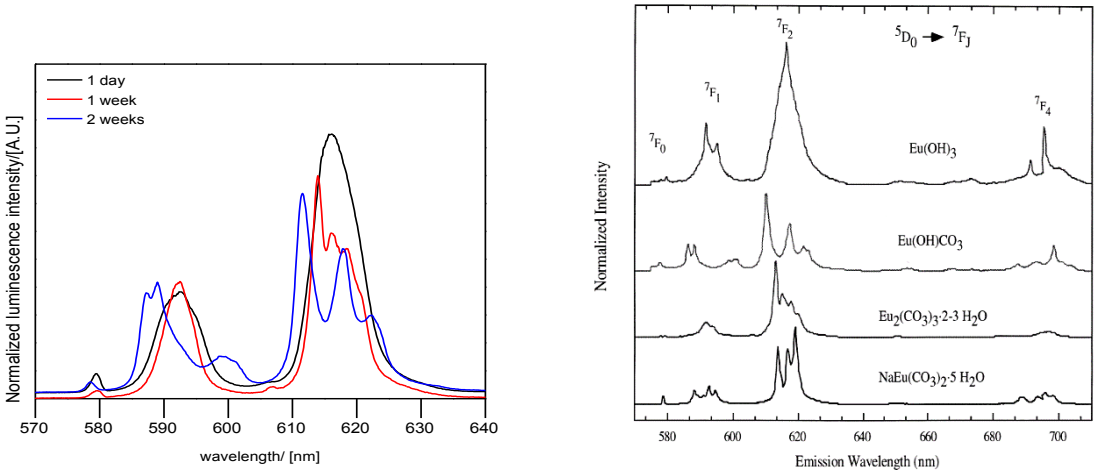

Figure 3.5: Left: Luminescence emission spectra of 10^{-3} mol.L^{-1} Eu(III) suspensions at pH ranging from 6.7 to 6.4 for different contact times (1 day, 1 week and 2 weeks). Right: Luminescence emission spectra of solids characterized by Runde et al. [56].

For 10^{-3} mol.L^{-1} Eu(III), after 1 day the spectrum is characterized by a broad $^5D_0 \rightarrow {}^7F_0$ peak, the $^5D_0 \rightarrow {}^7F_1$ peak is twofold split, and the $^5D_0 \rightarrow {}^7F_2$ peak is not split but very intense. This can be due to a mixture of several amorphous solid and diluted compounds; an assignment to a distinct species is not possible.

The spectrum obtained after 1 week shows a fourfold splitting of the $^5D_0 \rightarrow {}^7F_2$ transition and may be assigned to solid phase $Eu_2(CO_3)_3 \cdot 2{-}3H_2O$ (Figure 3.5 right, second lowermost spectrum) [56]. After 2 weeks, the spectrum can be attributed to solid $EuOHCO_3$ (Figure 3.5 right, second spectrum from above) [56]., based on the threefold splitting of both the $^5D_0 \rightarrow {}^7F_1$ and $^5D_0 \rightarrow {}^7F_2$ transitions, and their luminescence intensity ratios [56].

For lower concentrations, 10^{-5} and 10^{-4} mol.L^{-1} Eu(III), precipitation was observed with less than 5% of Eu(III) left in the supernatant. For both concentrations, over the whole investigation time scale, the same emission spectra (Figure 3.4 (B) and (C)) were recorded. According to the same splitting pattern and intensity ratios compared to Runde et al. [56], it might be the solid species $Eu_2(CO_3)_3 \cdot 2{-}3H_2O$. To further interpret the TRLFS spectra of the suspensions, calculation of luminescence lifetimes and number of water molecules in the first coordination sphere of Eu(III) has been carried out (Eq B.2). The data are listed in Table 3.3.

Table 3.3: Summarized lifetimes (µs) and number of water molecules of Eu(III) complexed with carbonates as a function of $[Eu(III)]_0$ and stirring time (measurements performed on suspensions).

Eu (III) (mol L^{-1})	10^{-3}			10^{-4}			10^{-5}		
Stirring time	**pH**	**t1**	**t2**	**pH**	**t1**	**t2**	**pH**	**t1**	**t2**
1 day	6.71	275 ± 8 (3.3 ± 0.5 H_2O)	411 ± 8 (2.0 ± 0.5 H_2O)	8.21	158 ± 17 (6.2 ± 0.5 H_2O)	400 ± 6 (2.1 ± 0.5 H_2O)	8.37	135 ± 3 (7.3 ± 0.5H_2O)	
1 week	6.46	117 ± 4 (8.5 ± 0.5 H_2O)	278 ± 5 (3.2 ± 0.5 H_2O)	8.20	232 ± 12 (4.0 ± 0.5 H_2O)	474 ± 11 (1.6 ± 0.5 H_2O)	8.28		328 ± 6 (2.6 ± 0.5 H_2O)
2 weeks	6.37	151 ± 7 (6.5 ± 0.5 H_2O)	316 ± 5 (2.8 ± 0.5 H_2O)	8.26	126 ± 13 (7.9 ± 0.5 H_2O)	390 ± 6 (2.1 ± 0.5 H_2O)	8.36		345 ± 8 (2.5 ± 0.5H_2O)
3 weeks	6.12	115 ± 2 (8.7 ± 0.5 H_2O)	284 ± 3 (3.1 ± 0.5 H_2O)	8.27	120 ± 7 (8.3 ± 0.5 H_2O)	375 ± 4 (2.2 ± 0.5 H_2O)	8.40		363 ± 14 (2.3 ± 0.5H_2O)
1 month	6.03	143 ± 5 (6.9 ± 0.5 H_2O)	340 ± 6 (2.5 ± 0.5 H_2O)	8.29	150 ± 8 (6.5 ± 0.5 H_2O)	398 ± 6 (2.1 ± 0.5 H_2O)	8.37		383 ± 4 (2.2 ± 0.5H_2O)
2 months	6.03	106 ± 3	278 ± 4 (3.2 ± 0.5 H_2O)	8.22	103 ± 7	362 ± 4 (2.3 ± 0.5 H_2O)	8.36		329 ± 6 (2.6 ± 0.5 H_2O)

For the highest concentration, 10^{-3} mol.L^{-1}, after 1 day reaction time, two lifetimes were identified, being attributed to a mixture of Eu(III) solid and aqueous species.

After 7 days reaction time, two luminescence lifetimes again indicated the presence of two distinct species. The shorter lifetime of 117 µs can be assigned to the free Eu^{3+} aquo ion, with possible minor contribution of $EuCl^{2+}$ or $EuOH^{2+}$. Taking into account the spectra shape (see Figure 3.5), the longer lifetime with a value of 278 µs can be assigned to solid species $Eu_2(CO_3)_3$·2-3 H_2O, according to Runde et al. [56], who measured a luminescence lifetime of 234 µs for this solid phase. This seems to be the main solid species at this time.

After 2 weeks the spectra shape changes, indicating that $EuOHCO_{3(s)}$ seems now to be the main solid phase. However, two luminescence lifetimes are identified corresponding to two distinct species. The shorter lifetime with values ranging between 106-151 µs may be attributed to the free aquo Eu^{3+} ion, with possible minor contribution of $EuCl^{2+}$ or $EuOH^{2+}$.The longer lifetime with values ranged between 278-340 µs might be assigned to $EuOHCO_{3(s)}$, based on the similar spectra shape to what Runde et al. [56] observed. One should not forget that Runde et al. [56] recorded their TRLFS spectra on isolated powders. In our study, we measured solids suspensded in water. The differences in the lifetimes compared to those of Runde et al. [56] can arise from a different water content in the crystal lattice.

For 10^{-4} mol.L^{-1} Eu(III) in all cases two lifetimes are identified no matter the reaction time. The shorter lifetime (values between 103 and 232 µs) could be attributed to $EuCO_3^+$ / $Eu(CO_3)_2^-{}_{(aq)}$ (Plancque et al. [61], Kim et al. [65]). Based on the spectra shape (Figure 3.4 (B), the solid phase $Eu_2(CO_3)_3$:2-3 H_2O seems to be the main species at all times. The longer lifetime (values between 362 and 474 µs) can be assigned to solid Eu(III) carbonate species, like $Eu_2(CO_3)_2$(s).

A similar behavior of Eu(III) is noticed for 10^{-5} mol.L^{-1} over time scale investigations. The luminescence emission bands (Figure 3.4 (C)) are comparable to the spectrum showed in Figure 3.5 right and correspond to solid $Eu_2(CO_3)_3$·2−3H_2O. After 1 week, only one lifetime was determined, in agreement with the fact that less than 1% of the initial Eu(III) concentreation was left in the supernantant. Again, the calculated lifetimes are higher than those reported by Runde et al. [56]) (luminescence lifetime of 234 µs).

A series of measurements by TRLFS were also performed for supernatants, after centrifugation of the suspensions. The spectra for the 10^{-3} mol.L^{-1} Eu(III) series are depicted in Figure 3.6.

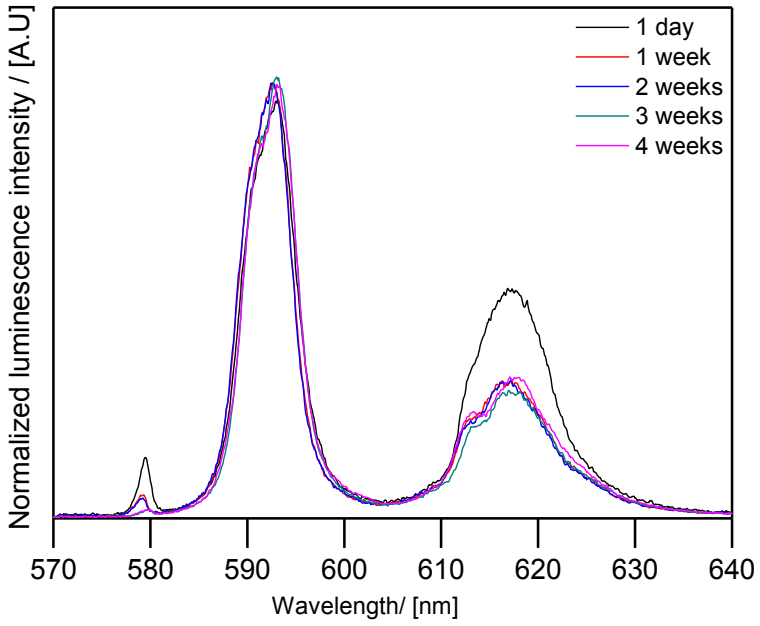

Figure 3.6: Luminescence emission spectra of 10^{-3} mol.L^{-1} Eu(III) supernatants as a function of stirring time, having the pH range between 6.6 and 6.1 $pCO_2=10^{-3.5}$ atm.

Spectra for 10^{-4} and 10^{-5} mol.L^{-1} initial Eu(III) concentration are very noisy because of the very low Eu(III) concentration remained in supernatant after precipitation (spectra not shown). For the 10^{-6} mol.L^{-1} Eu(III) series no precipitation occurred; the spectra are in principal the same as depicted in Figure 3.4 (D) and not analyzable because of the bad signal to noise ratio. Luminescence lifetimes are summarized in Table 3.4.

Table 3.4: Summarized lifetimes (µs) and number of water molecules of Eu(III) complexed with carbonates as a function of $[Eu(III)]_0$ and stirring time (measurements performed on supernatants).

Eu(III) (mol L^{-1})	**10^{-3}**			**10^{-4}**		**10^{-5}**	
Stirring time	**pH**	**Lifetime (µs)**		**pH**	**Lifetime (µs)**	**pH**	**Lifetime (µs)**
		t1	t2		t1		t1
1 day	6.59	112 ± 2 (8.9 ± 0.5 H_2O)	325 ± 21 (2.7 ± 0.5 H_2O)	8.12	198 ± 14 (4.8 ± 0.5 H_2O)	8.25	174 ± 11 (5.5 ± 0.5H_2O)
1 week	6.62	113 ± 1 (8.8 ± 0.5 H_2O)	/				/
2 weeks	6.41	113 ± 1 (8.8 ± 0.5 H_2O)	/				/
3 weeks	6.12	113 ± 1 (8.8 ± 0.5 H_2O)	/				/
1 month	6.12	119 ± 1 (8.4 ± 0.5 H_2O)	/				/

At an initial Eu(III) concentration of 10^{-3} mol.L^{-1}, the luminescence spectra (Figure 3.6) of the supernatants are similar to that measured by Plancque et al. [61] at pH=2 and pCO_2=0 except that after 1 day and can be assigned to free Eu(III) in solution. Also the lifetime values t_1 for initial 10^{-3} mol L^{-1} Eu(III) that are listed in Table 3.4 are very close to those presented in literature for $Eu^{3+}_{(aq)}$ (110 ± 10 µs [61-64]). This is also in agreement with the assignment to aqueous species of the shorter lifetimes determined for the suspensions.

For lower concentrations, 10^{-5} and 10^{-4} mol.L^{-1} Eu(III), less than 5% of Eu(III)) was left in the supernatant, the pH remains at ~ 8.1-8.2. Consequently, the luminescence lifetimes detected in these solutions after 1 day (around 200 µs; see Table 3.4) may correspond to $EuCO_3^+$.

In this part of the work, the speciation of four distinct Eu(III) concentrations at an initial pH of 8.3 in dependence of stirring time has been investigated by TRLFS. For the suspensions, the emission spectra have similar shapes for concentrations 10^{-5} and 10^{-4} mol.L^{-1} Eu(III), corresponding to solid species $Eu_2(CO_3)_3 \cdot 2\text{-}3\ H_2O$ whereas for 10^{-3} mol.L^{-1} the shape of spectra changes from 1 day (species not assignable) over 1 week ($Eu_2(CO_3)_3 \cdot 2\text{-}3\ H_2O$) to 2 weeks when the shape is kept constant and corresponds to $EuOHCO_{3(s)}$.

For supernatants, the lifetimes indicate the presence of Eu(III) carbonate aqueous species for 10^{-5} and 10^{-4} mol.L^{-1} initial Eu(III), whereas for 10^{-3} mol L^{-1} initial Eu(III) mainly free Eu^{3+} was identified by spectra shape and lifetime.

The increase of lifetimes by complexation of Eu(III) with carbonates reflects the exclusion of water molecules in the first sphere of coordination. The number of water molecules goes from 9 (corresponding to free Eu^{3+}) to 5−6 for monodentate complexes, around 3 for bidentate complexes and 2 for tridentate complexes. An explanation is given by Plancque et al. [61] who mentioned that carbonates are bidentate complexes and hence at least two water molecules are displaced through one carbonate ligand.

Besides the fluorescence measurements, additional XRD investigations were performed on the obtained precipitates. In Figure 3.7, the XRD pattern of the analyzed samples (10^{-3} mol.L^{-1} Eu(III) after 1 week and 1 month and 10^{-4} mol.L^{-1} Eu(III) after 1 month reaction time) are presented.

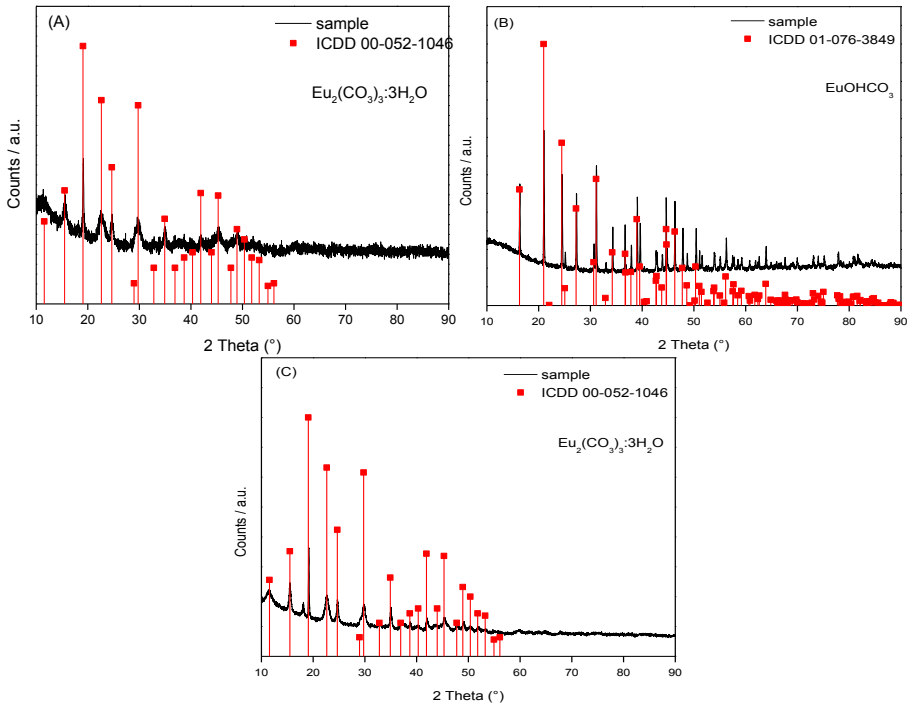

Figure 3.7: XRD diffraction patterns of the precipitates obtained from 10^{-3} mol L^{-1} Eu(III) after 1 week (A), 10^{-3} mol L^{-1} Eu(III) after 1 month (B) and 10^{-4} mol L^{-1} Eu(III) after 1 month (C).

According to the ICDD database (PDF2) [112], the sample prepared at an initial Eu(III) concentration of 10^{-3} mol.L^{-1} after 1 week of stirring (Figure 3.7 (A)) is an hydrated europium carbonate, i.e. $Eu_2(CO_3)_3{:}3H_2O$. The quality of the diffraction pattern is quite poor, which can be ascribed to the small particle size. In addition, the background is relatively high due to the X-ray fluorescence of Eu(III). Nevertheless, XRD results are in full agreement with TRLFS observations.

For 10^{-3} mol.L^{-1} Eu(III) after 1 month of stirring (Figure 3.7 (B)), the resulting precipitate is a well crystallized and pure europium hydroxo carbonate $Eu(CO_3)(OH)$ (ICDD card 01-076-3849). The phase transformation from $Eu_2(CO_3)_3{:}3H_2O$ to $EuOHCO_3$ observed by TRLFS is confirmed by XRD investigations.

For 10^{-4} mol.L^{-1} Eu(III) after 1 month of stirring (Figure 3.7 (C)), the solid can be identified as $Eu(CO_3)_3$:3 H_2O (ICDD card 01-052-1046). The peak at 2θ = 18.14 ° which seems to have been overlooked in the reference pattern can be indexed as (111) and ($1\bar{1}1$) during the refinement procedure. It fits perfectly to the monoclinic unit cell of hydrated Eu carbonate $Eu(CO_3)_3$:3 H_2O. XRD results are again confirming TRLFS observations.

As a conclusion, in the first part of this section, the main solid phases expected to precipitate in the experimental conditions of the sorption experiments (pH = 8.3, $pCO_2 = 10^{-3.5}$ atm), were identified with the use of speciation diagrams in the range 10^{-6} – 10^{-3} mol.L^{-1}. These are $Eu_2(CO_3)_3$:$3H_2O_{(s)}$ and $Eu(CO_3)OH_{(cr),}$ at 10^{-3} mol.L^{-1} and at ≤ 10^{-4} mol.L^{-1}, respectively. As aqueous species, $EuCO_3^+$ and $Eu(CO_3)_2^-$ are expected in the whole concentration range and at pH 8.3.

Macroscopic results have shown that precipitation proceeds fast for concentrations ≥10^{-5} mol.L^{-1}. They showed no precipitation for 10^{-6} mol.L^{-1}, contrary to results of speciation calculations: the kinetics of formation of phases, which must be slower for this low concentration, could be an explanation, together with the relatively high uncertainty in K_{sp} values from the literature.

TRLFS results are in agreement with the formation of the two solids $Eu_2(CO_3)_3$:$3H_2O_{(s)}$ and $EuOHCO_{3(s)}$. Indeed, for 10^{-3} mol.L^{-1} suspensions, the shape of spectra was different after 1 day, 1 week and 2 weeks of contact time. After 2 weeks and up to two months, the spectra shape remained constant. The obtained spectra are realistically comparable with those existent in literature and lead to the hypothesis of the formation of the solid phases $Eu_2(CO_3)_3$:$3H_2O_{(s)}$ which later transforms in $EuOHCO_{3(s)}$.

The emission spectra of 10^{-5} and 10^{-4} mol.L^{-1} Eu(III) suspensions had similar shapes overtime, indicating the formation of $Eu_2(CO_3)_3$ 2-3 $H_2O_{(s)}$.

For the two highest Eu(III) concentrations, XRD experiments confirmed the solid phases formed under our experimental conditions, which were identified by TRLFS. Depending on the four

distinct Eu(III) concentrations that have been investigated by TRLFS and XRD, the different solution behaviors of europium are summarized in Figure 3.8.

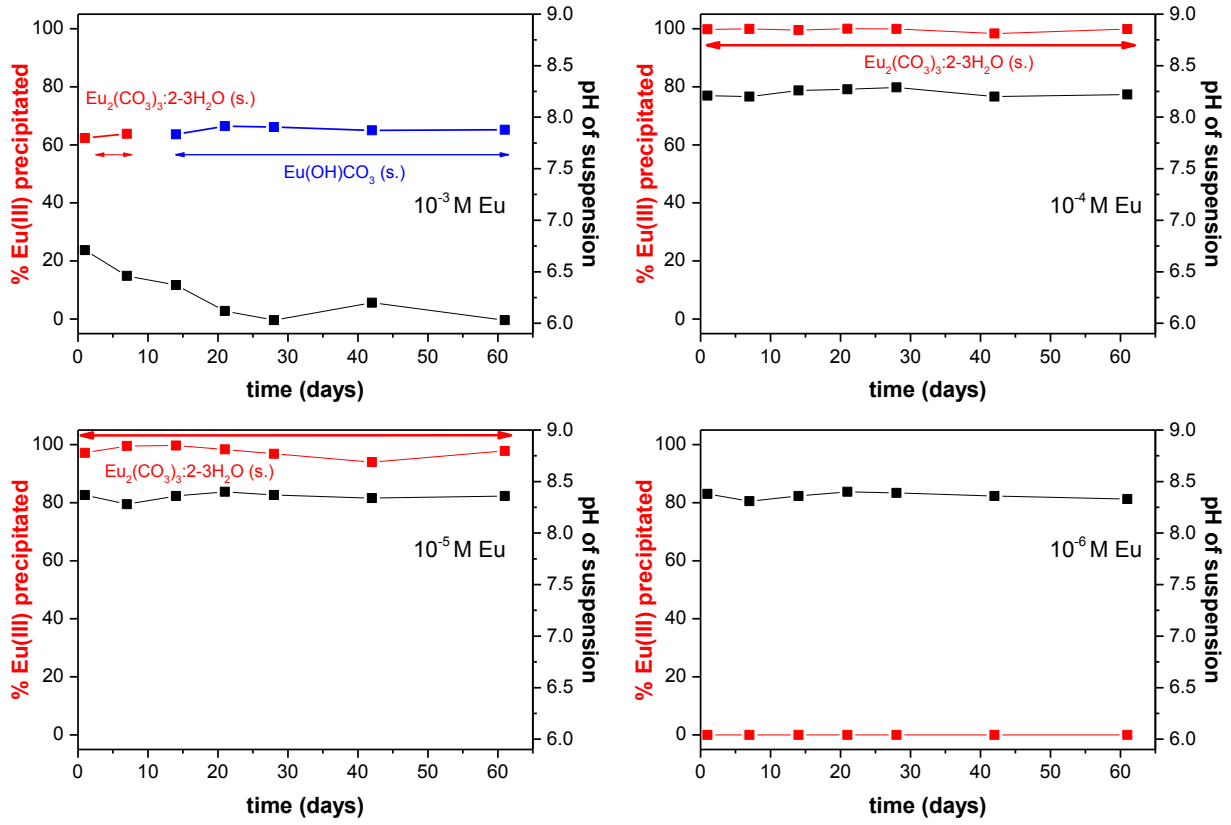

Figure 3.8: Percentage of Eu(III) precipitating as a function of time for different initial concentrations (left ordinate) and pH of the suspensions (right ordinate), with the identification of precipitating phases and their evolution with time.

3.2. Interaction of Eu(III) with calcite: macroscopic studies

Secondary phases can be formed as a result of geochemical transformation in a multiscale barrier system of a nuclear waste repository, because of the presence of interstitial ground water and physical and chemical factors. In contact with the ground water, radiochemical elements can be released in the environment or immobilized via sorption to the primary and secondary phases. Also, incorporation of radioelements in a secondary phase can be present. In this section, the mechanisms leading to the immobilization of europium onto calcite are investigated, in particular to determine if co−precipitation and incorporation into the bulk of calcite can be evidenced.

In the last few years, interaction of lanthanides with carbonate phases was extensively studied using various methods and different spectroscopic techniques, which highlighted the behavior of carbonate phases in various conditions [4, 5, 9, 10, 55, 113-116]. The purpose of this part of the Ph.D. is to investigate interaction of Eu(III) with calcite, in order to bring a better and fully understanding on Eu−NaCl−CO_2−calcite system. One of the objectives is to investigate interaction of Eu(III) as an analogue of trivalent actinides with carbonates under atmospheric conditions and under $pCO_2=10^{-2}$ atm for high level radioactive waste storage. If the actinides are released from the waste, their concentration would certainly be of the order of magnitude of trace levels. The chosen concentrations in our study were much higher and ranged between 10^{-6} and 10^{-3} mol.L^{-1} because of the requirements of the spectroscopic techniques (especially RBS). Concentration- and time-dependent experiments were performed with the purpose to differentiate between different mechanisms occurring at Eu(III)/calcite interface.

A first set of experiments using 1 and 5 g.L^{-1} of calcite equilibrated suspensions (SOLVAY (SOCAL U1-R)) with Eu(III) concentration ranging from 10^{-3} to 10^{-6} mol.L^{-1} revealed a complete removal of Eu(III) from aqueous solution. This was true for contact times ranging from 1 day to 6 months. Another set of macroscopic experiments were performed at 1 g.$L^{-1}$of calcite SOLVAY (SOCAL U1-R) using CPES under atmospheric conditions (which imposes a pH=8.3 for the system). Initial concentrations of 10^{-6}, 10^{-5} and 5×10^{-5} mol.L^{-1} Eu(III) were used with a contact time of 1 week. In all cases, Eu(III) was completely removed from the solution.

The results obtained under atmospheric conditions are not surprising, because many authors observed a similar effect. High affinity of Eu for calcite under atmospheric conditions can be compared with previous works. Zhong and Mucci [70] measured also sorption of REE (6.5×10^{-7}

mol.L^{-1}) onto calcite under seawater conditions and reported a high affinity of calcite for Eu(III) under atmospheric conditions. In Piriou et al. [6] study, Eu(III) is adsorbed by calcite especially on hydrated/hydroxylated sites. By co-precipitation experiments, Stipp et al. and Lakshtanov et al. [10, 71] reported a high affinity of Eu(III) by calcite. Similar sorption under atmospheric conditions by batch type experiments were reported by Hofmann et al. [9], where sorption was important as well.

Figure 3.9 presents the sorption of Eu(III) onto SOLVAY (SOCAL U1−R) powder at pCO_2=10^{-2} atm, imposing an equilibrium pH of 7.5±0.1. For that, a series of CPES containing fresh calcite (s/L = 1 g.L^{-1}) were spiked with Eu(III) stock solution to obtain the desired concentrations (10^{-6}, 10^{-5}, 10^{-4} and 10^{-3} mol.L^{-1}). Two contact times, i.e. 1 day and 1 week, were investigated.

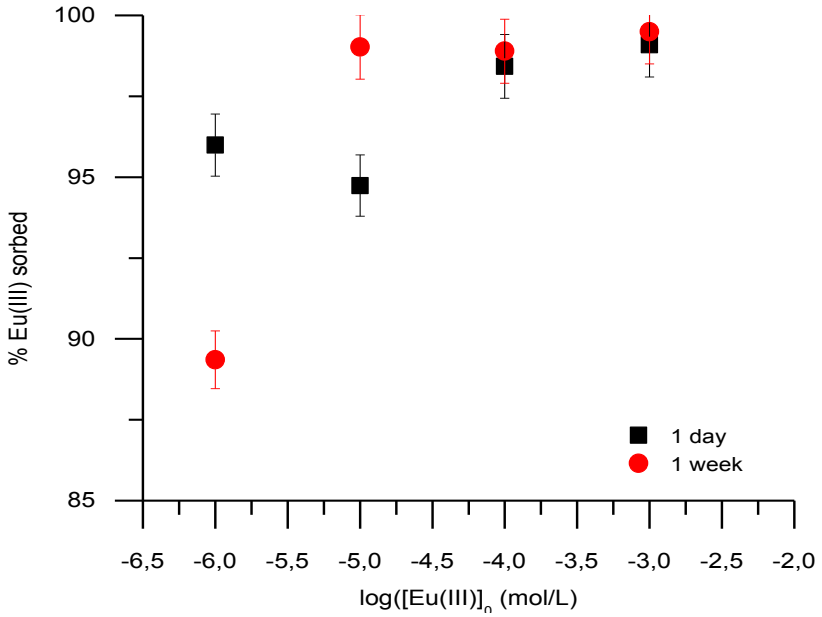

Figure 3.9: Sorption of Eu(III) onto calcite ([Eu]$_0$ = 10^{-6}, 10^{-5}, 10^{-4} and 10^{-3} mol.L^{-1}, I=10^{-1} mol.L^{-1} (NaCl), pCO_2 = 10^{-2} atm, pH=7.5±0.1, s/L=1 g.L^{-1}).

As a function of time, Eu(III) has a different behavior. From the results presented in Figure 3.9, almost 100 % sorption is reached for the two highest concentrations. For lower concentrations, the sorption fractions are slightly lowered. This slight decrease on sorption percentages can be

due to different speciation of Eu(III) in aqueous solution. Further experiments with longer contact times are required to understand undergoing mechanisms at $pCO_2=10^{-2}$ atm.

According to results obtained by Zavarin et al. [73], for 1% CO_2 and pH ranging between 7 and 7.5, the sorption fraction for a concentration of 10^{-7} mol.L^{-1} Eu(III) was 100%. This result can be compared with our experimental results for 10^{-6} mol.L^{-1} concentration. Even if in our case sorption fractions were below 100%, one possible explanation is a difference in the specific surface areas of calcites (18.3 m².g^{-1}for SOLVAY(SOCAL U1-R) compared to 0.26 m².g^{-1} in the study of Zavarin et al. [73]).

As a conclusion, our results are in agreement with the previous studies, especially for low concentrations, but novel since investigations under high Eu(III) concentrations and pH=8.3±0.1 at room temperature were not provided to our knowledge. Small differences between experiments at pCO_2 = 1 atm and 10^{-2} atm were highlighted for the lowest concentrations, which may be explained by a different behavior towards calcite.

In order to depict sorption mechanisms and species formed at Eu(III)/calcite interface, spectroscopic studies were carried out and described in sections below.

3.3. Eu(III) sorbed onto calcite powders: TRLFS investigations

3.3.1. Experiments under $pCO_2=10^{-3.5}$ atm

TRLFS measurements are aiming at determining the speciation of Eu(III) at calcite/water interface. Incorporation of Eu(III) into calcite bulk represents a very important retardation process and several studies concerning this topic are available in the literature [4-6, 114]. While the existent literature data are mainly focused on low concentrations of Eu(III) −precipitation studies, our work investigates in details various Eu(III) concentrations interacting with calcite which complete the current literature data and close existing gaps. Four different concentrations of Eu(III) (10^{-6}, 10^{-5}, 10^{-4} and 10^{-3} mol.L^{-1}) and several contact times between 4 hours and 6 months were selected in order to obtain a better understanding of Eu(III) behavior with calcite. The highest Eu(III) concentrations like 10^{-4} and 10^{-3} mol.L^{-1} were chosen to observe which precipitates can be formed on adsorbent's surface. Selected fluorescence emission spectra for the 4 concentrations after 4 hours are presented in Figure 3.10.

The lack of detectable fluorescence intensity in the supernatants confirms the complete removal of Eu(III), as observed by batch experiments, no matter the initial concentration. This was true not only for short reaction time, but also up to 6 months.

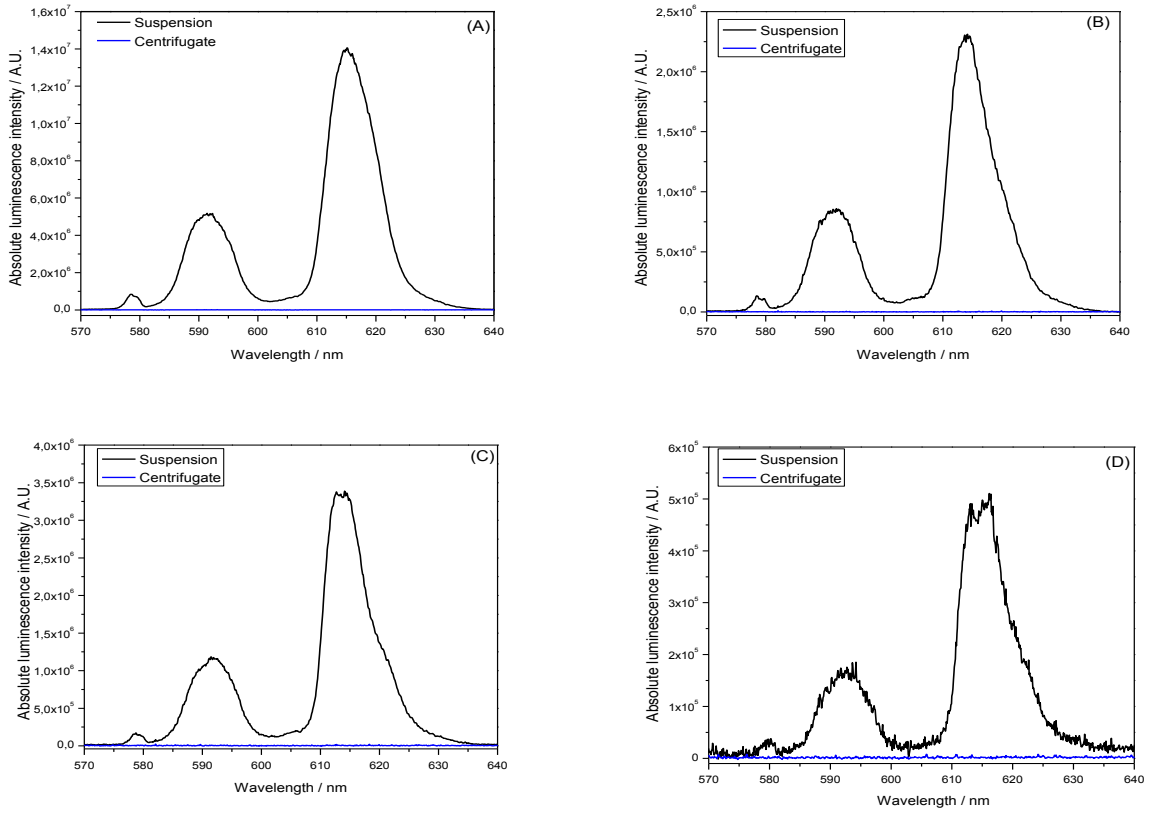

Figure 3.10: Luminescence emission spectra of Eu(III) suspension (black) and supernatant (blue) ($[Eu]_0 = 10^{-3}$ (A), 10^{-4} (B), 10^{-5} (C) and 10^{-6} (D) mol.L^{-1}, I=10^{-1} mol.L^{-1} (NaCl), s/L =5 g.L^{-1}, $pCO_2 = 10^{-3.5}$ atm, pH=8.3±0.1, t = 4 hours.

The fluorescence emission spectra for the 4 distinct concentrations and their evolution with time are presented in Figure 3.11.

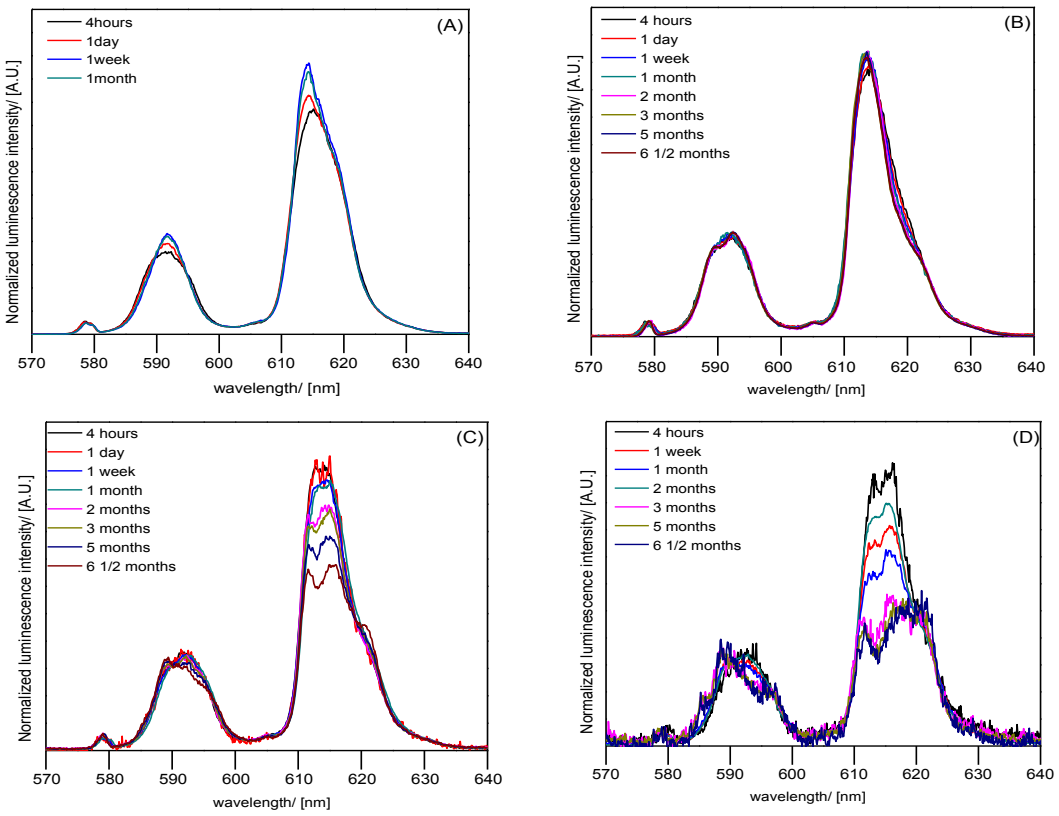

Figure 3.11: Luminescence emission spectra of Eu(III) sorbed onto calcite($[Eu]_0 = 10^{-3}$ mol.L^{-1} (A),10^{-4} mol.L^{-1} (B), 10^{-5} mol.L^{-1} (C) and 10^{-6} mol.L^{-1} (D), I=10^{-1} mol.L^{-1} (NaCl), s/L = 5 g.L^{-1}for samples 4 hours – 1 month and 1 g.L^{-1} for samples after 1 month. pCO_2 = $10^{-3.5}$ atm, pH=8.3±0.1).

For the lower concentrations, 10^{-6} and 10^{-5} mol.L^{-1} Eu(III), a splitting of the bands $^5D_0 \rightarrow {}^7F_1$ and $^5D_0 \rightarrow {}^7F_2$ and a decrease of the luminescence intensity from 4 hours to 6 months is noticed. The latter, can be due to incorporation of species into bulk caused by precipitation/dissolution of calcite.

An example of a time−resolved luminescence measurement (time-dependency spectra) of Eu(III) sorbed onto calcite is presented in Figure 3.12.

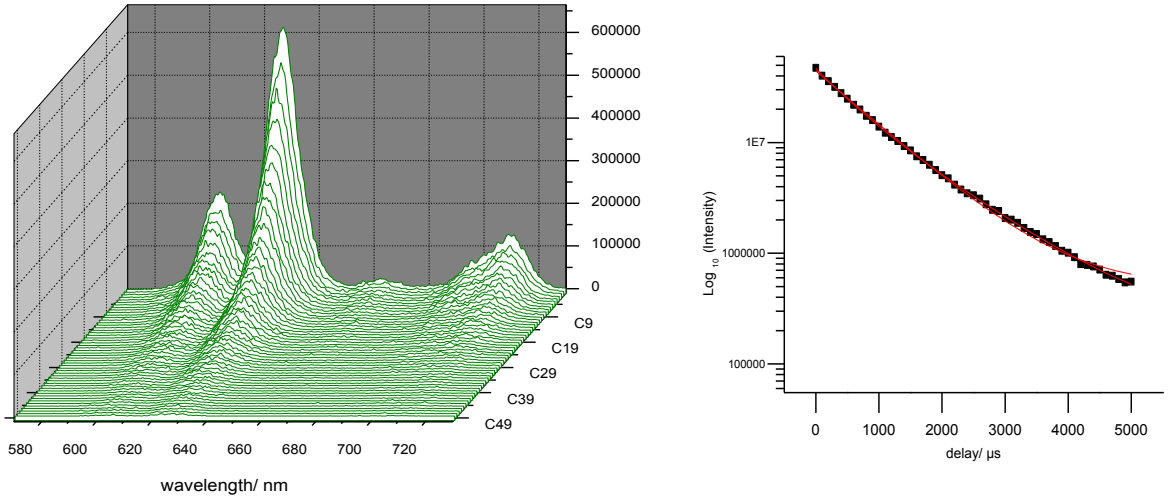

Figure 3.12: Time−resolved luminescence spectra (left) and decay curve (right) of $[Eu(III)]_0 = 10^{-4}$ mol.L^{-1}, I=10^{-1} mol.L^{-1}, s/L=5.g.L^{-1} $CaCO_3$, $pCO_2 = 10^{-3.5}$ atm, pH=8.3±0.1, t=1 month.

In the time-resolved spectra the luminescence intensity decreases as delay time increases. The obtained emission decay of Eu(III)/calcite species in Figure 3.12 is biexponential. This confirms the presence of two distinct species with luminescence lifetimes of 575±23 µs and 1241±32 µs which correspond to 1.2±0.5 H_2O and 0.2±0.5 H_2O, respectively, in the first coordination shell. This would indicate the formation of inner−sphere surface complexes. The lifetimes and corresponding water molecules of Eu(III) sorbed onto calcite are summarized in Table 3.5.

Table 3.5: Luminescence lifetimes and corresponding number of water molecules of Eu(III) sorbed onto calcite as a function of time (s/L=1 and 5 g.L^{-1}, $pCO_2 = 10^{-3.5}$ atm, pH=8.3±0.1).

Stirring time	10^{-3} mol/L Eu(III)		10^{-4} mol/L Eu(III)		10^{-5} mol/L Eu(III)		10^{-6} mol/L Eu(III)	
	t1	t2	t1	t2	t1	t2	t1	t2
4 hours	153 ± 4 (6.4 ± 0.5 H_2O)	342 ± 3 (2.5 ± 0.5 H_2O)	531 ±14 (1.4±0.5 H_2O)	1070 ± 18 (0.4 ± 0.5 H_2O)	608 ± 25 (1.1±0.5 H_2O)	1412±33 (0.1 ± 0.5 H_2O)		
1 day	190 ± 4 (5.0 ± 0.5 H_2O)	417 ± 3 (1.9 ± 0.5 H_2O)	590 ± 25 (1.2 ± 0.5 H_2O)	1160 ± 39 (0.3 ± 0.5 H_2O)	599 ± 20 (1.2 ± 0.5 H_2O)	1463 ± 25 (0.1 ± 0.5 H_2O)		
1 week	195 ± 4 (4.9 ± 0.5 H_2O)	434 ± 2 (1.8 ± 0.5 H_2O)	591 ± 25 (1.2±0.5 H_2O)	1189 ± 31 (0.3±0.5 H_2O)	709 ± 21 (0.9 ± 0.5 H_2O)	1765 ± 28 (0.0 ±0.5H_2O)	859 ± 37 (0.6 ± 0.5 H_2O)	2733 ± 105 (0.0 ±0.5H_2O)
1 month	211 ± 5 (4.5 ± 0.5 H_2O)	491 ± 3 (1.6 ± 0.5 H_2O)	575 ± 23 (1.2 ± 0.5H_2O)	1241±32 (0.2 ± 0.5H_2O)	827 ± 21 (0.7 ± 0.5 H_2O	1995 ± 44 (0.0 ± 0.5 H_2O)	894 ± 22 (0.6 ± 0.5 H_2O)	2535 ± 49 (0.0 ± 0.5 H_2O)
5 months	/	/	780± 60 (0.8 ± 0.5 H_2O)	1892 ± 92 (0.0 ± 0.5 H_2O)	616 ± 15 (1.2 ± 0.5 H_2O)	2095 ± 36 (0.0 ± 0.5 H_2O)	578 ± 61 (1.2 ± 0.5H_2O)	3151 ± 130 (0.0 ± 0.5 H_2O)
6 months	/	/	675 ± 12 (1.1 ± 0.5 H_2O)	1807 ± 26 (0.0 ± 0.5 H_2O)	735 ± 29 (1.0 ± 0.5 H_2O	2797 ± 92 (0.0 ± 0.5 H_2O)	912 ± 157 (0.5 ± 0.5 H_2O)	3772 ± 174 (0.0 ± 0.5 H_2O

For the upper limit Eu(III) concentration, 10^{-3} mol.L^{-1}, the time-dependent experiments were done from 4 hours to 1 month. Two distinct species were identified, one with a shorter lifetime between 153 and 211 μs and another with a longer lifetime between 342− 491 μs. This range of lifetimes can be attributed either to Eu(III) carbonate precipitates (shorter lifetime) or to sorbed or complexed Eu/calcite species (longer lifetime); the presence of 1−2 water molecules for the second species would indicate that inner−sphere surface complexes are formed.

Decreasing the Eu(III) concentration to 10^{-4} mol.L^{-1}, also two species were identified. The shorter lifetimes of 531−732 μs correspond to approximatively one water molecule in the first coordination sphere. These lifetimes can be attributed to a surface species. The longer lifetime increases with time from 1070 μs to 1807 μs, which would be in agreement with a graduate loss of the last water molecule. It can be attributed to an incorporated Eu(III) species after 2 months, which is in agreement with earlier studies evidencing incorporation of Eu(III) into carbonate phases [4, 6, 7, 62]. If we take into account that the studies mentioned before were made using low concentrations of Eu(III) (10^{-7}–10^{-6} mol.L^{-1}), this study proves that this phenomena is possible to occur even for higher Eu(III) concentrations, namely 10^{-4} mol.L^{-1}. This incorporation could be explained by the dynamic dissolution equilibrium of calcite. During the dissolution/re-crystallization process, Ca^{2+} ions would be replaced by Eu^{3+} which subsequently incorporates in the structure of calcite.

The 10^{-5} mol.L^{-1} Eu(III) concentration has a similar behavior like 10^{-4} mol.L^{-1}. The first lifetimes ranging from 599 to 827 μs corresponds to one remaining water molecule in the first coordination sphere and indicates the formation of a surface complex. The second lifetime increases likewise with time from 1412 μs to 2797 μs, corresponding to a total loss of water molecules, showing a trapping of europium−calcite species in the upper layer of calcite. It has to be mentioned that the total loss of water molecules around Eu(III) seem to proceed earlier than for 10^{-4} mol L^{-1}, the process being visible after 1 week.

The lowest investigated Eu(III) concentration, 10^{-6} mol.L^{-1}, presents also two lifetimes like the previous samples. The shorter lifetime has values comprised between 578 μs and 912 μs which are not in a graduate increasing. The hydration sphere of Eu(III) is not completely lost, which can indicate the formation of a surface complex. The higher lifetime increases gradually as a

function of reaction time from 2733 µs after 1 week to 3772 µs after 6 ½ months. The absence of water molecules after 1 week of reaction time indicates incorporation of Eu(III).

For the lower concentrations, lifetimes are comparable with those identified by Marques Fernandes et al. [4], where the values exceed 3000 µs for the same Eu(III) concentration and were attributed to incorporated species.

A possible mechanism that characterize the process, according to Marques−Fernandes et al. [4] is that two Ca^{2+} atoms are replaced with one Eu^{3+} atom and one Na^{+} atom. This phenomena is due to the capacity of calcite to precipitate/recrystallize in solution [10]. Also Schmidt et al. [115] presented the solid solution formation where solutes (trace metals) are incorporated in "solvent" which is assumed to be calcite. In the case of Eu(III), the charge compensation is provided by coupled substitution mechanism and the influence of Na^{+}/K^{+} ions in charge compensation has been highlighted [70, 115].

The results are also in agreement with former fluorescence data where Eu(III) co-precipitation with calcite was studied [4-6, 9, 116]. Comparing the results by batch type experiments from Hofmann et al. [9] using an Eu(III) concentration of 10^{-6} mol.L^{-1}, they identified two species which lifetimes are only of 200±20 µs and 740±90 µs after 1 month. In the case of mixed flow reactor experiments, the lifetimes exceed 3000 µs (3500±450 µs and 3700± 200 µs). Even longer lifetimes of 9.2 ms were identified in the three samples investigated by Yeghicheyan [7] for Eu(III) sorbed onto calcite. Lower lifetimes between 420 µs and 3500 µs were obtained by Yeghicheyan [7] for samples containing a mixture of calcite, vaterite and aragonite.

From this study, we can conclude that the reaction of Eu(III) with calcite has different behavior over time and Eu(III) concentrations. Eu(III) is first adsorbed, then by re-crystallization process it is trapped into bulk structure under graduate loss of water molecules. For low Eu(III) concentration (10^{-6} mol.L^{-1}), the incorporation was observed rapidly (even after 1 week reaction time). In contrast, for high Eu(III) concentration (10^{-3} mol.L^{-1}) no incorporation could be observed with time (up to 1 month), instead of that formation of Eu(III) carbonate precipitates beside sorbed species was assumed. The lack of incorporated species at high Eu(III) concentration is possibly caused by the relatively high amount on precipitated and sorbed Eu(III) species which covered the luminescence of incorporated Eu(III).

3.3.2. Experiments under $pCO_2=10^{-2}$ atm

The impact of pCO_2 on the interaction of Eu(III) was investigated. Samples were prepared as described in section 2.4.2 and investigated by TRLFS in order to determine the speciation. Fluorescence emission spectra were recorded for Eu(III) (10^{-6}, 10^{-5}, 10^{-4} and 10^{-3} mol.L^{-1}) after 1 day and 1 week stirring time using a s/L ratio of 1 g.L^{-1}(Figure 3.13).

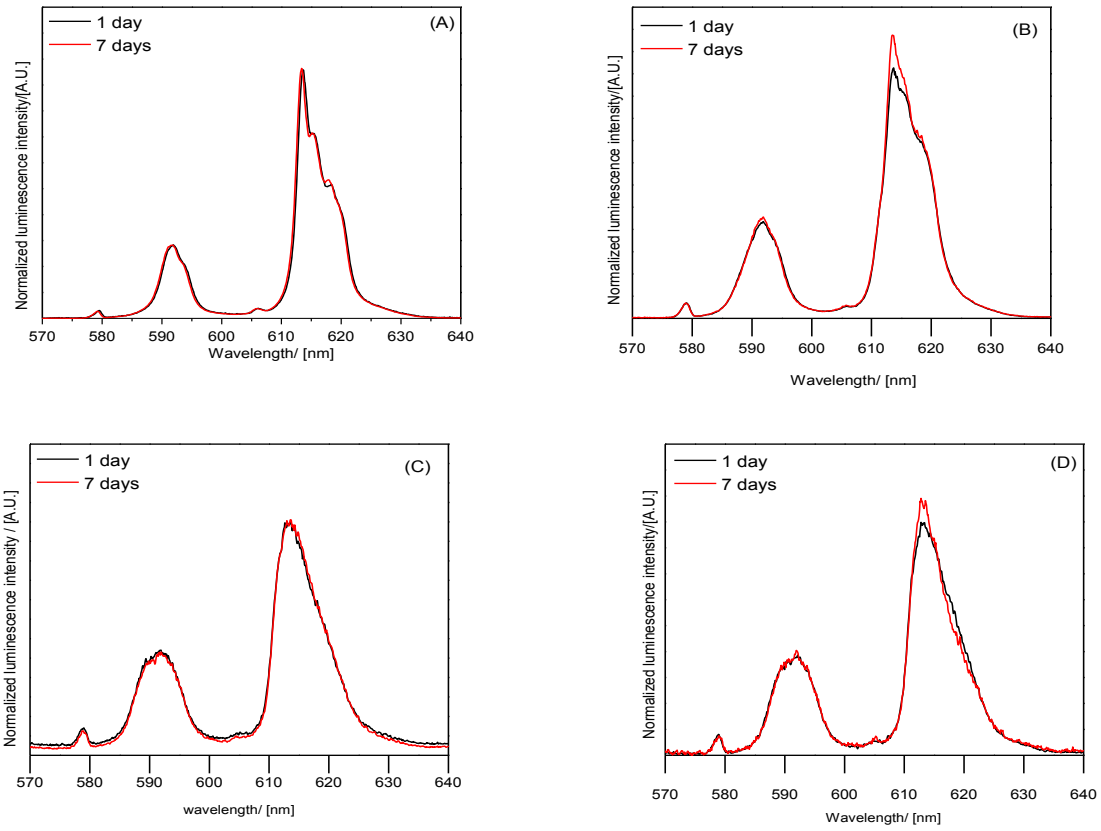

Figure 3.13: Luminescence emission spectra (A) 10^{-3} mol.L^{-1} Eu(III), (B) 10^{-4} mol.L^{-1} Eu(III), (C) 10^{-5} mol.L^{-1} Eu(III) and (D) 10^{-6} mol.L^{-1} Eu(III) sorbed on calcite (1 g.L^{-1}), stirred for 1 day and 7 days under $pCO_2=10^{-2}$ atm.

At Eu(III) concentrations of 10^{-3} and 10^{-4} mol.L^{-1}, the spectra show a threefold splitting of the $^5D_0 \rightarrow {}^7F_2$ transition and a twofold splitting of the $^5D_0 \rightarrow {}^7F_2$transition, similar to the luminescence spectra observed for CPES solutions (see chapter 3.1) which was assigned to $Eu_2(CO_3)_3 \cdot 2\text{-}3\ H_2O_{(s)}$ [56]. At lower Eu(III) concentrations no band splitting is observed.

For lifetime determination, the delay time follows a monoexponential or biexponential decay law confirming the presence of one or two Eu(III)/calcite species in the sample. The lifetime values are summarized in Table 3.6.

Table 3.6: Luminescence lifetimes of Eu(III) sorbed onto calcite under $pCO_2=10^{-2}$ atm and $[Eu(III)]_0 = 10^{-3}$, 10^{-4}, 10^{-5} and 10^{-6} mol.L^{-1}.

[Eu(III)] (mol.L^{-1})	Lifetimes (µs)			
	1 day		1 week	
	t_1	t_2	t_1	t_2
10^{-3}	416 ± 4 (1.9 ± 0.5 H_2O)		554 ± 8 (1.3 ± 0.5 H_2O)	
10^{-4}	178 ± 11 (7.5 ± 0.5 H_2O)	516 ± 40 (1.6 ± 0.5 H_2O)	259 ± 22 (3.5 ± 0.5 H_2O)	559 ± 10 (1.4 ± 0.5 H_2O)
10^{-5}	326 ± 28 (2.6 ± 0.5 H_2O)	794± 12 (0.6 ± 0.5 H_2O)	534 ± 31 (1.4 ± 0.5 H_2O)	1104 ± 62 (0.4± 0.5 H_2O)
10^{-6}	530 ± 33 (1.4 ± 0.5 H_2O)	1051 ± 66 (0.2 ± 0.5 H_2O)	593 ± 38 (1.2 ± 0.5 H_2O)	1289 ± 99 (0.2 ± 0.5 H_2O)

For all Eu(III) concentrations, the values of fluorescence lifetimes increased with reaction time.

For the highest Eu(III) concentration, 10^{-3} mol.L^{-1}, the decay was fitted best with the monoexponential decay law giving only one species with lifetimes of 416 µs after 1 day and 554 µs after 1 week, corresponding to 1.9 ± 0.5 and 1.3± 0.5 water molecules in the first coordination sphere, respectively. Considering the spectra shape, this might be attributed to a Eu(III) carbonate species sorbed onto calcite.

For the lower concentrations, 10^{-4}, 10^{-5} and 10^{-6} mol.L^{-1} Eu(III), biexponential fit was applied resulting in two distinct species.

For 10^{-4} mol.L^{-1} Eu(III) the longer lifetime is similar to that at 10^{-3} mol.L^{-1} Eu(III) and might also be assigned to an Eu(III) carbonate species sorbed onto calcite, considering the spectra shape. After 1 day reaction time, the shorter lifetime of 178 µs can be attributed to an aqueous Eu(III) carbonate species (maybe $EuCO_3^+$) [65]. After centrifugation and measuring the supernatant, luminescence signal of Eu(III) was still present (Figure 3.14). The luminescence decay was mono-exponential resulting in a lifetime of 252 ± 20 µs. This confirms the assignment made above.

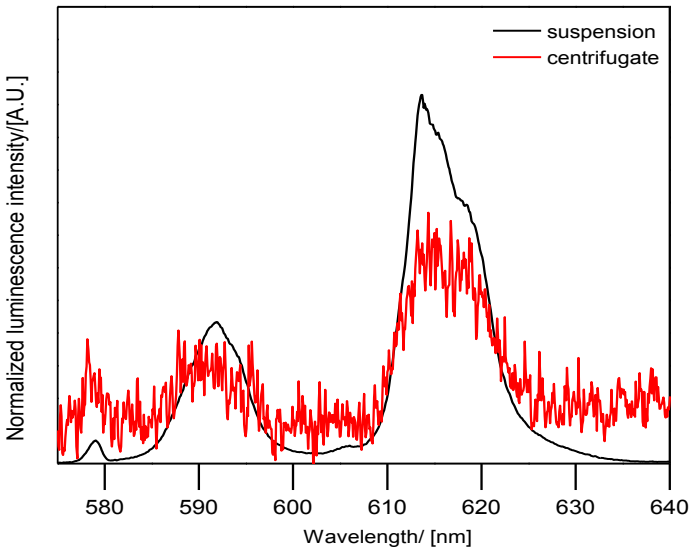

Figure 3.14: Normalized spectra of 10^{-4} mol.L^{-1} Eu(III), sorbed on calcite (1 g.L^{-1} $CaCO_3$) stirred for 1 day under $pCO_2=10^{-2}$ atm. The black lines represent the suspension and the red line the supernatant.

After 1 week reaction time and a concentration of 10^{-4} mol.L^{-1} both luminescence lifetimes can be dedicated to sorbed Eu(III)/calcite species. After centrifugation, there is no Eu(III) left in supernatant neither by TRLFS or ICP-MS.

For 10^{-5} mol.L^{-1} Eu(III), the shorter lifetime after 1 day may also be attributed to an aqueous Eu(III) carbonate species due to the presence of Eu(III) in supernatant after centrifugation (ICP-MS results, see section 3.2). The longer lifetime of 794 µs can be assigned to Eu(III)/calcite sorbed species. For 1 week contact time, both lifetimes can be attributed to sorbed species. The loss of almost all H_2O molecules indicates that the sorbed species are inner-sphere surface complexes.

For the lowest concentration, 10^{-6} mol.L^{-1}, the two calculated luminescence lifetimes after 1 day reaction time (530 µs and 1051 µs) are attributed both to sorbed species. After 1 week, the shorter lifetime of 593 µs can be assigned to sorbed species and the longer one (1289 µs) may correspond to slow/progressive incorporation into the bulk.

Comparing the results obtained under two distinct pCO_2, similarities and differences can be noticed.

The main general observation is the influence of reaction time on Eu(III) speciation onto calcite. The changes in the first coordination sphere of Eu(III) are given by the number of water molecules. As the reaction time increases, the number of water molecules decreases gradually. This implies that first Eu(III) is precipitated and/or sorbed onto the mineral as inner-sphere surface complexes, then its incorporation occurs by slow re-crystallization of calcite with time under graduate loss of hydration sphere.

However, a variation of the pCO_2 leads to significant differences in Eu(III)/calcite speciation. Except for Eu(III) concentration of 10^{-3} mol.L^{-1}, the calculated luminescence lifetimes are longer under atmospheric conditions compared to $pCO_2=10^{-2}$atm and same reaction time, standing for a faster surface complexation and incorporation process of Eu(III) into calcite under atmospheric conditions. At 10^{-3} mol.L^{-1} Eu(III) only precipitation and/or sorption could be observed for both pCO_2 conditions within the investigated timescale, whereas for the lower Eu(III) concentrations under $pCO_2 = 10^{-2}$ atm after 1 day reaction time aqueous Eu(III) carbonate species could be observed. Under atmospheric conditions complete sorption of Eu(III) was noticed already after 4 hours reaction time. At 10^{-4} mol.L^{-1} Eu(III) under atmospheric conditions incorporation into calcite could be detected after 3 months reaction time, while for 10^{-5} and 10^{-6} mol.L^{-1} Eu(III) actually after 1 week. In contrast, with higher pCO_2 (10^{-2} atm) the beginning of incorporation could be detected only for 10^{-6} mol.L^{-1} Eu(III) after 1 week reaction time and not for 10^{-5} mol.L^{-1} Eu(III).

As presented by Piriou et al. [6], Eu(III) can be included in a hydroxylated/hydrated sites for an Eu(III) concentration between 2 and 7.6×10^{-5} mol.m^{-2} for 5 hours contact time. These concentrations can be compared to ours, where for an Eu(III) concentration of 10^{-3} mol.L^{-1}, we obtain values of 1.09×10^{-5} mol.m^{-2}.The main finding in this study is that incorporation of Eu(III) could be observed under atmospheric conditions even for high concentrations such as 10^{-4} molL^{-1} Eu(III), whereas in former studies the initial Eu(III) concentration for incorporation experiments is very low, about 10^{-6} mol L^{-1} [4, 6, 9].

3.3.3. Experiments with calcite single crystals in CPES solutions under $pCO_2=10^{-3.5}$ atm

Earlier studies have been focused on interaction of calcite single-crystals with various elements like U, Se [117-120]. Based on these investigations and RBS requirements we have oriented our research work on single crystals too. A set of fluorescence measurements onto single crystals was performed. For contact time inferior to 1 week, no luminescence could be detected. So, only samples starting from 1 week up to 2 months contact time were recorded by TRLFS. Similar to the powder investigations, emission spectra and lifetimes were determined with the purpose to obtain speciation onto single crystals. The emission spectra of Eu(III) sorbed onto calcite crystals are presented in Figure 3.15.

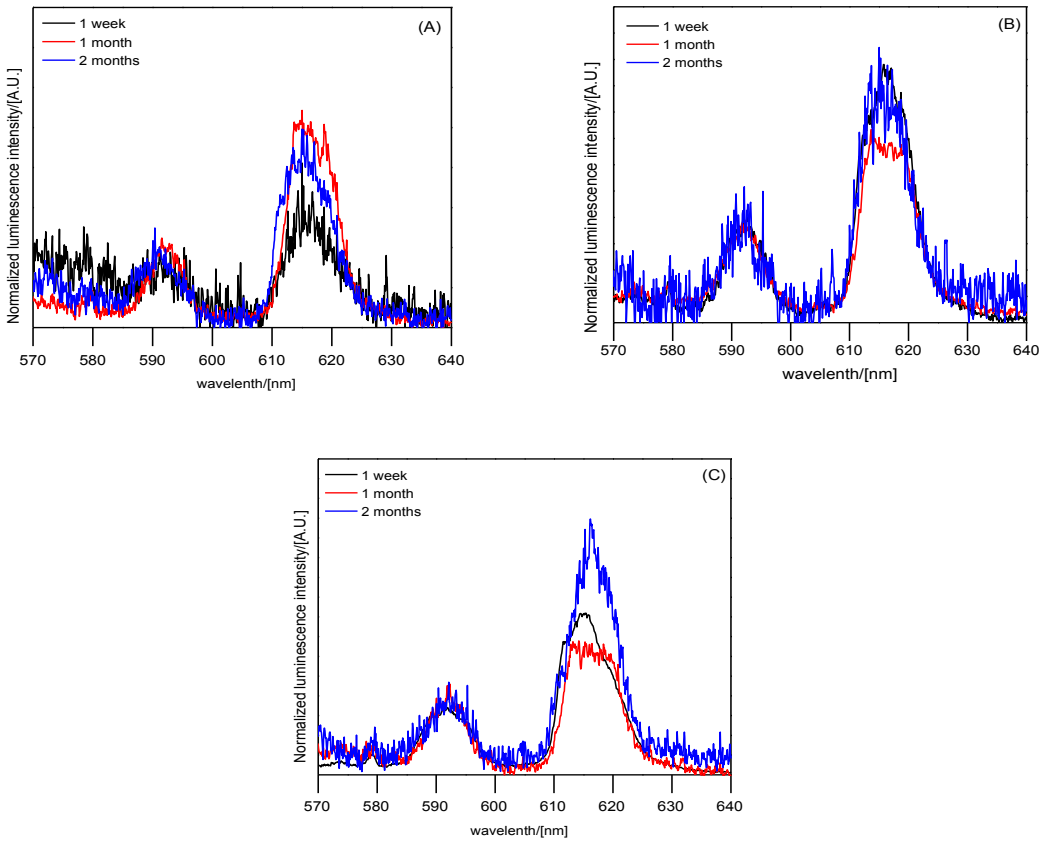

Figure 3.15: Luminescence emission spectra of Eu sorbed on calcite single crystals (A) 10^{-4} mol.L^{-1}, (B) 10^{-5} mol.L^{-1} and (C) 10^{-6} mol.L^{-1} Eu(III) under atmospheric condition ($pCO_2=10^{-3.5}$ atm), pH=8.3±0.1.

The incoherence of spectra intensities can be due to the size of crystals and the inhomogeneous distribution of Eu(III) on the crystal surface.

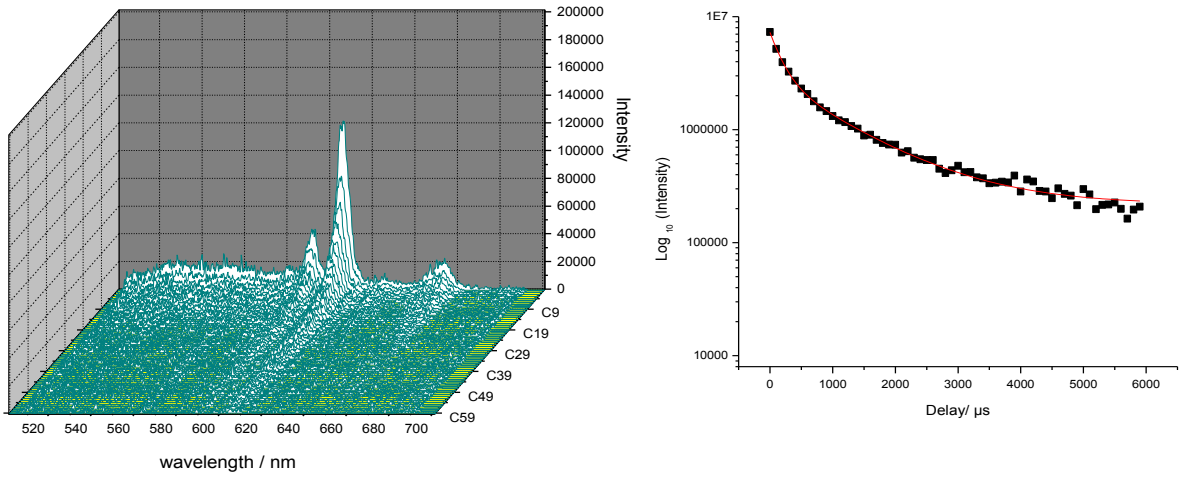

Figure 3.16: Time−resolved luminescence spectra (left) and time decay curve (right) of $[Eu(III)]_0 = 10^{-4}$ mol.L^{-1}, $CaCO_3$ single crystal, I=10^{-1} mol.L^{-1} NaCl, $pCO_2 = 10^{-3.5}$ atm, pH=8.3±0.1 and t=1 month.

Figure 3.16 depicts an example of a time-resolved luminescence measurement for 10^{-4} mol.L^{-1} Eu(III) after 1 month stirring time. The obtained emission decay is biexponential which confirms the presence of two distinct species with luminescence lifetimes of 214± 6 µs and 1195 ± 35 µs. The shorter lifetime may be attributed to a Eu(III) precipitate, whereas the longer lifetime (calculated number of water molecules: 0.3±0.5 H_2O) can be attributed to Eu(III)/calcite sorbed species.

All luminescence lifetimes are listed in Table 3.7.

Table 3.7: Luminescence lifetimes and corresponding water molecules of Eu(III) sorbed onto calcite single crystals.

Stirring time	Lifetimes (µs)					
	10^{-4} mol/L Eu(III)		10^{-5} mol/L Eu(III)		10^{-6} mol/L Eu(III)	
	t_1	t_2	t_1	t_2	t_1	t_2
1 week	615 ± 24 (1.1±0.5 H_2O)		250 ± 15 (3.7±0.5 H_2O)	1298 ± 30 (0.2±0.5 H_2O)	234 ± 22 (3.9±0.5 H_2O)	1206 ± 23 (0.2±0.5 H_2O)
1 month	214 ± 6 (4.4±0.5 H_2O)	1195 ± 35 (0.3±0.5 H_2O)	352 ± 21 (2.4±0.5 H_2O)	1138 ± 54 (0.1±0.5 H_2O)	-	-
2 months	154 ± 16 (6.3±0.5 H_2O)	1272 ± 73 (0.2±0.5 H_2O)	193 ± 29 (4.9±0.5 H_2O)	1100 ± 80 (0.3±0.5 H_2O)	352 ± 21 (2.4±0.5 H_2O)	1538 ± 54 (0.1±0.5 H_2O)

Since the results obtained onto powders reveal incorporation of Eu(III) by a graduate loss of water molecules in the first coordination sphere as a function of contact time, for single crystals the situation seems to be similar.

For the upper limit concentration, 10^{-4} mol.L^{-1} Eu(III), after 1 week only one Eu(III)/calcite sorbed species was identified. For 1 and 2 months, biexponential decay was matching best resulting in two distinct species, which can be attributed to Eu(III) precipitate for the shorter lifetime and to Eu(III)/calcite sorbed species for the longer lifetime.

For the intermediate concentration (10^{-5} mol.L^{-1} Eu) the measured lifetimes are expressing a biexponential behavior obtaining two distinct species. The luminescence lifetimes hardly vary with contact time. The shorter lifetime (between 193 – 352 µs) can be assigned to Eu(III) precipitate, and the longer one (1100 – 1300 µs) could be assigned to inner-sphere surface complex species.

For the lowest concentration, 10^{-6} mol.L^{-1} Eu(III), the shorter lifetime can be attributed to Eu(III) surface precipitate as in case of higher concentration presented above. The longer lifetime increases with contact time from 1206 µs (1 week) to 1538 µs (2 months) corresponding to almost no water molecules, which can show a progressive incorporation into the bulk lattice. Compared to powder studies under atmospheric conditions, the incorporation process seems to occur more slowly. This might be due to the much higher surface area of powder compared to the bigger single crystals.

Applying TRLFS on the Eu−NaCl−CO_2−calcite system, we can observe that Eu(III) presents a different behavior towards calcite depending on the pCO_2, the Eu(III) concentration, the contact time and the morphology of calcite. Generally, three kinds of Eu(III) species could be observed: first (especially at high Eu(III) concentrations) Eu(III) precipitates are formed. Then, a second mechanism which has been evidenced in all the concentration range is a sorption in the form of inner-sphere surface complexes. The last step is the incorporation of Eu(III) into the calcite structure. Under atmospheric conditions, at the highest Eu(III) concentration of 10^{-3} mol.L^{-1} and a contact time up to 1 month only precipitated and sorbed species could be observed. At lower concentration, 10^{-4} mol.L^{-1}, incorporation of Eu(III) into calcite could be observed after 2 months contact time. At lower Eu(III) concentrations (10^{-5} – 10^{-6} mol.L^{-1}), the incorporation process was even faster, starting already after 1 week contact time. The lower the Eu(III) concentration the faster is the further incorporation, deducible from the longest luminescence lifetimes at lowest Eu(III) concentration. This process is not only time- and concentration-dependent but also controlled by pCO_2. An advanced pCO_2 seems to cause a delay of the incorporation of Eu(III) into calcite. Also the morphology of calcite influences the time of incorporation. For calcite powder samples this process occurs much faster than for single crystals due to the much higher surface area in powdered solid compared to single crystals.

In order to have a deeper understanding of Eu(III) incorporation into calcite, RBS was used as a second technique in order to determine depth profile concentrations. This study presents a novel methodology based on the application of the nuclear ion beam technique Rutherford Backscattering Spectrometry to evaluate depth concentration profiles of heavy elements in a carbonate matrix. SEM−EDXS measurements were performed, too.

3.4. RBS and SEM-EDXS study of Eu(III) interaction with calcite

Rutherford Backscattering Spectrometry is a powerful tool to identify the element distribution on the mineral surface as a function of depth. Hence, it is of major interest in the case of our study if we take into account the results of the TRLFS study, which are in agreement with an incorporation mechanism, likely by a dissolution/precipitation process. Indeed, RBS will confirm or not the incorporation and will help to quantify the extent in depth and the kinetics of the process. RBS experiments were carried out using two types of ion beams: milli and micro beam, in order to get more information on the distribution of Eu(III) on the surface of calcite.

The samples that were measured by RBS were also investigated by SEM/EDXS. The purpose of these measurements is to investigate the surface of the crystals before and after Eu(III) sorption, check the morphology, homogeneity and distribution of possible europium-precipitates. Eu(III) surface concentrations were also determined. These results will be compared with the data obtained by RBS technique.

Additionally, the data obtained by these techniques will be examined and compared with previous results obtained by TRLFS onto single crystals in CPES solutions.

3.4.1. RBS milli-beam study of Eu(III) interaction with calcite powders

Two types of measurements were performed, using a milli−beam on two distinct types of samples, calcite powders (SOLVAY (SOCAL U1−R) and OMYA (BL 200)). The selected concentrations were high (10^{-4} and 10^{-3} mol.L^{-1}) because precipitation of Eu(III) is desired to be observed and because of RBS sensitivity, with the purpose to compare the results with the previous ones, obtained by TRLFS.

The calcite powders, without Eu(III), were analyzed by ICP-MS after total digestion and also by RBS (pellets), and no trace elements that can interact with the signal of Eu(III) were found. Concerning the RBS analyses of sorbed samples, calcite powders reacted during 1 month with Eu(III) and pressed to pellets afterwards have been analyzed with a 4 MeV ^{4}He incident beam. In Figure 3.17, the RBS spectra reacted for 1 month with 10^{-3} mol.L^{-1} Eu(III) onto OMYA (BL200) and SOLVAY(SOCAL U1-R) calcites are regrouped. At this concentration, the signal is more intense than for samples reacted with 10^{-4} mol.L^{-1}.

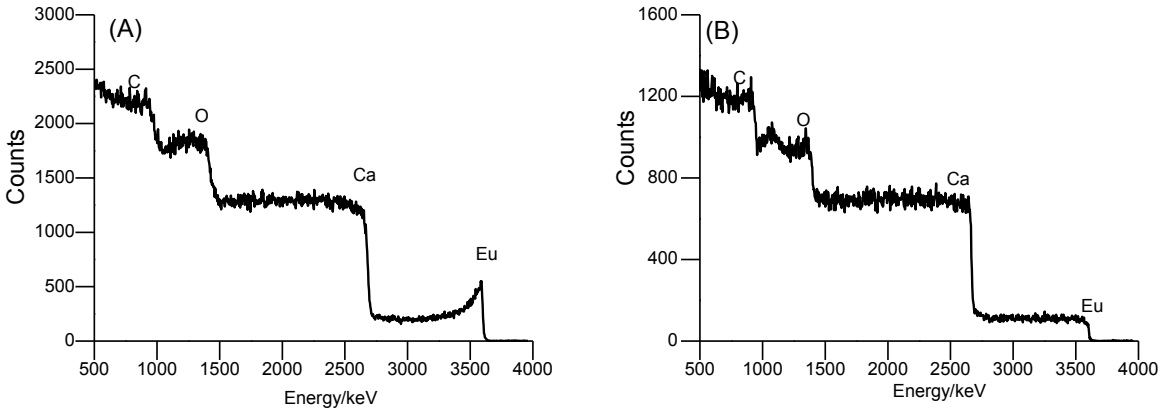

Figure 3.17: RBS spectra of 10^{-3} mol.L^{-1} Eu(III) reacted one month with calcite OMYA (A) and SOLVAY (B) at pH=8.3±0.1.

The spectra are composed of different steps, each one corresponding to a given chemical element. The edge of the step at the higher energy corresponds to the element at the surface of the sample, and the lower energies on each plateau correspond to the element in the depth.

At 4 MeV, the depth resolution is about 35 nm near the surface. It must be noted that two different analyses at different points have been made on each pellet and that a good reproducibility was obtained. Comparing the two powders, the calcite from SOLVAY had a smaller grain size (0.2 µm), and the attention was focused on the powder with higher grain size, both enriched in Eu(III) in the same conditions. It can be observed that the spectrum obtained on OMYA pellets (50 µm grain size) displays a sharp surface peak of Eu(III) that is not present for SOLVAY pellets. A large plateau is observed in our spectra, which intercepts the next element edge.

A first hypothesis of interpretation of the RBS spectrum on Figure 3.17 (A) (intense surface peak followed by a plateau) could be a concentration of Eu(III) on the surface together with a uniform distribution in the bulk of calcite. These features of the spectra should probably be assigned to the existence of artifacts on compacted samples, which are explained on Figure 3.18, where grey areas correspond to europium-rich zones and white areas to europium-poor zones. The alpha beam n°1 is backscattered by europium atoms at the surface of the sample, n°2 by the core of the sample in the case of the OMYA calcite. Beam n°2 intercepts several

grains in the SOLVAY calcite (artifact). Beam n°3 is backscattered by the europium atoms in the grain boundaries (artifact).

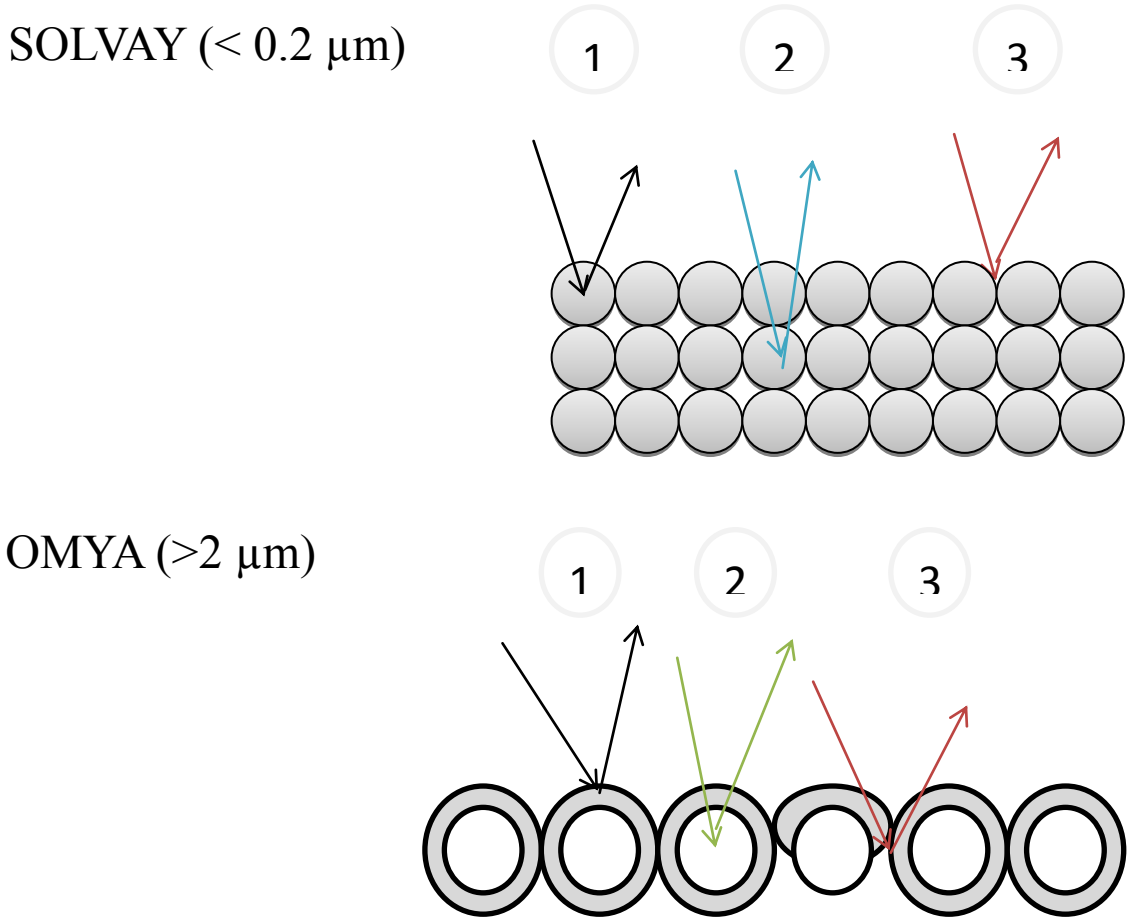

Figure 3.18: Schematic representation of the artifacts on powder samples

The constant signal of Eu(III) (large plateau after the surface peak) is a consequence of the compaction of the grains in the pellets and of the milli-meter beam size which averages the signals from all the probed grains. For the SOLVAY pellets, the artifact is so important that the surface peak cannot be seen. The first points should be spared by this artifact for the OMYA pellets, for which the surface peak is visible. The size and distribution of the powder grains has therefore been investigated by optical microscopy on OMYA powders enriched with Eu(III) without being pressed in pellets. A series of photographs were done by optical microscope, where agglomerates of calcite grains were identified and are presented in Figure 3.19.

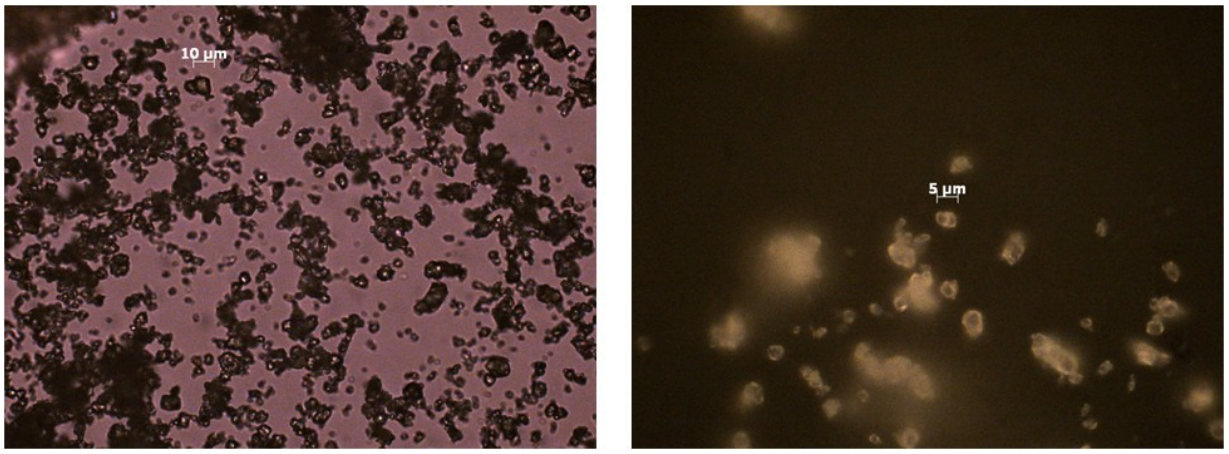

Figure 3.19: Images obtained by optical microscope of grain distribution of powder OMYA (BL 200) calcite general view (left) and a zoom of one selected zone (right).

The grain size of calcite reacted with Eu(III) was determined, and it is observed that from an initial size that was approximated to 50 µm as presented before it decreased to 5−10 µm. This can be due to the stirring mode of samples. The milli-beam RBS spectra of the OMYA samples would then be difficult to interpret. This fact was the initial reason why we chose to perform micro-beam RBS experiments which theoretically give us the possibility to focus on one grain. Anyway, as far as milli-beam experiments are concerned, we had to shift on another type of material to study the interaction mechanism of Eu(III) with calcite: milli-metric single crystals (Alfa Aesar).

3.4.2. RBS milli-beam and SEM-EDXS study of Eu(III) interaction with calcite single crystals Eu(III)

Single crystals were used and put in contact with europium solution (10^{-4} mol.L^{-1}) during 1 week and 1 month. For these preliminary experiments, the pH was increased from 5.5 to 8.3±0.1 by adding NaOH (10^{-1} mol.L^{-1}) because crystals are very small and the dissolution extremely slow, which means that pH cannot be reached very easily as for powders. This method to adjust the pH is not ideal, because of inhomogeneities in the local concentrations and since the pCO_2 could be modified at the bulk surface. For further experiments (microbeam analyses), the CPES method was used as described in Chapter 2.

The crystals were then analyzed separately and the incident beam was set to 1.5 MeV in order to improve the depth resolution and the backscattering yield. At this energy, the depth resolution is better than in the previous analyses performed on the pellets with a value of around 25 nm at the samples surface. Figure 3.20 presents the RBS spectra of a virgin calcite sample (left) and of a Eu(III) sorbed calcite (contact time: 1 month).

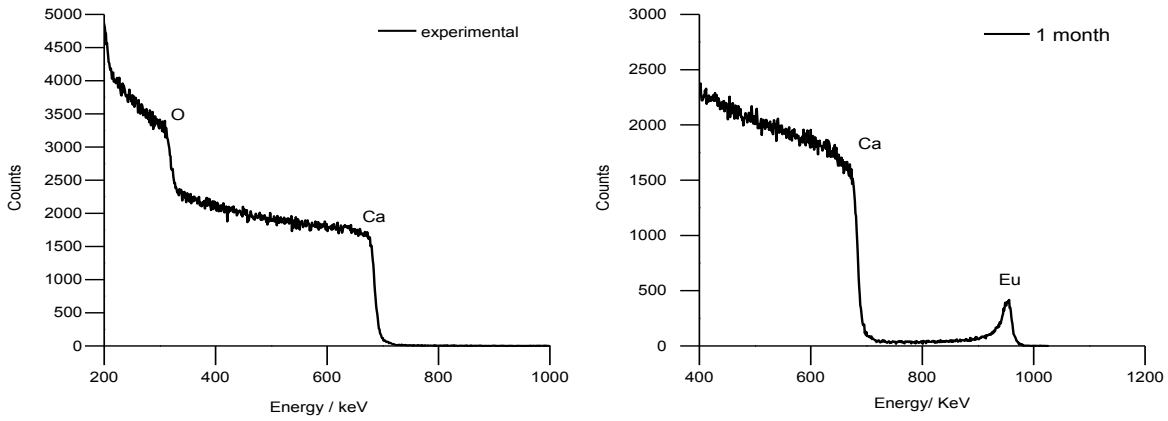

Figure 3.20: RBS spectra of virgin calcite (left) and Eu(III) (initial sorption with 10^{-4} mol.L^{-1} solution during 1 month) in calcite single crystals (right).

The shape of the Eu(III) steps show that at 10^{-4} mol.L^{-1} Eu(III) after 1 month at calcite-solution interface, is present both at the surface and in the bulk of the sample. This fact can be noted from the asymmetric peak of Eu(III) which appears around 900-1000 keV and tails off toward left, which can be assigned to element penetration on the substratum where concentration is decreasing by increasing bulk's depth [17], [104]. A similar asymmetric peak shape is observed by Carroll et al. [104] for Nd interacted with calcite. Nevertheless, in their study they do not conclude to a penetration in the substratum, but to the formation of a solid solution on the calcite surface, and the presence of Nd-Ca carbonate crystals was evidenced by SEM/EDXS. A series of spectra for diffusion are presented by Alonso et al. [17] for Eu(III) diffused in OPA clay, where the shape and intensity of the peaks are more pronounced than in the case of Eu(III) trapped in calcite.

Depth concentration profiles of Eu(III) were determined by simulation of the RBS spectra with the SIMNRA software and are presented in Figure 3.21.

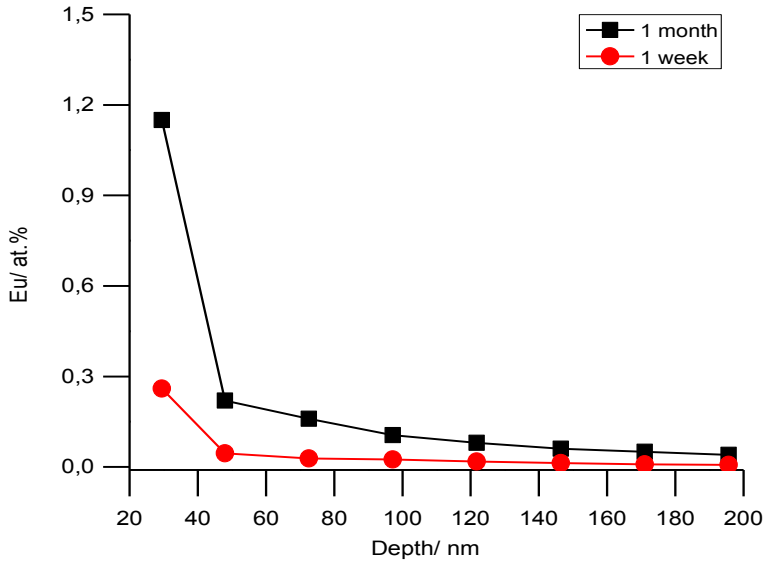

Figure 3.21: Depth concentration profiles of Eu(III) (initial sorption with 10^{-4} mol.L^{-1} solution during 1 week and 1 month) reacted with calcite single crystals. Lines are only plotted to guide the eyes.

The Eu(III) concentration decreases sharply in the first 40 nm and drops to zero only at a depth around 75 nm for the 1 week contact time sample. The profile corresponding to the 1 month contact time sample displays also a surface accumulation of Eu(III) with a sharp decrease in the first 20 nm but afterwards, the concentration decreases smoothly with the depth dropping to zero after 140 nm. So, taking into account the spectra shape and concentration profiles, it seems to indicate a surface accumulation and an incorporation of Eu(III) into the calcite crystal.

In order to get a better view of the morphology of the samples and to check the possible formation of a surface precipitate, SEM-EDXS measurements were carried out on the same samples. Several measurements with different scales have been performed onto single crystals. The lowest magnification of the image is used to have a general view of the surface of crystal (cracks, lumps), the highest to localize possible precipitated phases at the crystal surface.

Before starting the sorption experiments, the neat surface of some crystals were only examined by SEM to observe the initial morphology of the crystal without contact with solution (Figure 3.22).

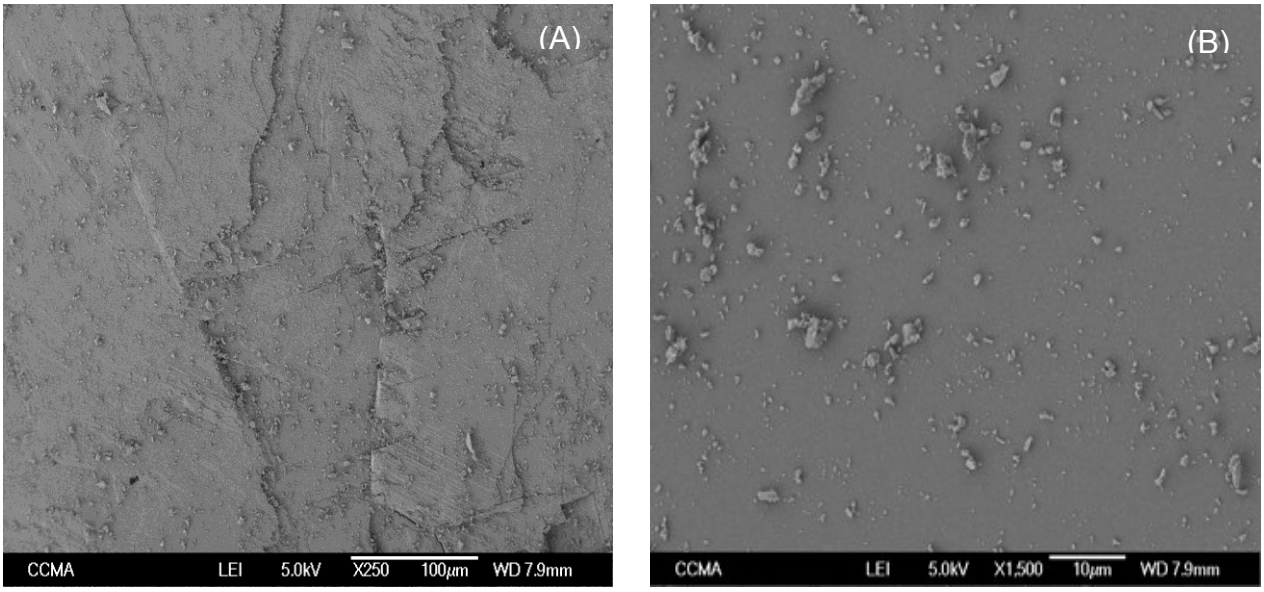

Figure 3.22: SEM photographs of calcite single crystal at 100 µm (A) and 10 µm (B) scales.

The surface of calcite is not smooth and presents defects and stripes (Figure 3.22 (A)) which in contact with solution can influence the crystal growth producing hillocks [19]. The (104) face of calcite is known to be often exposed to solution. The layer growth on this face was identified by Paquette and Reeder [36]. These results can be linked to XRD results on single−crystals, where the presence of this face is confirmed. Also, according to Harstad and Stipp [113] who investigated calcite dissolution by AFM, rhombohedral pits are formed by the (104) cleavage plane. In works presented before, the edge pits sides that are dissolving the most rapidly are in the $[\bar{4}41]_+$ and $[48\bar{1}]_+$ directions and slower in $[\bar{4}41]_-$ and $[48\bar{1}]_-$directions. As reported by Stipp et al. [20] calcite suffers a surface rearrangement in contact with air revealing the spontaneous development of pits and hillocks on (104) surface [19, 20]. The second image (Figure 3.22 (B)) represents a deep zoom on the crystal, and shows the presence of some granules on the crystal surface which can come from single crystals fragmentation.

SEM−EDXS analyses were then carried out on the Eu(III)-sorbed crystals and are presented in Figure 3.23.

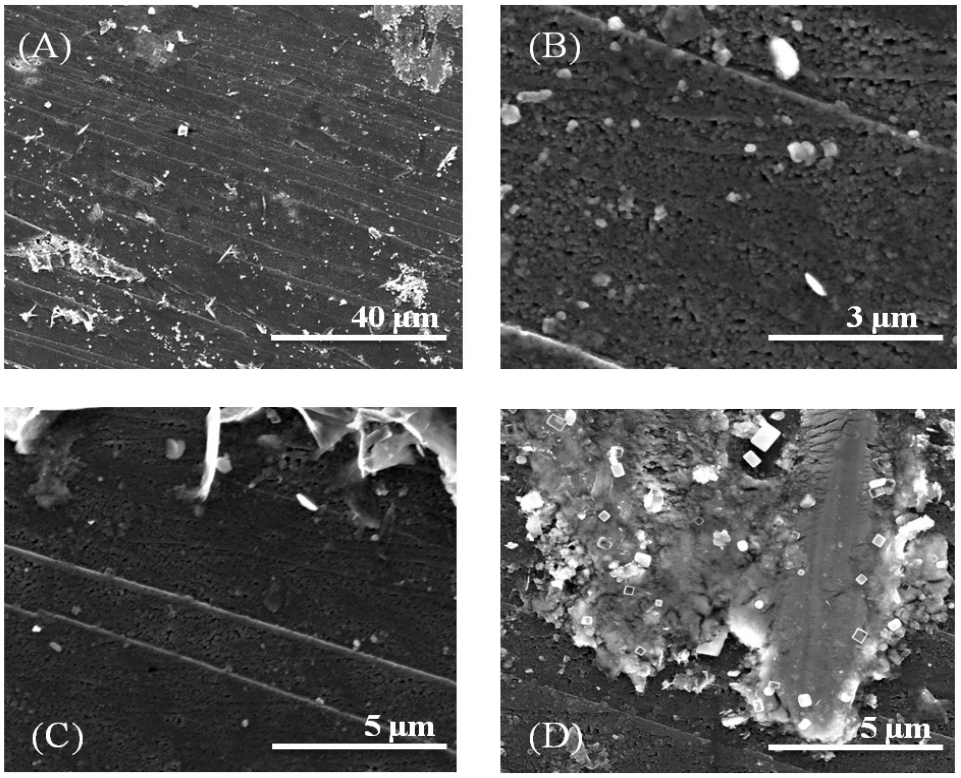

Figure 3.23: SEM images of a crystal reacted with Eu(III) 10^{-4} mol.L^{-1} during 1 month: general view (A) and zoom on three different regions of the sample surface (B, C, D).

The general overview of the crystal on Figure 3.23 (A) shows pronounced stripes, which can be seen with a higher magnification on Figure 3.23 (B) and Figure 3.23 (C). Compared to the surface of the virgin sample, more pronounced stripes are present on the surface which means that the surface has been modified by the Eu(III) solution and could have incorporated Eu(III). Figure 3.23 (A) shows also unhomogeneity of the sample: whereas rather homogeneous terraces can be seen between the stripes, some features can be seen on the photographs which would be in agreement with the formation of surface precipitates (bottom left and top right of the image). Figure 3.23 (B) shows a noticeable porosity of the crystal on one of the analyzed area. Figure 3.23(D)) shows a magnification of the zone in the upper right corner of Figure 3.23 (A). It can be seen that the surface is partially covered by a "tongue shaped" precipitate topped with some small white cubes and the underlying calcite surface has also a corroded aspect. Also, damages of calcite surface may be due to the addition of NaOH, which may be responsible for the porosity

observed on Figure 3.23 (B). The main conclusion that can be drawn is that Eu(III) is not uniformly distributed onto calcite surface.

Some EDXS analyses have been carried out on the area depicted in Figure 3.23 (D), and the results are presented on Figure 3.24. They reveal that the precipitate contains significant amounts of Eu(III) and that the white cubes are salt (presence of Na and Cl).

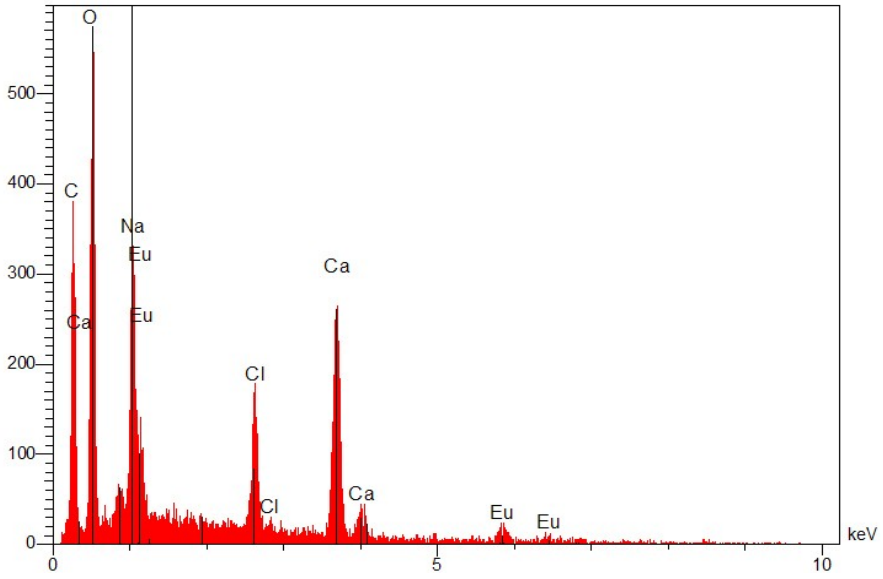

Figure 3.24: EDXS spectrum of 10^{-4} mol.L^{-1} Eu(III) on a single crystal, pH=8.3±0.1 (fixed by adding NaOH) and 1 month stirring time.

Beside the modification of porosity of the bulk, the inconvenient of the addition of NaOH to increase pH is that can cause local modifications of the pCO_2 on calcite crystal surface. This fact implied the implementation of a new manner to make the sorption experiments onto single crystals which is described in section 2.4.1. This method permits to keep constant the pH throughout the experiments without having to add NaOH during the pre-equilibration step.

Since there is a high heterogeneity on milli-metric single crystals as shown by SEM-EDXS study, we tried to refine our interpretation using RBS with µ-beam facility. The use of µ-RBS was also meant initially as a tool to analyze the powder samples (OMYA(BL 200)) with a mean 5 µm grain size without having to compact them into pellets. Unfortunately, preliminary tests on the powders were not successful since it was impossible to separate the grains (even under optical microscope) and to probe with the beam only one grain. Powders are well known to form

agglomerates and the possibility to probe agglomerates rather than one grain was very high. In order to avoid introducing measurement errors, we focused our attention only on milli-metric calcite single crystals.

3.4.3. RBS μ-beam and SEM-EDXS study of Eu(III) interaction with calcite single crystals

Single crystals were placed in a CPES solution as described in section 2.4.3 then spiked with Eu(III) resulting a concentration of 10^{-4} and 10^{-5} mol.L^{-1} and stirred for several contact times (1 day – 2 months). Samples were measured using a micro-beam which permits to study the bulk at small level and highlight spatial heterogeneities as inhomogeneous surface for example. The concentration profiles of Eu(III) in calcite were simulated considering layers with a thickness of a few tenth of nm. The surface of calcite in similar conditions (10^{-5} and 10^{-4} mol.L^{-1} Eu(III), several reaction times) has been investigated by SEM-EDXS analyses were also performed to get a better understanding of the surface morphology and composition, and were correlated with RBS maps which allowed to get a picture of the distribution of Eu on the surface and the depth of the crystals.

3.4.3.1 Experiments with low Eu(III) concentration (10^{-5} mol.L^{-1})

Figure 3.25 regroups the spectra for 10^{-5} mol.L^{-1} Eu(III) having a contact time of 24 hours, 1 week, 2 weeks and 2 months. The presence of Eu(III) is observed at an energy around 1350 keV. The spectra presented are the experimental (black) and the simulated (red).

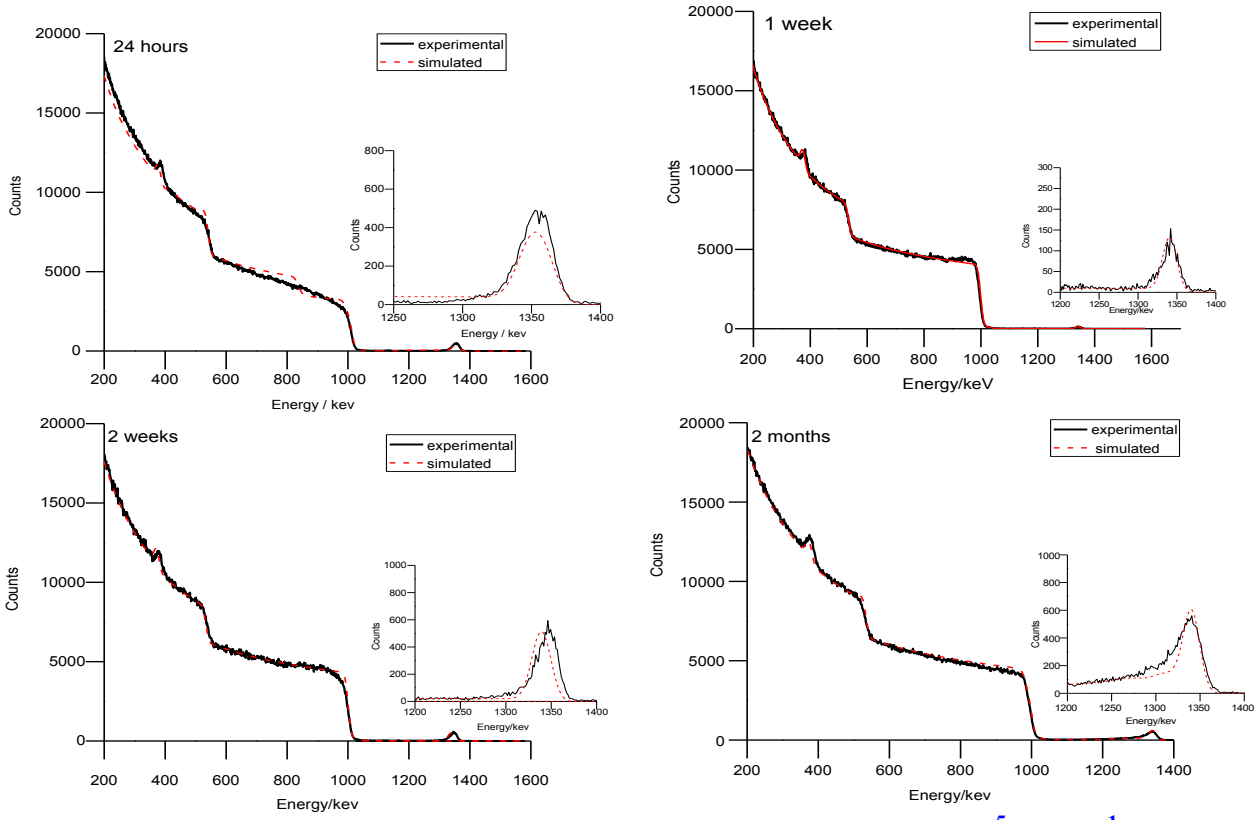

Figure 3.25: RBS spectra of calcite single crystals after reacting with 10^{-5} mol.L^{-1} Eu(III) for 24 hours, 1 week, 2 weeks and 2 months.

The RBS spectra indicate the presence of Eu(III) on the crystal surface over all the investigated contact times. From direct observation it is clear that spectrum of virgin calcite (Figure 3.22) and the spectra recorded for Eu(III) sorbed onto calcite single crystals are different. The shape of Eu(III) peak changes with reaction time, from a sharp symmetric peak for 1 day, 1 week and 2 weeks to a broad asymmetric peak for 2 months (zoomed images). A possible explanation for the change in the shape of the peaks can be that for symmetric peaks the main feature to be observed is an accumulation on the surface of the substrate (from 1 day until 2 weeks), whereas the asymmetric peak obtained for 2 months can be assigned to a more important penetration of Eu(III) onto calcite.

Figure 3.26 presents the depth concentration profiles of Eu(III) on calcite single crystals.

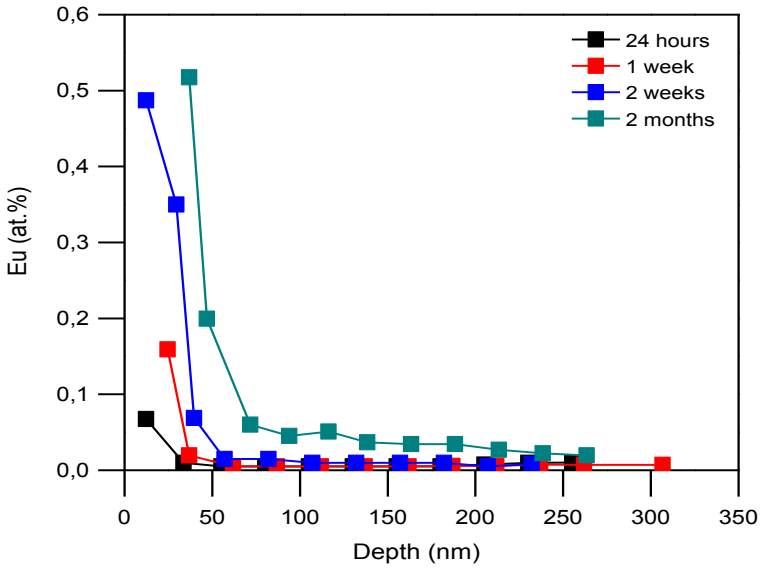

Figure 3.26: Depth concentration profiles of Eu(III) (initial sorption with 10^{-5} mol.L^{-1} solution during 24 hours, 1 week, 2 weeks and 2 months) on calcite single crystals. Lines are only plotted to guide the eyes.

The Eu(III) concentration decreases sharply in the first 40 nm and then drops towards zero only at a depth around 50 nm for the 1 day, 1 week and 2 weeks contact time sample, but the starting concentrations are very different at the extreme surface. The profile corresponding to the 2 months sample displays also a surface accumulation of Eu(III) with a sharp decrease in the first 50 nm but afterwards, the concentration decreases smoothly with the depth dropping to zero after 200 nm. This seems to indicate a surface accumulation together with an incorporation of Eu(III) into the calcite crystal. When we compare the depth concentration profiles and the aspect of spectra obtained for 2 weeks and 2 months it can be noticed that even if we have close values in the first 40 nm in for depth profiles, the shape of spectra as well as the modeling above 40 nm can highlight a different behavior of Eu(III) as a function of time. For 2 weeks we have only accumulation of Eu(III) on the surface, in the first 40 nm, while for 2 months the RBS peak tails off towards the left and the Eu(III) concentrations are detectable up to 200 nm in depth. This second type of behavior can be attributed to incorporation into calcite either by diffusion or by dissolution/re-precipitation.

In Figure 3.27, SEM images of one selected sample are presented among those that were investigated. A sample prepared with a long contact time was chosen since for such a low initial concentration EDXS signals were only obtained for long stirring times (and even in these conditions, the signal was generally close to the detection limit).

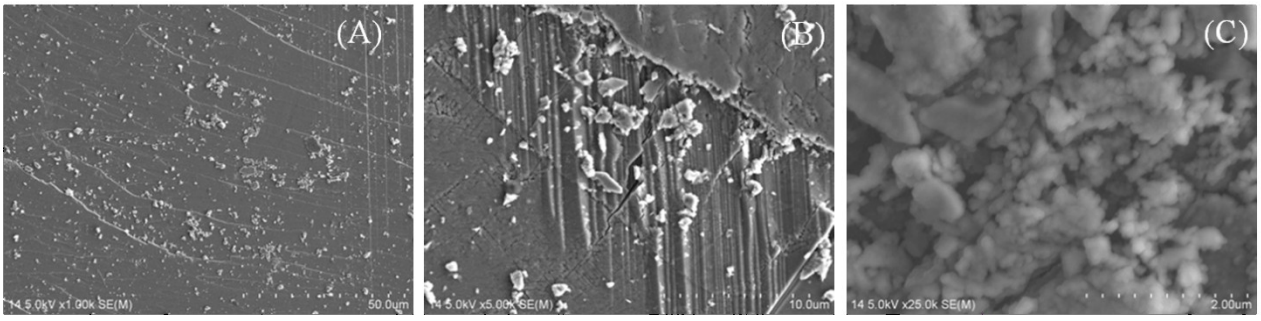

Figure 3.27: SEM image of a calcite crystal reacted with 10^{-5} mol.L^{-1} Eu(III), pH=8.3±0.1 and 2 months stirring time with a magnification of 50 µm (A), 10 µm (B) and 2 µm (C).

The first image corresponds to a scale of 50 µm and offers a general view of the crystal surface Figure 3.27(A). From the image, on crystal's surface there are observed granulations which can be perceived by human eye and may be Eu(III) precipitate. For the 10 µm scale, the presence of a precipitate is obvious and the solid is not very well crystallized. The aspect of calcite is corroded and some stripes are present on the surface that are visible also on calcite without contact with Eu(III) (Figure 3.22(A)).

The amounts of Eu(III) and other possible elements on the crystal surface were measured by EDXS in two distinct points of the crystal where the important surface accumulations or aggregates present on surface were suggesting the possible presence of Eu(III) precipitate (solid solution) (Figure 3.28). The same principle was applied for all selected samples for the same initial concentration.

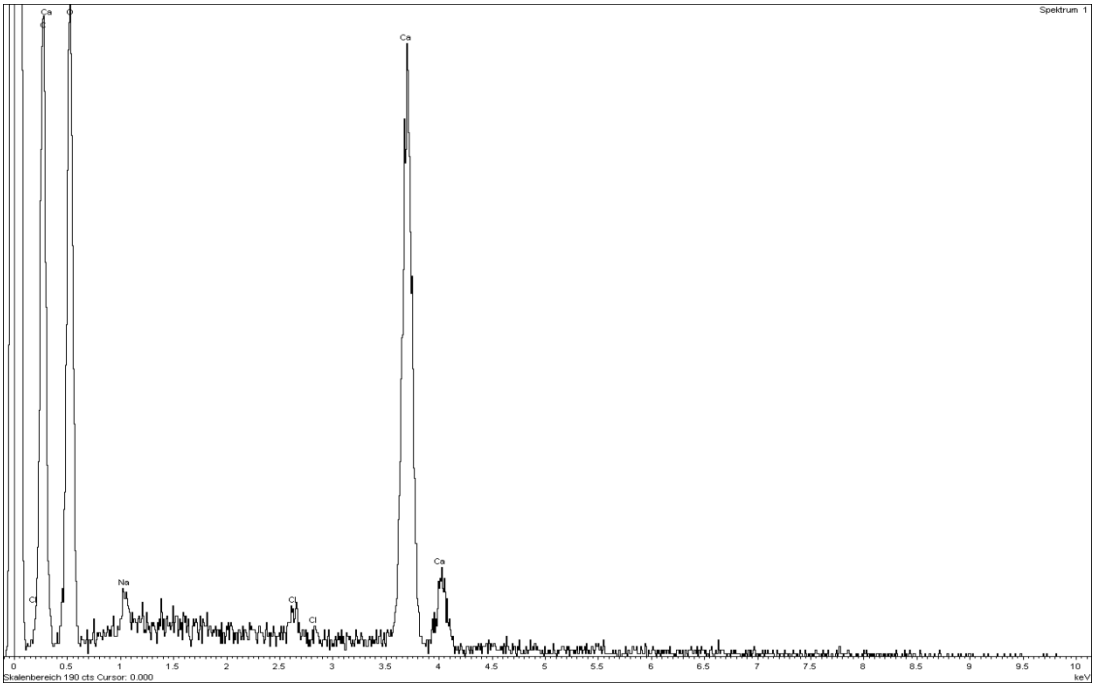

Figure 3.28: EDXS spectrum of a calcite crystal reacted with 10^{-5} mol·L^{-1} Eu(III), pH=8.3±0.1 and 2 months stirring time measured in one position.

The EDXS spectrum (Figure 3.28) indicates the presence of Na and Cl, but the presence of salt crystals is not visible by human eye on SEM images. The content of Eu(III) in the two probed areas was below the detection limit. Linking the results with those obtained by RBS where Eu(III) was clearly present, we may have analyzed different positions in the crystal by the two techniques.

For 10^{-5} mol.L^{-1} Eu(III) initial concentration sorbed onto calcite during 24 hours up to 2 months, the Eu(III) content detected by EDXS was close to the detection limit, but Eu(III) signals were obtained for a longer contact time than for RBS experiments (5 months). For this sample, the surface concentrations determined by EDXS were 1.20 at.% in the first position and 2.3 at.% in the second position.

Carroll et al. [104] investigated by SEM U, Nd and Th reacted with calcite for high concentrations (up to 10^{-2} mol.L^{-1}) under temperature (50°C). They observed the precipitation of U which forms a solid phase within the calcite surface and the precipitation of Nd with Ca and carbonate ions as individual crystals which subsequently rearrange to form a solid solution.

These results are different from the conclusions of our EDXS study from which we did not evidence any Eu(III) (co-)precipitate, at least for most of the investigated contact times. To have a better view of the distribution of Eu(III) on the surface of the samples, a series of Eu(III) maps were recorded concomitant with the RBS spectra, and the maps are presented for two stirring times (1 day and 2 months) in Figure 3.29.

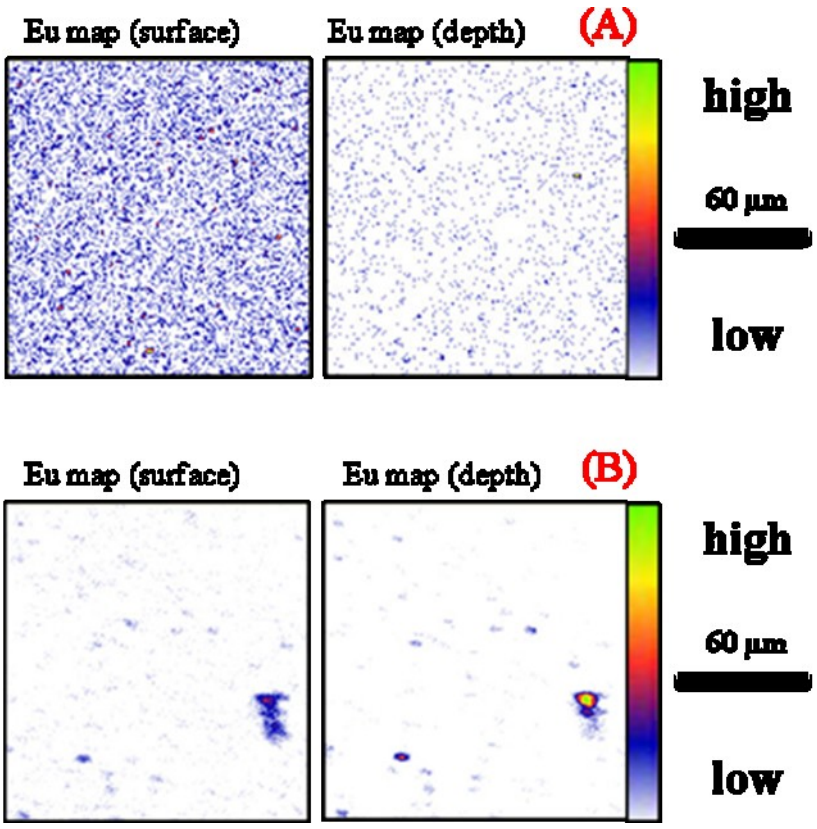

Figure 3.29: Eu(III) RBS elemental maps of 10^{-5} mol.L^{-1} Eu(III) on calcite, in surface and depth: (A) 24 hours and (B) 2 months. The concentration is presented as a function of the color, from less concentrated on bottom to more concentrate on the top.

The distribution of Eu(III) content is not uniform, more concentrated areas being localized especially on surface. For 24 hours and 2 months contact times, small spots with Eu(III) concentrated areas are very dispersed over the entire measured region.

As a conclusion, the results of the RBS study on low concentrated samples show an accumulation of Eu(III) on the surface of calcite together with an incorporation for the samples

reacted for long contact times. RBS maps and SEM-EDXS analyses highlighted the heterogeneities in the distribution of Eu(III) on the calcite surface and SEM showed the presence of precipitates on calcite. The presence of Eu(III) in these precipitates could not be evidenced by EDXS, probably because of the lower sensibility of the technique compared to RBS (order of magnitude of EDXS sensibility: a few 0.1 % in a probed thickness of 1 µm, whereas the RBS spectra were modeled with a few 0.1 % in a probed depth of 20-30 nm for the first simulated layer, which represents then a smaller concentration).

3.4.3.2. Experiments with high Eu concentration (10^{-4} mol.L^{-1})

A higher concentration, 10^{-4} mol.L^{-1} was investigated by RBS (Figure 3.30). The spectra presented are the experimental (black) and the simulated (red).

In all spectra the presence of Eu(III) on crystal surface is signaled for energies varying between 1200-1350 keV, and the intensity of Eu(III) peaks is increasing over time. The shape of the peak is rather symmetrical for 24 hours and 1 month samples, which could be interpreted as an accumulation of Eu(III) on the crystal. For the other samples, namely 2 weeks, 2 months and 5 months, an asymmetrical peak which tails off towards the left is noticed. This feature could be correlated to Eu(III) penetration into calcite.

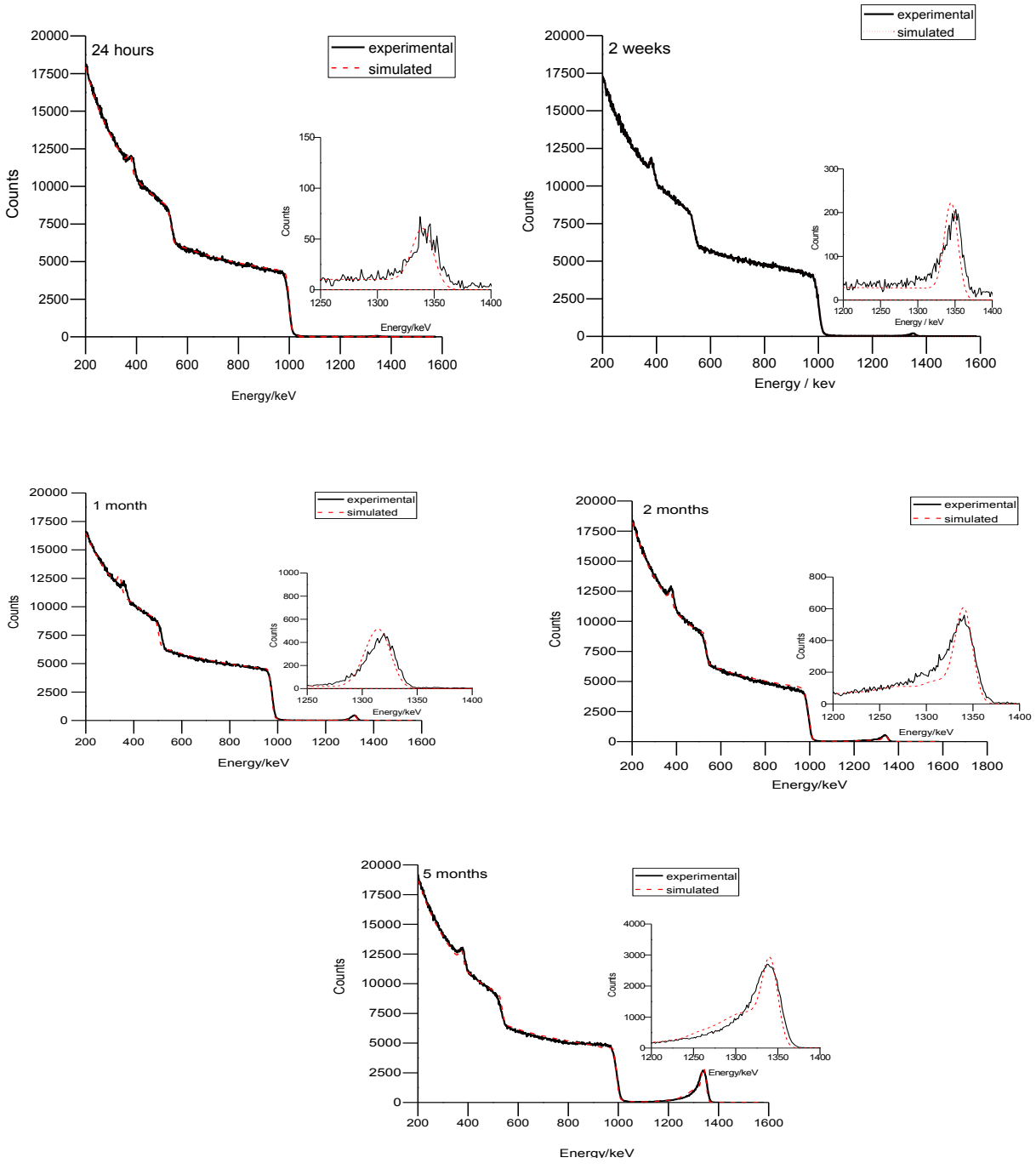

Figure 3.30: RBS spectra of calcite single crystals after reacting with 10^{-4} mol.L^{-1} Eu(III) for 24 hours, 2 weeks, 1 month, 2 months and 5 months.

In Figure 3.31, the depth concentration profiles of 10^{-4} mol.L^{-1} Eu(III) sorbed onto calcite are presented.

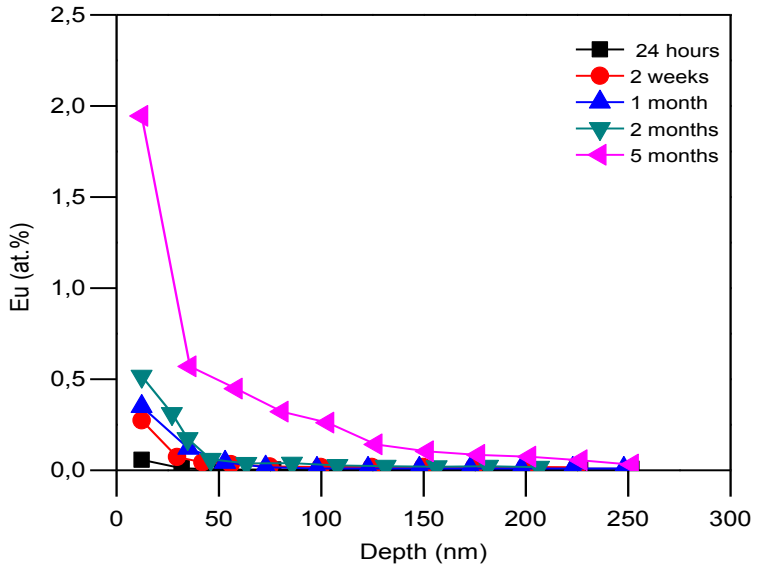

Figure 3.31: Depth concentration profiles of Eu(III) (initial sorption with 10^{-4} mol.L^{-1} solution during 24 hours, 2 weeks 1 month, 2 months and 5 months) in calcite single crystals. Lines are only plotted to guide the eyes.

For the first contact times (24 hours−2 months) the Eu(III) content on the surface has a value below 0.5 at.%, then drops to zero in the first 50 nm. After this depth no europium is found. For the higher contact time a more important Eu(III) content is present on the crystal surface, then decreases slowly up to 250 nm, where it drops to zero and remains constant. The concentration profiles are comparable with those obtained for 10^{-5} mol.L^{-1} Eu(III): for the shorter contact times, an accumulation of Eu(III) in the first 40-50 nm is observed whereas experiments carried out over the longest contact times highlight an incorporation of Eu(III) in the bulk of the sample.

SEM-EDXS measurements were carried out for 10^{-4} mol.L^{-1} Eu(III) and different contact times.

Figure 3.32 represents the SEM images for different scales on 10^{-4} mol.L^{-1} Eu(III) samples with a contact time of 5 months.

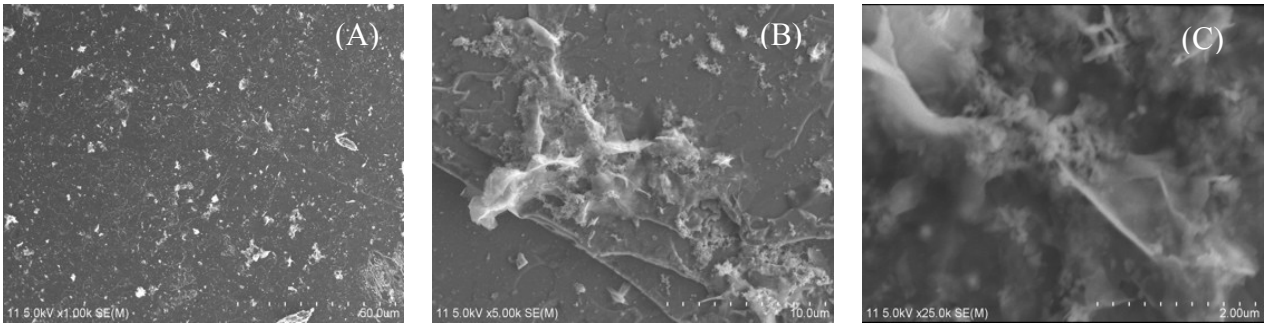

Figure 3.32: SEM images of a calcite crystal reacted with 10^{-4} mol.L^{-1} Eu(III), pH=8.3±0.1 and 5 months stirring time with a scale of 50 µm (A), 10 µm (B) and 2 µm (C).

The image recorded at 50 µm shows several zones where granulations are visible. These granulations are also present on calcite single crystals without contact with Eu(III).

For a magnitude of 10 µm, there is an obvious surface precipitate that presents an irregular shape. The fact that the surface of the crystal is not smooth and that some cracks are present can favor the accumulation of precipitates into the cracks. Also, for such a long reaction time, Eu(III) is expected to precipitate, as SEM-EDXS analyses showed for the samples prepared by the NaOH method and measured by milli-beam RBS. These images reveal that the precipitate is heterogeneously distributed. In Table 3.8, the Eu(III) fractions identified by EDXS for different contact times are summarized.

Table 3.8: Summary of Eu(III) surface concentrations measured by EDXS for 10^{-4} mol.L^{-1} Eu(III).

Stirring time (days)	Eu(III) pos 1 (at. %)	Eu(III) pos 2 (at. %)
1	–	–
14	–	–
30	1.90	4.95
60	4.26	4.81
150	5.15	5.56

Before 14 days no Eu(III) was detected, but after 1 month low Eu(III) concentration is identified on the crystal surface. A regular increase of surface concentration is then noticed as a function of contact time.

Compared with 10^{-5} mol.L^{-1} samples, the Eu(III) content is higher for each contact time since Eu(III) was not detected before 5 months for the samples with a low concentration, and since for the 10^{-4} mol.L^{-1} sample with a 5 months stirring time, an increase of Eu(III) content onto the surface of the crystal is observed compared to the 10^{-5} mol.L^{-1} sample for the same contact time. Nevertheless, it should be noted that we only selected the more concentrated areas to record the EDXS spectra; areas with no Eu(III) content were present on all the probed samples.

The SEM-EDXS results can be connected with the formation of a precipitate on the surface of the crystal, taking into account the features observed in the SEM photographs and the EDXS results which show a noticeable amount of Eu(III) in several areas where the precipitate can be seen on the SEM photographs. It should be noted though that the surface is highly heterogeneous.

Changes on calcite without contact with any solution were observed by Stipp et al. [20] using AFM during exposure to air, where pits appeared on surface over time (several minutes - ~24 hours). Stipp et al. [10] also followed in situ Eu(III) uptake by calcite and calcite behavior in water by AFM. They observed the formation of pits on the crystal surface and that after a longer exposure to water pits edges spread back and possibly another layer of deep pits nucleates again. In the case of calcite exposed to Eu(III) the rhombohedra outline that is seen for calcite exposed to water becomes elliptic, which shows that Eu(III) is adsorbed. They didn't observe precipitation, because by AFM no small particles were observed, but the dissolution of calcite was clearly evidenced. These results seem to be in disagreement with our results, since we have shown the presence of surface precipitates which contain a noticeable amount of Eu(III). Nevertheless, their contact time was very low, 1 minute exposure to solution and the pH was much lower. The formation of a surface complex could nevertheless be a possible supplementary mechanism in our case which cannot be evidenced by SEM-EDXS. RBS Eu(III) maps on calcite samples exposed to 10^{-4} mol.L^{-1} Eu(III) during 24h and 5 months are presented in Figure 3.33.

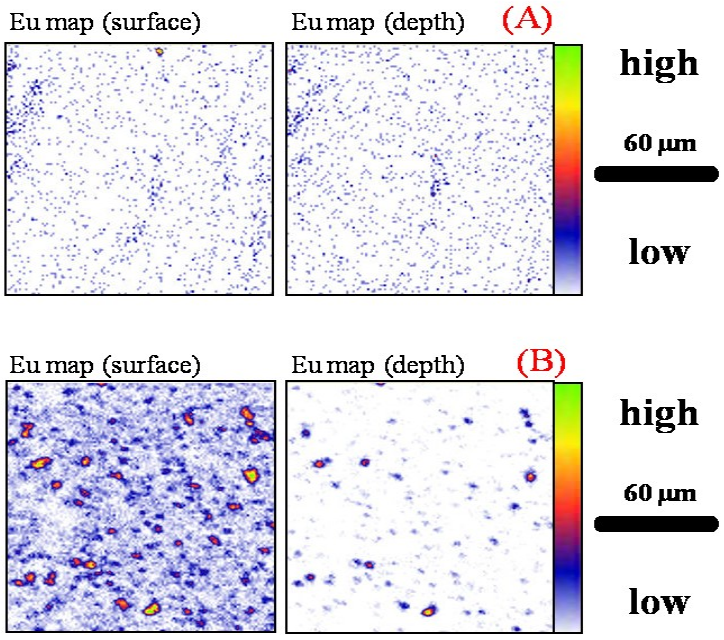

Figure 3.33: Eu(III) RBS elemental maps of 10^{-4} mol·L^{-1} Eu(III) on calcite, in surface and depth : (A) 24 hours, and (B) 5 months.

Distribution of Eu(III) on crystal's surface and depth is not homogeneous. For the 5 months sample, some Eu(III) clusters with high concentrations can be seen, which we may attribute to a surface coprecipitate. The RBS maps thus confirm the results of the SEM-EDXS study.

3.4.3.3. Apparent diffusion coefficients

The previous results seem to indicate incorporation of Eu(III) into calcite and we have tried to quantify the velocity of this incorporation. One way is to calculate diffusion coefficients. However these calculated coefficients do not presume on the incorporation mechanisms and are therefore called apparent diffusion coefficients.

The general equation of diffusion can be expressed by equation (Eq. 3.1).

$$\frac{\partial C}{\partial t} = D\frac{\partial^2 C}{\partial x^2} - \langle v \rangle \frac{\partial C}{\partial x} + kC \qquad \text{(Eq. 3.1)}$$

with: C, concentration of the studied element (Eu(III))

t, the time

x, the probed depth

D, <v> and k: diffusion coefficient, transport velocity and loss term

If diffusion is the main process (which will be our assumption), this equation can be simplified into Eq. 3.2 which is also called Fick's second law:

$$\frac{\partial C}{\partial t} = D\frac{\partial^2 C}{\partial x^2} \qquad \text{(Eq. 3.2)}$$

There are a lot of solutions of this equation depending mainly on the initial and limit conditions.

In our case, initial conditions (t=0) are for $x > 0$: $c(x,0) = c_0$

and limit conditions are: for $t > 0$ and $x = 0$: $c(0,t) = c_s$.

The solution of this equation with these conditions is given in equation 3.3:

$$\frac{c-c_s}{c_0-c_s} = \mathrm{erf}\left(\frac{x}{2\sqrt{Dt}}\right) \qquad \text{(Eq. 3.3)}$$

where erf stands for the mathematical error function (also called Gauss integral).

We can assume also that, at t=0, no reaction between calcite surface and solution occurs. Therefore $c_0 = 0$. The new solution is now given in equation 3.4:

$$\frac{c}{c_s} = \mathrm{erfc}\left(\frac{x}{2\sqrt{Dt}}\right) \qquad \text{(Eq. 3.4)}$$

Where erfc stands for the complementary error function (erfc = 1 – erf)

The last point which remains is the identification of the c_s value. As we have seen by SEM, the concentration of Eu(III) at the surface (x=0) is not homogeneous and does not remain constant with the sorption time. Therefore we added a Gaussian term to take into account the evolution of c_s.

Finally, the solution we used to fit our experimental points is (Eq. 3.5):

$$C(x) = C_S \operatorname{erfc}\left(\frac{x}{2\sqrt{Dt}}\right) + A\exp\left(-\frac{x}{2s^2}\right) \qquad \text{(Eq. 3.5)}$$

with C(x) = europium concentration at the distance x

c_s = europium concentration at the surface

x = distance between the surface and the i layer (cm)

D = diffusion coefficient ($cm^2 \cdot s^{-1}$)

t = contact time (s)

s = sigma of the function – equivalent to the size of the precipitate layer

A= Gaussian intensity (fixed by user)

The diffusion coefficients were calculated for both investigated Eu(III) concentrations presented above. The result of the modeling is that, in both cases, the order of magnitude is about 10^{-22} – 10^{-21} $m^2.s^{-1}$.

A series of diffusion coefficients for Pb and Sr in calcite under anhydrous conditions by Cherniak [101]. They identified the diffusion coefficients having magnitude orders of 10^{-23} – 10^{-21} $m^2 \cdot s^{-1}$ for both Sr and Pb at temperatures ranging from 435-445°C ($D \approx 3 \cdot 10^{-23}$ $m^2.s^{-1}$) to 650-650-660°C ($D \approx 2\text{-}5 \cdot 10^{-21}$ $m^2.s^{-1}$). Other set of annealed experiments of REE (La, Nd, Dy, Yb) diffusion into calcite were performed by Cherniak [79] and the diffusion coefficients that were calculated have a magnitude of $5 \cdot 10^{-23}$ – $3 \cdot 10^{-22}$ $m^2.s^{-1}$ at 650°C, also in anhydrous conditions. Even if the experimental procedures are not the same (dry/wet samples), our results are therefore inconsistent with the results of Cherniak, since the coefficients determined in our study are higher than the diffusion coefficients determined at 650°C for other REE. Lahav and Bolt [105] determined ^{45}Ca self-diffusion into calcite using an experimental procedure comparable to ours (calcite suspensions in water) obtaining a diffusion coefficient $D=8 \cdot 10^{-24}$ $m^2.s^{-1}$ at room temperature. Again, this is inconsistent with our coefficients which are higher

than the Ca coefficient: Eu(III) diffusion is unlikely to process faster than the self-diffusion of Ca in calcite.

Taking into account our obtained apparent diffusion coefficients, there are high inconsistencies when we compare them with real diffusion coefficients from literature data. It seems thus unlikely that Eu(III) incorporation proceeds as a diffusion mechanism into calcite, and this is the major result of this section. These apparent diffusion coefficients could nevertheless be useful to estimate the extent of Eu(III) incorporation in real calcite systems.

As a summary of the RBS and SEM/EDXS study of europium sorbed on calcite, milli-RBS performed on single crystals reveals that Eu(III) accumulates at the surface and is also incorporated into calcite, the amount increasing with time. For 10^{-4} mol.L^{-1} samples, after 1 week, Eu(III) can be found on a depth of 75 nm, whereas after 1 month contact time penetrates deeper, to 140 nm. μ-RBS permitted us to determine depth profile concentrations and obtain the distribution (elemental maps) of Eu(III) on samples. For both investigated concentrations (10^{-4} and 10^{-5} mol.L^{-1}), trapping of Eu(III) into calcite was determined to occur, and the surface atomic concentrations are comparable for all samples except for the 10^{-4} mol.L^{-1} sample with 5 months contact time, where it is significantly higher. From measured spectra, penetration of Eu(III) into calcite bulk was noticed after a few months for both concentrations (2 months in the case of 10^{-5} mol.L^{-1} Eu(III), 5 months in case of 10^{-4} mol.L^{-1}). For these two samples, Eu(III) penetrates up to 200-250 nm into calcite. For contact times below, respectively, 2 months for the 10^{-5} mol.L^{-1} sample and 5 months for the 10^{-4} mol.L^{-1} samples, the depth concentration on Eu(III) is visibly lower and localized in the first 50 nm. These differences between milli-RBS and μ-RBS can be due to the sample preparation, heterogeneity of crystal, but also to different probed areas. Also, Stipp et al. [10] shows that Eu(III) sorption alters calcite surface behavior and dissolution appears inhibited. Anyway, she confirms incorporation of Eu^{3+} (and other actinides which have the same behavior) during precipitation and crystal growth of natural calcite. As mechanism Carroll et al. [104] proposes precipitation of Nd-Ca carbonate crystals on the surface (confirmed also by SEM), which can later dissolve to rearrange as a Nd-Ca solid solution. These two studies are in agreement with ours, if we suppose the formation of a Eu/Ca/carbonate solid solution of a 200-250 nm thickness. Apparent diffusion coefficients were

determined in this study, and a comparison of the order of magnitude of the calculated apparent diffusion coefficients (10^{-22} – 10^{-21} $m^2.s^{-1}$) with the literature data show that these coefficients are only apparent. Diffusion, if taking place at all, is definitely not the only process occurring in the conditions of our study and surface calcite reactivity seems to be more relevant.

3.5. Summary and conclusions

On the first part of this chapter, prior to study the interaction of Eu(III) with calcite, solution chemistry of Eu(III) in CPES solutions was investigated by TRLFS and XRD. Speciation diagrams predicted that Eu(III), in our experimental conditions, should precipitate as $Eu_2(CO_3)_3{:}3H_2O_{(s)}$ and $EuOHCO_{3(s)}$, at 10^{-3} $mol.L^{-1}$ and at $\leq 10^{-4}$ $mol.L^{-1}$ respectively. The aqueous Eu(III)-carbonates that should predominate over the whole concentration range are $EuCO_3^+$ and $Eu(CO_3)_2^-$ at pH 8.3.

Precipitation for concentration $>10^{-5}$ $mol.L^{-1}$ was identified from macroscopic and spectroscopic results as a fast process. The emission spectra recorded for suspensions are similar for concentrations in Eu(III) of 10^{-4} and 10^{-5} $mol.L^{-1}$ during the whole investigated time scale. The shape of the spectra seem to indicate rather the presence of $Eu_2(CO_3)_3{:}3H_2O_{(s)}$. For the highest concentration, 10^{-3} $mol.L^{-1}$ different spectra are obtained for 1 day, 1 week and 2 weeks of contact time. Eu(III) is precipitating in solution forming the following solids: $Eu_2(CO_3)_3{:}3H_2O_{(s)}$ which later transforms into $EuOHCO_{3(s)}$ with time. This modification can be due to pCO_2 changes during the experimental period. This evolution of phases was confirmed by XRD.

The solid phases identified by speciation calculations, TRLFS and XRD analyses correspond to the end-members used by Lakshtanov and Stipp [71] in their modeling of solid solutions obtained by coprecipitation of europium, calcium and carbonate ions. They performed the experiments using co-precipitation method at pH 6, 10^{-1} $mol.L^{-1}$ $NaClO_4$ under pCO_2=1 atm. Their modeling was successful using either $Eu_2(CO_3)_3$ or $EuOHCO_3$, but they showed that the $NaEu(CO_3)_2$ stoichiometry was not adapted to fit the experimental data. It should be noted that the solid phase $NaEu(CO_3)_2{:}5H_2O$ (one of the solid phases with a saturation index superior to 1 in our speciation calculations) was not detected neither by TRLFS nor by XRD.

The TRLFS results on the solution behavior of europium in CPES solutions are a first basis for the TRLFS study on sorbed samples. The results obtained by TRLFS and XRD highlighted a

phase transformation with time. If surface precipitation occurs, TRLFS data (spectra shape as well as lifetimes) should be comparable.

Sorption of Eu(III) onto calcite (powders and single crystals) was investigated by spectroscopic tools (TRLFS and RBS) which permitted to identify the different processes occurring at Eu(III)/calcite interface. Same concentrations as for blank solutions were studied, as well as the impact of pCO_2. Generally two lifetimes were identified, some exceptions being seen for a few samples. Differences and similarities between samples measured under atmospheric conditions and $pCO_2=10^{-2}$ atm can be seen. Except for Eu(III) concentration of 10^{-3} mol.L^{-1}, the calculated luminescence lifetimes are longer under atmospheric conditions compared to $pCO_2=10^{-2}$ atm at same reaction time. This stands for a faster surface complexation and incorporation process of Eu(III) into calcite powder under atmospheric conditions.

The main general observation is the influence of reaction time on Eu(III) speciation onto calcite. Surface precipitates of Eu(III) onto all sorbent calcite were evidenced for every contact time by TRLFS for high concentrations such as 10^{-3} mol.L^{-1}. Onto powders investigated under ambient conditions, for a concentration of 10^{-4} mol.L^{-1}, incorporation is starting after 2 months and is evidenced by a very long lifetime (> 1 ms) which has been interpreted as a total loss of water molecules in the first coordination sphere. A second concomitant mechanism is identified, associated with a shorter lifetime which is the formation of inner-sphere complexes/sorbed species. For the last concentrations, 10^{-5} and 10^{-6} mol.L^{-1}, a short lifetime indicates as well sorbed species/inner-sphere complexes whereas long lifetime show incorporation which occurs much faster than for 10^{-4} mol.L^{-1}, after 1 week contact time. The calculated long lifetimes corresponding to the incorporated species increase with time for all studied concentrations. This does not seem to be consistent with a well-defined environment of europium in the solid. Another hypothesis in the interpretation of fluorescence decays would then be the presence of more than one incorporated species, which would be in agreement with previous studies [4, 7]. In this case, it would be highly interesting to complete the present study by site-selective TRLFS experiments.

Under $pCO_2=10^{-2}$ atm, like under ambient conditions, Eu(III) precipitates were identified for high concentrations and short reaction time, whereas for low concentration and long contact times progressive incorporation into bulk was evidenced. Compared to samples investigated

under ambient conditions, precipitation seems delayed under $pCO_2=10^{-2}$ atm. For calcite single crystals, incorporation is slower compared to powders. This can be due to the important differences of specific surface area between powders and single crystals. In this case, precipitation for short lifetimes of Eu(III)-carbonates and incorporation into bulk for long lifetimes is noticed.

The second technique used to highlight incorporation is RBS (milli-beam and μ-beam), where spectra together with depth concentration profiles confirmed this phenomenon. The two sorption methods for single crystals preparation turned to be appropriate both leading to incorporation of Eu(III) in calcite. The depth concentration profiles interpreted after milli-RBS analysis showed that for 10^{-4} mol.L^{-1}Eu(III) accumulates onto surface and penetrates up to 75 nm in one week, and up to 140 nm in one month. Similar results were obtained for two distinct concentrations, 10^{-5} mol.L^{-1} and 10^{-4} mol.L^{-1}. For lower concentration more important accumulation is noticed for longer stirring times, then penetration of Eu(III) up to 250 nm. For higher concentration the surface concentrations are more important for 10^{-4} mol.L^{-1} than 10^{-5} mol.L^{-1} as expected. The penetration of Eu(III) is at same depth, 250 nm. The heterogeneous distribution of Eu(III) onto calcite surfaces was highlighted by additionally SEM-EDXS and by RBS elemental maps.

The incorporation process does not proceed as a solid-state diffusion, as shown by the calculation of apparent "diffusion" coefficients. To our knowledge, this study is the first to have shown incorporation of Eu up to depths of 250 nm. The previous XPS study by Stipp et al. [10] showed that Eu(III) was present in calcite sorbed samples in the upper 4-5 nm but did not study the deeper incorporation due to the limitation of the technique. Some of the spectra in the RBS study by Carroll et al. [104] are comparable to ours from their shape but they did not extract any concentration profile from their data due to artifacts problems.

The results obtained by TRLFS, RBS, SEM−EDXS are in good agreement and highlight precipitation of Eu(III) on surface at high concentrations ($> 10^{-4}$ mol.L^{-1}) and incorporation for low concentrations ($< 10^{-4}$ mol.L^{-1}) and long contact times. Europium sorption on calcite appears to proceed according to three mechanisms:

- heterogeneous accumulation on surface as (co)-precipitate shown by TRLFS and RBS
- inner sphere- complex formation as shown by TRLFS

- incorporation into bulk produced by dissolution/re-crystallization process of calcite in order to form a solid-solution.

Chapter 4:
Interaction of nickel with calcite

4. Interaction of nickel with calcite

Nickel is a transition metal with a high toxicity and also an activation product (^{63}Ni and ^{59}Ni, with $t_{1/2}$ = 100.1 and 7.6 × 10^4 years, respectively), thus it is an important contaminant. Nickel carbonate phases and complexes are often found in underground water due to the ubiquity of carbonate ligands. This chapter groups macroscopic and spectroscopic results concerning the interaction between nickel and calcite. These results are compared with former studies on the same system and based on various spectroscopic tools.

4.1. Solution chemistry of nickel

4.1.1. Speciation calculations

The distribution and composition of aqueous solutions in the experimental conditions of our study regarding Ni(II) in carbonate media were calculated using the geochemical code PHREEQC Interactive (version 2.18.5570) [121]. The ThermoChimie database (version 9) [111] from ANDRA was used for these calculations. They were performed at constant ionic strength (10^{-1} mol.L^{-1} NaCl), at pCO_2 $10^{-3.5}$ atm and at 25 °C. The initial nickel concentrations, identical to those taken for the batch experiments, were ranging from 10^{-6} to 10^{-3} mol.L^{-1}. To reflect experimental conditions, a solution pre-equilibrated with calcite (pH 8.3) was used for the calculations. However, no calcite was introduced. The aqueous species and their formation constants used for speciation diagrams are summarized in Table 4.1.

Table 4.1: Ni(II) aqueous species and their equilibrium constants (I = 0) used for speciation calculations.

Aqueous Species	log K
$Ni^{2+} + Cl^- \rightleftharpoons \mathbf{NiCl^+}$	0.080
$Ni^{2+} + CO_3^{2-} \rightleftharpoons \mathbf{Ni(CO)_3}$	4.200
$Ni^{2+} + 2CO_3^{2-} \rightleftharpoons \mathbf{Ni(CO_3)_2^{2-}}$	6.200
$Ni^{2+} + H^+ + CO_3^{2-} \rightleftharpoons \mathbf{Ni(HCO_3)^+}$	11.730
$Ni^{2+} - H^+ + H_2O \rightleftharpoons \mathbf{Ni(OH)^+}$	−9.540
$Ni^{2+} - 2H^+ + 2H_2O \rightleftharpoons \mathbf{Ni(OH)_2}$	−18.000
$Ni^{2+} - 3H^+ + 3H_2O \rightleftharpoons \mathbf{Ni(OH)_3^-}$	−29.380
$2Ni^{2+} - H^+ + H_2O \rightleftharpoons \mathbf{Ni_2(OH)^{3+}}$	−10.600
$4Ni^{2+} - 4H^+ + 4H_2O \rightleftharpoons \mathbf{Ni_4(OH)_4^{4+}}$	−27.520

A list of the possible Ni(II) solid phases that can be formed, as well as their stability constants is presented in Table 4.2. Note that $Ni(OH)_{2(s)}$ refers to β-$Ni(OH)_2$ [111].

Table 4.2: Ni(II) solid phases and their equilibrium constants ($I = 0$) used for speciation calculations.

Solids	log K
Bunsenite NiO ⇌ $Ni^{2+} - 2H^+ + H_2O$	12.480
$NiCl_2$(s) ⇌ $Ni^{2+} + 2Cl^-$	8.670
$NiCl_2$:2H_2O(s) ⇌ $Ni^{2+} + 2Cl^- + 2H_2O$	4.920
$NiCl_2$:4H_2O(s) ⇌ $Ni^{2+} + 2Cl^- + 4H_2O$	3.820
$NiCl_2$:6H_2O(s) ⇌ $Ni^{+2} + 2Cl^- + 6H_2O$	3.040
Ni(CO_3):5.5H_2O(cr) ⇌ $Ni^{2+} + CO_3^{2-} + 5.5H_2O$	−7.520
Ni(OH)$_2$(s) ⇌ $Ni^{2+} - 2H^+ + 2H_2O$	11.030

Nickel should form insoluble hydroxide $Ni(OH)_{2(s)}$ in alkaline solutions or $NiCO_{3(s)}$ according to Guillard and Lewis [83], who mentioned that precipitation of $NiCO_{3(s)}$ occurs in competition with that of $Ni(OH)_{2(s)}$. Obviously, both thermodynamics and kinetics influence which solid phases really form.

Figure 4.1 presents the concentration of the different Ni(II) species as a function of the initial concentration as well as the saturation indices of solid phases.

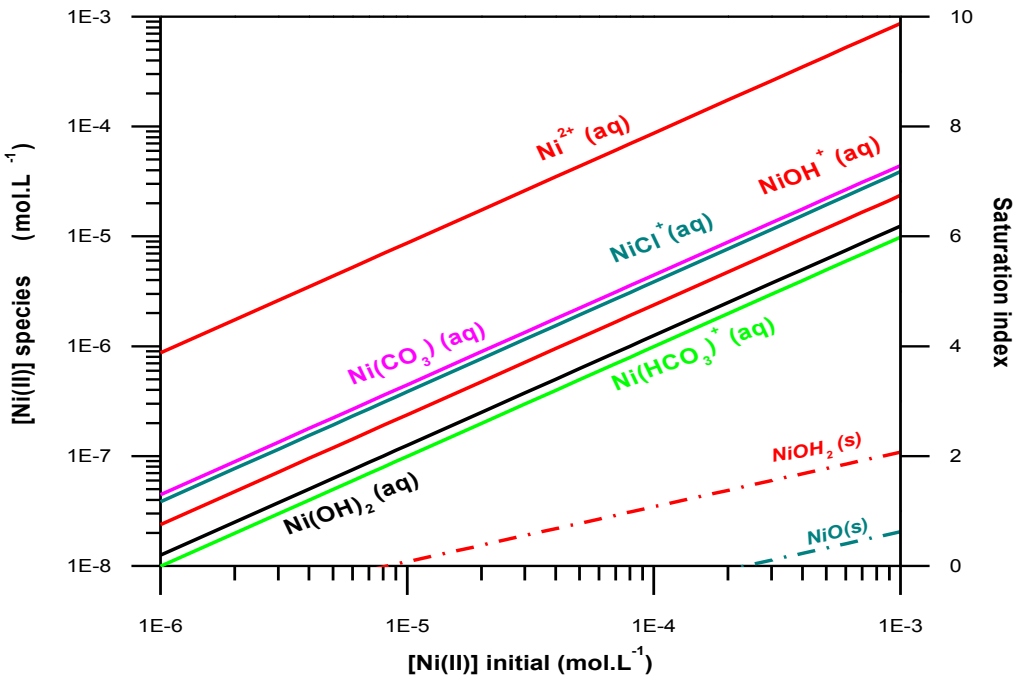

Figure 4.1: Concentration of aqueous species and saturation indices of solid phases as a function of the Ni(II) initial concentration (10^{-1} mol.L^{-1} NaCl, pCO_2 $10^{-3.5}$ atm and pH 8.3).

Equilibrium calculations (Figure 4.1) show that according to thermodynamic database used in our study, $Ni(OH)_{2(s)}$ is expected to precipitate at pH 8.3 and at Ni concentration above 8×10^{-6} mol.L^{-1}, since it shows a positive saturation index. Bunsenite ($NiO_{(s)}$) is predicted to be formed at Ni(II) concentration above 2×10^{-4} mol.L^{-1}. Solutions are expected to reach $Ni(OH)_{2(s)}$ saturation before saturation with respect to $NiO_{(s)}$. From these calculations, $Ni^{2+}_{(aq)}$ is the most abundant aqueous species for the whole concentration range of interest. The abundance of other aqueous phases like $Ni(CO_3)_{(aq)}$, $Ni(OH)_{2(aq)}$, $NiCl^{+}_{(aq)}$, $NiOH^{+}_{(aq)}$ is minor (less than 5%).

Other calculations (Figure 4.2) were done at pH 8.3 by considering this time the precipitation of $Ni(OH)_{2(s)}$ and $NiO_{(s)}$ only, i.e. the phases exhibiting positive saturation indexes.

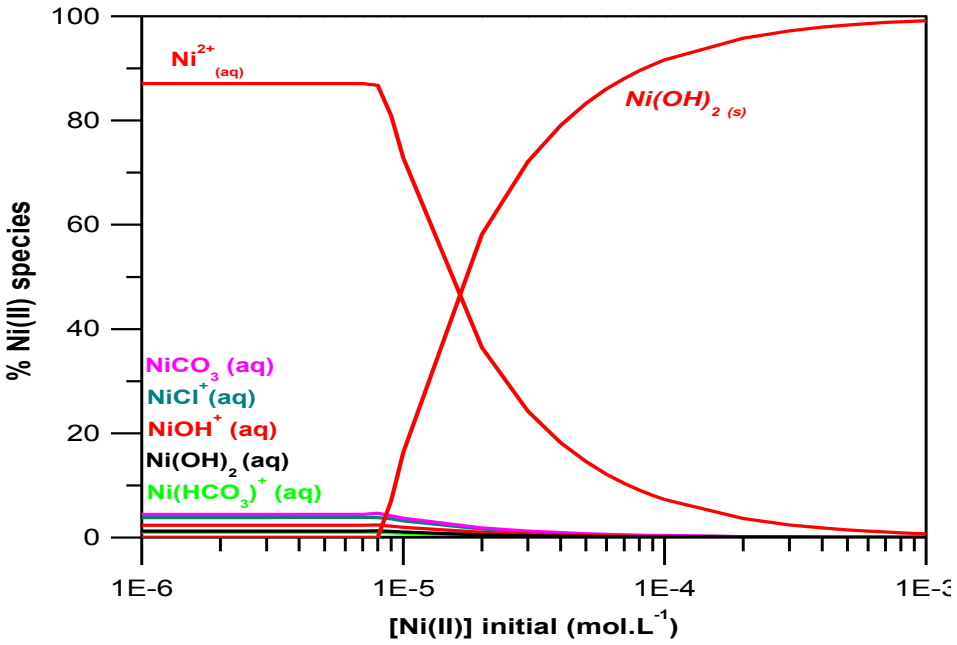

Figure 4.2: Concentration of aqueous species and solid phase as a function of the Ni(II) initial concentration (10^{-1} mol.L^{-1} NaCl, $pCO_2=10^{-3.5}$ atm and pH=8.3).

For concentrations higher than 10^{-5} mol.L^{-1}, $Ni(OH)_{2(s)}$ precipitates as predicted (Figure 4.2). The nickel precipitation is governed by the solubility of $Ni(OH)_{2(s)}$. In parallel to the increasing initial nickel concentration, the relative concentration of $Ni^{2+}_{(aq)}$, the predominant Ni(II) aqueous species, decreases.

Finally, speciation calculations were performed for a nickel concentration of 10^{-4} mol.L^{-1}, $pCO_2=10^{-3.5}$ atm and between pH 6 and 9. To reflect experimental conditions, a solution pre-equilibrated with calcite (pH 8.3) was used for the calculations. However, no calcite was introduced. Results are shown in Figure 4.3.

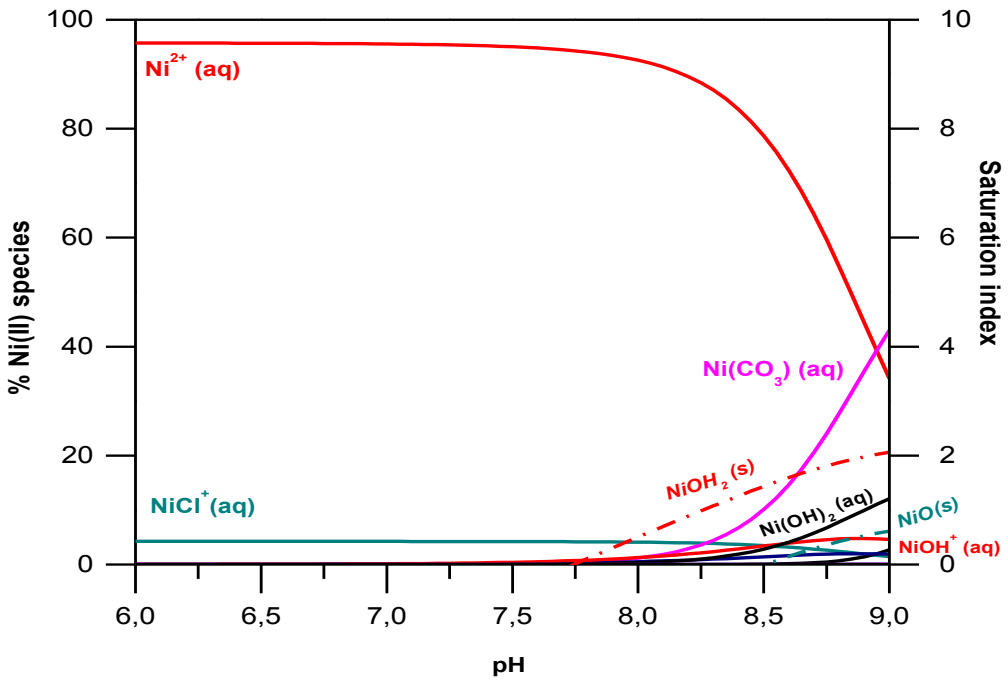

Figure 4.3: Concentration of aqueous species and saturation indexes of solid phases at 10^{-4} mol.L^{-1} Ni(II) as a function of pH (10^{-1} mol.L^{-1} NaCl, $pCO_2=10^{-3.5}$ atm).

For 0.1 mol.L^{-1} NaCl and atmospheric conditions, among the aqueous species, $Ni^{2+}_{(aq)}$ predominates in the pH range of 6−8, which can be compared with the results obtained by Lamana [14]. Another aqueous species that has an important abundance is $Ni(CO_3)_{(aq)}$ between pH 8.2 and 9.0. Contrary to Lamana's results, $Ni(CO_3)_2^{2-}{}_{(aq)}$ does not appear in our calculations. This is due to the differences in log K between those present in the WATEQ4f database [122] used by Lamana, and in Thermochimie 9.0 [111].

4.1.2. Nickel speciation in CPES: macroscopic results and XRD

Blank solutions were made up of CPES spiked with the appropriate volumes of nickel stock solution to obtain the desired final concentration. Time sequency experiments were performed on various initial Ni(II) concentrations such as 10^{-6}, 10^{-5}, 10^{-4} and 10^{-3} mol.L^{-1} to understand the behavior of nickel in CPES solutions. This study is very important especially to understand behavior of Ni(II) with ubiquitous carbonate ligands and to check the accuracy of our speciation calculations. In Figure 4.4, the concentration left in supernatant measured by ICP−MS as a function of stirring time is presented.

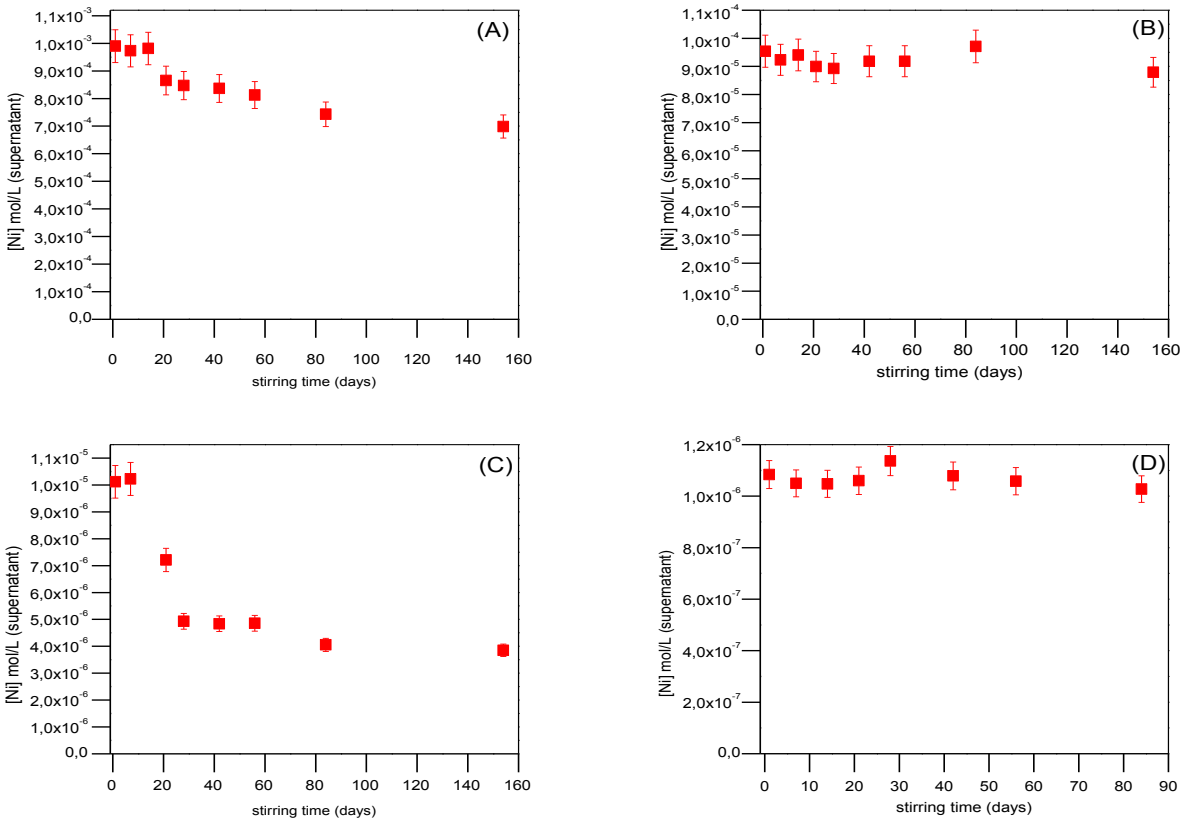

Figure 4.4: Concentration of Ni(II) left in supernatant for CPES solutions as a function of stirring time, for initial Ni concentrations of 10^{-3} mol.L^{-1} (pH = 8.1-8.3) (A), 10^{-4} mol.L^{-1} (pH = 8.3-8.4) (B), 10^{-5} mol.L^{-1} (pH = 8.3-8.4) (C) and 10^{-6} mol.L^{-1} (pH = 8.3-8.4) (D) ($pCO_2 = 10^{-3.5}$ atm, I = 0.1 mol.L^{-1} (NaCl)).

After approximately 20 days, for the 10^{-3} mol.L^{-1} initial concentration, the concentration of nickel left in the supernatant decreases, which means that the precipitation of nickel occurs (as a slow process). This fact is in agreement with speciation diagrams (Figure 4.1), which predict the formation of solid $Ni(OH)_2$. However, there is a discrepancy for the amount of nickel precipitated between speciation calculations (approximately 100 %) and that observed experimentally (about 30% after 150 days). This can be due to kinetic effects. One should also not forget possible differences in solubility products between freshly precipitated and well-crystalline phases.

For 10^{-4} mol.L^{-1}, the remaining concentration is close to the initial one and remains constant overtime, though precipitation could clearly be optically observed. Again, the amount of nickel

precipitating is in disagreement with our speciation calculations. For 10^{-5} mol.L^{-1}, precipitation occurred readily, but a significant decrease of nickel concentration left in the supernatant was noticed after 20 days. Again, precipitation turned out to be a slow phenomenon. The observed remaining concentration, i.e. 4×10^{-6} mol.L^{-1}, is about twice lower than predicted by thermodynamic calculations (Figure 4.2). Finally, no precipitation is occurring as expected from speciation diagrams for 10^{-6} mol.L^{-1}.

In order to check the nature of the precipitate, XRD analysis was performed on the solid phase obtained for a CPES sample spiked with 10^{-3} mol.L^{-1} Ni(II) stirred for 104 days. Results showed that the solid phase is $Ni(OH)_{2(s)}$ according to the ICDD file 01-075-6921 (Figure 4.5).

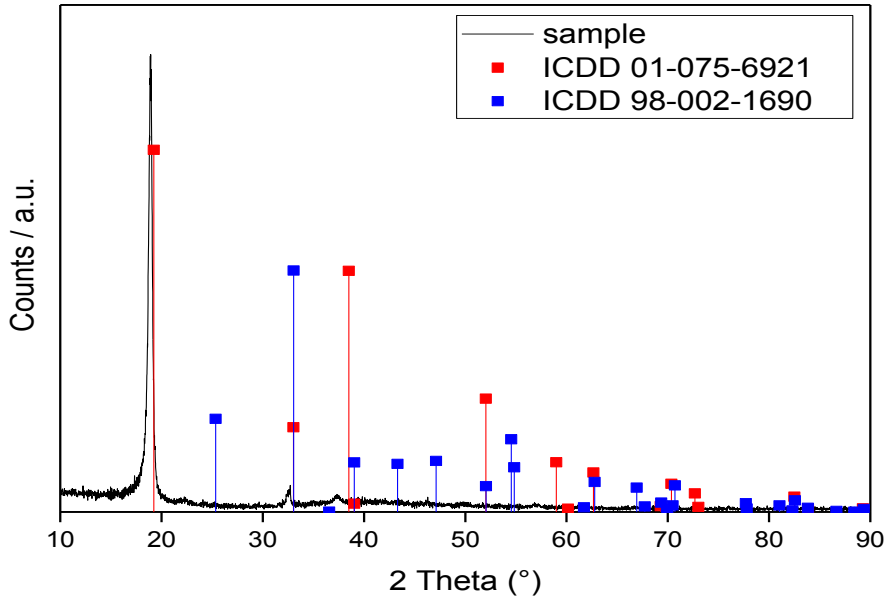

Figure 4.5: XRD of the solid phase precipitating after 104 days from a CPES solution spiked with 10^{-3} mol.L^{-1} Ni(II), with reference pattern of $Ni(OH)_2$(s) (red) (ICDD card 01-075-6921) and $NiCO_3$(s) (blue) (ICDD card 98-002-1690).

The precipitate resembles a fibrous felt, which was very difficult to grind. No dense sample with well-defined surface could thus be produced for the Bragg-Brentano XRD measurement. To minimize the obvious pattern shift compared to the literature data, a sample height correction was applied. Moreover, there are some intensity mismatches due to preferred orientation of the fibers. No hint for $NiCO_{3(s)}$ (ICDD 98-002-1690) was noticeable by XRD (Figure 4.5). The

peaks at 2θ = 19° and 37° would also fit with $Ni_3O_2(OH)_4$ (ICDD 00-006-0144) and β-NiOOH (ICDD 00-006-0141), but the quality of the ICDD references is doubtful. Nevertheless, in agreement with our speciation calculations (Figure 4.2), the nickel precipitation appears to be governed by the solubility of $Ni(OH)_{2(s)}$ under our experimental conditions.

In summary, precipitation of nickel occurs at 10^{-5}, 10^{-4} and 10^{-3} mol.L^{-1}, contrary to 10^{-6} mol.L^{-1}. However, speciation calculations overestimate the amount of nickel precipitating. Our blank experimental results show that precipitation of nickel under our experimental conditions is a slow process lasting up to several months.

4.2. Interaction of Ni(II) with calcite: macroscopic studies

4.2.1. Sorption isotherms

Nickel adsorption experiments were performed to investigate Ni(II) interaction with calcite as a function of time and concentration, and were followed by desorption experiments in order to test reversibility.

For our study, the concentrations that were chosen are 10^{-6}, 5×10^{-6}, 10^{-5}, 5×10^{-5}, 10^{-4}, 5×10^{-4} mol.L^{-1} Ni(II), ionic strength 10^{-1} mol.L^{-1} NaCl and 1 g.L^{-1} of calcite (SOLVAY(SOCAL U1−R). The solubility of Ni(II) according to the ANDRA's "Dossier Argile 2005" report [2] is close to 10^{-6} – 10^{-5} mol.L^{-1} in the conditions of COx clay rocks pore water. The lowest concentrations considered in our study match with ANDRA's requirements, but higher concentrations were also used to satisfy spectroscopic techniques' requirements. Also, these conditions were needed to distinguish between different possible mechanisms occurring at Ni(II)/calcite interface. All the experiments were performed under atmospheric conditions (pCO_2 = $10^{-3.5}$ atm imposing pH=8.3). The sorption fractions of nickel (% Ni adsorbed) were calculated with respect to the following formula:

$$\%\,\text{Ni adsorbed} = \frac{[\text{Ni initial}] - [\text{Ni supernatant}]}{[\text{Ni initial}]} \times 100$$

where:

- [Ni $_{initial}$] is the initial concentration of nickel added in the reactor (mol.L^{-1})

- [Ni $_{supernatant}$] is the concentration of nickel left in the supernatant measured by ICP−MS ($mol.L^{-1}$)

In Figure 4.6, classical sorption isotherms are represented for each reaction time as the concentration of sorbed nickel ($mol.g^{-1}$) versus the nickel concentration in solution ($mol.L^{-1}$).

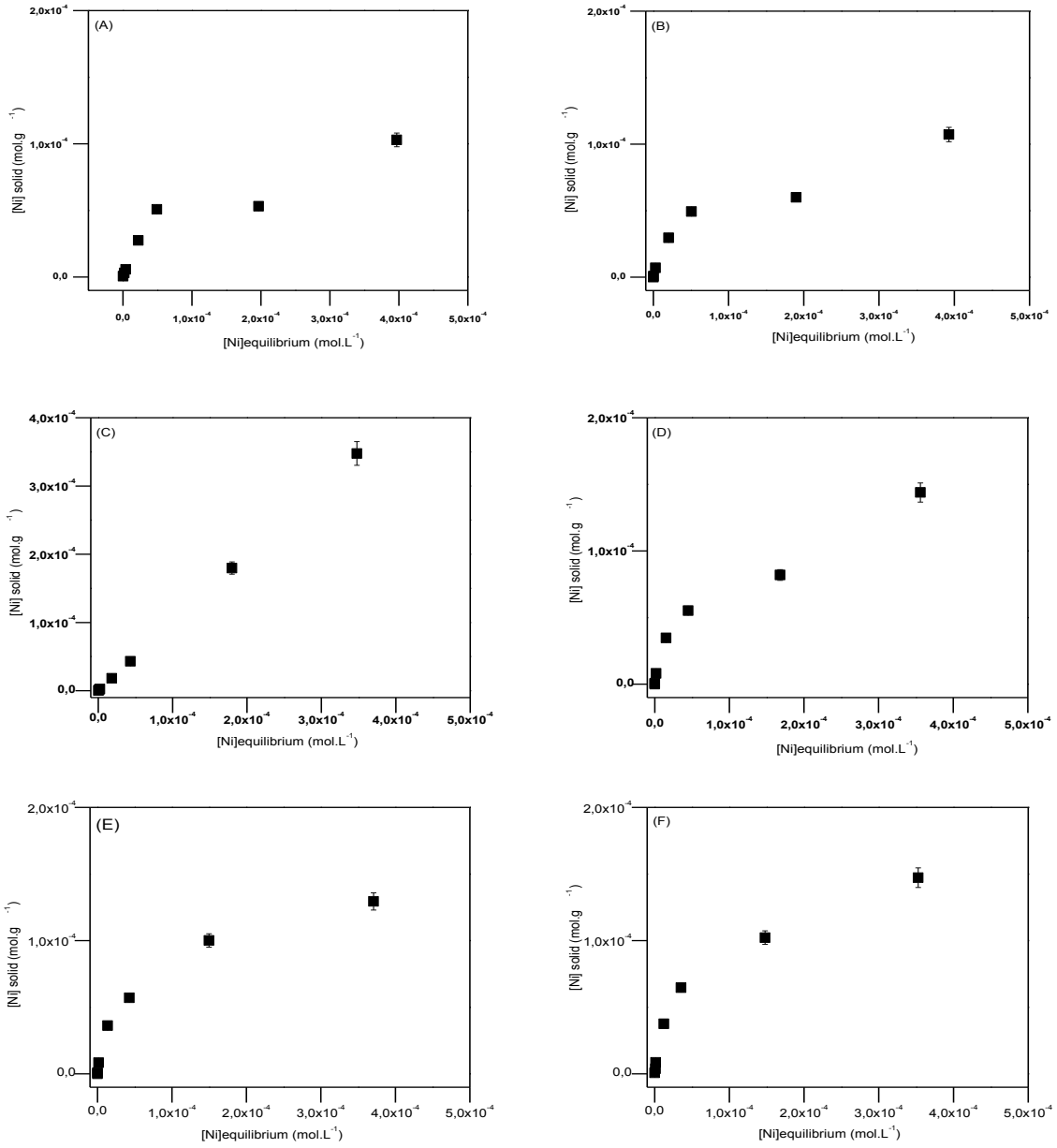

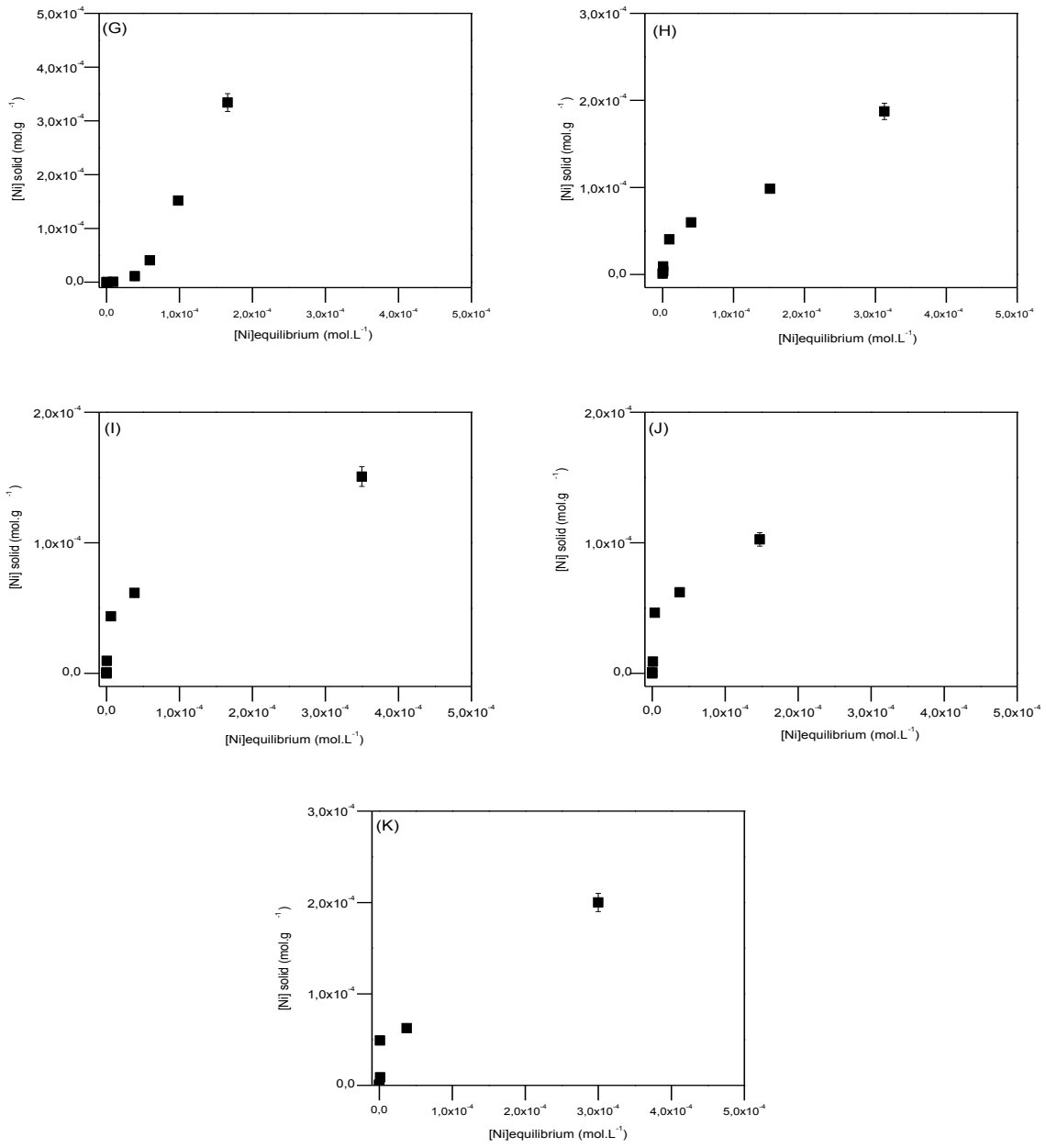

Figure 4.6 :Nickel isotherms for various contact times: (A) 1 day, (B) 4 days, (C) 1 week, (D) 2 weeks, (E) 3 weeks, (F) 4 weeks, (G) 6 weeks, (H) 8 weeks, (I) 10 weeks, (J) 12 weeks, and (K) 15 weeks
($[Ni]_0 = 10^{-6}$, 5×10^{-6}, 10^{-5}, 5×10^{-5}, 10^{-4}, 2.5×10^{-4}, 5×10^{-4} mol.L^{-1}, s/L = 1 g.L^{-1} $CaCO_3$ (SOLVAY), I = 10^{-1} mol.L^{-1} (NaCl), pH = 8.3-8.4 and stirring time 1 day – 15 weeks).

The presented isotherms do not present a plateau for high concentrations. This probably implies that the mechanisms are more complicated than a simple monolayer adsorption on homogeneous surface sites.

Results are presented as the fraction of sorbed nickel versus initial concentration in Figure 4.7 in order to have a better picture of the evolution with time of each sorption experiment.

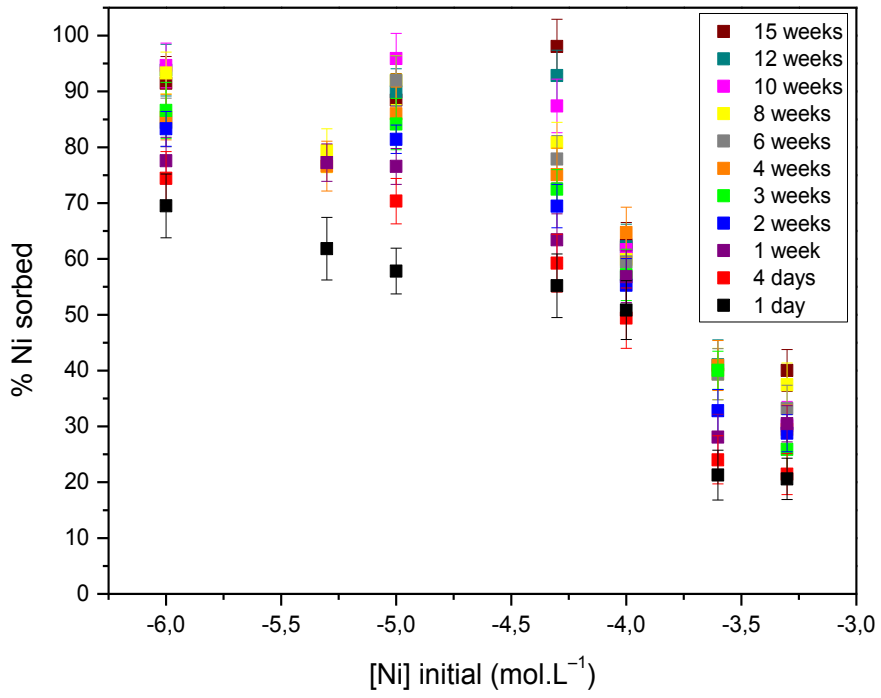

Figure 4.7: Nickel sorption onto calcite ($[Ni]_0 = 10^{-6}$, 5×10^{-6}, 10^{-5}, 5×10^{-5}, 10^{-4}, 2.5×10^{-4}, 5×10^{-4} mol.L^{-1}, s/L = 1 g.L^{-1} $CaCO_3$ (SOLVAY), I = 10^{-1} mol.L^{-1} (NaCl), pH = 8.3-8.4 and stirring time 1 day – 15 weeks).

The sorption fractions turned to be dependent of the initial concentration of Ni(II). As the concentration increases, the sorption fractions are decreasing. For the highest initial Ni(II) concentration (5×10^{-4} mol.L^{-1}), sorption is noticed after 1 day, the fraction being ~20%. For the lowest initial Ni concentration (10^{-6} mol.L^{-1}), ~70% of sorption is observed after 1 day. After 15 weeks of stirring time, fractions are increasing to 40% for $[Ni]_{initial}=5\times10^{-4}$ mol.L^{-1}), while for 10^{-6} mol.L^{-1} the sorption fractions are higher than 90%.

The evolution as a function of concentration seems logical: for lower concentrations, part of the surface sites of calcite should be occupied, whereas for higher concentrations in nickel the surface sites of calcite should be saturated and processes like multilayer adsorption or surface precipitation may occur. The evolution as a function of time shows that Ni(II) uptake increases with time for all the concentrations. More, there seems to be a fast sorption step followed by a slower one. Similar results were obtained by Lamana [14] for experiments with durations between 1 and 120 hours, a Ni(II) concentration of 1.2×10^{-4} mol.L^{-1}, and pH ranging from 7.8 to 9.0 with a fast step in the first 24 hours and then a slower increase of the sorbed quantity.

Nevertheless, interaction of Ni(II) with calcite was not previously studied in the literature for the longest contact times and for the highest nickel concentrations of our study.

Results show that calcite has a rather high affinity for Ni(II) and results are comparable with existent sorption data in literature [11, 13, 14, 84]. For higher concentrations, precipitation of Ni(II) should occur, but not for the lower concentrations as shown in speciation diagrams. Several authors [11, 13, 14, 84] (describe sorption of divalent metals as adsorption on calcite surface, followed by slow process of co-precipitation by re-crystallization or even entrapment into defect sites. According to Davis et al. [90] (for Cd), the first 24 hours are important for adsorption. In this study notable differences are observed over time.

Desorption studies were thus carried out to further investigate the sorption mechanism as a function of time.

4.2.2. Desorption studies

Following each sorption experiment, desorption experiments were carried out by replacing the nickel supernatant by Ni-free CPES solutions to each flask, after different sorption contact times, in similar experimental conditions (pH = 8.3±0.1, $pCO_2=10^{-3.5}$ atm). After the replacement of the supernatant, the concentration of nickel in solution was then measured for different desorption contact times. Desorption of Ni(II) from calcite has already been studied [11, 14]. Nevertheless, this study is novel since, to our knowledge, the Ni(II) behavior with carbonates and sorption behavior on calcite in NaCl solutions of various concentrations and such long contact times has never been investigated. In Figure 4.8, results corresponding to desorption experiments performed after 1 day, 1 week, 1 month and 2 months of sorption and various desorption contact

times are presented. The amount of remaining Ni(II) sorbed on the calcite surface is presented. A complete desorption is not expected, unless a new equilibrium would be established.

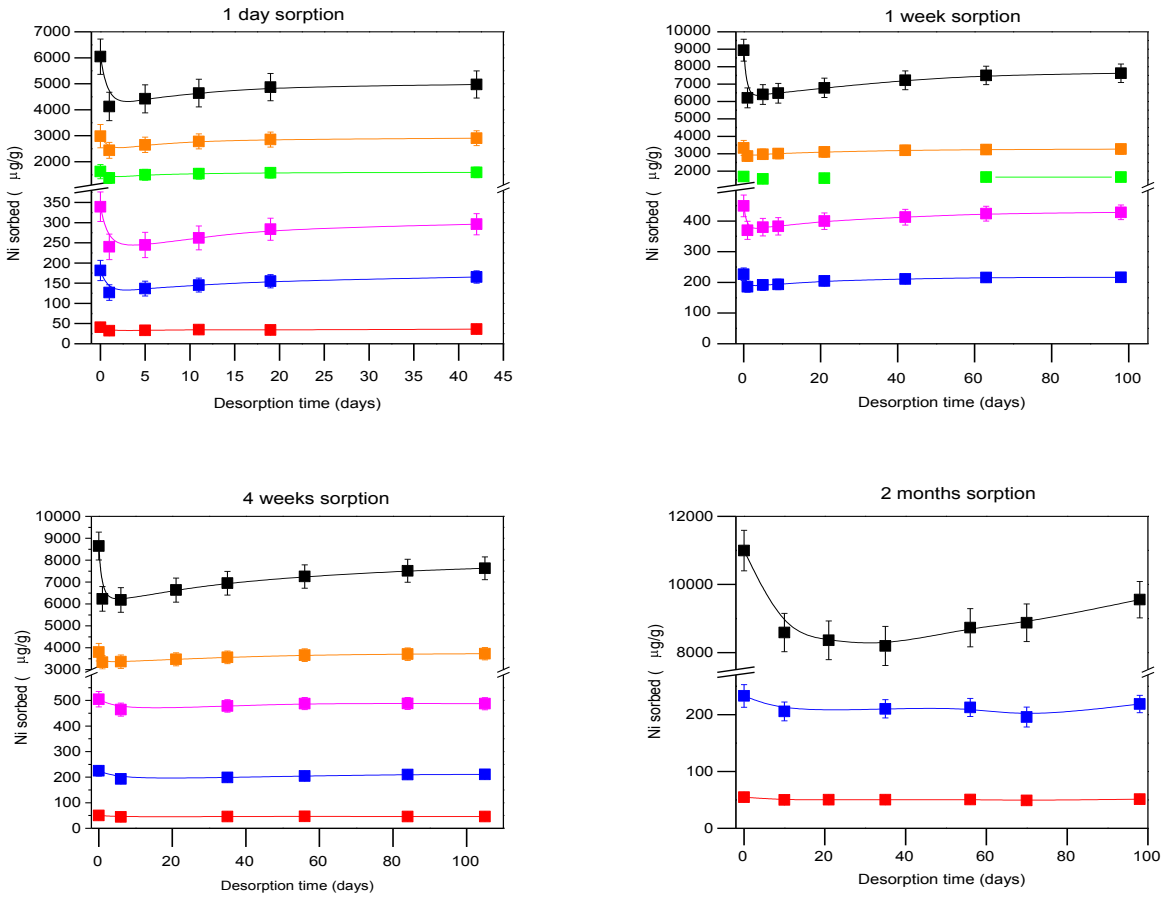

Figure 4.8: Desorbed fractions for Ni(II) as a function of stirring time and Ni(II) initial adsorbed concentration (10^{-6} mol.L^{-1} – red, 5×10^{-6} mol.L^{-1} – blue, 10^{-5} mol.L^{-1} – pink, 5×10^{-5} mol.L^{-1} – green, 10^{-4} mol.L^{-1} – orange and 5×10^{-4} mol.L^{-1} – black).

The first conclusion that we may draw from the experimental results is that desorption takes place for every concentration and duration of the sorption step. This assumption is not in agreement with results from Lamana's study [14], who investigated sorption of nickel onto calcite for 24 hours and then initiated desorption for 48 hours. They observed desorption for their weakest concentrations (initial concentration below ~10^{-4} mol.L^{-1}), but did not observe any desorption for higher concentrations. For desorption experiments performed after 1 day sorption the sorbed quantity decreases in a first step for all the studied concentrations. This means that desorption takes place, but if we consider longer desorption contact times, the sorbed quantity

increases. This behavior has never been observed before, but desorption of nickel onto calcite has never been studied for more than 48 hours [11, 14]. This increase of the sorbed quantity over time for longer experiments seems surprising at first sight, since we would have expected that as desorption takes place, the sorbed quantity would progressively decrease. The same tendency is observed for the desorption experiments carried out after 1 week sorption and 4 week sorption. After 2 months sorption, for the strongest concentration 5×10^{-4} mol.L^{-1}, the evolution of the sorbed quantity as a function of desorption time is more pronounced, and the evolution for the weaker concentrations is similar to the behavior observed for the shorter durations of the sorption step.

In order to estimate the degree of reversibility of nickel sorption on calcite as a function of contact time and concentration, we should introduce a new parameter. This new parameter has to take into account the fact that a completely reversible reaction does not result in a null sorbed quantity on the solid but in a sorbed quantity corresponding to sorption equilibrium. We then have to estimate what this quantity should be if a new equilibrium takes place after replacing the supernatant by a Ni(II) free solution. If the reaction is fully reversible, we should obtain the same quantity on the solid either after the sorption of nickel on a neat, Ni(II) free calcite, from a solution with a C_0 nickel concentration (in mol.L^{-1}), or after desorption from a Ni(II)-sorbed calcite with a C_0 concentration (also expressed in mol.L^{-1} of solution) put in contact with a Ni(II) free solution.

For each duration of desorption step and each concentration, we thus estimated the theoretical sorbed quantity in a full reversible case. For this, we used the results of the sorption experiments presented in section 4.2.1., for approximately the same initial concentration as the initial C_0 on the solid for desorption experiments, and the same contact time.

Based on the definition proposed by Zachara et al. [11], we then defined a desorption index D.I. as:

$$D.I. = \frac{theoretical\ sorbed\ quantity\ in\ a\ reversible\ case}{measured\ sorbed\ quantity\ after\ desorption}$$

The D.I. is thus equal to 1 when the reaction is fully reversible and it becomes smaller as the irreversibility of the reaction increases. The deviation from the ideal value (1) is then an

indication of the degree of reversibility of the reaction. The D.I. calculations for the different initial concentrations before the sorption step, and after 1 day, 1 week, 1 month and 2 months of sorption and various desorption contact times are shown in Figure 4.8.

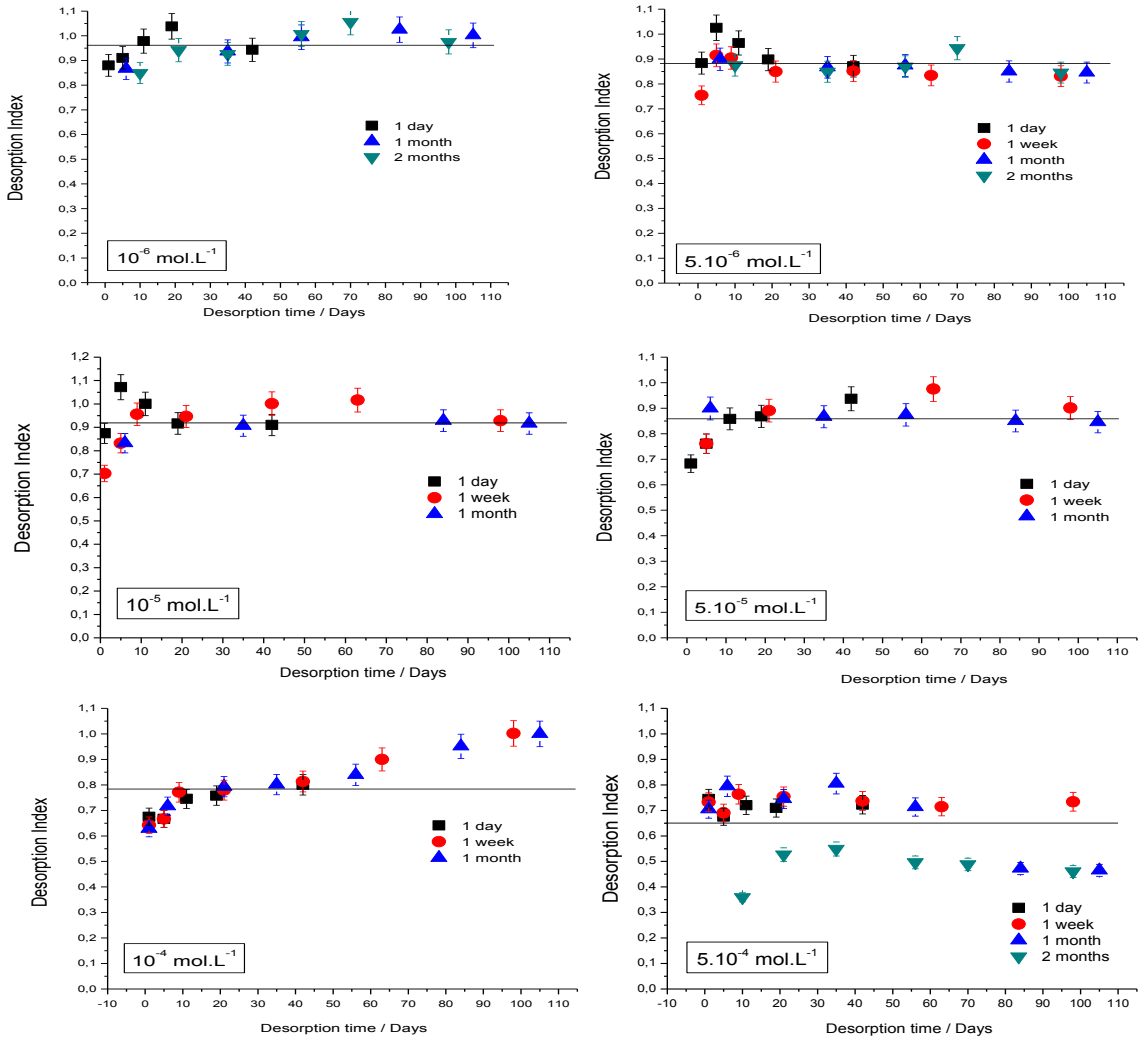

Figure 4.9: Desorption indexes as a function of desorption time, for Ni initial concentrations ranging from 10^{-6} mol.L^{-1} to 5.10^{-4} mol.L^{-1}, for 4 durations of the sorption step (■: 1 day, ●: 1 week, ▲: 1 month and ▼: 2 months). The horizontal lines on the graphs stands for the mean value of the desorption indices for each concentration.

From Figure 4.9 , a decrease of the D.I. can be seen when the Ni(II) concentration increases, from a mean value around 0.95 for a Ni(II) initial concentration of 10^{-6} mol.L^{-1} to a mean value around 0.65 for a Ni(II) initial concentration of 5.10^{-4} mol.L^{-1} if we take the average of the desorption indexes. To better visualize this evolution, the evolution of the mean D.I. as a function of the initial concentration is plotted on Figure 4.10. A clear decrease as a function of the concentration is observed, which implies that, whereas reversibility is almost achieved for the lowest concentrations, irreversibility becomes higher for the highest concentrations. This would mean that different mechanisms are to be considered when dealing with low and high concentrations, probably adsorption when the concentration is low and surface precipitation or co-precipitation (or even uptake into the calcite structure) when the concentration is higher.

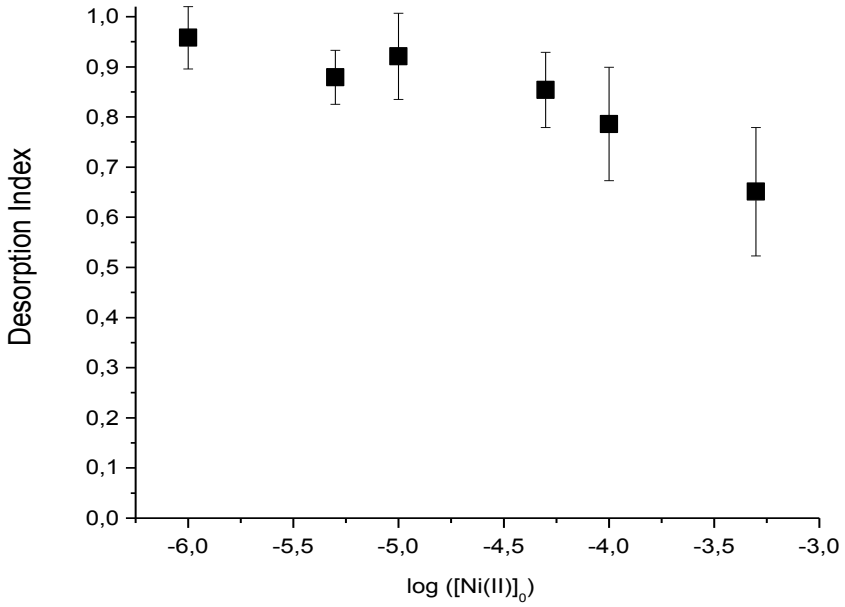

Figure 4.10: Mean desorption indexes as a function of Ni(II) initial concentration.

Our obtained D.I results for an initial nickel concentration of 10^{-6} mol.L^{-1} are somewhat different from the results of Zachara et al. [11], who obtained a D.I. of 0.8 for a concentration of 10^{-7} mol.L^{-1}. Indeed, 0.8 is the value that we obtain for higher concentrations (10^{-4} mol.L^{-1}). Nevertheless, the experimental procedure in Zachara et al. [11] for desorption experiments is

different from ours: in their study, desorption was achieved by decreasing the pH. Desorption results obtained by the two methods cannot thus be directly compared.

From Figure 4.10, a relative independency of the D.I. as a function of the durations of the sorption and desorption steps can be observed, which should result in two conclusions:

1) As the D.I. is independent of desorption time, this implies that desorption should occur rapidly and then remain constant.
2) As the D.I. is independent of the duration of the sorption step, the ratio between the reversible and irreversible part of the mechanism of the reaction between nickel and the calcite surface remains constant with the duration of the sorption step. This seems to be in contradiction with the conclusions drawn from the sorption study as a function of time in Section 4.2.1., where we proposed a fast adsorption (which is thought to be reversible) followed by a slower mechanism like incorporation by dissolution/re-precipitation (which is thought to be irreversible). One explanation may be that, even if slower mechanisms occur with time, some of them may also be reversible. Besides an irreversible trapping of nickel in the calcite lattice by dissolution/re-precipitation, we may then think of surface precipitation as a second slow mechanism occurring with time. This is in agreement with the blank experiments where we showed that Ni(II) precipitation is a long process.

As a conclusion, from the results of the time-dependent sorption experiments, desorption experiments, and the D.I. calculations, we may propose a sorption mechanism composed of two processes:

a) One fast reversible process, adsorption being a good candidate.
b) One long and partially reversible mechanism, which may correspond to surface precipitation.

A better understanding of the sorption mechanisms of nickel onto calcite (powder and single crystals) can be achieved by spectroscopic tools, among which we chose RBS, which is a powerful tool to determine the surface and depth concentrations of Ni. The extent of Ni(II) penetration into calcite can indeed be a clue to understand sorption mechanisms, as we showed in our study of interaction of europium with calcite. SEM-EDXS measurements were carried out mainly to assess the homo/heterogeneity of our samples.

4.3. Interaction of Ni(II) with calcite: spectroscopic studies

Preliminary tests using RBS were performed at IPNL (Institut de Physique Nucléaire de Lyon) at the milli−beam facility, on powders and single crystals.

4.3.1. Milli-beam RBS study on calcite powders

Calcite powders OMYA (BL 200) and SOLVAY (SOCAL U1-R) reacted during 1 month with Ni(II) (10^{-3} mol.L^{-1}). For this, a calcite equilibrated suspension was used. After interaction with Ni(II), powders were pressed to pellets and were analyzed with a 4 MeV ^{4}He incident beam. At this energy, the depth resolution is about 35 nm near the surface. It must be noted that two different analyses at different points have been made on each pellet and that a good reproducibility was obtained. RBS spectra of calcite reacted during 1 month with Ni(II) are exemplarily presented in Figure 4.11. Two distinct calcites were tested: OMYA (BL 200) with an initial average grain size of 50 µm and SOLVAY (SOCAL U1-R) with an initial average grain size of 0.2 µm. The nickel signal was detectable on the OMYA calcite only.

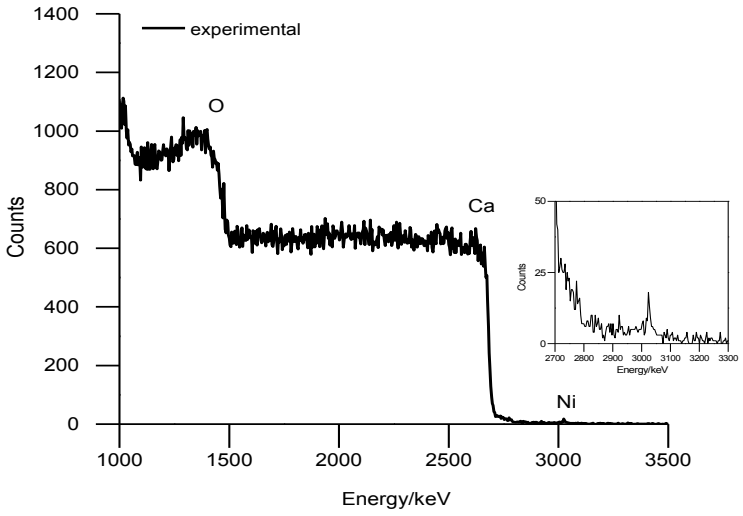

Figure 4.11: RBS spectra of calcite powder OMYA (BL 200) after 1 month contact time with 10^{-3} mol.L^{-1} Ni(II).

From Figure 4.11, the surface peak of nickel is shown at an energy of about 3000 keV, and the signal then becomes constant for lower energies (see zoom in the spectrum), before the Ca peak starts at about 2800 keV. As for the results obtained for the europium samples on pressed powders, this constant signal is the consequence of average effects when the beam interacts with

the Ni-rich region either located at the surface of the pellets or at the boundaries between grains. To solve the problem of averaging the signal on small grains, other preliminary experiments were performed at the milli-beam facility onto calcite millimetric single crystals.

4.3.2. Milli-beam RBS study on single crystals

The experiment was carried out for 10^{-3} mol.L^{-1} Ni(II) with a reaction time of 1 week and 3 weeks. The method of sample preparation is presented more detailed in chapter 2, wherein the same method was used for preliminary RBS milli-beam results on Eu(III) (use of a CSC-ES - calcite singe crystal equilibrated suspensions). The crystals were then analyzed and the incident beam was set to 1.5 MeV in order to improve the depth resolution and the backscattering yield. The RBS spectrum of one calcite single crystal after 3 weeks contact time with 10^{-3} mol.L^{-1} Ni(II) and pH = 8.3±0.1 (adjusted by NaOH) is presented in Figure 4.12.

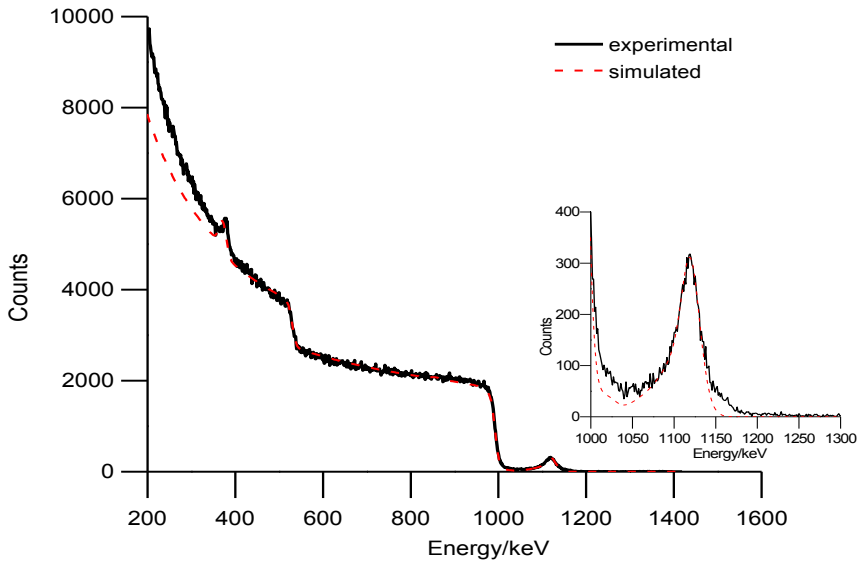

Figure 4.12: RBS spectrum of one calcite single crystal after 3 weeks contact time with 10^{-3} mol.L^{-1} Ni(II) and pH = 8.3±0.1 (adjusted by NaOH) (experimental spectra – black and simulated – red).

From this spectrum, Ni is observed onto the surface of the crystal, where the peak around energy of 1150 keV appears. Figure 4.13 shows the depth concentration profiles for Ni (10^{-3} mol.L^{-1} with a contact time of 1 and 3 weeks).

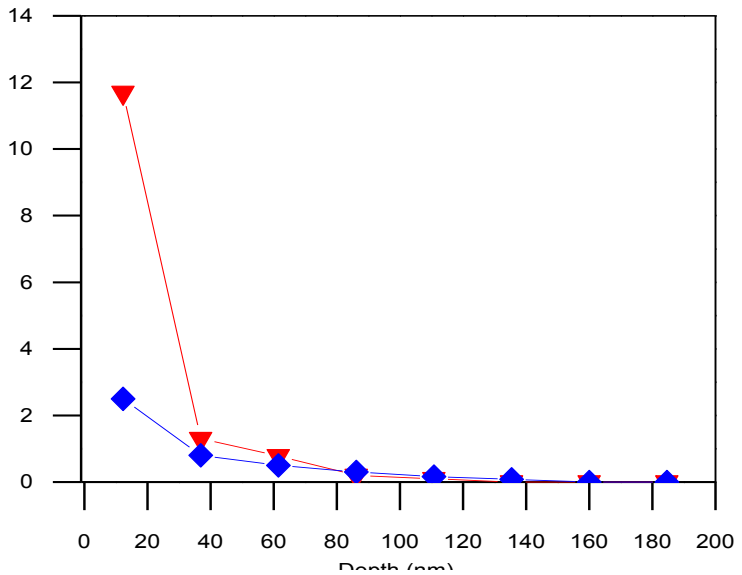

Figure 4.13: Depth concentration profiles of Ni(II) (sorption with 10^{-3} mol.L^{-1} solution during 1 week (▼) and 3 weeks (♦) in calcite single crystals. Lines are only plotted to guide the eyes.

The surface accumulation is present for both profiles, with high Ni(II) concentrations at the extreme surface of the sample. The Ni(II) concentration decreases sharply from the extreme surface to the bulk, which would indicate a surface accumulation rather than incorporation into the single crystals.

Table 4.3 presents the results considering 2 layers in the modeling of the results by the SIMNRA software (plus the layer corresponding to carbon covering): one layer at the extreme surface of the sample, where the Ni(II) content is important, and one layer defined in the depth of the sample, where the amount of nickel is smaller. The thickness of the first layer (the second layer being infinite) was chosen as the depth resolution of the milli-beam facility at IPNL in our experimental conditions, which is 25 nm. The table contains the atomic percentages calculated in the two layers.

Table 4.3: Ni(II) concentrations (at. %) in surface and in depth for calcite single crystals immersed in 10^{-3} mol.L^{-1} Ni(II) for 1 week and 3 weeks.

Contact time	Surface layer (at.%)	Depth (at.%)
1 week	11.70	0.34
3 weeks	2.50	0.26

Table 4.3 shows that there is an order of magnitude between the concentrations measured at the extreme surface of the samples and the concentrations measured in the bulk. This confirms the surface accumulation of nickel which would be in agreement with the formation of a surface precipitate. The differences on surface concentration can be due to a change in mechanisms or possible penetration of precipitate into the damage irregular calcite surface due to NaOH addition. The heterogeneities on the calcite surface analyzed by SEM-EDXS were already presented in section 3.5 for Eu(III).

In order to confirm our preliminary results obtained by milli-beam and to get more insight into the sorption mechanisms of Ni(II) into calcite, experiments using a micro-beam were performed at the CEA Saclay accelerator in order to enhance the spatial beam resolution and to obtain elemental maps. SEM-EDXS measurements were carried out in parallel to get information on the modifications in the morphology of the crystal and on the homo/heterogeneity of the sample.

4.3.3. µ-beam RBS and SEM-EDXS studies on single crystals

A µ−beam with energy of 1.5 MeV for a better depth resolution and backscattering yield was used. For these experiments, calcite single−crystals were put in contact with CSC-PES (calcite single-crystals pre-equilibrated solution), then spiked with Ni(II) to obtain an initial concentration of 10^{-4} or 10^{-3} mol.L^{-1} and stirred for different contact times (1 week − 2 months). Ni(II) elemental maps (Ni onto the surface and the depth) were drawn using the RBS spectra for each sample after being in contact with 10^{-4} mol.L^{-1} Ni solution for 1 week (Figure 4.14) and 1 month (Figure 4.15). Ni(II) relative content is indicated as a function of the color (very low contents – blue and higher ones – red−yellow).

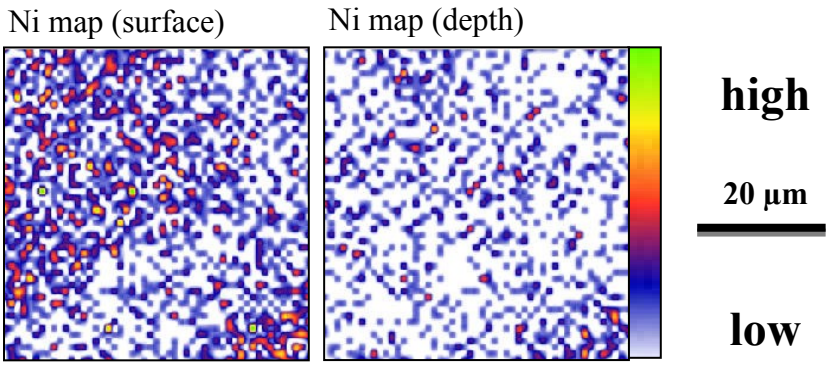

Figure 4.14: Ni(II) elemental maps in surface and depth obtained for 10^{-4} mol.L^{-1} Ni(II), 1 week contact time, extracted from RBS spectra.

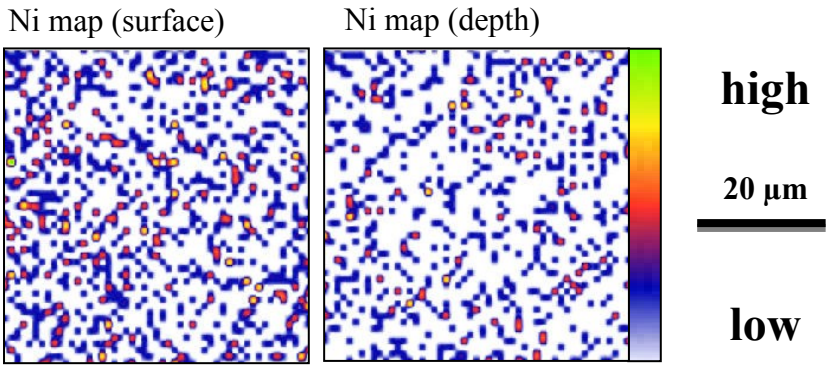

Figure 4.15: Ni(II) elemental maps in surface and depth obtained for 10^{-4} mol.L^{-1} Ni(II), 1 month contact time, extracted from RBS spectra.

As can be observed, nickel is not uniformly distributed on surface. Some red−yellow spots signals the presence of more significant concentration of nickel.

The RBS spectrum of one calcite single crystal after 1 week contact time with 10^{-4} mol.L^{-1} Ni(II) is presented in Figure 4.16. The general shape of the spectrum, with a Ni(II) peak located at around 1150 keV, is the same as for the spectra recorded at the micro-beam facility.

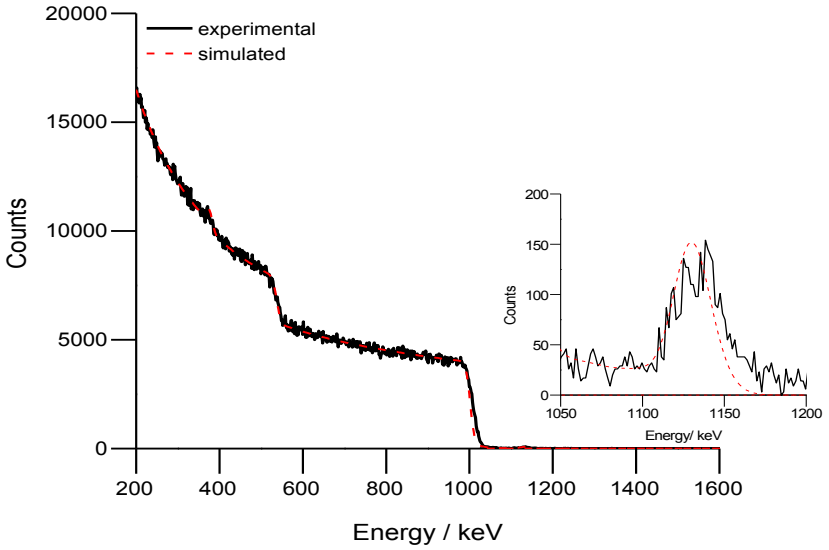

Figure 4.16: RBS spectrum of a calcite single crystal after 1 week contact time with 10^{-4} mol.L^{-1} Ni(II) (experimental spectra – black and simulated – red).

Simulations of the spectra for 1 week and 1 month contact times and 10^{-4} mol.L^{-1} Ni(II) are shown in Table 4.4. Two layers were used to model the RBS spectrum. The thickness of the first layer was chosen to be 12-15 nm, which was necessary for modeling the spectra, but this value is inferior to the depth resolution of our experiments at the CEA Saclay micro-beam facility which is around 30 nm. This value (30 nm) is then the value to be considered when interpreting the results.

Table 4.4: Ni(II) concentrations (at. %) in surface and in depth for calcite single crystals immersed in 10^{-4} mol.L^{-1} Ni(II) for 1 week and 1 month.

Contact time	Surface layer (at.%)	Depth layer (at.%)
1 week	0.50	0.04
1 month	0.38	0.04

From the table, concentrations are weaker than for the two samples measured at the milli-beam facility, but the experiments should be compared with 10^{-3} mol.L^{-1} samples (see later in this section). The same general features are observed as for the milli-beam experiments: Ni(II) is located at the extreme surface of the sample, in the first 30 nm, then the concentration drops nearly to zero. There is also an order of magnitude between the concentration at the surface and

in the bulk. This location of Ni(II) on the surface of the sample is even more pronounced than for the milli-beam results described in section 4.3.2 which showed a somewhat higher Ni(II) content in the bulk. This could be explained by the experimental procedure used to prepare the samples. Indeed, for the preliminary milli-beam experiments, crystals were prepared in a 0.1 mol.L^{-1} NaCl equilibrated suspension instead of a CSC-PES solution and the pH was thus initially weaker (around 5-6) which may have altered the calcite surface and made possible a dissolution/co-precipitation mechanism. SEM−EDXS measurements were then carried out to confirm the variable distribution of nickel, to check the homogeneity of the solid samples and to check the state of the surface in order to identify possible surface precipitate.

SEM-EDXS measurements were performed in two distinct positions of each crystal to check the homogeneity of the samples and EDXS measurements were conducted to identify areas where Ni(II) was more concentrated, which may be surface phases that are formed. In Figure 4.17, three measurements done on a calcite single crystal for different scales (50, 10 and 2 µm) at 10^{-4} mol.L^{-1} initial nickel concentration are presented.

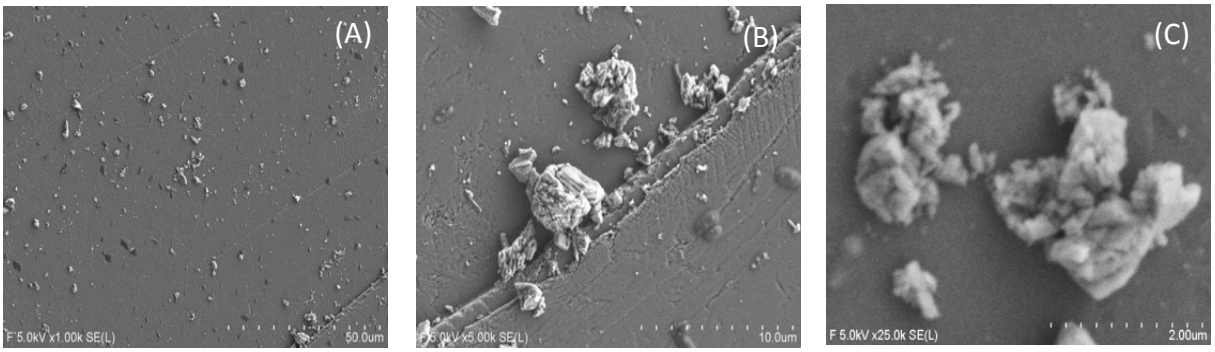

Figure 4.17: SEM images at different scales: 50 µm (A), 10 µm (B) and 2 µm (C) of 10^{-4} mol.L^{-1} Ni(II) sorbed onto calcite single crystal during 1 month.

From Figure 4.17 (A), shown with a scale of 50 µm, pits on the surface of the crystal in contact with Ni(II) for 1 month are noticed. In Figure 4.17 (B), one crack of the crystal can be observed but also some flakes that are present on the surface. One of these flakes was measured by EDXS to determine the elemental composition, and turned out to be pure calcite. By EDXS in all cases, low Ni(II) content was measured, very close to detection limit (data not shown).

To investigate the impact of the initial Ni(II) concentration and subsequent surface loading, another set of experiments were performed for a higher concentration, 10^{-3} mol.L^{-1} which additionally gives the possibility to obtain a good signal/noise ratio. Ni(II) elemental maps were obtained from RBS spectra, and the maps are presented for two stirring times in Figure 4.18 (1 month) and Figure 4.19 (2 months). It should be noted that, as the acquisition time was different for the two samples, the relative scale of the concentrations is not the same in the two figures, so the concentrations cannot be compared for the two samples from the maps.

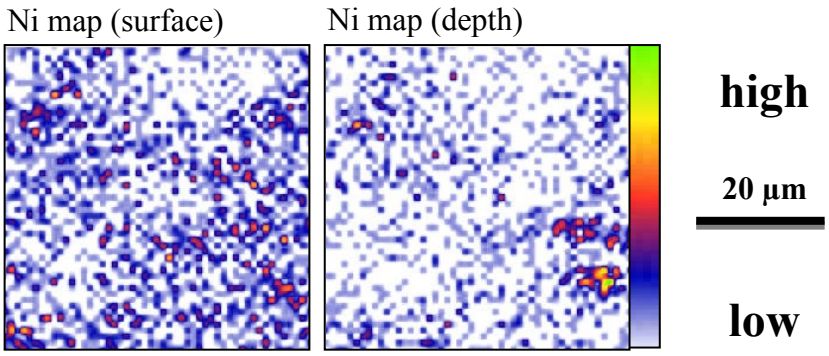

Figure 4.18: Ni(II) elemental maps in surface and depth obtained for 10^{-4} mol.L^{-1} Ni(II), 1 month contact time, extracted from RBS spectra.

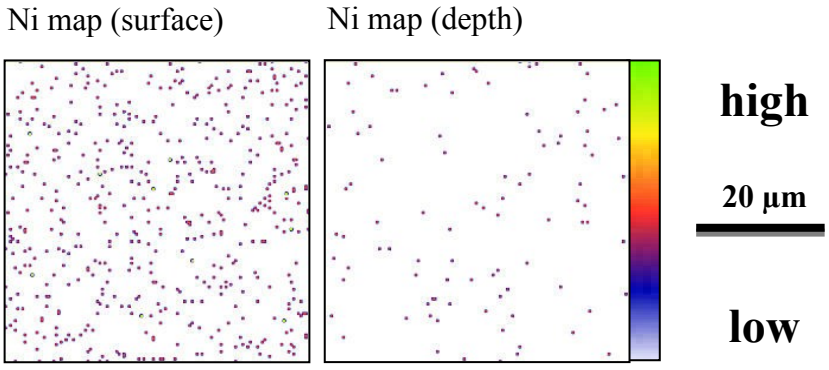

Figure 4.19: Ni(II) elemental maps in surface and depth obtained for 10^{-3} mol.L^{-1} Ni(II), 2 months contact time, extracted from RBS spectra.

The distribution of nickel content is not uniform, some concentrated spots are observed on the two samples as well as areas where the Ni(II) content is weaker. The concentrated spots (yellow-reddish), heterogeneously located on the surface, can be seen more clearly on Figure 4.18.

SEM−EDXS measurements were then carried out to get more information on the surface heterogeneity. In Figure 4.20, three different scales 50, 10 and 2 µm as in the previous case are presented.

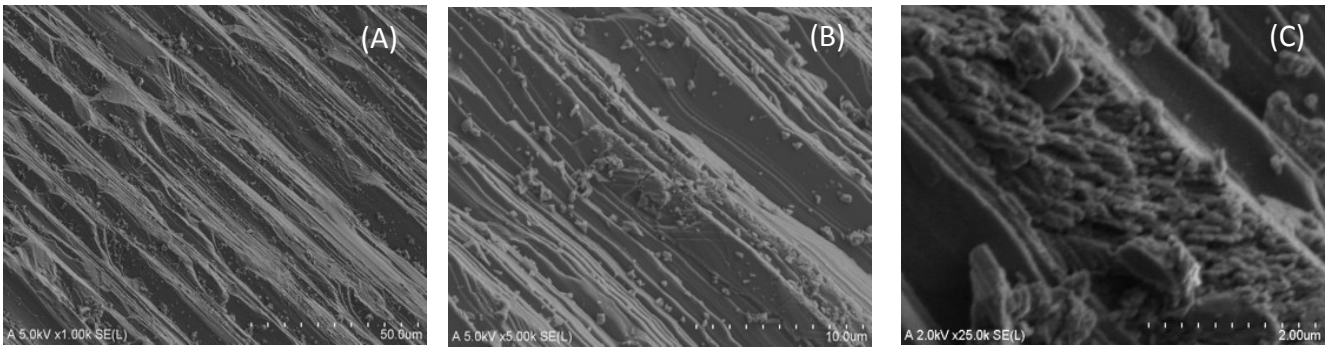

Figure 4.20: SEM images of 10^{-3} mol.L^{-1} Ni(II) sorbed onto calcite single crystals during 1 month with different magnifications 50 µm (A), 10 µm (B) and 2 µm (C).

From Figure 4.20 (A) on crystal, are noticed linear stripes. One of these stripes was analyzed and turned out to be calcite. Apart from the stripes, by EDXS analysis of Ni(II) on near surface probed area was identified having a content of 0.4 at.% in first probed position and 0.8 at.% in the second probed position. Table 4.5 presents the simulations of the RBS spectra of nickel sorbed onto calcite for an initial concentration of 10^{-3} mol.L^{-1} Ni(II) and two contact times, 1 month and 2 months. Two layers were used to model the RBS spectrum as for the 10^{-4} mol.L^{-1} samples.

Table 4.5: Ni(II) concentrations (at. %) in surface and in depth for calcite single crystals immersed in 10^{-3} mol.L^{-1} Ni(II) for 1 month and 2 months.

Contact time	Surface layer (at.%)	Depth layer (at.%)
1 month	0.74	0.06
2 months	0.74	0.06

Results show that Ni(II) is localized at the extreme surface of the sample, in the first 30 nm, as for the 10^{-4} mol.L^{-1} experiments. Concentrations are similar to the 10^{-4} mol.L^{-1} samples, and there is also an order of magnitude between the concentration in the surface layer and the

concentration in the bulk. Compared with the milli-beam experiments, the concentrations are lower. It can be explained by the heterogeneities of the samples, as shown by RBS elemental maps and SEM-EDXS analyses.

In conclusion to the RBS experiments, a localization of Ni(II) in the first tens of nanometers has been observed either at the milli-beam facility at IPNL or at the micro-beam facility at CEA Saclay.

This surface accumulation would be in agreement with an adsorption or a surface precipitation of nickel. Strong heterogeneities were highlighted by RBS elemental mapping and SEM-EDXS measurements: if there is a surface precipitate, the precipitation does not occur uniformly on the crystal. The discrepancies revealed by surface techniques RBS and SEM-EDXS as a function of the stirring time can be due to different mechanisms occurring for each contact time. At these high initial nickel concentrations, the formation of the expected surface precipitate $Ni(OH)_{2(s)}$, which is not uniformly distributed, could be another explanation.

4.4. Summary and conclusions

Nickel sorption onto calcite but also other divalent metals were investigated by many authors [11, 14, 90, 91] who observed an initial adsorption followed by slower uptake which has often been interpreted as co-precipitation or re-crystalization. Anyway, hypotheses concerning the mechanism of Ni(II) interaction with calcite are various in the literature. Zachara et al. [11] highlight that sorption of Ni(II) onto calcite can be depicted as surface exchange between Ni^{2+} and Ca^{2+}, whereas Lamana [14] interprets the long progressive increase with time as co-precipitation or diffusion into the bulk. Carlsson and Aalto [13] who investigated Ni(II) co-precipitation with calcite using liquid scintillation observed Ni(II) incorporation by re-crystallization. SEM−EDXS investigations of Carlsson and Aalto [13] showed that Ni(II) can be found in recrystallized calcite. Since re-crystallization is driven by the difference in surface free energy for crystals of different sizes and that metastable solid phases can be formed [11], the likelihood of co-precipitation of an adsorbed Ni(II) into freshly formed calcite surface layers is considerable [84]. AFM and XPS studies were performed by Hoffmann and Stipp [12] on calcite single crystals in contact with $Ni(ClO_4)_2$ during 1 minute who found out that Ni(II) is adsorbed on calcite surface even though dissolution of solid's surface. Also, from samples exposed to Ni(II) solutions, the surface topography is modified by re-crystallization and this process can

bury a small amount of Ni(II) in the bulk. Later, Lakshtanov and Stipp [84] showed that Ni(II) is taken up/incorporated by solid solution formation.

In this study, we investigated at first the solution chemistry of Ni(II). Precipitation of Ni(II) was identified as a slow phenomenon by means of blank experiments in CPES solutions and precipitation of $Ni(OH)_{2(s)}$ at 10^{-3} mol.L^{-1} was evidenced by XRD, in agreement with speciation diagrams.

Nickel interaction with calcite was investigated as a function of time and concentration, at constant pH (8.3 ± 0.1), ionic strength (0.1 mol.L^{-1} (NaCl)), and $pCO_2 = 10^{-3.5}$ atm. Batch sorption experiments revealed high sorption fractions for Ni(II) initial concentrations such as 10^{-6}, 5×10^{-6}, 10^{-5} and 5×10^{-5} mol.L^{-1}, and lower ones for higher concentrations 10^{-4} mol.L^{-1}, 2.5×10^{-4} mol.L^{-1} and 5×10^{-4} mol.L^{-1}. Sorption was evidenced as a slow process which lasted several months. Desorption experiments revealed the release of Ni(II) over time for all concentrations. Desorption indexes were calculated and enabled to assess an almost complete reversibility for low concentrations (below 10^{-5} mol.L^{-1}), the irreversibility becoming higher when the concentration increases. To interpret the data, a two-step mechanism was proposed: a first initial fast adsorption followed by a slower mechanism such as surface precipitation or coprecipitation with calcite. RBS using both milli and micro beams showed accumulation of Ni(II) onto surface. RBS elemental maps showed a heterogeneous distribution of Ni(II) on single crystals surface, which was confirmed by SEM−EDXS measurements.

Taking into account the literature data, the most probable mechanism for the interaction of nickel with calcite may be the formation of a solid solution by co-precipitation. We would then expect, as we had in like in europium case, incorporation into the bulk. RBS experiments showed the contrary: a surface accumulation was noticed in almost every sample that was analyzed, in agreement with the formation of a surface precipitate. If we compare the RBS results to the macroscopic study, the slower mechanism that was evidenced in our time-dependent sorption experiments after the initial fast adsorption, could then be surface precipitation. This hypothesis is in agreement with the blanks experiments that were carried out in the first part of our study which showed that nickel precipitation in solution in the conditions of our experiments is a slow phenomenon.

The results are innovative and highlight the effect of time and Ni(II) concentration in calcite pre−equilibrated solutions and dried single crystals which were not investigated yet by other authors.

Conclusions

Conclusions

The storage of nuclear waste is a major issue for the sustainability of French nuclear power. The safety of long-term deposition of radioactive waste is mandatory. It is therefore necessary to ensure that the engineered and host rock barriers inhibit the migration of radioelements in the environment. Calcite, being one of the components of clay stones (host rock in the French concept) and secondary phases, must be able to immobilize/retain radioelements.

This work permitted to investigate interaction of Eu(III) and Ni(II) with calcite under specific conditions.

The main results obtained during this thesis work will be summarized here:

I. Calcite as starting material

Preliminary characterization (XRD, BET, IR, SEM, TOC, ICP-MS after total digestion) permitted us to choose two types of powders (SOLVAY (SOCAL U1-R) and OMYA (BL 200)) for our studies, based on the spectroscopic tools requirements. For the same reason, single crystals were also used in our study.

II. Europium

❖ *Europium in solution*

Europium complexation with carbonates was investigated in CPES solutions over a large range of concentrations and for several contact times, as a preliminary study before dealing with the interaction with calcite.

At pH 8.3, speciation calculations predicted that Eu(III) should precipitate as $Eu_2(CO_3)_3{:}3H_2O_{(s)}$ and $Eu(CO_3)OH_{(cr)}$, at 10^{-3} mol.L^{-1} and at $\leq 10^{-4}$ mol.L^{-1} respectively. These theoretical calculations are confirmed by macroscopic results who revealed the precipitation of Eu(III) for concentrations superior to 10^{-5} mol.L^{-1}. No precipitation is noticed for 10^{-6} mol.L^{-1} in solution. The formation of the two aforementioned solids was confirmed by TRLFS. Static spectra for

10^{-3} mol.L^{-1} showed the formation of $Eu_2(CO_3)_3$ – 2-3 H_2O and $EuOHCO_3$ solid phases. The presence of the solid $EuOHCO_3$ is confirmed from static spectra shape (after 14 days) and is kept until the last investigated stirring time. The emission spectra of 10^{-5} and 10^{-4} mol.L^{-1} Eu(III) suspensions were identical and were not modified with increasing reaction time, indicating the formation of $Eu_2(CO_3)_3$ – 2-3 $H_2O_{(s)}$.

❖ *Eu(III) sorbed onto calcite powders and single crystals under various conditions*

The interaction of Eu(III) with calcite was investigated on both powders and single crystals, as a function of time, initial concentration of Eu(III) and pCO_2. TRLFS and RBS were applied aiming at characterizing the occurring mechanisms.

❖ *Macroscopic results*

Experiments that were performed under atmospheric condition and $pCO_2=10^{-2}$ atm on powders showed a very quick and almost complete Eu(III) uptake, in agreement with former studies.

❖ *TRLFS results*

Time-dependency experiments permitted to discriminate different mechanisms for the sorption of Eu(III) on calcite powders and single crystals by TRLFS. Static spectra showed two different bands characteristic to $^7F_1$ and $^7F_2$ transitions of sorbed Eu(III) no matter the contact time and the adsorbent type. An overall view of Eu(III) interaction with calcite can be seen as precipitation (for concentration superior to 10^{-5} mol.L^{-1}), concomitant to the formation of Eu(III) inner sphere complexes. Incorporation of Eu(III) within the calcite structure has also been evidenced. Each concentration of Eu(III) will be treated as follows.

One observation is the influence of reaction time on Eu(III) behavior on speciation onto calcite. Generally, two lifetimes were observed whatever the initial concentration, the values of the longer lifetimes for low concentrations and long contact times being remarkably long for a sorbed species (up to 3700 μs). Thus, at least two chemical environments of europium are present on the sorbed samples.

As mechanisms, for 10^{-3} mol.L^{-1} under atmospheric conditions, TRLFS results on powders and single crystals permitted to identify Eu(III)-precipitate for the shorter lifetimes, whereas inner-sphere surface complexes for the longer lifetimes are probable. However, only one sorbed species was highlighted over all investigation time for $pCO_2=10^{-2}$ atm on powders.

Decreasing the concentration to 10^{-4} mol.L^{-1}, inner-sphere surface complexes were identified on powders for both lifetimes, assuming that several H_2O/HO^- ligands surrounded europium in the first coordination sphere. Under atmospheric conditions, for 2 months contact time, Eu(III) progressive incorporation starts, as the number of water molecules decreases. Results obtained under $pCO_2=10^{-2}$ atm on powders, show smaller lifetimes than those under atmospheric conditions, precipitation of Eu(III) still exists as showed from low calculated lifetimes as well as inner-sphere surface complexation-similar mechanisms were identified on single crystals and atmospheric conditions.

For the last concentrations, 10^{-5} and 10^{-6} mol.L^{-1}, as for higher ones, low lifetimes indicate sorbed species/inner-sphere complexes and the high lifetimes show incorporation, which happens much faster, this phenomena occurring after 1 week contact time under atmospheric conditions. The inner-sphere complexes are also found for lower concentration 10^{-5} mol.L^{-1} for contact times between 4 hours and 1 day. The 7 days stirring time is a border contact time, because incorporation of Eu(III) into solid starts, by seeing a clear increasing of the value of second species and complete loss of water molecules from the first coordination sphere. The lower values are as well inner-sphere complexes surrounded by water molecules. For 10^{-6} mol.L^{-1}, shorter lifetimes are assigned to sorbed species and the higher lifetimes are assigned to incorporated species, having a complete loss of H_2O/HO^- molecules.

Looking to Eu(III) sorbed onto calcite single crystals compared to powders, incorporation is delayed due to the different shape of crystals and lower specific surface area.

- *RBS results*

Milli-RBS analyses have been performed on compacted pellets of sorbed calcite powders (SOLVAY (SOCAL U1-R) and (OMYA (BL 200)). The SOLVAY powder has a grain size of 0.2 µm, which was too small to extract any information from the RBS data. For the OMYA powder, the shape of the spectra corresponds to an incorporated sample but the spectra cannot be

fully quantitatively interpreted for milli-beam experiments, due to the same artifacts than for SOLVAY powders. Micro-beam experiments were this carried out but the impossibility to separate grains rendered the results´ interpretation very difficult. For that reason, further RBS experiments were performed on single crystals.

The two sorption methods (CES and CPES) for single crystals preparation turned to be appropriate, both leading to incorporation of Eu(III) in calcite. The depth concentration profiles interpreted by milli-RBS analysis showed that for 10^{-4} mol.L^{-1} Eu(III) accumulates onto surface then penetrates up to 75 nm for 1 week, whereas for 1 month the penetration occurs up to 140 nm (this would represent as an order of magnitude about 100 atomic layers). The surface accumulation can correspond to a surface (co)-precipitate as shown by the SEM-EDXS analyses.

Similar results were obtained for two distinct concentrations, 10^{-5} mol.L^{-1} and 10^{-4} mol.L^{-1} by μ-RBS. For lower concentration more important accumulation is noticed for longer stirring times, then penetration of Eu(III) up to 250 nm. For higher concentration, 10^{-4} mol.L^{-1} the surface accumulations are more important than 10^{-5} mol.L^{-1} as expected. The penetration of Eu(III) is at same depth, 250 nm. The heterogeneous distribution of Eu(III) onto calcite surfaces was showed both by additionally SEM-EDXS analyses and by RBS elemental maps. Last, concentration profiles were modeled with the help of apparent diffusion coefficients, leading to a value of $10^{-22} – 10^{-21}$ m².s^{-1}. These values have been compared to diffusion coefficients in the literature and were shown to be incompatible with a real diffusion mechanism.

The obtained results by two distinct techniques are in agreement highlighting three sorption mechanisms on the surface of calcite:

- heterogeneous accumulation on surface as (co)-precipitate shown by TRLFS, RBS and additionally SEM-EDXS
- inner-sphere surface complex formation as shown by TRLFS
- incorporation into bulk produced by dissolution/re-crystallization process of calcite in order to form a solid solution rather than solid-state diffusion.

III. Nickel

❖ *Nickel in solution*

The speciation of Ni(II) in CPES solutions was investigated. Speciation calculations predicted Ni(II) to precipitate as $Ni(OH)_{2(s)}$ at concentrations higher than 10^{-5} mol. L^{-1}. Precipitation of Ni(II) was experimentally confirmed and identified as a slow process. XRD patterns showed the formation of $Ni(OH)_{2(s)}$ for 10^{-3} mol.L^{-1}. For 10^{-3} and 10^{-4} mol.L^{-1}, Ni(II) precipitation is not complete, contrary to 10^{-5} mol.L^{-1} where Ni(II) turned out to be completely removed from the solution.

❖ *Ni(II) sorbed onto calcite powders under atmospheric conditions*

We studied the uptake of Ni(II) as a function of initial Ni(II) concentration and time. Adsorption was maximal for the longest contact times, as expected. For low concentrations such as 5×10^{-5}, 10^{-5} and 10^{-6} mol.L^{-1}, the sorbed fractions ranged between 90-100%. For concentrations of 2.5×10^{-4} and 5×10^{-4} mol.L^{-1}, the adsorption is lower, not exceeding 40%. Uptake kinetics allowed hypothesizing a dual nature of the process: a significant fraction of total Ni(II) was sorbed to the surface within the first 24 hours, followed by slow continuous progressive sorption as time passes, which might interpreted as metal co-precipitation or diffusion into the bulk solid phase.

Desorption of Ni(II) was investigated and represented as Desorption Indexes (D.I.) which were introduced to estimate the reversibility. Decreasing of the mean D.I. at increasing initial Ni(II) concentration was showed. The D.I. was found to be relatively insensitive to the durations of the sorption and desorption steps. Two assumptions were drawn from D.I: (a) desorption is fast and then remains constant over time (b) since D.I. is independent of the duration of the sorption step, the ratio between the reversible and irreversible part of the mechanism of the reaction between nickel and the calcite surface remains constant with the duration of the sorption step.

The second hypothesis seemed to contradict observations from sorption experiments, which could be explained by the occurrence of fast adsorption followed by a slower mechanism (surface precipitation). As for Eu(III), RBS measurements together with SEM-EDXS were performed on single crystals to characterize the Ni(II)/calcite system.

❖ *RBS results of Ni(II) sorbed onto calcite single crystals under atmospheric conditions*

Both milli- and micro-RBS studies showed accumulation of Ni(II) onto calcite surface. A heterogeneous distribution of Ni on single crystals surface, confirmed by SEM−EDXS measurements, was revealed by RBS elemental maps. This surface accumulation would be consistent with the mechanisms proposed based on the sorption/desorption batch experiments, i.e. adsorption and/or surface precipitation. A not uniformly distributed $Ni(OH)_2(s)$ could explain the differences observed by RBS and SEM-EDXS as a function of time.

As this study was performed in the context of nuclear waste disposal, an important question to be answered is:

« What are the environmental consequences of interaction of Eu(III) and Ni(II) with calcite for a long term safety of a nuclear waste repository ? »

In the introduction of this study, the importance of calcite as trapping material was highlighted as it is one of the main phases in COx composition. Calcite will definitively immobilize dissolved Eu(III) and surely will retard its migration in the geosphere. Therefore, beside sorption on clay surfaces, the contribution of calcite to the immobilization of europium should be significant when modeling the system. Ni(II) is also readily sorbed by calcite, though in a reversible way for low concentrations (desorption occurs then quantitatively in the first 24 hours) and in an partly reversible way for the higher studied concentrations (up to 5.10^{-4} $mol.L^{-1}$). This reversible/partly reversible sorption of nickel is then probably not relevant with respect to clay contribution. It has been shown that Eu(III) is readily incorporated into the calcite structure, whereas Ni(II) accumulates at the surface. A highly relevant retardation mechanism for the long-term fate of Eu(III) in the geosphere is the structural incorporation of Eu(III) into calcite on equilibrium conditions. Such reactions are to some extent expected if the resulting solid solution is thermodynamically stable.

There are some perspectives to give to this work.

An apparent discrepancy between RBS and SEM-EDXS results was encountered during this work, when surface precipitation was observed. This was due to the difficulty to probe the same areas on the crystal sample with these two techniques. This could be solved by using marked areas on SEM-probed samples before RBS analyses.

It would also be interesting to perform AFM experiments on crystal samples to get information on the height of the surface precipitates and the roughness of the surface. This would complete our representation of the surface that is drawn from SEM photographs only, by adding a third dimension to the 2D - images. Optical interferometry could also be a good choice to complete AFM results.

For carbonate complexation with Eu(III), site selective-TRLFS could be applied to confirm/infirm the results that were so far obtained. This would allow discriminating among the different species in case of intermixtures. Also, the interaction of Eu(III) with calcite (powders and single crystals) under atmospheric conditions could also be investigated then by site-selective TRLFS.

Other set of experiments under $pCO_2=10^{-2}$ atm should be continued for longer reaction times, in order to further understand the impact of pCO_2 on the interaction of Eu(III) with calcite. The impact on the Eu(III) aqueous speciation should also be determined by TRLFS and site-selective TRLFS. Further investigations by RBS to determine depth profile concentration would also be of interest.

Other interesting technique to be used onto single crystals is XRR (Specular X-ray Reflectivity) coupled with XRD that permits the characterization of thin-film and multilayer structures, but also identifies interface roughness [120].

The impact of temperature on the interaction of Eu(III) and Ni(II) with calcite could also be studied. Aqueous speciation, surface charge and solubility of calcite will be impacted by the increase in temperature and should also be investigated.

A more complex model that should include several processes like precipitation (formation of solid-solutions), surface complexes formation and incorporation and kinetics identified during this study should be developed. Most of the existent models such as surface complexation [23, 47, 123], surface precipitation [124] or solid solution formation [71, 125, 126] are proposed independently and do not consider all the processes within the same model. The data acquired during this Ph.D. for different contact times (up to 6 months) would serve as input data to parametrize the model and take into account kinetic aspects.

Bibliographic references

1. ANDRA, *Evaluation of the feasibility of a geological repository in an argillaceous formation*, in *Dossier 2005 Argile,* 2005.
2. ANDRA, *Evolution phénoménologique du stockage géologique*, in *Dossier 2005 Argile,* 2005.
3. ANDRA, *The CIGEO Project - Meuse/Haute Marne reversible geological disposal facility for radioactive waste*, 2013.
4. Marques-Fernandes, M., et al., *Site-selective time-resolved laser fluorescence spectroscopy of Eu^{3+} in calcite.* Journal of Colloid and Interface Science, 2008. **321**: p. 323-331.
5. Marques-Fernandes, M., et al., *Incorporation of trivalent actinides into calcite: A time resolved laser fluorescence spectroscopy (TRLFS) study.* Geochimica et Cosmochimica Acta, 2008. **72**(2): p. 464-474.
6. Piriou, B., et al., *Characterization of the Sorption of Europium(III) on Calcite by Site-Selective and Time-Resolved Luminescence Spectroscopy.* Journal of Colloid and Interface Science, 1997. **194**(2): p. 440-447.
7. Yeghicheyan, D., *Etude expérimentale du partage des terres rares entre carbonates de calcium et solutions aqueuses: Influence de la cinétique de cristallisation et de la spéciation des terres rares en solution*, 1996, Ph.D. Thesis, Université Paul Sabatier de Toulouse, France.
8. Brandt, H., et al., *Structural incorporation of Cm(III) in trioctahedral smectite hectorite: A time-resolved laser fluorescence spectroscopy (TRLFS) study.* Geochimica et Cosmochimica Acta, 2007. **71**(1): p. 145-154.
9. Hofmann, S., et al., *Trace concentration – Huge impact: Nitrate in the calcite/Eu(III) system.* Geochimica et Cosmochimica Acta, 2014. **125**: p. 528-538.
10. Stipp, S.L.S., et al., *Eu^{3+} uptake by calcite: Preliminary results from coprecipitation experiments and observations with surface-sensitive techniques.* Journal of Contaminant Hydrology, 2003. **61**: p. 33-43.
11. Zachara, J.M., C.E. Cowan, and C.T. Resch, *Sorption of divalent metals on calcite.* Geochimica et Cosmochimica Acta, 1991. **55**: p. 1549-1562.

12. Hoffmann, U. and S.L.S. Stipp, *The behavior of Ni^{2+} on calcite surfaces.* Geochimica et Cosmochimica Acta, 2001. **65**: p. 4131-4139.
13. Carlsson, T. and H. Aalto, *Coprecipitation of Ni with calcite: an experimental study.* Materials Research Society Symposium Proceedings, 1998. **506**: p. 621–627.
14. Lamana, R.T., *Nickel sorption on calcite surface: a macroscopic experimental study*, 2010, Master Thesis, McGill University, Montréal, Canada.
15. Stipp, S.L.S., et al., *Cd^{2+} uptake by calcite, solid-state diffusion, and the formation of solid-solution: Interface processes observed with near-surface sensitive techniques (XPS, LEED, and AES).* Geochimica et Cosmochimica Acta, 1992. **56**: p. 1941-1954.
16. Stipp, S.L.S., et al., *Spontaneous movement of ions through calcite at standard temperature and pressure.* Nature, 1998. **396**: p. 356-359.
17. Alonso, U., et al., *Diffusion coefficient measurements in consolidated clay by RBS micro-scale profiling.* Applied Clay Science, 2009. **43**: p. 477-484.
18. Stipp, S.L.S. and F.M. Hochella Jr, *Structure and bonding environments at the calcite surface as observed with X-ray photoelectron spectroscopy (XPS) and low energy electron diffraction (LEED).* Geochimica et Cosmochimica Acta, 1991. **55**: p. 1723-1736.
19. Stipp, S.L.S., C.M. Eggleston, and B.S. Nielsen, *Calcite surface structure observed at microtopographic and molecular scales with atomic force microscopy (AFM).* Geochimica et Cosmochimica Acta, 1994. **58**: p. 3023-3033.
20. Stipp, S.L.S., W. Gutmannsbauer, and T. Lehmann, *The dynamic nature of calcite surfaces in air.* American Mineralogist, 1996. **81**: p. 1-8.
21. Rachlin, L.A., S.G. Henderson, and M.C. Goh, *An atomic force microscope (AFM) study of the calcite cleavage plane; image averaging in Fourier space.* American Mineralogist, 1992. **77**: p. 904-910.
22. Heberling, F., et al., *A thermodynamic adsorption/entrapment model for selenium(IV) coprecipitation with calcite.* Geochimica et Cosmochimica Acta, 2014. **134**: p. 16-38.
23. Van Cappellen, P., et al., *A surface complexation model of the carbonate mineral-aqueous solution interface.* Geochimica et Cosmochimica Acta, 1993. **57**: p. 3505-3518.
24. Villegas-Jimenez, A., et al., *Acid-Base Behavior of the Gaspeite ($NiCO_{3(s)}$) Surface in NaCl Solutions.* Langmuir, 2010. **26**: p. 12626-12639.

25. Nehrke, G. and P. Van Cappellen, *Framboidal vaterite aggregates and their transformation into calcite: A morphological study.* Journal of Crystal Growth, 2006. **287**: p. 528-530.
26. Jacobson, R.L. and D. Langmuir, *Dissociation constants of calcite and $CaHCO_3^-$ from 0 to 50°C.* Geochimica et Cosmochimica Acta, 1974. **36**: p. 1023-1045.
27. Berner, R.A., *The solubility of calcite and aragonite in seawater at atmospheric pressure and 34.5 ‰ salinity.* American Journal of Science, 1976. **276**(6): p. 713-730.
28. Plummer, L.N. and E. Busenberg, *The solubilities of calcite, aragonite and vaterite in CO_2-H_2O solutions between 0 and 90°C, and an evaluation of the aqueous model for the system $CaCO_3$-CO_2-H_2O.* Geochimica et Cosmochimica Acta, 1982. **46**: p. 1011-1040.
29. Garvin, D., V.B. Parker, and H.J. White Jr., *CODATA thermodynamic tables : Selection of some compounds of calcium and related mixtures: A prototype set of tables,* 1987, Washington D.C.: Hemisphere Publishing Corporation.
30. Stumpf, T. and T. Fanghänel, *A Time-Resolved Laser Fluorescence Spectroscopy (TRLFS) Study of the Interaction of Trivalent Actinides (Cm(III)) with Calcite.* Journal of Colloid and Interface Science, 2002. **249**: p. 119-122.
31. Nielsen, A., *Electrolyte crystal growth kinetics.* Journal of Crystal Growth, 1984. **67**: p. 278-288.
32. Curti, E., *Coprecipitation of radionuclides with calcite: estimation of partition coefficients based on a review of laboratory investigations and geochemical data.* Applied Geochemistry, 1999. **14**: p. 433-445.
33. Markgraf, S.A. and R.J. Reeder, *High-temperature structure refinement of calcite and magnesite.* American Mineralogist, 1985. **70**: p. 590-600.
34. Kashkai, M.A., *Structural Analysis of the Most Commonly Encountered Habit Faces of Calcite Crystals from Skarn Deposits.* Mineralogical Magazine, 1970. **37**: p. 929-933.
35. Skinner, A.J., J.P. LaFemina, and H.J.F. Jansen, *Structure and bonding of calcite; a theoretical study.* American Mineralogist, 1994. **79**: p. 205-214.
36. Paquette, J. and J.R. Reeder, *Relationship between surface structure, growth mechanism, and trace element incorporation in calcite.* Geochimica et Cosmochimica Acta, 1995. **59**: p. 735-749.

37. Ruiz-Agudo, E., et al., *Effect of pH on calcite growth at constant aCa^{2+}/aCO_3^{2-} ratio and supersaturation.* Geochimica et Cosmochimica Acta, 2011. **75**: p. 284-296.
38. Perry IV, T.D., R.T. Cygan, and R. Mitchell, *Molecular models of a hydrated calcite mineral surface.* Geochimica et Cosmochimica Acta, 2007. **71**: p. 5876-5887.
39. Spagnoli, D., S. Kerisit, and S.C. Parker, *Atomistic simulation of the free energies of dissolution of ions from flat and stepped calcite surfaces.* Journal of Crystal Growth, 2006. **294**: p. 103-110.
40. Heberling, F., et al., *Structure and reactivity of the calcite-water interface.* Journal of Colloid and Interface Science, 2013. **354**: p. 843-857.
41. Sposito, G., *On Points of Zero Charge.* Environmental Science & Technology, 1998. **32**: p. 2815-2819.
42. Somasundaran, P. and G.E. Agar, *The zero point of charge of calcite.* Journal of Colloid and Interface Science, 1967. **24**: p. 433-440.
43. Sø, H.U., *Sorption and desorption of arsenate onto calcite*, 2007, Master Thesis, Technical University of Denmark, Kongens Lyngby, Denmark.
44. Rouff, A.A., J.R. Reeder, and N.S. Fisher, *Pb (II) Sorption with Calcite: A Radiotracer Study.* Aquatic Geochemistry, 2002. **8**: p. 203-228.
45. Stumm, W., L. Sigg, and L.J. Schnoor, *Aquatic chemistry of acid deposition.* Environmental Science & Technology, 1987. **21**: p. 8-13.
46. Chiarello, P.R. and C.N. Sturchio, *The calcite (10-14) cleavage surface in water: Early results of a crystal truncation rod study.* Geochimica et Cosmochimica Acta, 1995. **59**: p. 4557-4561.
47. Wolthers, M., L. Charlet, and P. Van Cappellen, *The surface chemistry of divalent metal carbonate minerals; a critical assessment of surface charge and potential data using the charge distribution multi-site ion complexation model.* American Journal of Science, 2008. **308**: p. 905-941.
48. Dove, M.P. and F.M. Hochella Jr, *Calcite precipitation mechanisms and inhibition by orthophosphate: In situ observations by Scanning Force Microscopy.* Geochimica et Cosmochimica Acta, 1993. **57**: p. 705-714.

49. Teng, H.H., *The thermodynamics and kinetics of calcite crystallization: Baseline for understanding biomineral formation*, 1999, Ph.D. Thesis, Georgia Institute of Technology, Atlanta, USA.
50. Heberling, F., et al., *Reactivity of the calcite-water-interface, from molecular scale processes to geochemical engineering.* Applied Geochemistry, 2014. **45**: p. 158-190.
51. Fenter, P., et al., *Surface speciation of calcite observed in situ by high-resolution X-ray reflectivity.* Geochimica et Cosmochimica Acta, 2000. **64**: p. 1221-1228.
52. Geissbühler, P., et al., *Three-dimensional structure of the calcite-water interface by surface X-ray scattering.* Surface Science, 2004. **573**: p. 191-203.
53. Pokrovsky, O.S., et al., *Surface Speciation Models of Calcite and Dolomite/Aqueous Solution Interfaces and Their Spectroscopic Evaluation.* Langmuir, 2000. **16**: p. 2677-2688.
54. Fanghänel, T., et al., *Thermodynamics of Cm(III) in Concentrated Salt Solutions: Carbonate Complexation in NaCl Solution at 25°C.* Journal of Solution Chemistry, 1999. **28**: p. 447-462.
55. Stumpf, T., et al., *Inner-sphere, outer-sphere and ternary surface complexes: a TRLFS study of the sorption process of Eu(III) onto smectite and kaolinite.* Radiochimica Acta, 2002. **90**: p. 345-349.
56. Runde, W., C. Van Pelt, and P.G. Allen, *Spectroscopic characterization of trivalent f-element (Eu, Am) solid carbonates.* Journal of Alloys and Compounds, 2000. **303-304**: p. 182-190.
57. Runde, W., G. Meinrath, and J.I. Kim, *A Study of Solid-Liquid Phase Equilibria of Trivalent Lanthanide and Actinide Ions in Carbonate Systems*. Radiochimica Acta, 1992. **58-59**: p. 93-100.
58. Horrocks, W.D. and D.l.R. Sudnick, *Lanthanide ion luminescence probes of the structure of biological macromolecules.* Accounts of Chemical Research, 1981. **14**: p. 384-392.
59. Horrocks, W.D., Jr. and D.R. Sudnick, *Lanthanide ion probes of structure in biology. Laser-induced luminescence decay constants provide a direct measure of the number of metal-coordinated water molecules.* Journal of the American Chemical Society, 1979. **101**: p. 334-40.

60. Barthelemy, P.P. and R.G. Choppin, *Luminescence study of complexation of europium and dicarboxylic acids.* Inorganic Chemistry, 1989. **28**: p. 3354-3357.
61. Plancque, G., et al., *Europium speciation by time-resolved laser-induced fluorescence.* Analytica Chimica Acta, 2003. **478**(1): p. 11-22.
62. Stumpf, T., et al., *Incorporation of Eu(III) into Hydrotalcite: A TRLFS and EXAFS Study.* Environmental Science & Technology, 2007. **41**: p. 3186-3191.
63. Moulin, C., et al., *Europium complexes investigations in natural waters by time-resolved laser-induced fluorescence.* Analytica Chimica Acta, 1999. **396**(2-3): p. 253-261.
64. Heller, A., A. Barkleit, and G. Bernhard, *Chemical Speciation of Trivalent Actinides and Lanthanides in Biological Fluids: The Dominant in Vitro Binding Form of Curium(III) and Europium(III) in Human Urine.* Chemical Research in Toxicology, 2011. **24**: p. 193-203.
65. Kim, J.I., et al., *A study of the carbonate complexation of Cm(III) and Eu(III) by time-resolved laser fluorescence spectroscopy.* Journal of Alloys and Compounds, 1994. **213**: p. 333-340.
66. Pointeau, I., *Etude mécanistique et modélisation de la rétention des radionucléides par les silicates de calcium hydratés (CSH) des ciments*, 2000, Ph.D. Thesis, Université de Reims Champagne-Ardenne, France.
67. Vu-Do, L., *Influence de la matière organique naturelle mobile sur la rétention de l´europium sur l'argilite de Bure*, 2013, Ph.D. Thesis, Université Paris XI, Orsay, France.
68. Parekh, P.P., et al., *Distribution of trace elements between carbonate and non-carbonate phases of limestone.* Earth and Planetary Science Letters, 1977. **34**: p. 39-50.
69. Palmer, M.R., *Rare earth elements in foraminifera tests.* Earth and Planetary Science Letters, 1985. **73**: p. 285-298.
70. Zhong, S. and A. Mucci, *Partitioning of rare earth elements (REEs) between calcite and seawater solutions at 25°C and 1 atm, and high dissolved REE concentrations.* Geochimica et Cosmochimica Acta, 1995. **59**(3): p. 443-453.
71. Lakshtanov, L.Z. and S.L.S. Stipp, *Experimental study of europium (III) coprecipitation with calcite.* Geochimica et Cosmochimica Acta, 2004. **68**(4): p. 819-827.
72. Tesoriero, J.A. and F.J. Pankow, *Solid solution partitioning of Sr^{2+}, Ba^{2+}, and Cd^{2+} to calcite.* Geochimica et Cosmochimica Acta, 1996. **60**: p. 1053-1063.

73. Zavarin, M., et al., *Eu(III), Sm(III), Np(V), Pu(V), and Pu(IV) sorption to calcite.* Radiochimica Acta, 2005. **93**: p. 93-102.

74. Schmidt, M., et al., *Incorporation versus adsorption: substitution of Ca^{2+} by Eu^{3+} and Cm^{3+} in aragonite and gypsum.* Dalton Transactions, 2009. **33**: p. 6645–6650.

75. Kowal-Fouchard, A., et al., *Structural identification of Europium(III) adsorption complexes on montmorillonite.* New Journal of Chemistry, 2004. **28**: p. 864-869.

76. Ghaleb, K.A., et al., *Speciation of Europium (III) Surface Species on Monocrystalline Alumina Using Time-Resolved Laser-Induced Fluorescence-Scanning Near-Field Optical Microscopy.* Applied Spectroscopy, 2008. **62**: p. 213-219.

77. Holliday, K., et al., *Discriminating factors affecting incorporation: comparison of the fate of Eu^{3+}-Cm^{3+} in the Sr carbonate-sulfate system.* Dalton Transactions, 2012. **41**: p. 3642-3647.

78. Cherniak, D.J., *An experimental study of strontium and lead diffusion in calcite, and implications for carbonate diagenesis and metamorphism.* Geochimica et Cosmochimica Acta, 1997. **61**(19): p. 4173-4179.

79. Cherniak, D.J., *REE diffusion in calcite.* Earth and Planetary Science Letters, 1998. **160**(3-4): p. 273-287.

80. Nieminen, M.T., et al., *Biogeochemistry of Nickel and Its Release into the Environment*, in *Metal Ions in Life Sciences, Vol. 2,* 2007, Wiley: . p. 1-30.

81. Gamsjäger, H., et al., *Chemical thermodynamics of Nickel,* 2005, Amsterdam: Elsevier Science Publishers B. V.

82. Isaacs, T., *The mineralogy and chemistry of the nickel carbonates.* Mineralogical Magazine, 1963. **33**: p. 663-678.

83. Guillard, D. and E.A. Lewis, *Nickel Carbonate Precipitation in a Fluidized-Bed Reactor.* Industrial & Engineering Chemistry Research, 2001. **40**: p. 5564-5569.

84. Lakshtanov, L.Z. and S.L.S. Stipp, *Experimental study of nickel(II) interaction with calcite: Adsorption and coprecipitation.* Geochimica et Cosmochimica Acta, 2007. **71**: p. 3686-3697.

85. Belova, D.A., L.Z. Lakshtanov, and S.L.S. Stipp, *Experimental study of Ni adsorption on chalk: preliminary results.* Mineralogical Magazine, 2008. **72**: p. 377-379.

86. Palmer, D.A., P. Bénézeth, and D.J. Wesolowski, *Solubility of Nickel Oxide and Hydroxide in Water*, in *Proceedings of the 14th International Conference on the Properties of Water and Steam,* 2005: Kyoto.

87. Palmer, D.A., P. Bénézeth, and D.J. Wesolowski, *Aqueous high temperature solubility studies. I. The solubility studies of boehmite as functions of ionic strength (to 5 molal, NaCl), temperature (100-290°C), and pH as determined by in situ measurements.* Geochimica et Cosmochimica Acta, 2001. **65**: p. 2081-2095.

88. Plyasunova, V., N., Y. Zhang, and M. Muhammed, *Critical evaluation of thermodynamics of complex formation of metal ions in aqueous solutions. IV. Hydrolysis and hydroxo-complexes of Ni^{2+} at 298.15 K.* Hydrometallurgy, 1998. **48**: p. 43-63.

89. Mattigod, V.S., et al., *Solubility and solubility product of crystalline $Ni(OH)_2$.* Journal of Solution Chemistry, 1997. **26**: p. 391-403.

90. Davis, A.J., C.C. Fuller, and D.A. Cook, *A model for trace metal sorption processes at the calcite surface: Adsorption of Cd^{2+} and subsequent solid solution formation.* Geochimica et Cosmochimica Acta, 1987. **51**: p. 1477-1490.

91. Zachara, J.M., J.A. Kittrick, and J.B. Harsh, *The mechanism of Zn^{2+} adsorption on calcite.* Geochimica et Cosmochimica Acta, 1988. **52**: p. 2281-2291.

92. Rouff, A.A., et al., *The influence of pH on the kinetics, reversibility and mechanisms of Pb(II) sorption at the calcite-water interface.* Geochimica et Cosmochimica Acta, 2005. **69**(22): p. 5173-5186.

93. Rouff, A.A., J.R. Reeder, and N.S. Fisher, *Electrolyte and pH effects on Pb(II)-calcite sorption processes: the role of the $PbCO_3°_{(aq)}$ complex.* Journal of Colloid and Interface Science, 2005. **286**: p. 61-67.

94. Hummel, W. and E. Curti, *Nickel Aqueous Speciation and Solubility at Ambient Conditions: A Thermodynamic Elegy.* Monatshefte Fur Chemie, 2003. **134**: p. 941-973.

95. Doner, H. and M. Zavarin, *Nickel and manganese interaction with calcite, UCRL-ID-135402*, 1999: Lawrence Livermore National Laboratory.

96. Lorens, B., R., *Sr, Cd, Mn and Co distribution coefficients in calcite as a function of calcite precipitation rate.* Geochimica et Cosmochimica Acta, 1981. **45**: p. 553-561.

97. McBride, M.B., *Chemisorption of Cd^{2+} on Calcite Surfaces.* Soil Science Society of America Journal, 1980. **44**: p. 26-28.

98. Sato, M. and S. Matsuda, *Structure of vaterite and infrared spectra.* Zeitschrift für Kristallographie, 1969. **129**: p. 405–410.

99. Sivakumar, S., et al., *FTIR Spectroscopic Studies on Coastal Sediment Samples from Cuddalore District, Tamilnadu, India.* Indian Journal of Advances in Chemical Science 2012. **1**: p. 40-46.

100. Khan, E. and S. Pillai. *Effect of Leaching from Filters on Laboratory Analyses of Collective Organic Constituents*. in *Proceedings of the 79th Annual Water Environment Federation Technical Exposition and Conference*. 2006. Dallas, TX: Water Environment Federation.

101. Cherniak, D.J., *An experimental study of strontium and lead diffusion in calcite, and implications for carbonate diagenesis and metamorphism.* Geochimica et Cosmochimica Acta, 1997. **61**: p. 4173-4179.

102. Cherniak, D.J. and F.J. Ryerson, *A study of strontium diffusion in apatite using Rutherford backscattering spectroscopy and ion implantation.* Geochimica et Cosmochimica Acta, 1993. **57**: p. 4653-4662.

103. Alonso, U., et al., *Study of the contaminant transport into granite microfractures using nuclear ion beam techniques.* Journal of Contaminant Hydrology, 2003. **61**: p. 95-105.

104. Carroll, A.S., et al., *Interactions of U(VI), Nd, and Th(IV) at the Calcite-Solution Interface.* Radiochimica Acta, 1992. **58-59**: p. 245.

105. Lahav, N. and G.H. Bolt, *Self-Diffusion of ^{45}Ca into certain carbonates.* Soil Science, 1964. **97**: p. 293-299.

106. Hummel, W., et al., *Nagra/PSI Chemical Thermodynamic Data Base 01/01.* Radiochimica Acta, 2002. **90**: p. 805-813.

107. Tits, J., et al., *The uptake of Eu(III) and Th(IV) by calcite under hyperalkaline conditions, PSI Bericht 02-03*, 2002, Paul Scherrer Institut, Villigen, Switzerland, and Nagra Technical Report NTB 02-08, Wettingen, Switzerland.

108. Rao, R.R. and A. Chatt, *Characterization of Europium(III) carbonate complexes in simulated groundwater by solvent extraction.* Journal of Radioanalytical and Nuclear Chemistry 1988. **124**: p. 211-225.

109. Haas, R.J., L.E. Shock, and C.D. Sassani, *Rare earth elements in hydrothermal systems: Estimates of standard partial molal thermodynamic properties of aqueous complexes of*

the rare earth elements at high pressures and temperatures. Geochimica et Cosmochimica Acta, 1995. **59**: p. 4329-4350.

110. Spahiu, K. and J. Bruno, *A Selected Thermodynamic Database for REE to Be Used in HLNW Performance Assessment Exercises, SKB 95-35: Svensk Kärnbränslehantering AB*, 1995.
111. Giffaut, E., et al., *Andra thermodynamic database for performance assessment: ThermoChimie.* Applied Geochemistry 2014. **49**: p. 225–236.
112. *PDF-2, International Centre for Diffraction Data, Newtown Square, PA, U.S.A.*, 2008.
113. Harstad, A.O. and S.L.S. Stipp, *Calcite dissolution: Effects of trace cations naturally present in Iceland spar calcites.* Geochimica et Cosmochimica Acta, 2007. **71**: p. 56-70.
114. Sabau, A., et al., *Interaction of europium and nickel with calcite studied by Rutherford Backscattering Spectrometry and Time-Resolved Laser Fluorescence Spectroscopy.* Nuclear Instruments and Methods in Physics Research Section B: Beam Interactions with Materials and Atoms, 2014. **332**: p. 111-116.
115. Schmidt, M., et al., *Charge Compensation in Solid Solutions.* Angewandte Chemie International Edition, 2008. **47**: p. 5846-5850.
116. Stumpf, T., et al., *Structural characterization of Am incorporated into calcite: A TRLFS and EXAFS study.* Journal of Colloid and Interface Science, 2006. **302**: p. 240-245.
117. Chada, V.G.R., et al., *Divalent Cd and Pb uptake on calcite cleavage faces: An XPS and AFM study.* Journal of Colloid and Interface Science, 2005. **288**: p. 350-360.
118. Alexandratos, V.G., J. Elzinga, E., and J. Reeder, R., *Arsenate uptake by calcite: Macroscopic and spectroscopic characterization of adsorption and incorporation mechanisms.* Geochimica et Cosmochimica Acta, 2007. **71**: p. 4172-4187.
119. Reeder, J.R., et al., *Coprecipitation of Uranium(VI) with Calcite: XAFS, micro-XAS, and luminescence characterization.* Geochimica et Cosmochimica Acta, 2001. **65**: p. 3491-3503.
120. Sturchio, C.N., et al., *Lead adsorption at the calcite-water interface: Synchrotron X-ray standing wave and X-ray reflectivity studies.* Geochimica et Cosmochimica Acta, 1997. **61**: p. 251-263.
121. Parkhurst, D.L. and C.A.J. Appelo, *User's guide to PHREEQC (version 2) – A computer program for speciation, batch-reaction, one dimensional transport, and inverse*

geochemcal calculations, U.S. Department of the Interior, U.S. Geological Survey, Water-Resources Investigations Report 99-4259, 1999.

122. Ball, J.W. and D.K. Nordstrom, *User's Manual for WATEQ4F, with Revised Thermodynamic Data Base and Test Cases for Calculating Speciation of Major, Trace, and Redox Elements in Natural Waters, Report 91-183*, 1991: Menlo Park, California.
123. Pokrovsky, O.S., G.S. Pokrovski, and J. Schott, *Gallium(III) adsorption on carbonates and oxides: X-ray absorption fine structure spectroscopy study and surface complexation modeling.* Journal of Colloid and Interface Science, 2004. **279**: p. 314-325.
124. Farley, J.K., A.D. Dzombak, and M.M.F. Morel, *A surface precipitation model for the sorption of cations on metal oxides.* Journal of Colloid and Interface Science, 1985. **106**: p. 226-242.
125. Curti, E., D.A. Kulik, and J. Tits, *Solid solutions of trace Eu(III) in calcite: Thermodynamic evaluation of experimental data over a wide range of pH and pCO_2.* Geochimica et Cosmochimica Acta, 2005. **69**(7): p. 1721-1737.
126. Kulik, D.A., et al., *$(Ca,Sr)CO_3$ aqueous-solid solution systems: From atomistic simulations to thermodynamic modelling.* Physics and Chemistry of the Earth, Parts A/B/C, 2010. **35**(6-8): p. 217-232.
127. Brunauer, S., P.H. Emmett, and E. Teller, *Adsorption of Gases in Multimolecular Layers.* Journal of the American Chemical Society, 1938. **60**: p. 309-319.
128. *HighScorePlus (V. 3.0), PANalytical B. V.*, 2009: Almelo, The Netherlands.
129. *Apex Suite (V. 2013.4-1), Bruker-AXS*, 2013: Madison, WI, U.S.A.
130. Müller, K., *The sorption of uranium(VI) and neptunium(V) onto surfaces of selected metal oxides and alumosilicates studied by in situ vibrational spectroscopy*, 2009, Ph.D. Thesis, Technische Universität Dresden, Germany.
131. Schultz, L.N., et al., *High surface area calcite.* Journal of Crystal Growth, 2013. **371**(0): p. 34-38.
132. http://www.purdue.edu/rem/rs/sem.htm. [cited 2015 June 18].
133. Skoog, D.A., D.M. West, and F.J. Holler, eds. *Chimie analytique*. 1997, De Boeck Supérieur: Bruxelles.

134. Tertre, E., *Adsorption de Cs^{+}, Ni^{2+} et des lanthanides sur une kaolinite et une smectite jusqu'à 150°C : Etude expérimentale et modélisation*, 2005, Ph.D. Thesis, Université Paul Sabatier, Toulouse, France.

135. Takahashi, Y., et al., *Characterization of Eu(III) Species Sorbed on Silica and Montmorillonite by Laser-Induced Fluorescence Spectroscopy.* Radiochimica Acta, 1998. **82**: p. 227-232.

136. Tan, X., M. Fang, and X. Wang, *Sorption Speciation of Lanthanides/Actinides on Minerals by TRLFS, EXAFS and DFT Studies: A Review.* Molecules, 2010. **15**: p. 8431-8468.

137. Kimura, T., et al., *Determination of Number of Cm(III) in various aqueous solutions.* Radiochimica Acta, 1996. **72**: p. 61-64.

138. Moll, H., et al. *Curium(III) as intrinsic luminescence probe for direct speciation studies in biogeochemical systems*. in *International Workshop on Advanced Techniques in Actinide Spectroscopy, HZDR*. 2012.

139. Moll, H., et al., *Curium(III) complexation with pyoverdins secreted by a groundwater strain of Pseudomonas fluorescens.* Biometals, 2008. **21**: p. 219-228.

140. Daudin, L., H. Khodja, and J.P. Gallien, *Development of ''position–charge–time'' tagged spectrometry for ion beam microanalysis.* Nuclear Instruments and Methods in Physics Research Section B: Beam Interactions with Materials and Atoms, 2003. **210**: p. 153-158.

141. Raepsaet, C., et al., *Ion beam analysis of radioactive samples.* Nuclear Instruments and Methods in Physics Research Section B: Beam Interactions with Materials and Atoms, 2009. **267**(1213): p. 2245-2249.

142. Khodja, H., et al., *The Pierre Sue Laboratory nuclear microprobe as a multi-disciplinary analysis tool.* Nuclear Instruments and Methods in Physics Research Section B: Beam Interactions with Materials and Atoms, 2001. **181**(1-4): p. 83-86.

143. Mayer, M., *SIMNRA user's guide*, 1997, Max Planck Institut fur Plasmaphysik.

Appendix A: Analytical and standard spectroscopic methods

A.1. Specific surface area (SSA) and total organic carbon (TOC) determination

Specific surface area of calcite was determined using the analysis of the gas sorption isotherm after the Brunauer, Emmett and Teller model, also called BET method [127]. The BET method assumes the sorption of gas molecules in multi-layers on energetically homogeneous surfaces excluding any interactions between molecules. The gases that are used for such measurements are inert gases, and in our case N_2. For all types of calcite, total organic carbon (TOC) was determined as well.

Total organic carbon is an indirect measurement of organic content existent in a solution. Analytical technologies utilized to measure TOC share the objective of completely oxidizing the organic molecules in an aliquot of liquid sample to carbon dioxide (CO_2), measuring the resultant CO_2 concentration, and expressing this response as carbon concentration. All technologies must discriminate between the inorganic carbon, which may be present in the water from sources such as dissolved CO_2 and bicarbonate, and the CO_2 generated from the oxidation of present organic molecules in the sample The total organic carbon was determined by a multi Multi-point Beckman Coulter surface analyzer SA 3100.

A.2. X-ray diffraction (XRD)

X-ray diffraction (XRD) provided crystallographic data to determine the phases present and possible crystalline phases present in the aimed sample. This method allows a quantitative and qualitative analysis, but in our case only qualitative analysis was performed. X-ray Diffraction is a non-destructive analytical technique that provides detailed information about the internal lattice of crystalline substances. A briefly background is presented in this section. In 1912 Max von Laue discovered that crystalline substances act as three-dimensional diffraction gratings for X-ray wavelengths similar to the spacing of planes in a crystal lattice. X-ray diffraction is now used to study crystal structures and atomic spacing. X-rays are produced by a cathodic tube, filtered to produce a monochromatic radiation, collimated to concentrate then and directed to target.

Powder diffraction has been mainly used to verify the purity of the starting materials and the absence of polymorph phases.

The physical background of this technique will be shortly explained. The X-Ray is produced when high-speed electrons are interacting with a metal target. The energy of electrons is ranging between 10 - 40 keV. A monochromatic energy having a wavelength λ deploy through a crystalline material at angle θ. In a crystal, the atoms are arranged periodically, thus the diffracted X-rays can interact very good. The relation A.1 gives the difference between the two waves:

$$2\lambda = 2d \sin(\theta) \qquad \text{(Eq. A.1)}$$

W. L. Bragg has elaborated this relationship in 1912. For a constructive interference between these waves, the path difference must be an integrated number of wavelengths:

$$n\lambda = 2d_{hkl} \sin(\theta_{hkl}) \qquad \text{(Eq. A.2)}$$

where:

n = integer number

λ = wavelength of incident X-ray

d_{hkl} = distance between the atomic plans in a crystal

θ_{hkl} = diffraction angle from hkl plans

Powders XRD measurements are performed on θ-θ diffractometer D-8 (Bruker/Axs) with Bragg-Brentano-geometry using a graphite secondary monochromator and a scintillator. These measurements were done at The X-ray laboratory at the HZDR (Institute of Ion Beam Physics and Materials Research).

The single crystals were ground and characterized by powder X-ray diffraction at the Dresden University of Technology (TUD). A PANalytical XPert diffractometer with Cu Kα1 radiation, operating in Bragg-Brentano mode at 40 kV and 40 mA, was used. Each pattern was measured in ten individual runs from 5 to 100° 2θ (step-scan mode, 0.013° step, 45.9 seconds per step for

each run). Qualitative phase analysis was performed by the software package HighScorePlus [128] using the PDF-2 database from ICDD [112].

In order to explore which facets were exposed to the solution during sorption experiments, several native crystals were characterized by single crystal X-ray diffraction. The as-received crystals were fixed on glass rods with epoxy, mounted on a goniometer head and investigated on a Kappa Apex 2 diffractometer (Bruker-AXS) with graphite-monochromatized Mo Kα radiation (50 kV, 30 mA). Thirty frames per crystal were recorded in different section of the Ewald sphere and evaluated with the Bruker Apex Suite [129]. The crystal quality was checked on the basis of the diffraction image and orientation matrix and the crystals facets were determined.

A.3. Infra-red (IR) spectroscopy

Since it is well known that XRD is not sensitive enough and cannot deliver information about the presence of all phases in the analyzed material (if there is less than 5 % of phase), powders were investigated by attenuated total reflectance infrared spectroscopy (ATR-FT-IR) too, suitable to measure the lattice vibrations of wet pastes or liquid samples.

Infrared (IR) spectroscopy is an extremely reliable and well recognized fingerprinting method. The technique of Attenuated Total Reflectance (ATR) is used on solid and liquid sample analyses because it combats the most different aspects of infrared analyses, like sample preparation and spectral reproducibility. An attenuated total reflection accessory operates by measuring the changes that occur in a totally internally reflected infrared beam when the beam comes into contact with a sample. An infrared beam is directed onto an optically dense crystal with a high refractive index at a certain angle. This internal reflectance creates an evanescent wave that extends beyond the surface of the crystal into the sample held in contact with the crystal.

The measurements were performed using Bruker Vertex 80/v spectrometer with a MCT (mercury-cadmium-telluride) detector. More details are given elsewhere [130]. According to Schultz et al. [131] ATR-FT-IR technique reduces the effects of scattering artifacts in the IR spectrum, which are quite large for commercial calcite with a particle size of ≈5 mm. Also, this technique is used to make the difference between the possible existences of several phases in the

investigated material. The presence of water molecules or other phases that may contain organic phases (who have e.g. –OH groups) can be investigated by this technique.

A.4. Inductively Coupled Plasma Mass Spectrometry (ICP-MS) and Inductively Coupled Plasma – Optical Emission Spectrometry (ICP-OES)

Concentration in solution and in solid is determined by inductively coupled plasma mass spectrometry (ICP-MS - model ELAN 9000, Perkin Elmer; error ± 10%) and inductively coupled plasma – optical emission spectrometry (ICP-OES- model Perkin Elmer Optima 7300 DV; error ± 10%).

A.5. Scanning Electron Microscopy (SEM)

A scanning electron microscope is an electron microscope where images are produced by scanning a sample with a focused beam of accelerated primary electrons and detecting signals (e.g. secondary electrons or back-scattered electrons), which result from the interaction with the sample. SEM has various purposes, such as microstructure investigation or chemical analysis. All samples were investigated under vacuum. A schematic representation of an SEM is shown in Figure A.2. An electron gun containing e.g. a W/La cathode is emitting electrons.

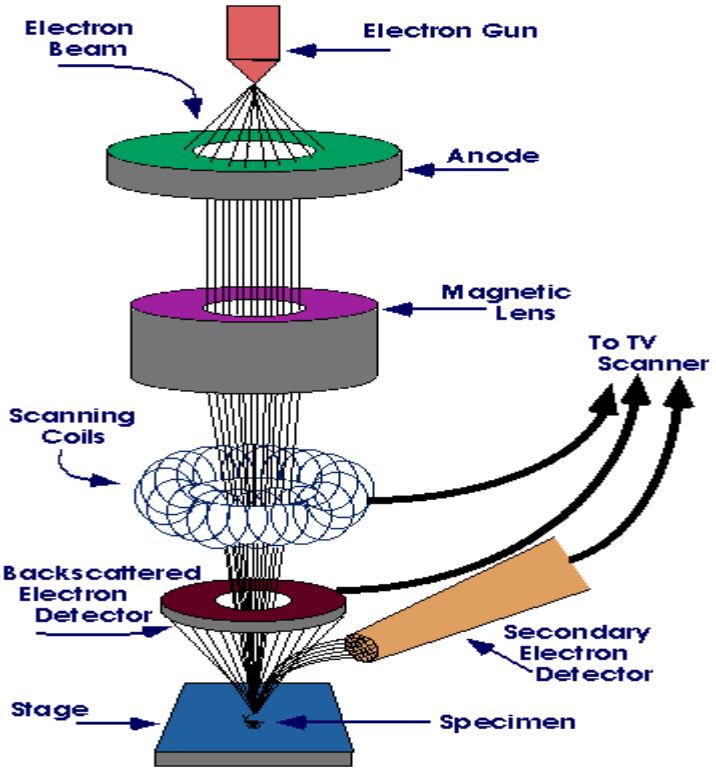

Figure A.2: SEM principle [132].

The beam of primary electrons with energy in the energy range of 20-40 keV is formed to a spot with a size of 0.4-5 nm by magnetic condenser lens. Then the beam passes through the scanning coils in the electron column, allowing it to scan the sample in x and y direction. The sample (or at least the surface) has to be conductive. If this is not the case, it can be coated with a thin layer of conductive material (e.g. Au, C, Pt). To prevent the accumulation of charges at the sample surface, the sample holder has to be electrically grounded. The quality of the obtained images depends on the electron spot size and the interaction volume. Because our investigated samples were not conductive, they were covered with a thin layer of carbon and the measurements conditions were adapted to the samples. The aim of these measurements is to determine the particle size, the grain distribution and the shape of grains. SEM measurements were taken using the scanning electron microscope FEG JEOL 6700F with an acceleration voltage of 3.0 kV. The measurements were done in the Centre Commun de Microscopie Appliquée (CCMA) - University of Nice.

A.6. Scanning Electron Microscopy coupled with Energy Dispersive X-ray Spectroscopy (SEM-EDXS)

SEM-EDXS is an analytical technique that is widely used to determine elemental composition of a solid sample. Quantitative analysis involves identification of specific peaks for each element and is relatively easy due to the simplicity of X-ray techniques. A short physical background will be exposed as follows. In SEM, as presented before, the electrons interact with the sample surface. When the electrons are interacting with samples, several signals are generated and detected as an image or X-ray spectrum (this information is given by the secondary electrons). Energy Dispersive X-ray Spectroscopy (EDXS) is a qualitative and quantitative X-ray microanalytical technique that can provide information on the chemical composition of a sample for elements with atomic number (Z) >3.

The spatial resolution of EDXS analysis in the SEM depends on the size of the interaction volume, which in turn is controlled by the accelerating voltage and the mean atomic number of the sample, Z. For EDXS in the SEM, spatial resolution and depth resolution is on the order of a few microns. The detection limit of EDXS analysis in the SEM depends on the composition of the sample being analyzed, but is in the range 0.1-0.5 wt%.

A set of measurements onto calcite single-crystals not doped and doped with Eu(III)/Ni(II) were done at the Centre Technologique des Microstructures of University Lyon 1 and the Electron Microscopy Laboratory at HZDR. These measurements were performed only for calcite single-crystals at the end of each sorption experiments and were aiming at giving us information about the distribution of europium or nickel onto the surface of the crystal. These measurements permitted us to determine the distribution of Ni/Eu onto surface, the precipitation phenomena and help to distinguish between different mechanisms that can occur on the adsorbent surface. This technique gives the possibility to see the defects and edge pits onto the surface of the single crystals (which are present because the single crystals are natural calcite crystals) and to discriminate the different mechanism occurring at element/calcite interface.

Appendix B: Principle of Time Resolved Laser-induced Fluorescence Spectroscopy (TRLFS)

B.1 The fluorescence

Fluorescence is an important process from analytical point of view. This phenomenon is observed when atoms or molecules excited by absorption of an electromagnetic radiance, return to elementary state releasing the energy excess as photons [133].

The fluorescence is a luminescence phenomenon of a light substance that adsorbed other electromagnetic radiation. Fluorescence corresponds to transitions between states of the same spin in a very short time (10^{-9} – 10^{-6} s) [133]. Luminescence permits to bring an atom (Eu atom in our case) in an excited state by submitting it to UV excitation. The released energy to fundamental state produces a secondary emission where the time dependency and the frequency are characteristic of the symmetry of occupied sites by an atom in a crystal. An example of the main energy transfers who are taking place in the energetic levels of the elements with a $4f^6$ configuration (Eu(III)) are presented in the figure below (Figure B.1).

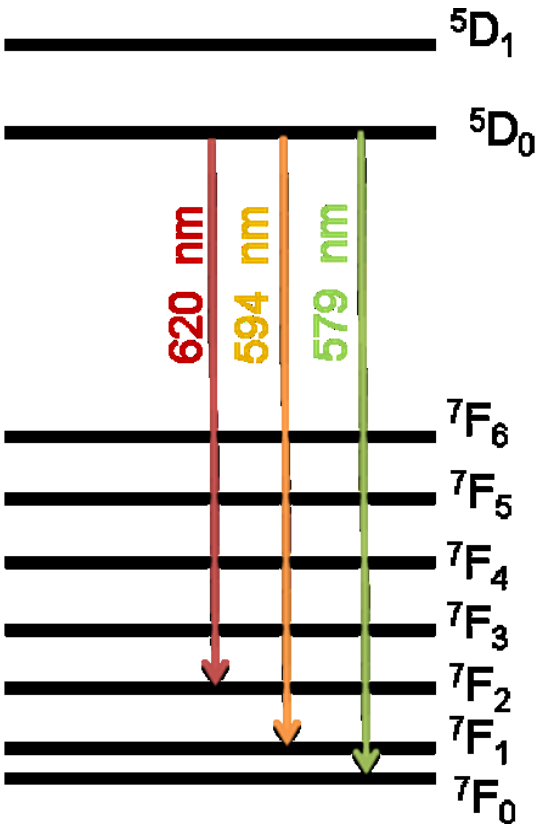

Figure B.1: Electronic Eu(III) scheme for energy levels distributions (the wavelengths are in nm) [134].

With a non-selective UV excitation not only the $^5D_0$ level but also higher energy levels are excited. After radiationless relaxation to the first excited state, that is $^5D_0$, luminescence emission to the groundstate ^7F_J (J = 0-6) occurs. The most relevant electron transitions for the investigation of Eu(III) complexation are these with J = 0-2. The $^5D_0 \rightarrow {}^7F_0$ (λ=579 nm) transition should show up only one band as the level is not degenerated. For the transition $^5D_0 \rightarrow {}^7F_1$ (λ=594 nm) up to three stripes can appear and up to five stripes for $^5D_0 \rightarrow {}^7F_2$ (λ=620 nm) due to the degeneration rule 2J+1. The transition $^5D_0 \rightarrow {}^7F_2$ (λ=620 nm) is hypersensitive and is very important in complexation studies [132]. The intensity ratio of the $^5D_0 \rightarrow {}^7F_1$ and $^5D_0 \rightarrow {}^7F_2$ transitions and the luminescence lifetimes give information about the Eu(III) speciation. These information are important to understand the sorption mechanism and Eu(III) species that may form in aqueous solutions or at water/solid interface [135, 136].

B.2 Correlation between luminescence lifetime and water molecules calculations

The measured luminescence intensity, Y at time x is the sum of fluorescent intensities of the i-th species at t = 0. The τ_i is the calculated luminescence lifetime for the i-th species [136] :

$$Y = \sum_n \left(A_i e^{-\tau_x/\tau_i} \right) \qquad \text{(Eq. B.1)}$$

The luminescence lifetimes of Eu(III) in solution are quite short because of the energy transfer from f level (which are excited) to the lower vibronic states of H_2O molecules in the first coordination sphere of lanthanides. When the ions are complexed or sorbed onto a mineral surface by inner-sphere complexation, a part of the water molecules is displaced [136].

Horrocks and his collaborators [59] established a linear relation between the lifetime and the number of H_2O in the first coordination sphere of Eu(III) by determination the lifetimes of crystalline complexes with a known number of water molecules in H_2O and D_2O , assuming that we have one coupling with H_2O and the coupling with D_2O was considered negligible. An empirical formula to determine the number of H_2O was developed for Eu(III) [137]:

$$n_{H_2O-/} = \frac{1.07}{\tau} - 0.62 \qquad \text{(Eq. B.2)}$$

where:

τ = luminescence lifetime (ms).

There is applied also a standard error for nH_2O calculation of ± 0.5 water molecules. The equation presented before has been calculated for europium solids prepared in the manner in which the number of water molecules is varies from 0 to nine (corresponding to Ln(III)), but also can be transferred to aqueous complexes as well.

B.3 TRLFS measurements with Eu(III)

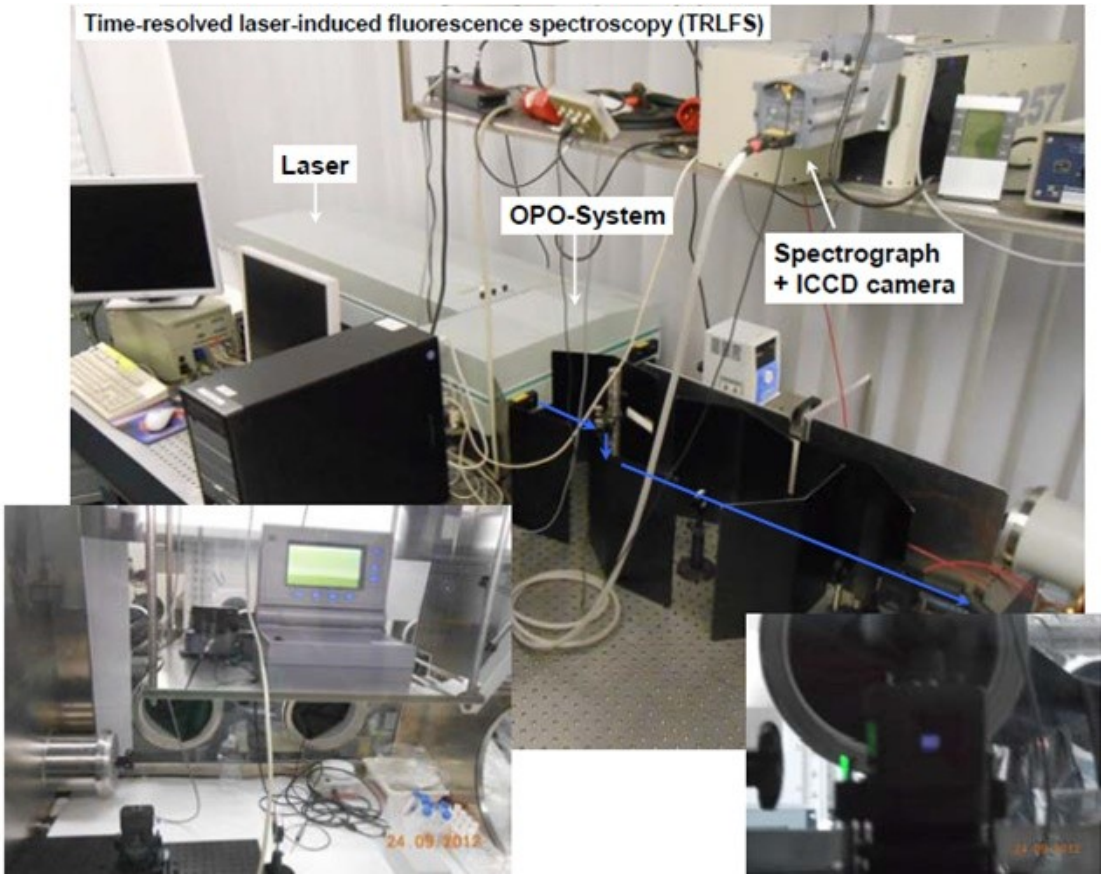

Figure B.2: Image of the laser system [138].

Figure B.2 represents the laser system used for measurements. The TRLF spectra were recorded using a pulsed flash lamp pumped Nd:YAG OPO (optical parametrical oscillator) laser system (Powerlite Precision II 9020 laser equipped with a Green PANTHER EX OPO, Santa Clara (CA,USA)) from Continuum. An optical parameter oscillator (OPO) was used to adjust the wavelength which was emitted by the laser beam and was pumped by a second harmonic oscillation of the Nd:YAG laser (532 nm). A photodiode is monitoring the laser pulsed energy which was around 1 – 1.5 mJ during the measurements. The detector for the fluorescence emission consists of a spectrograph (Oriel MS 257), with different gratings (300 and 1200 lines per mm, respectively), and an ICCD camera (Andor iStar); all components were purchased from the Lot-Oriel Group. A detailed description of the used equipment is given by Moll and his collaborators [139]. A constant time window of 1 ms and an excitation wavelength of 394 nm

were applied for all measurements. The emission spectra were recorded in the 570-650 nm (1200 line mm^{-1} grating, static spectra) and 440-780 nm (300 line mm^{-1} grating, time-resolved spectra) ranges. For time-resolved measurements, spectra with delay time steps between 50 and 250 μs were recorded.

Appendix C: Principle of Rutherford Backscattering Spectrometry

C.1 Presentation of the technique

Rutherford Backscattering Spectrometry (RBS) was developed by Ernest Rutherford in 1910 and the first applications were made in the 1960s (including the analysis of a lunar soil). When the incident ion passes close enough to the core of the target, the Coulomb repulsion (electrostatic interactions between the positive charges of the two nuclei) becomes sensitive. Incident particle energy E_0 collides then bounces off the target nucleus, resulting in a loss of energy ΔE. Then the incident particle is released with energy E_1 lower than E_0 (Figure C.1).

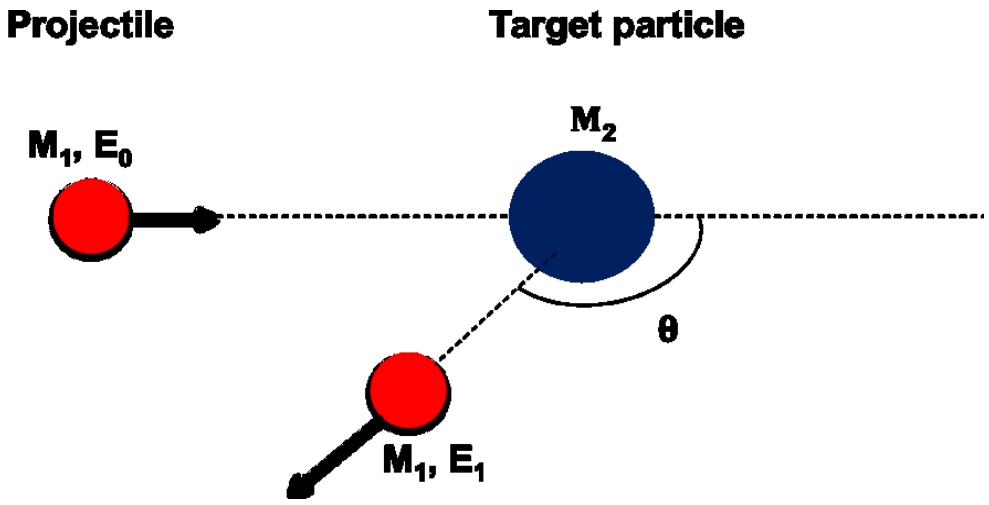

Figure C.1: Schematics of an elastic collision and backscattering of a lighter projectile with a heavier target particle.

Energy loss driven during this elastic scattering is characteristic of the element analyzed. The energy of the ion will be distributed according to its weight, the detection angle θ (relative to the position of the detector in the analysis chamber), and the mass of the nucleus diffuser. This energy E_d is proportional to the energy of the incident beam (Eq. C.1) ions.

$$E_d = K \cdot E_0 E_d = K \cdot E_0 \qquad \text{(Eq. C.1)}$$

where:

E_d = backscattered energy

K= kinematic factor

E_0 = incident ion energy

The conservations of kinetic energy and momentum give access to the kinematic factor K (Eq. C.2).

$$K = \frac{\sqrt{M_2^2 - M_1^2 \sin^2\theta} + M_1 \cos\theta}{(M_1 + M_2)} \qquad \text{(Eq. C.2)}$$

where:

M_1 = mass of projectile

M_2 = mass of target

θ = scattering angle

A RBS spectrum of a compound is composed of several signals corresponding to the different elements present in the sample. The total RBS signal of a A_xB_y compound is the sum of two signals: one for the A element at high energy and the other for B atom at lower energy if $A_A > A_B$ (where A and B are the respective masses of the elements). The higher is the thickness of the sample, the larger the width of each signal. The concentration of each element is proportional to the signal height (see Figure C.2).

Through matter, the incident ions loose a certain amount of energy (Eq. C.3), proportional to the energy stopping power of the elements present in the material (dE /dx).

$$\Delta E = \int_{x=0}^{x} \left(\frac{dE}{dx}\right) dx \Delta E = \int_{x=0}^{x} \left(\frac{dE}{dx}\right) dx \qquad \text{(Eq. C.3)}$$

Thus, a projectile coming from a collision inside the bulk has a lower energy compared to a projectile coming from a collision at the surface of the sample.

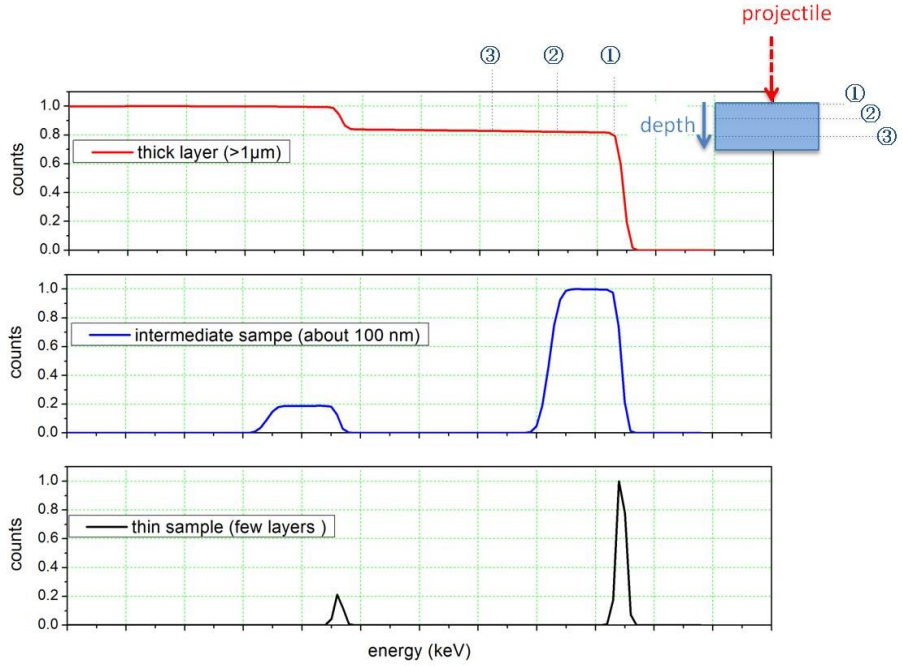

Figure C.2: RBS signals representing the interaction of a light particle with a A_xB_y compound with varying sample thicknesses.

C.2 Description of the experimental conditions

The analyses have been carried out using two different facilities: the 4 MV Van de Graaff facility at IPN Lyon and the 3.75 MV Van de Graaff facility at CEA Saclay / LEEL.

C.2.1 Experiments performed at IPN Lyon

The experiments were done using a millibeam on compacted powders on one hand and on millimetric sized single crystals on the other hand.

Beam was normal to the sample surfaces and ^{4}He detection was performed at 172° using a surface barrier silicon detector. Two different energies have been used for the incident beam: 4 and 1.5 MeV. The 4 MeV beam allowed probing Eu and Ni in order to measure the incorporation of Eu and Ni in function of depth and the 1.5 MeV experiments were performed with the purpose to increase the surface resolution and to accurately probe the first hundreds nanometers near the surface. The circular incident beam was around 1 mm in diameter and the current density was

kept low with a maximum value of 2 μAcm^{-2} in order to avoid element (Eu or Ni) migration or calcite degradation during RBS analysis [114].

C.2.2 Experiments performed at CEA Saclay / LEEL

Other set of experiments were performed at the nuclear microprobe LEEL laboratory (Laboratoire d'Etude des Eléments Légers) located at the CEA of Saclay, in order to get elemental maps at a micrometric scale and to get more insight into the sorption mechanisms of Eu into calcite, experiments using a microbeam. The microprobe is equipped with a 3.75 MV single stage accelerator. Two microbeam lines are available. One of these, situated at 90° to the injection line, is used to measure non-active samples. The other one, located in a controlled shielded area, offers the unique feature of being devoted to radioactive samples. More details were given elsewhere [140-142]. A schematic representation of the installation is presented in the figure below (Figure C.3).

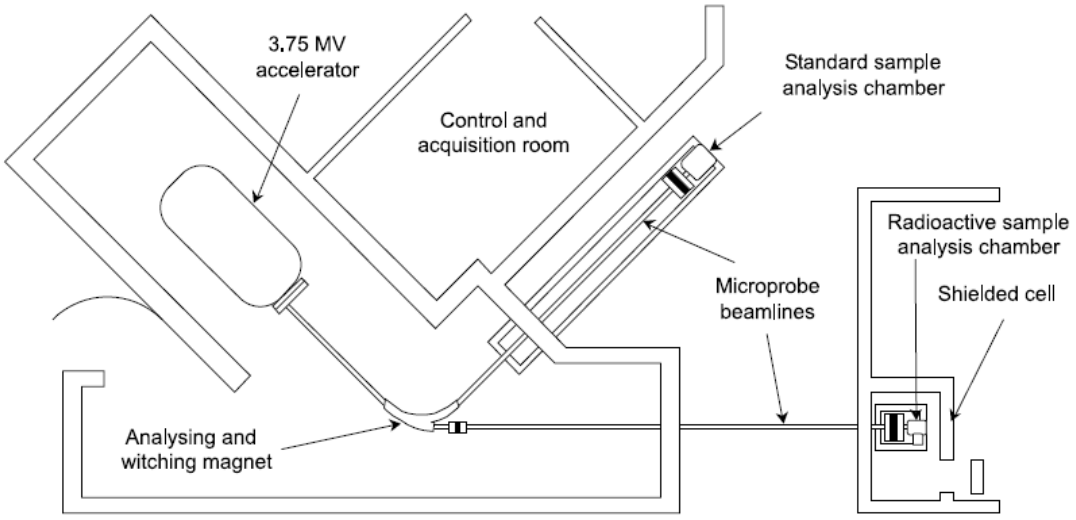

Figure C.3: Schematic representation of LEEL nuclear microprobe [142].

The accelerator can generate beams of $^{1}H^{+}$, $^{3}He^{+}$ and $^{4}He^{+}$ with an energy ranging from 800 keV to 3.5 MeV, $^{2}H^{+}$ from 800 keV to 1.9 MeV. They are redirected to the relevant microfocusing line by the switching magnet. After the magnet, a set of four independent stainless steel slits

defines the object size and shape for the quadrupole doublet. The minimum size of the microbeam, image produced by this focusing lens 25 cm behind in the analysis chamber, can reach 2 × 2 μm^2 on the target. The analysis chamber is equipped with several detectors, allowing various currently used IBA methods (Ion Beam Analysis) as it is shown in Figure C.4.

A 4-axis goniometer permits a precise positioning on the sample before recorded experiment [140, 142]. Two cameras are also used, the first one to overview the sample and the other is connected to a 400X confocal optical microscope. Using this camera the field of view is 150 × 100 µm [140, 142].

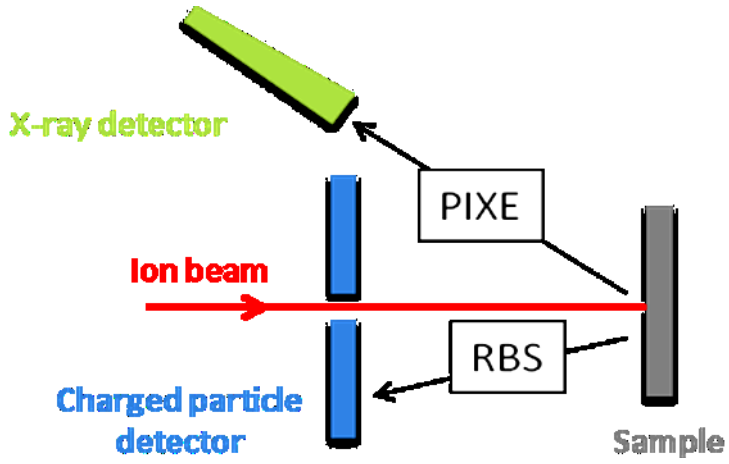

Figure C.4: Configuration of the analysis chamber.

Signal acquisition is done through a charged particle detector for RBS spectra. Simultaneous analysis of the samples by PIXE (Particle X-Ray Emission) is also available at the CEA facility but will not be developed in this appendix.

C.3 Data processing

The SIMNRA [143] 6.06 simulation program was used to simulate the RBS experimental spectra (performed at IPN Lyon and CEA Saclay).

SIMNRA is an analytical code based on the single scattering approximation. In this code, the sample target is subdivided into shallow sublayers. Each simulated spectrum is made up of the

superimposed contributions from each isotope of each sublayer of the sample target. The thickness of each sublayer is put equal to the value of the depth resolution (around 20 nm) determined by the RESOLNRA code. When the incident particles penetrate a sublayer, they lose energy due to electronic and nuclear energy loss (calculated with the Doolittle algorithm) and the beam energy is spread due to straggling (it is assumed that the particle energy distribution is Gaussian). SIMNRA calculates the energy of backscattered particles from the front and the backside of the sublayer. This allows calculating the energy spectrum of each isotope in each sublayer. The number of counts in each channel is consequently given by integrating this energy spectrum. At the end, the signal of the detector is calculated taking into account the number of counts, the detector solid angle and the cross-sections on each considered element (Ni or Eu, Ca, C and O).

Figure C.5 shows a typical RBS spectrum obtained on a single calcite crystal put into contact with a solution enriched with Ni (10^{-3} mol.L^{-1}) during 3 weeks and analyzed at IPN Lyon. The red points represent the experimental data and the blue line represents the spectrum fitted with SIMNRA [143].

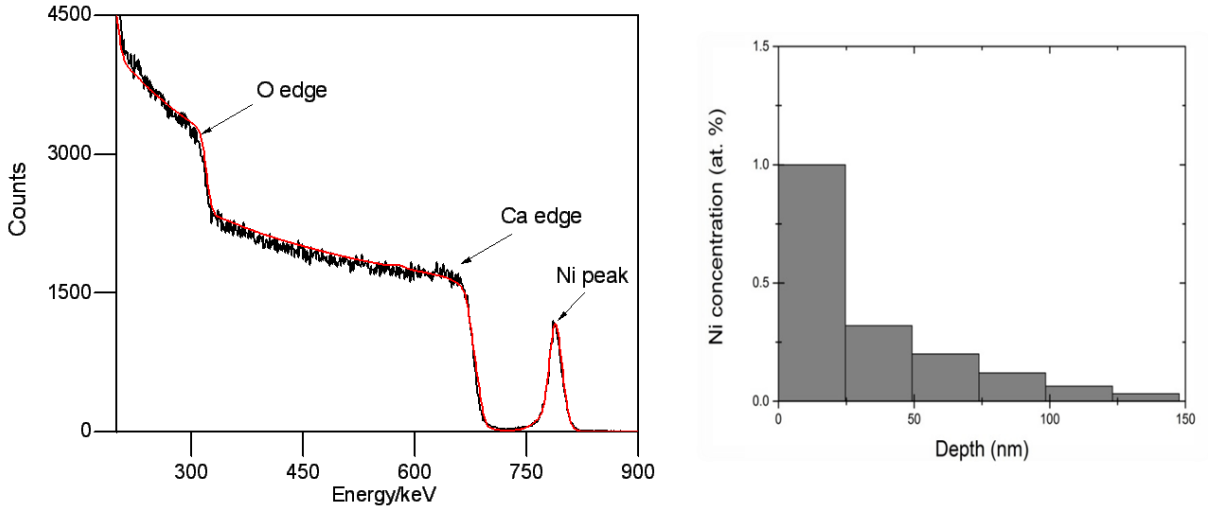

Figure C.5: Ni(II) concentration as a function of depth after processing the data for the previously cited sample.

Moreover, at CEA Saclay, the RISMIN program [140] was used to build an X-Y map which reflects the lateral distribution of each element and to extract the spectra linked to the map (Figure C.6).

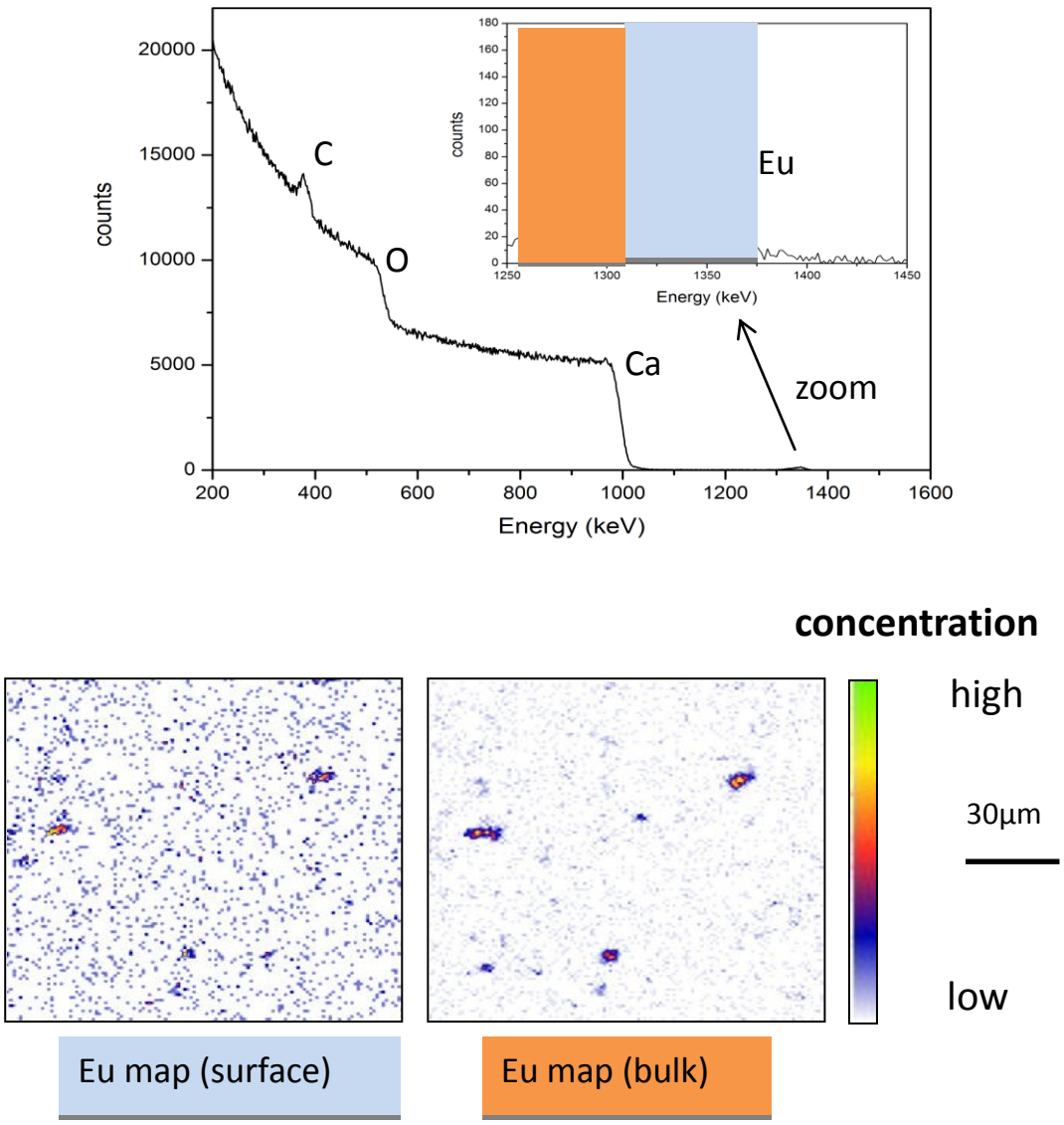

Figure C.6: RBS spectra obtained on single crystal of calcite (10^{-5} mol.L^{-1} Eu(III)/ contact time 5 months), together with RBS elemental maps for Eu, drawn from the colored region of interest.

Abstract

In the context of the safety assessment of an underground repository for nuclear waste, sorption reactions are one of the main processes to take into account to predict the migration of the radionuclides which might be transferred from the waste canisters to underground waters over geological time scales. Sorption of aqueous species on minerals can include adsorption processes, surface (co)-precipitation, and even incorporation in the bulk of the material, which can lead to the irreversibility of some sorption reactions.
This work is focused on two elements: Eu(III) as an analogue of trivalent actinides and Ni(II) as activation product. Calcite was chosen as adsorbent due to its presence in Callovian-Oxfordian clay rocks. Our study combines batch experiments with spectroscopic techniques (TRLFS, RBS and SEM-EDXS) to elucidate the mechanisms occurring at Eu(III)/Ni(II) calcite interface. To obtain a better understanding on the systems, before starting sorption experiments, aqueous chemistry of Eu(III) and Ni(II) was carefully investigated.
Macroscopic results showed a strong retention of Eu(III) on calcite, no matter the initial concentration, contact time and CO_2 partial pressure. Ni(II) was also readily sorbed by calcite, but the retention was influenced by contact time and concentration. Time-dependent sorption experiments showed a marked and slow increase of retention upon a long time range (up to 4 months).Desorption results indicated a partly reversible sorption for Ni(II).
TRLFS highlighted the influence of initial concentration and contact time on the interaction of Eu(III) with calcite. With the help of RBS and SEM-EDXS, it enabled to discriminate between different mechanisms like surface precipitation, inner-sphere complexation and incorporation. RBS showed incorporation of Eu(III) into calcite up to 250 nm, contrary to Ni(II) which was located at the surface.

Key words: sorption, calcite, Eu(III), Ni(II), TRLFS, RBS

Résumé

Dans le contexte de l'évaluation de la sûreté d'un stockage de déchets radioactifs en site géologique profond, les réactions de sorption sont un des principaux processus à prendre en compte pour prédire la migration des radionucléides qui pourraient être transférés des colis de déchets vers les eaux souterraines à l'échelle des temps géologiques. La sorption d'espèces aqueuses sur les minéraux peut inclure des processus d'adsorption, de (co-)précipitation de surface, et aller jusqu'à l'incorporation au sein des phases solides, ce qui peut entraîner l'irréversibilité de certaines réactions de sorption.
Ce travail est axé sur deux éléments: l´Eu(III) comme analogue des certains actinides trivalents et le Ni(II) en tant que produit d'activation. La calcite a été choisie comme solide d´étude en tant que composant des argilites du Callovo-Oxfordien. Notre étude combine des expériences de type batch avec des techniques spectroscopiques (SLRT, RBS et MEB-EDXS) pour élucider les mécanismes qui se produisent à l'interface Eu(III) / Ni(II) – calcite. Pour obtenir une meilleure compréhension des systèmes, avant de commencer les expériences de sorption, la chimie en solution de l'Eu(III) et du Ni(II) a été systématiquement étudiée.
La calcite a montré une forte rétention de l'Eu(III), quelle que soit la concentration initiale, le temps de contact et la pression partielle de CO_2. Ni(II) est également aisément retenu par la calcite, mais la rétention est dépendante de ces deux paramètres. Les expériences de sorption en fonction du temps ont montré une augmentation nette et progressive de la rétention sur de longues durées (jusqu'à 4 mois). Les résultats de désorption indiquent une réversibilité partielle pour Ni(II).
La SLRT a montré l'influence de la concentration et du temps de contact sur l'interaction de l'Eu(III) avec la calcite. Avec l'aide de la RBS et de la MEB/EDX, elle a permis de discriminer différents mécanismes tels que la précipitation de surface, la formation de complexes de surface de sphère interne et l'incorporation. La RBS a démontré l'incorporation de l'Eu(III) dans la calcite jusqu'à une profondeur de 250 nm, contrairement au Ni(II) qui lui reste situé en surface.

Mots clés : sorption, calcite, Eu(III), Ni(II), SLRT, RBS